UNIVERSITÀ VITA-SALUTE SAN RAFFAELE

CORSO DI DOTTORATO DI RICERCA
INTERNAZIONALE IN MEDICINA MOLECOLARE

Curriculum in Cellular and Molecular Biology

How to become a secretory cell: lessons from endometrial stromal cell decidualization

DoS: Prof. Roberto Sitia
Second Supervisor: Prof. Maya Schuldiner

Tesi di DOTTORATO DI RICERCA di Marco Dalla Torre
Matr. 017375
Ciclo di Dottorato XXXVI
SSD BIO11/BIO13

Anno Accademico 2022/2023

UNIVERSITÀ VITA-SALUTE SAN RAFFAELE

CORSO DI DOTTORATO DI RICERCA INTERNAZIONALE
IN MEDICINA MOLECOLARE

Curriculum in Cellular and Molecular Biology

How to become a secretory cell: lessons from endometrial stromal cell decidualization

DoS: Prof. Roberto Sitia
Second Supervisor: Prof. Maya Schuldiner



Tesi di DOTTORATO DI RICERCA di Marco Dalla Torre
Matr. 017375
Ciclo di Dottorato XXXVI
SSD BIO11/BIO13

Anno Accademico 2022/2023

RELEASE OF PHD THESIS

Il sottoscritto *I, the undersigned*	Marco Dalla Torre
Matricola/*Registration number*	017375
Nato a *Born in*	Magenta (MI)
Il/ *on*	03/06/1996

Autore della tesi di Dottorato di ricerca dal titolo *Author of the PhD Thesis titled*

How to become a secretory cell: lessons from endometrial stromal cell decidualization

☐ AUTORIZZA la Consultazione della tesi/*AUTHORIZES the public release of the thesis*

■ NON AUTORIZZA la Consultazione della tesi per 12 mesi/DOES NOT AUTHORIZE the public release of the thesis for 12 months

a partire dalla data di conseguimento del titolo e precisamente/*from the PhD thesis date, specifically*

Dal/*from* 13/12/2023 Al/*to* 13/12/2024

Poiché/*because:*

☐ l'intera ricerca o parti di essa sono potenzialmente soggette a brevettabilità/*The whole project or part of it might be subject to patentability;*

■ ci sono parti di tesi che sono già state sottoposte a un editore o sono in attesa di pubblicazione/*Parts of the thesis have been or are being submitted to a publisher or are in press;*

☐ la tesi è finanziata da enti esterni che vantano dei diritti su di esse e sulla loro pubblicazione/*the thesis project is financed by external bodies that have rights over it and on its publication*

È fatto divieto di riprodurre, in tutto o in parte, quanto in essa contenuto/Copyright the contents of the thesis in whole or in part is forbidden

Data/*Date* 09/11/2023 Firma/*Signature* 

Declaration

This thesis has been:

- composed by myself and has not been used in any previous application for a degree. Throughout the text I use both 'I' and 'We' interchangeably.

- has been written according to the editing guidelines approved by the University.

Permission to use images and other material covered by copyright has been sought and obtained. For all the image included, it was possible to obtain permission and is/are therefore included in thesis under the "fair use" exception (Italian legislative Decree no. 68/2003).

All the results presented here were obtained by myself, except for:

1) ***Hematoxylin and Eosin staining***

   The staining phase of the protocol was performed by Dr. Amleto Fiocchi, from the Advanced Light and Electron Microscopy Centre, San Raffaele Hospital, Milan, Italy

2) ***Transmission electron microscopy***

   Fixation, resin embedding and image acquisition were performed by Dr. Maria Carla Panzeri, from the Advanced Light and Electron Microscopy Centre, San Raffaele Hospital, Milan, Italy

3) ***Time-course transcriptome analysis***

   The bioinformatic analysis of the T-HESC transcriptome was performed in collaboration with Daniele Pittari, MEng. As a former member of Protein Transport and Secretion Unit, he performed the computational analyses and the graphical representation of the results.

Some of the results presented in this thesis, obtained by myself, was previously published in peer-reviewed journals:

-Results corresponding to Figures 4-14 were published in *Anelli et al. "Profound architectural and functional readjustments of the secretory pathway in decidualization of*

endometrial stromal cells." Traffic (Copenhagen, Denmark) vol. 23,1 (2022), of which I am co-author.

-Results corresponding to Figure 3, Figures 15-18 and Figures 20-31 were published in *Pittari, Dalla Torre, et al. "CREB3L1 and CREB3L2 control Golgi remodelling during decidualization of endometrial stromal cells." Frontiers in cell and developmental biology vol. 10 986997. 13 Oct. 2022*, of which I am co-first author.

All sources of information are acknowledged by means of reference.

Acknowledgments

First, I would like to thank my Director of Studies, Professor Roberto Sitia, who always guided, encouraged and supported me during the three years of my PhD project.

I also want to express my gratitude towards Dr. Tiziana Anelli, who also guided and assisted me since my very first days in the lab, and teaching me most of what I can do.

I gratefully acknowledge Professor Maya Schuldiner, who carefully supervised my project and always provided useful suggestions and exciting scientific discussion.

I would like to thank all my internal and external collaborators, who contributed to my project with reagents and technical support, but even more importantly with invaluable ideas and advices: Dr. Alessandra Boletta and Dr. Laura Cassina, for their invaluable suggestions and their support in the analysis of the mitochondrial compartment; Professor Paola Panina, for her role in the initial development of the project, and for the support she always provided; Daniele Pittari, for his significant contribution to the transcriptome analyses; all the ALEMBIC staff, and Laura Cassina in particular, for the support they provided me before, during and after all my microscopy acquisitions; Professor Kenji Inaba and Dr.Yuta Amagai, for kindly providing me the reagents required for pH and zinc quantifications.

Last, but not least, I want to thank all the presents and former lab mates: during these three years they always helped me by fruitful scientific discussion, but even more importantly they became true and sincere friend.

Abstract

Every biological process depends, in some measure, on protein transport and secretion. These processes are accomplished by all cell types, but specialized cells can convert, by their differentiation program, into real *protein factories*.

The *decidualization* of Endometrial Stromal Cells (EnSC) is a clear example of inducible secretory differentiation: upon hormonal stimulations, these fibroblast-like cells completely switch their phenotypes, and provide the factors needed for successful embryo implantation through a massive and efficient secretory activity. Accordingly, these cells are fundamental for human health and fertility, and defects of the decidualization program can have serious pathological implications.

To understand how EnSC can build-up their secretory capacity, I decidualized them *in vitro* and analyzed their differentiation program with different approaches (expression analysis at transcriptome and single gene level, biochemical assays, and high-resolution microscopy).

In my project, I clearly demonstrated that this secretory differentiation program is far more complex than simply *building bigger organelles*: ER and Golgi enlarge, as expected for a secretory cell, but some compartments are clearly prioritized, with modifications of their luminal chemical characteristics (including pH and ion concentrations).

These morphological reshapings are regulated by complex transcriptional networks, which include the activation of the transcription factors CREB3L1 and CREB3L2, but not of the ER unfolded protein response.

EnSC rearrangements are not limited to the secretory organelles: indeed, I observed a coordinated reshaping of all the cellular compartments, including a massive enlargement of the mitochondrial compartment. This corresponds to a complete rewiring of the energy metabolism, with a radical switch from glycolysis to mitochondrial respiration.

Together, my results provide a detailed picture on how EnSC achieve quickly and efficiently a massive secretory capacity, by a careful preparation and a coordinated reorganization of all the cellular components.

TABLE OF CONTENTS

TABLE OF CONTENTS **1**

ACRONYMS AND ABBREVIATIONS **5**

LIST OF FIGURES AND TABLES **9**

INTRODUCTION **13**

1 THE ENDOMETRIUM 13

1.1 The role of implantation in human reproduction *13*

1.2 Anatomical and histological organization of the endometrium *14*

1.3 Regulation of the endometrial dynamics: uterine and ovarian cycle *15*

1.4 The secretory phase: decidualization of the endometrium *17*

2 ENDOMETRIAL STROMAL CELLS: MASTER REGULATORS OF THE ENDOMETRIUM 19

2.1 General description of endometrial stromal cells *19*

2.2 Regulation of EnSC decidualization *20*

2.3 Decidualized EnSCs reshape the endometrial environment *22*

2.3.1 The decidualization markers: prolactin and IGFBP-1 ..... *23*

2.3.2 Extracellular matrix deposition and remodeling *24*

2.3.3 Regulation of angiogenesis and blood vessel maturation *25*

2.3.4 Regulation of immune cell populations *26*

2.4 Pathological implications of defective decidualization *27*

3 BECOMING A *PROTEIN FACTORY*: THE SECRETORY PATHWAY ORGANELLES 28

3.1 Secretory pathway organelles: a brief overview *28*

3.1.1 The endoplasmic reticulum *29*

3.1.2 Golgi complex *32*

3.1.3 Homeostasis of the secretory pathway *34*

AIMS OF THE WORK **37**

RESULTS 38

1 CHARACTERIZATION OF THE SECRETORY ORGANELLES IN DECIDUALIZATION 38

1.1 Validation of T-HESC as an EnSC decidualization model 38

1.2 Secretory organelle enlargement: immunofluorescence and morphometry 42

1.3 Characterization of chaperone and enzyme induction 50

1.4 A broader view: time-course transcriptome analysis 54

2 REGULATION OF THE SECRETORY ORGANELLES: CREB3L1 AND CREB3L2 58

2.1 Identification of co-regulated transcriptional clusters of secretory pathway genes 59

2.2 CREB3L1 and CREB3L2 are induced during decidualization 63

2.3 CREB3L1 and CREB3L2 are required for efficient decidualization 67

2.4 Effect of CREB3L1/2 silencing on secretory organelle volume and morphology 73

2.5 Silencing of CREB3L1 and CREB3L2 impairs protein trafficking and secretion 76

3 NOT ONLY A MATTER OF SECRETORY ORGANELLES: MITOCHONDRIAL NETWORK REWIRING 81

3.1 Mitochondria enlarge in decidualization 82

3.2 Morphological reshaping of the mitochondrial network 85

3.2 Ultrastructural analysis of mitochondria and ER-mitochondria interactions ... 88

3.3 ER and mitochondria closely associate in endometrial stromal cells 93

3.4 A metabolic switch: increase in respiration, decrease in glycolysis 95

3.5 Transcriptional analysis of mitochondrial genes 99

3.6 A glimpse of regulation: the nuclear translocation of PGC-1a 102

4 A GENERAL CHANGE IN THE CELLULAR LANDSCAPE: PRELIMINARY DATA ON ZINC QUANTIFICATION IN ENSC SECRETORY PATHWAY 105

4.1 Generation and validation stable cell lines for subcellular zinc quantification 106

4.2 Golgi measurement of pH and zinc at a sub-organelle level.....110

DISCUSSION 116

1 MORPHOLOGICAL AND FUNCTIONAL RESHAPING OF THE SECRETORY PATHWAY ORGANELLES 116

2 TRANSCRIPTIONAL REGULATION OF ORGANELLE RESHAPING 118

3 MITOCHONDRIAL NETWORK RESHAPING AND REWIRING OF THE MITOCHONDRIAL ...121

4 THE DYNAMICS OF ZINC IN ENSC SECRETORY PATHWAY 124

5 CLOSING REMARKS 126

MATERIALS AND METHODS 128

REAGENTS 128

CELL LINES AND CULTURE CONDITIONS 128

IN VITRO DECIDUALIZATION PROTOCOL 128

ISOLATION, CULTURE AND *IN VITRO* DECIDUALIZATION OF MURINE ENSC 129

IMMUNOFLUORESCENCE 129

HAEMATOXYLIN/EOSIN STAINING 130

MORPHOMETRIC AND MORPHOLOGICAL ANALYSIS 130

SECRETOME COLLECTION 131

ELISA 131

WESTERN BLOT 132

SYPRO RUBY PROTEIN STAINING 132

REAL TIME QPCR 133

SILENCING OF GENE EXPRESSION 134

TRANSMISSION ELECTRON MICROSCOPY 134

MITOTRACKER STAINING 136

SEAHORSE ASSAY FOR MITOCHONDRIAL ACTIVITY 136

MOLECULAR BIOLOGY: PLASMID GENERATION 136

T-HESC TRANSFECTION 137

Transcriptome analysis 138
HeLa cell transfection 140
Generation of stable T-HESC cell lines 140
Microscopy-based in vivo measurement of pH and zinc 141
Graphical representations and statistical analysis 143
Table 1: Antibodies 143
Table 2: Synthetic oligonucleotides 145
REFERENCES 147

ACRONYMS AND ABBREVIATIONS

$[Zn^{2+}]$ = Zinc concentration

ACSS1 = Acyl-CoA Synthetase Short Chain Family Member 1

ATF6 = Activating Transcription Factor 6

ATP = Adenosine Triphosphate

BiP = Binding Immunoglobulin Protein

cAMP = cyclic Adenosine Monophosphate

CD = Cluster of Differentiation

cDNA = complementary DNA, from RNA retrotranscription

COX1/2 = Cyclooxygenase 1/2

CPT1A/C = Carnitine Palmitoyltransferase 1A/C

CREB3L1/2 = cAMP Responsive Element Binding 3-Like protein ½

CRT = Calreticulin

C_t = threshold cycle, in qPCR

DEA = Differential Expression Analysis

DEG = Differentially Expressed Gene

e.g. = *exempli gratia*, that is "for example"

ECAR = Extra-Cellular Acidification Rate

ECM = Extracellular Matrix

EnSCs = Endometrial Stromal Cells

ER = Endoplasmic Reticulum

ERGIC = ER-Golgi Intermediate Compartment

ERGIC53 = ER-Golgi Intermediate Compartment 53 kDa protein

ERp44 = Endoplasmic Reticulum resident protein 44

FGF = Fibroblast Growth Factors

FSH = Follicle-Stimulating Hormone

GM130 = Golgi Matrix protein 130

GnRH = Gonadotropin Releasing Hormone

GO = Gene Ontology

h = hours

HBSS = Hank's balanced saline solution

HLA = Human Leukocyte Antigen

Hsp47 = Heat shock protein 47

IF = Immunofluorescence

IGF-1 = Insulin-like Growth Factor

IGFBP-1 = Insulin-like Growth Factor Binding Protein 1

IL = interleukin

IRE1α = Inositol-Requiring Enzyme 1α

IVF-ET = In Vitro Fertilization and Embryo Transfer

k = Cluster number

K_d = Dissociation coefficient

LH = Luteinizing Hormone

MERC = Mitochondria-Endoplasmic Reticulum Contact site

MIC-1 = Macrophage Inhibitory Cytokine 1

min = minutes

MMP = Matrix Metalloprotease

mtDNA = Mitochondrial DNA

Nrf1/2 = Nuclear Respiratory Factor ½

OCR = Oxygen Consumption Rate

ORA = Over-Representation Analysis

OXPHOS = Oxidative Phosphorylation

PAI-1 = Plasminogen Activator Inhibitor 1

PAM = Partition Around Medioids

PDI = Protein Disulfide Isomerase

PERK = PKR-like Endoplasmic Reticulum Kinase

PGC-1α = Peroxisome Proliferator-Activated Receptor Gamma Coactivator 1α

PGE_2 = Prostaglandin E2

PKA = Protein Kinase A

PPARα/γ = Peroxisome Proliferator-Activated Receptor α/γ

PR = Progesterone Receptor

PRL = Prolactin

qPCR = semi-quantitative real-time PCR

R_{max} = Maximum signal, upon zinc addition

R_{min} = Minimum signal, upon zinc chelation

ROI = Region Of Interest

R_{ss} = Basal signal, at the steady state

RT = Room Temperature

RTN4 = Reticulon 4

s = seconds

SBD = Shape-Based Distance

siRNA = small interfering RNA

TEM = Transmission Electron Microscopy

TF = Tissue Factor

TGN46 = Trans Golgi Network

T-HESC = TERT-immortalized Human Endometrial Stromal Cells

TIMP = Tissue Inhibitor of Metalloproteases

TOM20 = Translocase of the Outer Membrane 20

uDCs = uterine Dendritic Cells

uNKs = Uterine Natural Killer Cells

UPR = Unfolded Protein Response

VDAC = Voltage Dependent Anion Channel

VEGF = Vascular Endothelial Growth Factor

ΔC_t = difference between the C_t of the gene of interest and the C_t of the reference gene

$\Delta\Delta C_t$ = difference between the ΔC_t of a sample and the ΔC_t of the control sample

LIST OF FIGURES AND TABLES

Figure 1. Decidualized EnSCs reshape the endometrial environment. 23

Figure 2. Homeostasis of the secretory pathway: Unfolded Protein Response of the ER… 36

Figure 3. Visualization of endometrial stromal cell decidualization. 40

Figure 4. Decidualization markers are transcriptionally induced during T-HESC in vitro decidualization. 41

Figure 5. Decidualized T-HESC secrete prolactin and interleukin 6. 42

Figure 6. Secretory pathway organelles enlarge in decidualization. 42

Figure 7. Decidualization reshapes morphology and distribution of secretory pathway organelles. 46

Figure 8. ER and Golgi enlarge during decidualization. 46

Figure 9. ER and ERGIC enlarge and reorganize during decidualization. 47

Figure 10. Volume of the secretory pathway organelles increases during decidualization. 48

Figure 11. Relative proportions of secretory pathway organelles change in decidualization. 49

Figure 12. Decidualization induces re-adjustment of the organelle composition. 51

Figure 13. Genes encoding for secretory pathway chaperones and enzymes are induced during decidualization. 52

Figure 14. In vitro decidualization of primary murine EnSCs validates the secretory pathway reshaping observed in the T-HESC cell line. 53

Figure 15. Decidualization entails an extensive transcriptional reshaping. 55

Figure 16. Transcriptional reshaping of the secretory organelles is an early event in decidualization. 56

Figure 17. Transcriptional profile of decidualizing T-HESC reflects the physiological differentiation program. 58

Figure 18. Time-series clustering dissects the transcriptional orchestration of secretory pathway reshaping 60

Figure 19. Representation of CREB3L1/2 activation mechanism. 64

Figure 20. CREB3L1 and CREB3L2 are transcriptionally induced in T-HESC decidualization 65

Figure 21. CREB3L1 and CREB3L2 are expressed and activated during decidualization. 66

Figure 22. Silencing of CREB3L1 and CREB3L2 is effective and specific. 67

Figure 23. Silencing of CREB3L1 and CREB3L2 does not affect the transcriptional induction of the decidualization marker prolactin. 68

Figure 24. Silencing of CREB3L1 and CREB3L2 impairs expression and induction of secretory pathway genes during decidualization. 70

Figure 25. Silencing of CREB3L1 and CREB3L2 impairs the expression of specific secretory pathway proteins. 72

Figure 26. Silencing of CREB3L1/2 in decidualization does not impair the overall morphological reshaping, but affects the morphology of ER and Golgi. 74

Figure 27. Silencing of CREB3L1/2 in decidualization impairs Golgi complex enlargement. 75

Figure 28. Silencing of CREB3L1/2 disrupts Golgi morphology in decidualized cells. 76

Figure 29. Silencing of CREB3L1/2 induces aberrant ER accumulation of secretory protein cargoes in decidualized EnSCs. 77

Figure 30. Silencing of CREB3L1 and CREB3L2 causes intracellular accumulation of procollagen and impairs collagen secretion. 78

Figure 31. CREB3L1 and CREB3L2 are required for efficient protein secretion in decidualized endometrial stromal cells. 80

Figure 32. Mitochondria are reorganized and redistributed during decidualization. 83

Figure 33. Mitochondrial network enlarges in decidualization. 83

Figure 34. Mitochondrial volume significantly increases upon decidualization. 84

Figure 35. Decidualization increases the expression of mitochondrial proteins. 85

Figure 36. Decidualization reshapes the mitochondrial network morphology. 86

Figure 37. The elongation of mitochondria increases with decidualization. 86

Figure 38. Despite their elongation, mitochondrial of decidualized cells are highly dynamic. 87

Figure 39. Transmission electron microscopy reveals close interactions between ER and mitochondria. 88

Figure 40. Highly elongated mitochondria are detected by TEM in decidualized T-HESCs 89

Figure 41. Ultrastructural analysis confirms mitochondrial elongation in decidualized cells. 91

Figure 42. ER and mitochondria increase their association during decidualization. 92

Figure 43. Mitochondria partially colocalize with different ER markers. 94

Figure 44. Seahorse mitochondrial stress test. 95

Figure 45. Decidualization increases mitochondrial respiration of T-HESC and modifies their respiratory profile. 96

Figure 46. Detailed analysis of mitochondrial respiration rewiring in decidualization. 97

Figure 47. Decidualization reduces glycolysis and induces a switch in the energy metabolism. 98

Figure 48. Decidualization reshapes the transcription pattern of mitochondrial genes. 100

Figure 49. Analysis of individual genes confirms transcriptional induction or repression of key mitochondrial functions. 100

Figure 50. Time-course analysis of mitochondrial gene transcription reveals early and profound functional changes during the decidualization process. 102

Figure 51. Nuclear translocation of PGC-1α is an early event of T-HESC decidualization. 104

Figure 52. Co-immunofluorescence with Golgi markers confirmed the correct sub-organelle organelle localization of the Halo-tagged probes. 108

Figure 53. The Halo-tagged probes are expressed and correctly localized in the stable T-HESC cell lines. 109

Figure 54. Cell lines expressing the Halo-tagged probes can be correctly decidualized. ..110

Figure 55. TMR and ZnDA-1H can be correctly detected in the T-HESC lines expressing the Halo-tagged probes, as required for the labile zinc quantification. 111

Figure 56. ZnDA-1H fluorescent signal can be modulated, as expected, by zinc chelation and by addition of exogenous zinc. 111

Figure 57. Golgi-localized fluorescent pH probes (pHluorin-2) can be correctly expressed in control and decidualized T-HESC by transient transfection. 112

Figure 58. Decidualization induces a slight acidification of different sub-compartments of the Golgi complex.....113

Figure 59. The labile fraction of zinc in different sub-compartments of the Golgi complex is modified by decidualization.....114

Figure 60. Zinc concentration controls localization and function of ERp44. 125

Figure 61. Structure of the ZnDA-1H fluorescent probe. 142

Figure 62. Graphical representation of pHluorin-2 signal calibration. 143

INTRODUCTION

1 The endometrium

1.1 The role of implantation in human reproduction

In the human species, the probability of successfully establishing a pregnancy is surprisingly low, especially in comparison to what observed in other mammals. It has been estimated that, at the peak of fertility, the reproductive success is not higher than 30% per ovulatory cycle, a value that quickly declines with age (Kim 2017, Ng 2020); as a comparison, the probability of establishing a pregnancy in outbred mice strains can be as high as 70-75% per reproductive event (Mader 2009).

The main individual cause of reproductive unsuccess, in humans, is represented by defects in the embryo implantation process, accounting for as many as 65-75% of overall reproductive failures (Norwitz 2001, Wilcox 1988). Indeed, the endometrium receptivity for the embryo is extremely limited in time, with an optimal *implantation window* of about 24-36 hours; outside this limited timeframe, even in the absence of any pathological condition, the likelihood of embryo implantation, and pregnancy progression drop dramatically (Ng 2020, Gellersen 2014).

Similar results were obtained by comparative studies on the probability of success of *in vitro* fertilization and embryo transfer (IVF-ET) procedures. Depending on the study considered and the IVF-ET strategies taken into consideration, the probability of successful pregnancy upon transfer of viable embryos is limited to 25-35% for a single IVF-ET procedure, with the success of implantation representing also in this case the limiting step (Smith 2015, Modest 2018).

The biological causes of the low efficiency of embryo implantation in the human species are complex, and only partially understood. A main aspect of the phenomenon is clearly the complete independence between the fecundation and the receptivity dynamics of the endometrium: as the two processes occur independently, any slight temporal mismatch between the two can completely hinder the successful establishment of pregnancy (Ng 2020, Gellersen 2014, Okada 2018).

The next sections will briefly discuss the histological organization of the endometrium, the morphological and functional changes required for a correct embryo implantation, and the pathological implications of defects in the tissue remodeling process.

1.2 Anatomical and histological organization of the endometrium

The uterus is a pear-shaped organ, formed by three tissues layers concentrically organized around the uterine cavity. Each of the layers has different histological features, and a different physiological role in the organ function. The outermost layer, the *perimetrium*, is a thin layer of connective tissue that surrounds the uterus, in continuity with the peritoneum. The intermediate layer, the *myometrium*, is a thick muscular layer, which represents the bulk of the organ; the myometrium is mostly formed by an alternation of smooth muscle fibers with different orientation, responsible for the uterine contractions upon delivery. The innermost layer, the *endometrium*, lines the uterine cavity, and is the one involved in embryo implantation and placenta formation (Thiyagarajan 2023).

The endometrium is formed by a simple columnar epithelium, covering a layer of highly cellular stromal tissue. Several tubular glands cross the endometrium, spanning from the uterine cavity to the basal layer of the stromal tissue. The tissue also contains abundant vasculature and lymphatic vessels, mostly concentrated close to the myometrium-endometrium junction (Yamaguchi 2021, Gellersen 2014).

Endometrium is conventionally divided into *stratum functionalis*, which includes the epithelium, the neck of the glands, and the upper part of the stromal tissue; and *stratum basalis*, which instead contains the base of the glands, most of the vasculature, and the deep layer of the stromal tissue. Although there is no clear histological difference between the two layers, and no clear boundary between them can be identified in basal conditions, the two *strata* acquire completely different organization and functions during the uterine cycle, as more widely described in the following sections (Yamaguchi 2021, Gellersen 2014, Thiyagarajan 2023).

Different cell populations populate the endometrial tissue. Specialized glandular epithelial cells form the columnar epithelium lining the uterine cavity and the uterine glands. In the

stroma, instead, the main cellular component is represented by the endometrial stromal cells (EnSCs), fibroblast-like cells with a peculiar secretory differentiation program, that represents the main topic of this thesis. Specialized immune cells are also abundant in the stromal tissue. Uterine natural killer cells (uNKs) represent the most abundant lymphoid population, accounting for up to 30-40% of the total cells present in the post-ovulatory phase (Gellersen 2014). These cells, positive for the cluster of differentiation 56 (CD56), but not for the CD16 antigen, are likely involved in the immune recognition and tolerance towards the trophoblast, and do not seem to have a significant cytotoxic activity. Macrophages positive for CD163 are also abundant in the tissue, while tissue-resident uterine dendritic cells (uDCs) and T lymphocytes are present in lower numbers.

It has been demonstrated that the *stratum basalis* of the endometrium also contains Epithelial Stem/Progenitors Cells (Cousins 2021) and Mesenchymal Stem Cells, endowed with high proliferation and clonogenic potential. The role of these stem cell populations is to reconstitute the epithelial and the stromal cell compartments, respectively, after the endometrial tissue is shed during menstruation (Cousins 2021, Gellersen 2014).

1.3 Regulation of the endometrial dynamics: uterine and ovarian cycle

The endometrium is a highly dynamic tissue, that undergoes a complex series of cyclical modifications, collectively known as the *uterine cycle*. The morphological and functional changes of the tissue are extensive, and involve all the residing cell populations, the vascular system, and the extracellular matrix. The process is fundamental to allow a correct embryo implantation, and is tightly connected with the *ovarian cycle*, that instead controls the maturation and release of the oocyte. Together, the uterine and the ovarian cycle constitute the *menstrual cycle.*

The menstrual cycle is controlled by the hypothalamus-pituitary-gonadal axis, through positive and negative feedback mechanisms controlling hormone release by different endocrine tissues. Each cycle is triggered by the release of a pulse of Gonadotropin Releasing Hormone (GnRH) by the hypothalamus. Once secreted, GnRH quickly reaches the adenohypophysis, where it triggers specialized cells (the *gonadotrophs*) to release two

glycoprotein hormones (*gonadotropins*), the Follicle-Stimulating Hormone (FSH) and the Luteinizing Hormone (LH). Through the systemic circulation, FSH and LH reach the ovaries, where they trigger the maturation of several follicles, of which only one (the *dominant follicle*) will complete maturation; the other ones, instead, will degenerate into *atretic follicles*. During follicle maturation, FSH and LH induce respectively *granulosa cells* and *theca cells* to produce and modify steroid hormones: upon stimulation, the *theca cells* produce and release large amounts of progesterone and androstenedione, which in turn is converted into 17-beta-estradiol by granulosa cells.

As the ovarian cycle proceeds and the estrogen levels rise, the dominant follicle completes maturation and breaks, releasing the oocyte in the *ovulation* process. During the following days, the ruptured follicle develops into the *corpus luteum*, that continues producing estrogens and progesterone. If embryo implantation does not occur, negative feedback loops drive the decrease of circulating FSH and LH, followed by the regression of the corpus luteum and the return of 17-beta-estradiol and progesterone to basal levels (Thiyagarajan 2023).

The changing levels of steroid hormones couple the ovarian cycle with the uterine cycle, ensuring that the remodeling of the endometrium is synchronized with the follicular maturation and oocyte release: in case of fecundation, this ensures that the peak of the endometrial receptivity corresponds to the moment in which the implantation probability is the highest. This tight coordination between the two cycles is particularly important for the mammalian species in which the uterine remodeling is under complete *maternal control* (humans, non-human primates, some bats and few other small mammals), meaning that it precedes and is independent from the implantation of the embryo (Gellersen 2014).

The uterine cycle is conventionally divided in three phases, even though the transition from one phase to the other is not sharp and well defined. The first phase is the *menstruation* and corresponds to days 0-5 of each menstrual cycle. In this phase, the *stratum functionalis* of the endometrium, that was extensively remodeled during the previous cycle, is shed from the tissue. This phase temporarily corresponds to the beginning of the release of the gonadotropins from the pituitary gland, and the beginning of the maturation of a new follicle (early *follicular phase* of the ovarian cycle).

After menstruation, the endometrium begins the *proliferative phase*, corresponding to days 5-14 of the cycle. In this phase, the endometrial tissue is repaired, and its overall architecture is reconstituted. The process is induced by the estrogens released by the developing follicle (late *follicular phase*), previously described in this paragraph (Gellersen 2014, Thiyagarajan 2023).

The third phase of the uterine cycle is the *secretory phase*, in which the endometrial tissue is massively remodeled in preparation for a possible embryo implantation, in a process defined *decidualization.* Accordingly, the secretory phase begins at day 14 of the cycle, corresponding to the moment of ovulation, and lasts until the end of the cycle, at day 28. The main driver of this phase is the rise of progesterone levels, massively produced by the *corpus luteum* (during the *luteal phase* of the ovarian cycle).

At the end of the secretory phase, unless implantation has occurred, the progesterone levels drop rapidly, as the *corpus luteum* regresses. This causes the *stratum functionalis* of the endometrial tissue to degenerate and detach, leading to the menstrual phase of the following cycle (Thiyagarajan 2023).

From menarche to menopause, a woman experiences on average 450 menstrual cycles, each of which corresponds to the maturation of one oocyte, and to extensive but reversible rearrangements of the endometrial tissue (Okada 2018, Gellersen 2014).

1.4 The secretory phase: decidualization of the endometrium

As described in the previous section, the endometrial layer is deeply remodeled during the uterine cycle, first to repair the tissue after menstruation, and then in preparation for the possible implantation of the embryo. The tissue changes are extensive, and clearly evident at both an anatomical and a histological level: for this reason, the formation of a specialized tissue of maternal origin involved in embryo implantation was recognized as early as 1826 (Gellersen 2014). Due to its transitory nature, this tissue was called *decidua*, from the Latin adjective *deciduus* (falling off, e.g. referred to the leaves of trees).

All the elements of the endometrial tissue are involved in the rearrangements. In menstruation, the whole *stratum functionalis* is shed from the endometrium. Therefore, as

the cycle progresses into the proliferative phase, the whole architecture of the vasculature, of the epithelium, and of the upper stromal layers must be completely reconstituted. This process seem to completely rely on progenitors located in the *stratum basalis*, although bone-marrow derived progenitors have also been proposed to play a role in the reconstitution of the resident endometrial stromal cells (Gellersen 2014, Thiyagarajan 2023).

The most extensive tissue rearrangements, however, are the ones observed in decidualization, that is the formation of the endometrial *decidua* during the secretory phase of the uterine cycle. In decidualization, the epithelial layer lining the uterine cavity acquires a pseudostratified organization and thickens, as the cells forming it enlarge their secretory organelles and accumulate glycogen granules. At the same time, the uterine glands enlarge their lumens and increase their complexity, giving rise to extremely coiled, intricate structures (Yamaguchi 2021).

Even more importantly, the stromal layer of the *stratum functionalis* is completely reorganized: the tissue thickens and swells, as abundant extracellular matrix proteins are secreted by the residing stromal cells (Cornillie 1985, Gellersen 2014, Okada 2018); the residing immune cell populations, and in particular the uNKs, significantly increase their number in the tissue (Dunn 2003); and the endometrial stromal cells themselves *decidualize*, undergoing a dramatic differentiation program into a secretory phenotype (Okada 2018, Gellersen 2014, Dunn 2003).

At the same time, new blood vessels sprout from the radial arteries in the myometrium and invade the endometrium: these vessels, called spiral arteries, are fundamental to support the endometrial cell populations during the secretory phase, and to establish the placental circulation in case of successful embryo implantation (Pijnenborg 2006, Gellersen 2014). Accordingly, any defect in the development, invasion or maturation of spiral arteries, almost inevitably results in pregnancy complications or failure (Pijnenborg 2006, Thiyagarajan 2023).

It is important to underline that all the morphological and functional changes described only involve the *stratum functionalis*, while the *stratum basalis* of the endometrium is completely unaffected by the decidualization process. This is likely fundamental to ensure

the efficient reconstitution of the *stratum functionalis* at the end of the menstruation, and to preserve the progenitor cells and the overall organization of the uterine glands.

2 Endometrial stromal cells: master regulators of the endometrium

2.1 General description of endometrial stromal cells

Endometrial stromal cells represent the main cellular population of the endometrial stroma, as well as the main regulators of the endometrial structure and reorganization.

EnSCs are sometimes defined as endometrial fibroblasts, mostly due to their morphological features and their localization in the stroma. However, they also have unique features, clearly identifying them as a specific cell type.

During the proliferative phase of the uterine cycle, endometrial stromal cells are chiefly involved in the reconstitution of the correct endometrial architecture. In this phase, the new endometrial stromal cells generated by the progenitors localized in the *stratum basalis* undergo extensive proliferation, regenerating the upper layer of the endometrial stroma. EnSC are also responsible for the secretion of extracellular matrix (ECM) proteins, including but not limited to Collagen type I, III and VI. The secretory activity observed in this phase, however, is not comparable to the one of decidualized EnSCs (Carbone 2006, Okada 2018, Shi 2020). In a physiological context, the endometrial regeneration occurs without any scar or tissue fibrosis, further confirming that EnSCs are indeed a cellular type with unique features (Gellersen 2014).

During the secretory phase, as extensively described in the following paragraphs, EnSCs decidualize, terminally differentiating into a secretory phenotype. Upon decidualization, these cells stop proliferating, enlarge and change their morphology, acquiring an epithelioid appearance. Even more importantly, decidualized EnSCs secrete large amounts of a wide array of secretory cargo proteins, that reshape the local environment to promote a successful embryo implantation (Dunn 2003, Gellersen 2014, Okada 2018).

2.2 Regulation of EnSC decidualization

During the secretory phase of the uterine cycle, endometrial stromal cells undergo a complete phenotypic switch, terminally differentiating into a secretory phenotype. This differentiation program is induced by ovarian steroid hormones, progesterone in particular, that reach the endometrium through the systemic circulation. Accordingly, decidualization begins first for the cells in close contact with the endometrial blood vessels, and gradually propagates to all the other EnSCs in the *stratum functionalis* (Gellersen 2014).

At the beginning of the secretory phase, estrogens prime the expression of the progesterone receptor (Maruyama 2008, Okada 2018), that is in turn strongly activated by the surge of progesterone levels (Okada 2018). Results based on murine models suggest that the PR-A isoform is required for EnSC response to progesterone, while the other isoform (PR-B) appears instead to be dispensable (Conneely 2000).

In response to progesterone itself, other signaling molecules with a paracrine effect are locally produced by endometrial stromal cells (Dunn 2003).

In response to progestins themselves, other signaling molecules with a paracrine effect are locally produced by endometrial cells. Indeed, steroid hormones stimulate the expression of COX-1 and COX-2 enzymes, leading to the production of signaling lipids with a local effect, including prostaglandin E2 (PGE_2) and other lipokines (Dunn 2003), but also to the upregulation of their receptors (Houserman 1989). In subsequent phases, IL-1β and other paracrine cues, released by both immune cells and by the embryo itself, further sustain the expression of COX-2 (Tamura 2002), maintaining and reinforcing the signaling cascade.

Hormonal stimulation also induces the expression of relaxin, a small peptide hormone with both paracrine and systemic effects (Palejwala 2002, Dunn 2003, Gellersen 2003). Relaxin has fundamental roles in the correct maturation of the endometrial vasculature (Albrecht 2010), but also acts as autocrine and paracrine signal, sustaining EnSC decidualization (Palejwala 2002).

Several other signal molecules and growth factors contribute to the decidualization program, in many cases in a non-dispensable manner (Matsuoka 2010, Li 2007). These signals include, but are not limited to, Wnt5a (Matsuoka 2010), BMP-2 (Li 2007), and

members of the TGF- β superfamily, secreted by both EnSCs and uterine epithelial cells (Jones R 2006). All these molecules induce the expression of important decidualization markers, but even more importantly they are often involved in positive feedback loops, providing robustness to the differentiation program (Gellersen 2014).

Interestingly, most of the paracrine signals involved in decidualization converge to a rise of the intracellular levels of cyclic AMP (cAMP), either due to the induction of adenylyl cyclase activity, or due to the inhibition of cAMP-degrading phosphodiesterases (Brar 1997, Gellersen 2003). The increased intracellular levels of cAMP determine the activation of EPAC (Kusama 2013) and PKA, resulting in the activatory phosphorylation of CREB (Telgmann 1998, reviewed in Yoshie 2015).

Cyclic AMP signaling, moreover, further sensitize cells to progesterone, as PKA activity prevents the inhibitory SUMOylation of progesterone receptor (Jones M 2006), and its binding with co-repressors (Wagner 1998), but also by directly promoting the expression of progesterone receptor (Brosens 1999, Dunn 2003).

Together, the activation of progesterone and cAMP-dependent signaling cascades determines an extensive transcriptional response in decidualizing cells, including the induction of C/EBPβ, FOXO1, homeobox A1, HAND2 and STAT (Yoshie 2015, Okada 2018). These transcription factors, in combination with progesterone receptor itself and CREB, determine the correct gene expression during the decidualization program.

Interestingly, the interaction among the different signals appears to be complex and dynamic, and the role of each molecule may change during the progression of the decidualization program (Okada 2018).

For example, progesterone has been variously reported to antagonize or promote the production of PGE_2 (Dunn 2003), but also to promote the expression of PGE_2 receptor (Houserman 1989). Moreover, despite progesterone alone is sufficient to induce decidualization *in vitro* (Gellersen 2014), progesterone signaling can in some conditions dampen prolactin expression.

Paracrine signals released by tissue-resident immune cell populations are also thought to contribute to the precise spatiotemporal control of EnSC decidualization: interferon γ,

secreted by lymphoid aggregates in the *stratum basalis*, reduces the expression of decidualization markers, counterbalancing the effects of cAMP-dependent signals elicited by progesterone and paracrine cues (Christian 2001).

Together, these data suggest a tight connection between the different signaling cascades controlling decidualization, likely ensuring robustness to the decidualization program and minimizing the impact of stochastic fluctuations of hormone levels.

2.3 Decidualized EnSCs reshape the endometrial environment

In their proliferative state, EnSCs substantially represent the stromal compartment of the endometrium. They actively proliferate, and secrete ECM proteins, actively contributing to the post-menstrual repair of the endometrial tissue (Gellersen 2014, Shi 2020). This is a clear difference between EnSC and most other secretory cell types, as in this case the progenitor of the terminally differentiated secretory cell already has a well-defined physiological function and specialized secretory capacity.

With decidualization, the phenotype of EnSCs, as well as their role in the endometrial tissue, change dramatically. With this differentiation program, indeed, EnSCs become specialized *protein factories*, that with their secretory cargoes completely reshape the local environment and direct the activity of all the other residing cell populations (Gellersen 2014, Okada 2018).

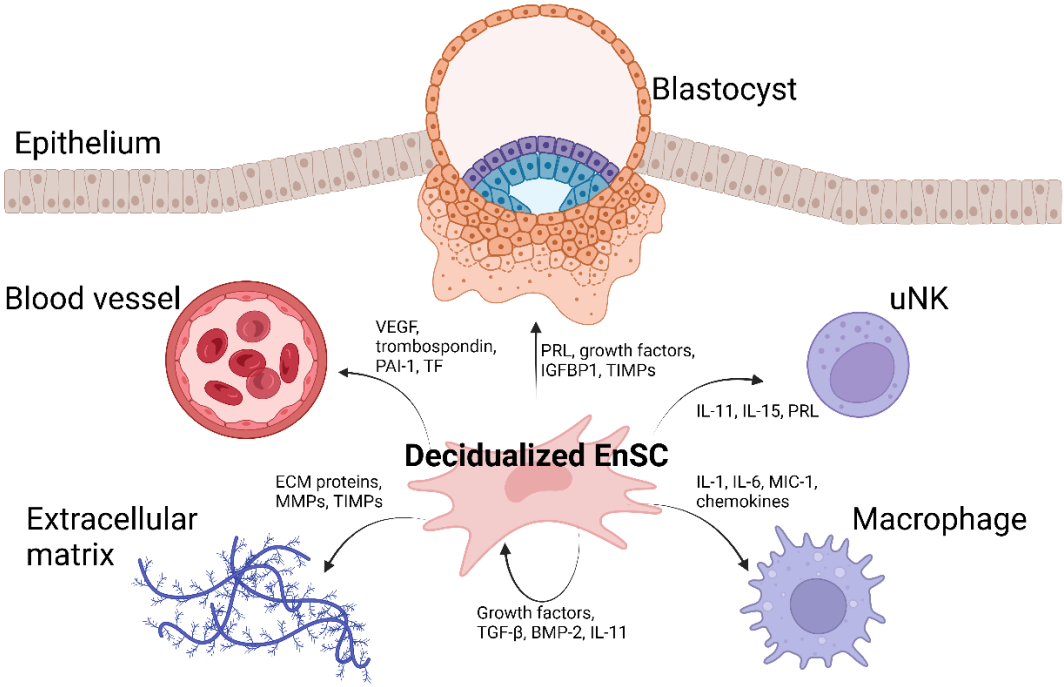


Figure 1. Decidualized EnSCs reshape the endometrial environment.
Schematic representation of the crosstalk between decidualized endometrial stromal cells and the other components of the endometrium, including the trophoblast in early invasion phase. Different proteins secreted by EnSCs and their respective targets are indicated (Gellersen 2014, Okada 2018). Created in BioRender, publication agreement number LT26A0SA27.

2.3.1 The decidualization markers: prolactin and IGFBP-1

Upon decidualization, endometrial stromal cells express, among several other cargoes, high levels of Prolactin (PRL) and Insulin-like Growth Factor Binding Protein 1 (IGFBP-1) (Dunn 2003, Gellersen 2014, Okada 2018). Both these proteins are easily detectable in the amniotic fluid and in the decidualized endometrial tissue (Ben-Jonathan 1996, Rutanen 1985). Due to their early identification as decidua-specific proteins, and their abundant expression in decidualized EnSCs, PRL and IGFBP-1 are considered conventional markers of decidualization , both *in vitro, ex vivo* and *in vivo* experiments (Gellersen 2014).

In the endometrial context, PRL is expected to act as a paracrine signal acting on epithelial cells, uNKs, blood vessels and, in case of implantation, on the trophoblast (Gellersen 2014). Several functions have been proposed for PRL in decidualized endometrium, alone or in synergy with progesterone: among them, promotion of trophoblast invasion (Stefanoska

2013, Sharma 2016), immune regulation (Jabbour 2001), stimulation and /or control of angiogenesis (Corbacho 2002), and induction of glandular-epithelial cell differentiation (Jabbour 2001).

IGFBP-1, as indicated by its name, binds the Insulin-like Growth Factors (IGF-1 and IGF-2), preventing the binding with their receptor (Lee 1993) and thus reducing their availability in the tissue (Carter 2004). Apart from its canonical function, IGFBP-1 was also reported to directly promote trophoblast invasion, through direct signaling mechanisms (Gleeson 2001).

In the endometrium, IGFBP-1 is cleaved by matrix metalloproteases (in particular, by MMP-3 and MMP-9), secreted by both decidualized EnSCs and by the trophoblast (Coppock 2004). However, decidualized EnSCs also secrete inhibitors of the same proteases (TIMP-1, TIMP-2, α2-macroglobulin), thus protecting IGFBP-1 from degradation (Coppock 2004).

This system likely ensures a precise spatiotemporal control of IGFBP-1, through a precise coordination of its secretion, degradation and protection (Gellersen 2014). In this way, IGF-1 and IGF-2 signaling can be precisely modulated in the endometrium, and possibly connected with the matrix remodeling processes.

2.3.2 Extracellular matrix deposition and remodeling

One of the most evident aspects of endometrial decidualization is the formation of a thick layer of extracellular matrix in the *stratum functionalis*. This matrix has the fundamental function of providing the optimal environment to accommodate the embryo after implantation, but also to limit the invasion of the trophoblast to the superficial layers, therefore avoiding potentially catastrophic damages to the underlying vasculature (Sharma 2016). This ECM layer is deposed by decidualized EnSCs: indeed, these cells secrete large amounts of collagen type I, IV and VIII (Carbone 2006, Shi 2020), fibronectin, laminin, decorin, and heparan-sulfate proteoglycans (Schatz 2016, Gellersen 2014, Okada 2014).

Decidualized EnSCs are also actively involved in the remodeling of the ECM, as they secrete matrix metalloproteases (MMPs), but also tissue inhibitors of metalloproteases (TIMP), likely to prevent an excessive trophoblast invasion (Sharma 2016).

2.3.3 Regulation of angiogenesis and blood vessel maturation

As previously described, the endometrial vascular system is extensively remodeled during the secretory phase, with the formation of the spiral arteries that extend in the functional layer of the endometrium (Gellersen 2014, Brosens 2019).

This process is of capital importance for the establishment of a successful pregnancy: defects in the formation of the endometrial blood vessels, or in the maturation of their endothelium, inevitably lead to pregnancy failure or to serious complications (Brosens 2019, Ng 2020).

Decidualized EnSC play a crucial role in the development of the endometrial vasculature. As a part of their secretory cargoes, indeed, these cells produce and secrete proangiogenic and vasoactive molecules, including the growth factor VEGF (Shifren 1996) and FGF (Albrecht 2010, Okada 2018), angiopoietins, relaxin (Palejwala 2002, Albrecht 2010). Other proteins with antiangiogenic function, such as trombospondin, are also secreted to counterbalance the pro-angiogenic cues (Albrecht 2010). Moreover, upon decidualization, EnSCs also express tissue factor (TF), one of the main activators of the coagulation cascade, and plasminogen activator inhibitor 1 (PAI-1), a key inhibitor of fibrinolysis (Dunn 2003). Taken together these results highlight the crucial role of decidualized EnSCs in the induction of early endometrial angiogenesis, in the local regulation of hemodynamics, and in the control of coagulation upon vascular damage. All these aspects are of capital importance in case of successful implantation of the embryo, to support the developing placenta with an adequate blood flow, but also to prevent excessive bleeding when the trophoblast erodes the endometrial vasculature.

In later phases of embryo implantation and invasion, the endometrial vasculature undergoes a further, extensive remodeling, resulting in the establishment of the placental circulation: the diameter of the vessels increases, resulting in a decrease in the blood flow velocity, and the endothelium undergoes a maturation process, allowing more efficient exchanges between fetal and maternal circulation (Brosens 2019). These processes, essential

for the embryo development and for a complication-free pregnancy progression, are mostly regulated by uNKs and resident macrophages (Gaynor 2017, Brosens 2019).

Since decidualized EnSCs are directly responsible for the recruitment, the proliferation and the correct differentiation of both these cell types, they likely contribute also to the regulation of these later vascular remodeling events, although mostly through an indirect mechanism (Vinketova 2016).

2.3.4 Regulation of immune cell populations

As previously described, peculiar immune cell types reside in the endometrial tissue, and mediate fundamental functions such as the immune tolerance towards the fetus (Santoni 2008), and the correct development of placental vasculature (Brosens 2019). Both uNKs and tissue resident macrophages actively participate to the decidualization of the endometrial tissue: they proliferate extensively, and secrete signaling molecules that sustain EnSC decidualization, vascular remodeling and embryo implantation (Dunn 2003, Hanna 2006, Vinketova 2016). As immune cells of the endometrium do not express the progesterone receptor (Henderson 2003), however, other cell types must necessarily direct their response to the hormonal changes.

Also in this context, decidualized EnSCs represent the master regulators of the endometrial environment. Upon decidualization, EnSCs secrete a wide array of different cytokines and chemokines, which induce the resident immune populations to acquire peculiar tolerogenic phenotypes (Petracco 2012, Vinketova 2016).

Decidualized cells also express several cytokines, including IL-1, IL-6, IL-8, IL-11, IL-15, and LIF, and several chemokines (Dunn 2003, Petracco 2012, Viketova 2016).

Among them, IL-15 appears to be particularly crucial for the endometrial dynamics: this cytokine, expressed (Okada 2000) and secreteed (Okada 2004) upon decidualization, is indeed the main inducer of uNK proliferation and differentiation (Hanna 2006).

The precise role of other cytokines in the endometrial context is not always completely clear: for example, highly inflammatory cytokines (IL-1, IL-6) are secreted in a generally tolerogenic immune environment, and apparently interfere with the decidualization program

(Simon 1995); at the same time, they appear to be fundamental for the successful implantation (Simon 1994). Other cytokines, such as IL-11, appear to have a mostly autocrine role, as they are secreted by EnSCs themselves, and are required for both *in vitro* and *in vivo* decidualization (Dimitriadis 2002).

Decidualized EnSCs, probably to promote tolerance towards the embryo, also secrete Macrophage Inhibitory Cytokine 1 (MIC-1), a cytokine impairing macrophage and dendritic cell maturation: MIC-1, indeed, interferes with the differentiation of antigen presenting cells (Segerer 2012).

2.4 Pathological implications of defective decidualization

Due to the multifunctional role of decidualized EnSCs in the endometrium, defects in their differentiation program can have serious effects on women's health and successful pregnancy establishment.

Embryo implantation has been reported to represent the most critical step in the establishment of pregnancy (Norwitz 2001), also due to the narrow window of endometrial receptivity (Ng, 2020). The existence of this tight *implantation window*, although apparently detrimental, allows a precise coordination between the development of the embryo and the dynamics of the endometrium (Norwitz 2001, Salker 2010, Ng 2020), and at the same time provides a strict negative selection against embryos with severe developmental defects (Salker 2010). Accordingly, delayed implantation does not impair early embryo development, but frequently results in a negative pregnancy outcome (Wilcox 1999).

Taking these points into consideration, correct EnSC decidualization appear to be critical for the implantation outcome: cells with a defective differentiation fail to provide a receptive environment for the embryo, thus leading to reduced fertility and early pregnancy loss (Salker 2010, Lucas 2020).

A delay in decidualization, in turn, can abnormally extend the implantation window, leading to a *paradoxical superfertility*: the lack of a strict temporal selection of the embryo results in a higher number of implantation events, which however also corresponds to a high rate of early miscarriage (Salker 2010). Physiologically, the narrow implantation window has

indeed been proposed as a barrier mechanism against the implantation of embryos with severe chromosomal anomalies, often corresponding to delays in the early phases of development; an extension of endometrial receptivity removes this important checkpoint, thus allowing also pregnancies with limited probability of success and high risk of complications (Salker 2010).

On the same line, the temporal mismatch between the embryo transfer and the physiological *implantation window* appears to be a critical aspect for the low success rate of FIV-ET procedures (Ng 2020), estimated around 25-35% per treatment (Smith 2015). Even though a direct comparison with the clinical setting is not possible, it is important to note that in animals in which decidualization is directly induced by embryo implantation, such as mice, the same procedure has a success rate close of 90-95% (Vasudevan 2010).

Alterations of endometrial stromal cell decidualization have been implicated in the pathogenesis of other clinical conditions. Impaired EnSC decidualization and defective expression of annexin A2 in EnSCs have been described in pre-eclampsia (Garrido-Gomez 2020), a severe pregnancy complication characterized by defects in the placental vasculature and severe maternal hypertension (Gellersen 2014, Chaiworapongsa 2014).

Resistance to decidualization has also been described in endometriosis, a pathology characterized by hyper-proliferation of EnSCs in both the endometrium and ectopic regions (Klemmt 2006, Gellersen 2014). In this context, the incomplete differentiation state probably promotes the survival and the invasiveness of EnSCs (Klemmt 2006).

3 Becoming a *protein factory*: the secretory pathway organelles

3.1 Secretory pathway organelles: a brief overview

In eukaryotic cells, the vast majority of the proteins exposed on the plasma membrane or secreted in the extracellular environment is synthetized in the lumen of the secretory pathway organelles. This complex system of membranes and vesicles has the fundamental function of creating a series of isolated compartments, characterized by specific chemical properties and well-defined sets of proteins and enzymes. Secretory proteins can therefore be synthetized

and processed through a series of incompatible chemical reactions, acquiring their native structure and the correct post-translational modifications.

While all the cells synthetize proteins destined to the extracellular environment, some cell types specialize in the secretion of protein cargoes, turning themselves into *protein factories.* Endometrial stromal cells represent a clear example of this: upon decidualization, they devote completely to the production of secretory cargoes, through which they mediate their physiological functions.

3.1.1 The endoplasmic reticulum

The endoplasmic reticulum (ER) represents the largest organelle of the secretory pathway. It is formed by a complex system of tubules and *cisternae* (that is, large, flattened vesicles), in continuity with the outer membrane of the nuclear envelope (Baumann 2001, Lynes 2011, Westrate 2015).

The organelle is conventionally divided in *rough* and *smooth* ER, based on the presence of ribosomes on its membrane, with the former involved in protein synthesis, and the latter mediating all the other functions (Alberts 2015). This sharp, dichotomic division of the ER, however, is becoming more and more outdated: the organelle appears to be instead formed by several specialized subdomains, each of which contains all the proteins required for a specific function (Lynes 2011, Sasaki 2019).

For secretory cell types, the synthesis, folding and quality control of protein cargoes clearly represent the most important functions of the endoplasmic reticulum.

Secretory proteins, as well as membrane proteins and resident proteins of the secretory pathway, are synthesized by the ribosomes localized on the rough ER membrane, and co-translationally imported in the organelle lumen by the translocon system (Deshaies 1991, Johnson 1999).

Inside the ER, proteins acquire their native conformation, in a process driven by weak interactions among the amino acid side chains. The final conformation of the protein is entirely determined by the sequence of its amino acids, based on the minimization of the free

energy of interaction, and could in principle be reached also *in vitro*, in the absence of any other element (Anfinsen 1973, Ellgaard 2016, Nelson 2017).

In the ER, protein folding is facilitated by a wide array of chaperone proteins. Chaperones interact transiently with the unfolded proteins, preventing the aggregation of exposed hydrophobic patches and de-stabilizing aberrant conformations (Gidalevitz 2013, Saibil 2013). Moreover, chaperones also contribute to the translocation of polypeptides (Bar-Lavan 2016), the formation of protein complexes (Adams 2021), and the sensing of ER stress (Hetz and Papa 2018). Considering the fundamental roles of chaperones, it is not surprising that chaperones are among the most abundant proteins in human cells, accounting for 10% of the total protein mass (Finka 2013).

The endoplasmic reticulum contains several different types of chaperones, often associated in large, transient complexes. Some of them, such as BiP, have a broad cargo specificity and are involved in the folding of most of the proteins (Pobre 2019): just to provide an example, a random polypeptide would in average contain a BiP-binding site every 36 amino acids (Blond-Elguindi 1993). Due to its abundance, its wide specificity, and its fundamental roles in protein folding, BiP is indeed considered the master regulator of ER functions (Pobre 2015).

Other chaperones have a small number of selected substrates (such as GRP94, involved in the folding of some growth factors and membrane receptors) or are even substrate-specific (such as Hsp47, specific for procollagen): their abundance, therefore, depends on the specific cell type, and on the nature of its secretory cargoes (Nagata 2003, Graner 2015).

Additional modifications contribute to the achievement and stabilization of the correct conformation of a protein. The co-translational addition of an oligosaccharide contributes to the primary folding of the polypeptides and has a fundamental role in the quality control mediated by calnexin and calreticulin (Danilczyk 2000, Aebi 2013, Ellgaard 2016).

Another important aspect is the formation of disulfide bonds between couples of cysteines, a process mediated by dedicated oxidoreductases. The formation of these covalent bonds significantly stabilizes the tridimensional structure of a folded polypeptide, as well as the

interaction among different subunits. In this way, the correct structure of proteins is better maintained in the harsh extracellular environment (Betz 1993, Braakman 2011).

In this process PDI, a protein with both chaperone and enzymatic function, plays a pivotal role: according to the oxidation status of its exposed cysteines (2 CXXC motifs in the thioredoxin-like domains of the protein), it mediates disulfide bond formation, reduction or isomerization through the formation of mixed disulfides and their subsequent resolution.

The endoplasmic reticulum also contains several PDI-like enzymes, such as ERp72, ERp57 (the oxidoreductase associated with calnexin and calreticulin), ERp46, ERp18 and P5, with very similar functions but acting on different substrates or in different phases of the folding (Ellgaard 2005, Jessop 2009, Araki 2013).

The formation of disulfide bonds consumes the available pool of oxidized PDI; this problem is solved by a specific mechanism based on the oxidation or reduction of Ero1, a

FAD-dependent enzyme: with a mechanism very similar to the one described before, Ero1 oxidizes the cysteines of PDI (and of the related enzymes) reducing a disulfide bond in its own active site (Araki 2013, Soares 2013). After that, Ero1 transfers the electrons acquired from PDI to molecular oxygen, oxidizing again its cysteines and producing hydrogen peroxide (Tu 2004, Araki 2013).

The glutathione peroxidases GPX7 and GPX8, as well as the thiol-containing enzyme PRX4 mediate the scavenging of H2O2, highly reactive and therefore potentially dangerous for the cell. PRX4, moreover, contains couples of cysteines that are oxidized in the process; in this way, with another disulfide bridge exchange reaction, it brings back oxidizing equivalents to PDI, making the whole process more efficient (Jessop 2009, Araki 2013).

Synthesis and modification of proteins, although important, represents only one of the many functions of the endoplasmic reticulum. The organelle, indeed, represents the main storage site for calcium, a fundamental second messenger in several signaling pathways; it is involved in synthesis and maturation of several lipids, such as phospholipids, steroidal hormones and GPI-anchors; it contains fundamental enzymes, involved in detoxification of xenobiotics and dangerous endogenous molecules.

Interestingly, the ER is also involved in a plethora of complex interactions with all the other intracellular organelles, including mitochondria, Golgi complex, endosomes, lysosomes, peroxisomes, and lipid droplets (Valm 2017). While the different components are for simplicity often considered as separate units, indeed, they should rather be considered a highly interconnected functional network (Phillips and Voeltz 2016, Valm 2017). These contacts, stabilized by tethering specific tethering molecules, allow for instance non-vesicular shuttling of sterols between the membrane of the ER and ones of *trans*-Golgi and endosomes (Phillips and Voeltz 2016), but also the direct transport of amino acids from lysosomes to the ER (Choi 2023).

The contacts between ER and mitochondria are by far the most characterized form a functional point of view. These interactions mediate a fundamental crosstalk between the two organelles, including the transport of calcium from the ER to the mitochondrial matrix, the transport of sterols, and the synthesis of phospholipids, mediated by enzymes localized in both organelles (Phillips and Voeltz 2016, Sasaki 2019).

Moreover, the contacts between ER and mitochondria also have a crucial role in the control of mitochondrial network dynamics, as they define the position of both mitochondrial fusion and fission events (Sasaki 2019).

3.1.2 Golgi complex

The Golgi complex is the second main organelle of the secretory pathway. This organelle is formed by a stack of 5-7 *cisternae,* organized in a directional way (Farquhar 1985, Li 2019). This organization is maintained by structural proteins called *golgins*, that tether the *cisternae* and anchor them to the microtubule cytoskeleton (Barr 2001, Gosavi 2017).

Differently from most organelles, the Golgi complex is characterized by marked asymmetry and a precise directionality: vesicles arrive from the endoplasmic reticulum to one side of the organelle (the *cis* Golgi), while vesicles containing processed cargoes leave from the opposite side (the *trans* Golgi) (Rothman 1996, Pelham 2000). The borders of the Golgi apparatus are quite faded: upstream, a network of large, interconnected vesicles called ERGIC (ER-Golgi Intermediate Compartment) receives cargoes from the endoplasmic

reticulum and sorts them to the *cis* Golgi network (the receiving side of the organelle) or back to the ER (Appenzeller-Herzog 2006); downstream, the last *cisterna* becomes a sort of hub, called Trans Golgi Network, that directs proteins to the extracellular environment, the lysosomes or to the stable pool of secretory vesicles (Gu 2001, Di Martino 2019).

Despite the extensive vesicular transport across the Golgi complex, that according to some models even includes the progression and maturation of the *cisternae* themselves (Glick 2011), the identity of the *cis, medial*, and *trans* compartments of the organelle remains stable, with a well-defined localization of structural proteins and enzymes (Pulvirenti 2008, Glick 2011). Similarly, a precise gradient of pH, zinc and copper is maintained across the organelle, probably through a precise localization of the Golgi proton pump (GPHR) and of the different ion transporters (Paroutis 2004, van Baelen 2004, Maeda 2008, Amagai 2023).

Inside the organelle, more than 250 different glycosidases and glycosyltransferases add new sugars to the proteins and modify the simple oligosaccharides added in the ER (Stanley 2011). The sugars can also be modified by different enzymes, such as sulfurylases and epimerases, further increasing the complexity of the modifications (Cooper 2000, Stanley 2011, Conway 2011). For some proteins, such as proteoglycans and other ECM proteins, the glycosylations are particularly extensive, and can account for several times the molecular weight of the unmodified polypeptide (Stanley 2011). Specific modifications of the terminal sugars are also added to some proteins, defining their final subcellular localization: the presence of a mannose phosphorylated in position 6, for instance, directs enzymes and other proteins to the lysosomal compartment (Coutinho 2012).

Different mechanisms, such as recognition of consensus signals on the polypeptide, accessibility of the sugar moieties and precise localization of the enzymes across the *cisternae* are thought to contribute to the specificity of Golgi glycosylation, but the precise mechanisms are not completely understood to the state of the art (Stanley 2011, Sasaki 2019).

The second, fundamental function of the Golgi complex is to act as a sorting hub for the whole secretory pathway: all the proteins transported to the Golgi complex are indeed directed by this organelle to the correct compartment, may that be the extracellular space, the lysosomes, specialized vesicular pools or the Golgi itself (Gu 2001, Glick 2011, Sasaki

2019). This is particularly critical in highly polarized cells, in which the vesicles directed to the cell membrane must be directed either to the lateral or the basolateral domain (Glick 2011, Ford 2021). Different mechanisms have been proposed to explain the precise sorting of proteins into different vesicular pools: specific features of cargo proteins are thought to be recognized by dedicated receptors, that either include or exclude the cargo from the vesicle (Di Martino 2019). To the state of the art, however, only a limited number of sorting signals and receptors have been clearly identified (Gu 2001, Gary-Bobo 2007, Ford 2021).

3.1.3 Homeostasis of the secretory pathway

In their physiological functions, secretory cell types must produce, transport, modify and secrete large amounts of protein cargoes. The efficiency of the secretory process entirely depends on the capacity of the secretory pathway organelles to maintain their identity, and to respond to perturbations, including sudden variations of the cargo workload.

In the ER, the accumulation of misfolded protein cargoes induces a homeostatic response, defined Unfolded Protein Response (UPR), with an intensity proportional to the severity and duration of the stress (reviewed in Walter and Ron 2011, Hetz and Papa 2018).

The UPR depends on the activation of three main sensors: ATF6 (Haze 1999), IRE1α (Cox 1999) and PERK (Mori 1993). The activation mechanism and the downstream effectors of each UPR sensor are different, but all of them converge to a restoration of organelle homeostasis, by modulating the synthesis of new proteins, and increasing the folding and degradation capacity of the ER (DuRose 2006, Walter and Ron 2011).

The three branches of the UPR are often activated in the differentiation program of several secretory cell types, independently from the accumulation of misfolded proteins (Hetz 2012, So 2018). This mechanism is fundamental to increase the capacity of the endoplasmic reticulum to efficiently accommodate and fold large amounts of secretory protein cargoes (Pincus 2010), and to prevent an overloading of the organelle, by dampening an excessive production of proteins (Gao 2012).

Important roles of UPR sensors and signaling cascades have been described in the differentiation of several secretory cell types, including plasma cells (Iwakoshi 2003, Hetz 2012, So 2018) and pancreatic β cells (Gao 2012).

Interestingly, this is not the case of other secretory cells, such as thyrocyte differentiation (Christis 2010) and EnSC decidualization (Anelli 2021): indeed, no overt activation of the UPR branches is observed in the differentiation of these cell types.

Tight control mechanisms also maintain the identity and content of the different secretory organelles: this is particularly true for the Golgi complex, that continuously receives a massive flow of vesicles from the much larger endoplasmic reticulum. Dedicated mechanisms prevent ER proteins from reaching the Golgi, and retrieve them if they escape the retention mechanisms (Ma W. 2017). The bulk of the ER chaperones and the enzymes, together with the newly synthetized proteins, is thought to form a huge, supramolecular assembly, the so-called *ER matrix* (Ma W. 2017); these mechanism likely prevents the massive leakage of ER-resident proteins, although specific exclusion mechanisms have also been proposed (Ma W. 2017).

When ER-resident proteins are transported to downstream compartments, they are promptly retrieved, either by direct assembly of COPI on a double lysine motif (for transmembrane proteins), or by the interaction with the KDEL-receptors (KDELR), which in turn induce vesicle formation (Capitani 2009, Gao 2014). The KDELRs, as the name suggests, recognize the consensus motif KDEL on the C-terminus of proteins (Capitani 2009); for soluble ER enzymes not bearing a KDEL, and for unassembled intermediates of multimeric proteins, the interaction with the KDELR depends on a mediator, the protein ERp44 (Anelli 2003, Sannino 2014, Anelli 2018). A similar sorting process is thought to mediate the cis-trans organization of Golgi proteins, but the precise mechanisms are unknown to the state of the art (Di Martino 2019).

A complex signaling network is thought to exist at the interface between the ER and the Golgi complex, to regulate and coordinate the bi-directional flow of proteins and vesicles (Farhan 2011, Centonze 2019). Proteins with a signaling function have been identified in the secretory organelles, and signaling events correlated with protein trafficking have been

described: examples of this are the kinase LTK, localized at the ER-exit sites, or the signaling cascades associated with the activity of the KDELRs (Farhan 2011, Centonze 2019, Cancino 2014, Pulvirenti 2008). However, a general understanding of these signaling mechanisms, and their precise role in the homeostasis of the secretory pathway, are to the state of the art largely unknown.

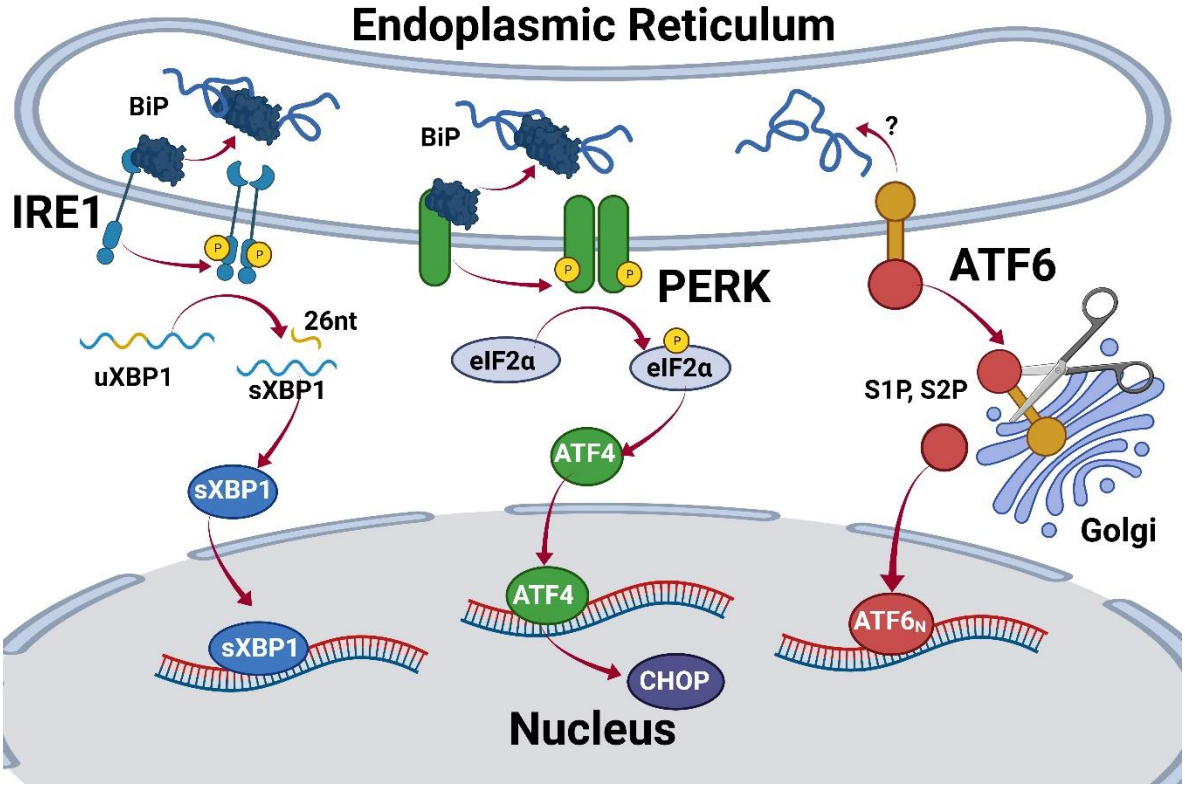


Figure 2. Homeostasis of the secretory pathway: Unfolded Protein Response of the ER. Schematic representation of the three branches of the canonical UPR of the ER, with their activation mechanism and their downstream effectors. Created in BioRender, publication agreement number LH26A0VT06

AIMS OF THE WORK

Despite the great physiological importance of endometrial stromal cells, several aspects of their decidualization program are still poorly understood.

In this project, I aimed to characterize the different steps required to convert a fibroblast-like cell into a specialized *protein factory* with a unique phenotype.

Taking advantage of an *in vitro* model of decidualization, I investigated the morphological and functional reshaping of the organelles during the differentiation program; to the best of my knowledge, this was the first detailed characterization of EnSC decidualization from a cell biology point of view.

More in detail, I tried to answer to the following questions:

-How are the secretory pathway organelles reorganized in decidualization?

-Which are the transcriptional mechanisms controlling their dynamics?

-How does decidualization impact the mitochondrial network and the cellular metabolism?

-Are other aspects, such as organellar content of metal ions, also affected in the differentiation program?

During the three years of my PhD, I assessed these questions by several different experimental approaches, combining high-resolution microscopy, RNA analyses and biochemical assays.

The results I obtained, although preliminary in some of their parts, provide new, interesting insights on endometrial stromal cell decidualization, characterizing aspects of the differentiation program which were never investigated before.

RESULTS

1 Characterization of the secretory organelles in decidualization

Decidualization of endometrial stromal cells represents an amazing example of inducible secretory differentiation. In response to simple environmental cues, namely the levels of estrogens and progesterone, EnSCs completely reshape their phenotype, terminally differentiating into specialized *protein factories*. In a matter of a few days, all the EnSCs of the *stratum functionalis* radically change their role in the tissue: they stop proliferating, dramatically change their morphology, and direct most of the events occurring in the tissue through the protein cargoes they secrete (Krikun 2004, Gellersen 2014).

Considering the sudden increase in protein synthesis and secretion experienced by EnSC during decidualization, achieving and maintaining high efficiency in the secretory pathway organelles must clearly be a paramount aspect of this differentiation program. However, this aspect has never been extensively investigated.

In the following sections, I characterized the reshaping of the secretory pathway organelles during endometrial stromal cell decidualization, in terms of morphological rearrangements, functional reorganization and transcriptional changes.

1.1 Validation of T-HESC as an EnSC decidualization model

To investigate the different aspects of the decidualization process, I employed the cell line T-HESC as an experimental model. This line, derived from primary human endometrial stromal cells immortalized with telomerase, has previously been validated as a reliable model of EnSC decidualization (Krikun 2004).

Based on the previous literature, I selected an *in vitro* decidualization protocol based on 1µM MPA (medroxyprogesterone acetate) and 0.5 mM cAMP (8-bromoadenosine 3′, 5′ cyclic monophosphate) (Brosens 1999, Gellersen 2014). MPA is a progesterone analogue, routinely used in clinical practice for contraception and for the correction of hormonal imbalance (Sathe 2023); its presence in the medium mimics the hormonal changes between the proliferative and the secretory phase of the menstrual cycle. The 8-bromoadenosine cyclic monophosphate is a cell permeant analogue of cAMP. In physiological decidualization,

activators of adenylate cyclase (such as prostaglandin E2) and inhibitors of phosphodiesterases (such as relaxin) represent key inducers of decidualization (Palejwala 2002, Dunn 2003). During *in vitro* decidualization, exogenous cAMP provides a priming for the progesterone signaling, that normally would be provided by signaling molecules increasing the intracellular cAMP levels.

As confirmed also by previous results obtained in the lab, cAMP alone can induce an early response of some genes, but not proper decidualization. Conversely, progesterone is able to induce decidualization, but the process is slower and the gene induction is limited, compared to the complete stimulation.

To verify that T-HESC decidualization can effectively be achieved in the experimental setting, I analyzed different hallmarks of decidualization at different days after treatment with cAMP and progesterone.

Decidualization reshaped T-HESC morphology: as clearly visible in both hematoxylin/eosin staining and by immunofluorescence for cytoskeleton proteins, cells switched from a fibroblast-like appearance to an epithelioid morphology (Figure 3).

As shown in Figure 3, proliferative T-HESC are elongated cells, generally spindle-shaped and sometimes with several long protrusions. After decidualization, instead, the cells become larger, and acquire a polygonal shape; the “empty space” surrounding the nucleus, representing both the cytoplasm and the organelles, enlarges significantly, and is more intensely stained by eosin, a nonspecific protein dye (Figure 3).

The morphological changes observed reflect the ones observed in histological sections (Gellersen 2014), and recapitulate what was previously described for the *in vitro* decidualization protocol chosen (Brosens 1999). These observations were also in line with previous experiments performed in the lab, in which this *in vitro* decidualization protocol induced analogue morphological changes in primary human and murine EnSC.

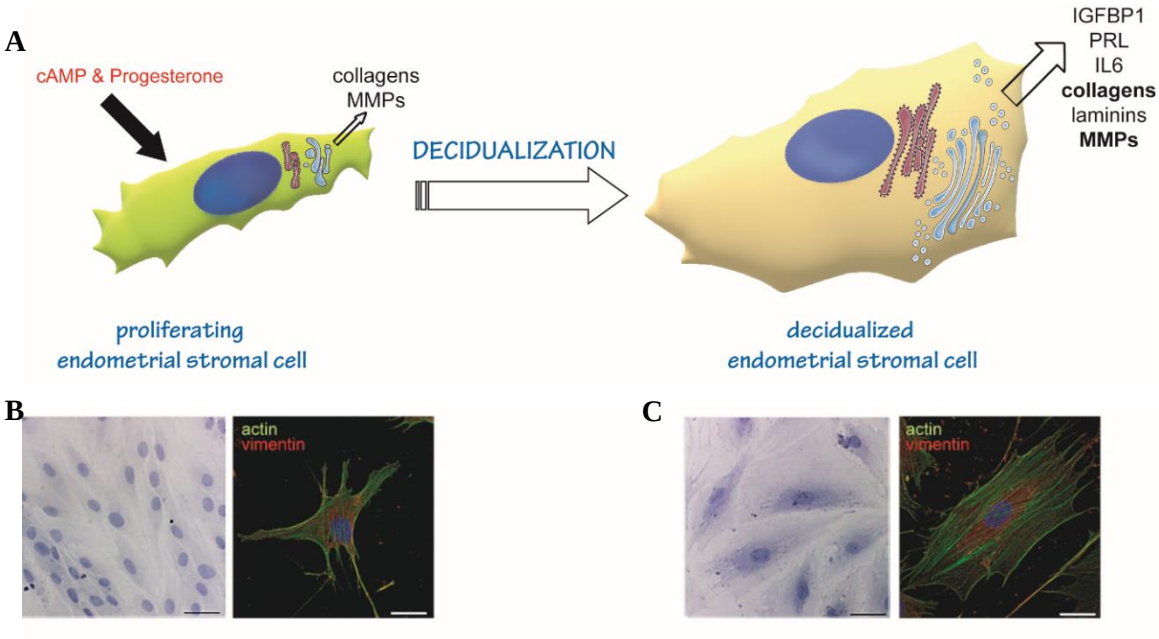


Figure 3. Visualization of endometrial stromal cell decidualization.
A. Graphical representation of EnSC decidualization. B. Microscopy of proliferative T-HESC. Left panel: Hematoxylin and eosin staining, bright field microscopy; acquired with a 20x magnification, bar: 60 µm. Right panel: Fluorescence microscopy of the cytoskeleton (phalloidin-FITC; anti-vimentin immunofluorescence); acquired with a 60x magnification, bar: 20 µm. C. Microscopy of decidualized T-HESC (6 days of *in vitro* decidualization). Organized as panel B.

To further validate the model, I evaluated by semi-quantitative real-time PCR (qPCR) the expression, during the differentiation protocol, of conventional decidualization markers (Dunn 2003, Gellersen 2014 Okada 2018). The expression of prolactin (PRL), insulin growth factor binding protein-1 (IGFBP-1) and Tissue Factors (TF) was already strongly enhanced at day 3 of the differentiation program, and was further increased at day 5, corresponding to complete decidualization (Figure 4).

Transcriptional induction of these genes was also verified by qPCR in parallel with all the following experiments, to confirm the successful decidualization of the analyzed cells.

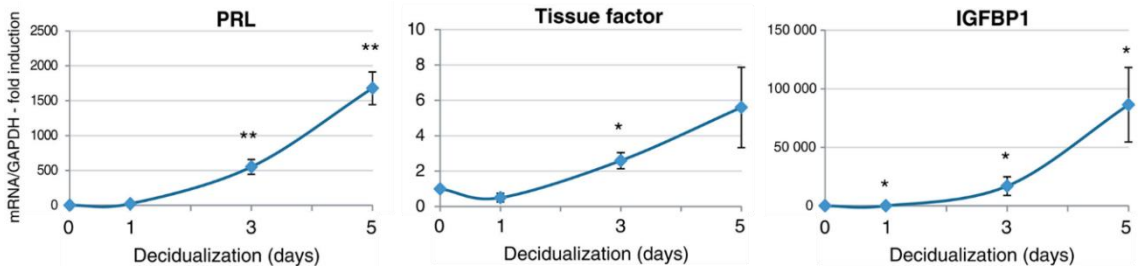


Figure 4. Decidualization markers are transcriptionally induced during T-HESC *in vitro* decidualization.

Real-time qPCR analysis of the indicated genes. Results corresponding to three independent replicates, normalized on GAPDH mRNA and represented as mean ± SEM. *: $p \leq 0.05$; ** $p \leq 0.01$, t-test of each time-point versus d0.

To ensure that *in vitro* T-HESC decidualization corresponds as closely as possible to the physiological process, besides the changes in gene expression, the secretion of PRL and interleukin-6 (IL-6) was tested by ELISA assay. These proteins are among the paracrine signals secreted by EnSC during physiological decidualization (Dunn 2003, Okada 2018). Prolactin, in particular, is considered a primary hallmark of the decidualization process (Gellersen 2014), and mediates fundamental functions in the endometrium, includingpromotion of trophoblast invasion (Stefanoska 2013, Sharma 2016), immune regulation (Jabbour 2001), stimulation and /or control of angiogenesis (Corbacho 2002), and induction of glandular-epithelial cell differentiation (Jabbour 2001).

The role of IL-6 in decidualization is more complex, and not completely understood. This cytokine is clearly upregulated at a transcriptional level in decidualization (Deb 1999), and is present in the healthy decidual tissue (Pietro 2020), where it is thought to contribute to regulate trophoblast implantation and local secretion of metalloproteases (Bischof 2001); at the same time, excessive amounts of IL-6 in the placenta, e.g. as a consequence of a viral infection, may be detrimental for embryo development (Deb 1999, Dudley 1992).

Nonetheless, abundant secretion of IL-6 is consistently observed in *ex vivo* cultures of decidualized cells (Deb 1999). Therefore, the increasing secretion of PRL and IL-6 in the medium along the *in vitro* decidualization of T-HESC was perfectly in line with what could have been observed for physiological decidualization, and further confirmed the validity of the experimental system (Figure 5).

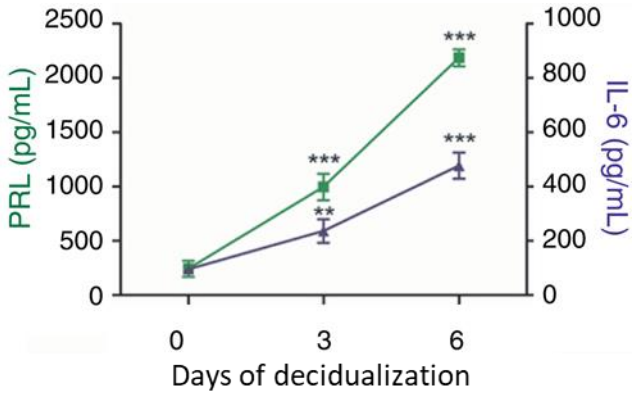


Figure 5. Decidualized T-HESC secrete prolactin and interleukin 6.
ELISA assay for PRL and IL-6. The calculated concentrations of the two proteins in the conditioned medium are represented by color code, and reported at the sides of the graph. Results correspond to four independent replicates, represented as mean ±SEM. **: $p \leq 0.01$; ***: $p \leq 0.001$, t-test of each time-point versus d0.

1.2 Secretory organelle enlargement: microscopy and morphometry

As a first step of the characterization, I analyzed the secretory pathway organelles of T-HESC by immunofluorescence (IF) and transmission electron microscopy (TEM), both in control conditions and upon decidualization.

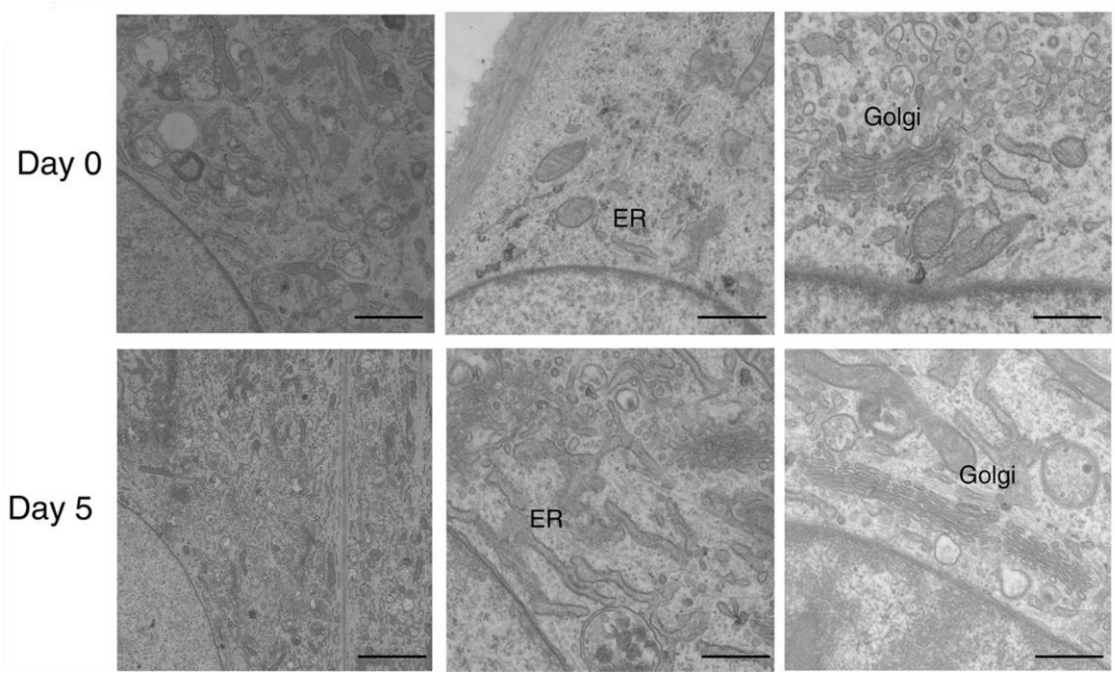


Figure 6. Secretory pathway organelles enlarge in decidualization.

Transmission electron microscopy of T-HESC before and after decidualization. The images show a general overview of the cellular ultrastructure (left) and the morphological changes of ER (middle) and Golgi complex (left). Representative images of four independent experiments. Scale bar: 1 μm (left panels) or 0.5 μm (middle and right panels).

The electron microscopy analysis revealed interesting changes in the organization of the secretory pathway organelles (Figure 6). In decidualized cells, I could observe a significant expansion of the rough ER (easily identified by the presence of ribosomes), and of the structure corresponding to the smooth ER (which appear as clusters of single-membrane tubules and vesicles): both the components appeared far more developed in decidualized cells, with larger cisternae and a larger and more complex tubular system.

An apparent enlargement was observed also for the Golgi complex. The two-dimension nature of electron microscopy didn't allow a complete evaluation of the organelle structure. However, an increased number of Golgi structures was consistently observed in decidualized cells, which often also contained particularly elongated Golgi stacks.

In general terms, the intracellular environment of decidualized cells appeared particularly "crowded", completely occupied by ER and Golgi structures, but also vesicles of various size, mitochondria and autophagosomes.

Together, these results suggested that, with decidualization, endometrial stromal cells increase the size and activity of their secretory pathway organelles, with a massive increment of the intracellular vesicular transport.

To better characterize the changes of the secretory pathway organelles in decidualization, different proteins were chosen for the immunostaining, as representative markers of different compartments of the secretory pathway organelles (Figures 7-10).

Calreticulin (CRT) and Protein Disulfide Isomerase (PDI) were used for the imaging of the protein-folding compartment of the ER, based on their pivotal role in primary quality control and oxidative folding (Gidalevitz 2013).

Reticulon 4 (RTN4) was used as additional ER marker, to visualize also other components of the organelle: this protein stabilizes the curvatures of the ER membrane (Rämö 2016, Wang 2016), and is therefore enriched at the ER tubules and on the edge of ER sheets (Voeltz

2006, Rämö 2016). Immunofluorescence for RTN4, therefore, allows visualization of the tubular structures corresponding to the smooth ER (Shibata 2006).

Endoplasmic Reticulum resident protein 44 (ERp44) and ER-Golgi Intermediate Compartment 53 kDa protein (ERGIC53) were used for the imaging of the ER-Golgi Intermediate compartment, where these proteins are localized, and act as a functional couple in protein cargo transport and retrieval (Tempio 2021).

Giantin and Golgi Matrix protein 130 (GM130) were used for the staining of the cis/medial Golgi compartment; and Golgin 97 and Trans-Golgi Network protein 46 (TGN46), for the trans-Golgi and the trans-Golgi network, based on their localization in the organelle (Munro 2011).

All the compartments analyzed displayed profound and extensive morphological changes. In general terms, all the organelles expanded during decidualization, something not completely unexpected, considering the increased secretory activity of decidualized EnSCs.

The protein-folding compartment of the ER progressively enlarged, as the cells progressed through the differentiation program (Figures 7-10). The Golgi complex also became significantly bigger, and completely reorganized its structure: the small, compact organelle observed in proliferative cell became indeed a large structure with a net-like morphology, occupying a large region of the perinuclear area (Figures 7-8).

Sharp morphological differences were observed between the ER markers associated to protein folding and other components of the same organelle, possibly corresponding to a well-defined “regionalization” of different functions.

The former, indeed, appeared to be concentrated in the perinuclear area of the cells, both in control conditions and after decidualization: when compared to a staining for the cell membrane, such as the one for the class I Human Leukocyte Antigen (HLA), performed before cell permeabilization, the signals of PDI and CRT left a wide “empty” area in the cell periphery (Figure 7).

Conversely, the RTN4 staining (roughly corresponding to the smooth ER) labeled an extended network of tubules, reaching the very periphery of the cell. An important enlargement was observed also for this component of the ER, possibly corresponding to an

increased biosynthesis of the lipids needed for the observed enlargement of the endomembrane system (Figure 9).

A particularly striking reorganization was observed for the ERGIC, as shown in Figures 8-9. The compartment, indeed, did not only massively enlarge upon decidualization, but seemed to also change its general organization. Indeed, the vesicles corresponding to this compartment became significantly more, and extended on a larger area of the cell.

These modifications likely correspond to a massive increase of the bi-directional vesicular trafficking connecting the ERGIC with upstream and downstream compartments: the ERGIC, indeed, represents both a fundamental intermediate station in the ER-to-Golgi transport of secretory cargoes (Appenzeller-Herzog 2006), and the main site of distal quality control, allowing retrieval of incomplete polymeric proteins (Anelli 2008).

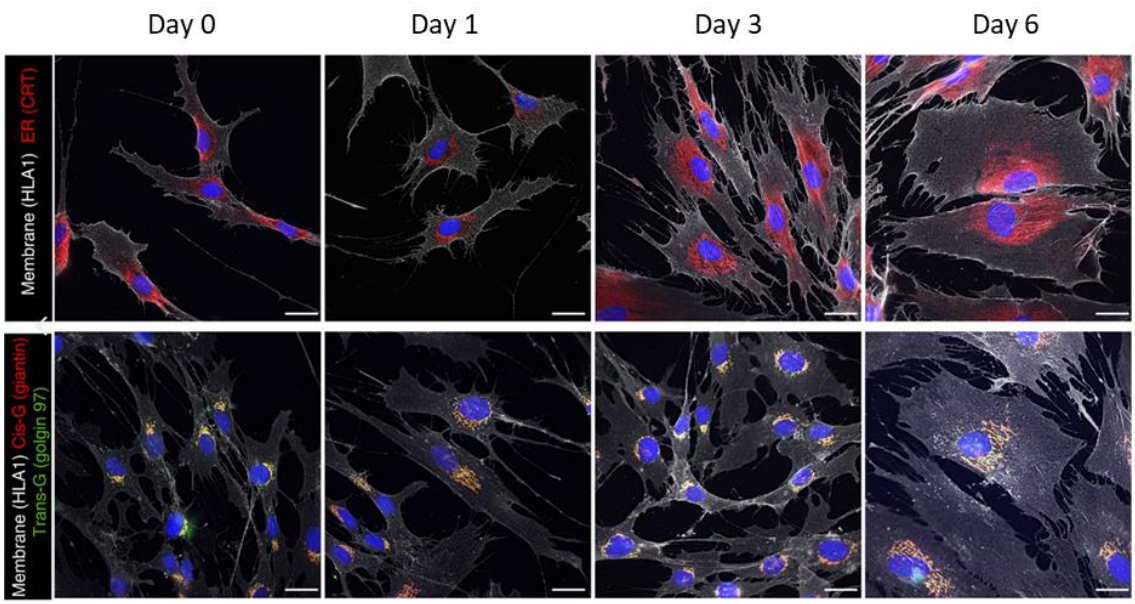


Figure 7. Decidualization reshapes morphology and distribution of secretory pathway organelles.

Combined immunofluorescence of secretory pathway organelle and plasma membrane markers during in vitro decidualization. Upper panel: calreticulin (ER, red) and HLA1 (plasma membrane, grey). Lower panel: giantin (*cis*-Golgi, red), golgin-97 (*trans*-Golgi, green) and HLA1 (plasma membrane, grey). Nuclei are counter-stained with DAPI (blue). 60x magnification, bar: 15 µm.

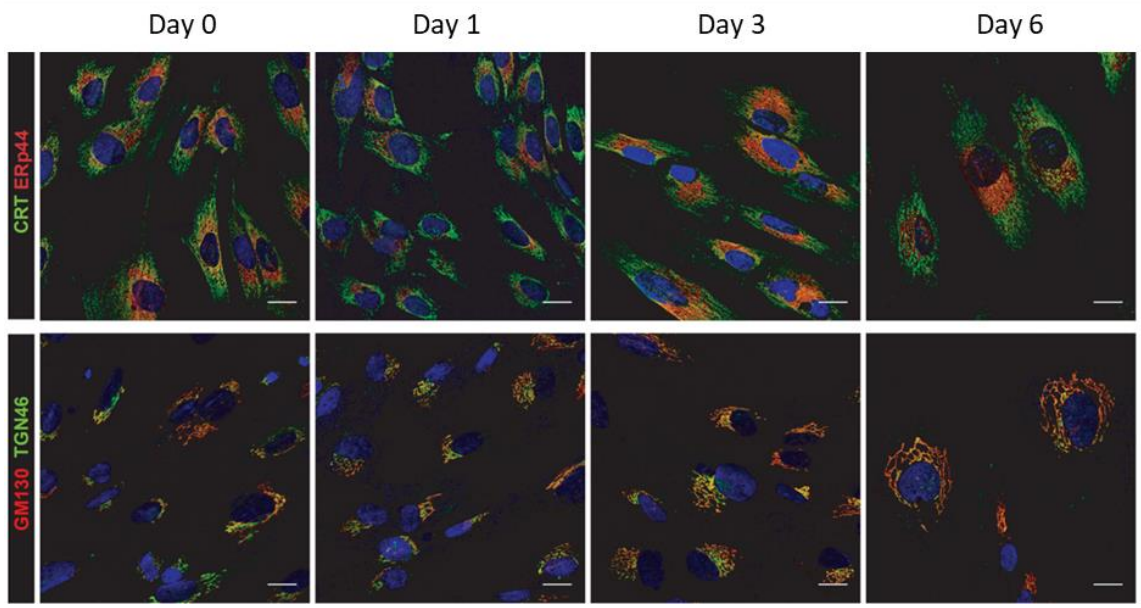


Figure 8. ER and Golgi enlarge during decidualization.

Combined immunofluorescence of secretory pathway organelle markers during *in vitro* decidualization. Upper panel: calreticulin (ER, green), and ERp44 (ERGIC, red). Lower panel: gm130 (*cis*-Golgi) and TGN46 (*trans*-Golgi). Nuclei are counter-stained with DAPI (blue). 60x magnification, bar: 15 µm.

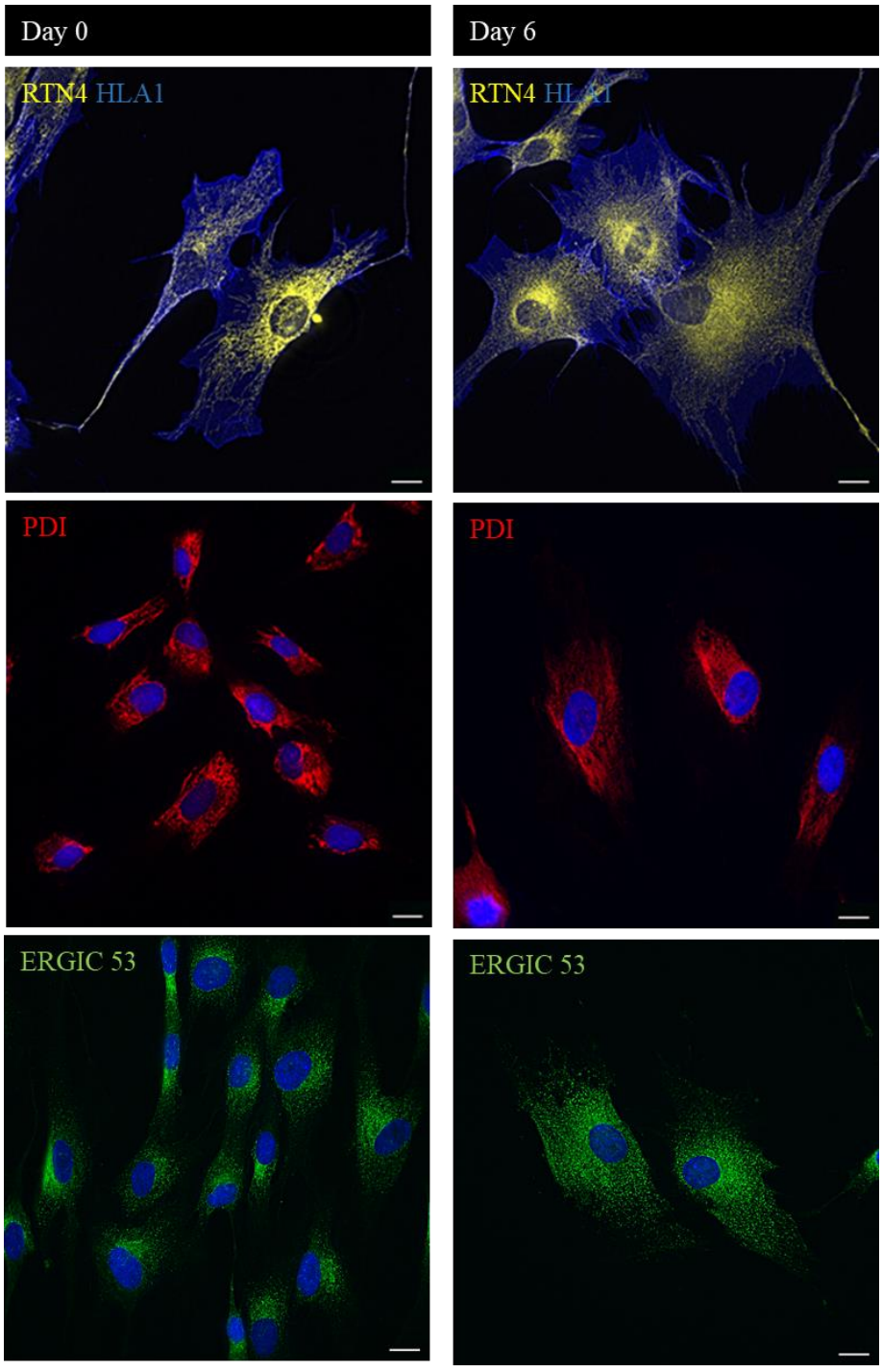


Figure 9. ER and ERGIC enlarge and reorganize during decidualization.
Immunofluorescence of secretory pathway organelle markers during *in vitro* decidualization. Comparison between proliferative (Day 0) and decidualized (Day 6) cells. Upper panel: reticulon 4 (rough and smooth ER, yellow) and HLA1 (plasma membrane). Middle paned: PDI (rough ER, red). Lower panel: ERGIC-53 (ERGIC, green). In middle and lower panels nuclei are counter-stained with DAPI (blue). 60x magnification, bar: 15 µm.

As decidualization entails a general reorganization of the cellular morphology, including a significant enlargement of the overall cell volume, a morphometric analysis was performed to better describe and quantify the changes of the secretory pathway organelles.

In the analysis, I quantified the volume corresponding to the organelle of interest, and the total volume of the cell (based on the membrane HLA staining). Coherently with the previous observations, both the total cell volume and the volume of rough ER (CRT), cis-Golgi (giantin) and trans-Golgi (golgin 97) were increased of several times from control conditions to the decidualized state (Figure 10). Due to the peculiar morphology of the ERGIC, formed by a Golgi-localized region, and an extremely extended vesicular pool, the same analysis could not be performed for this compartment.

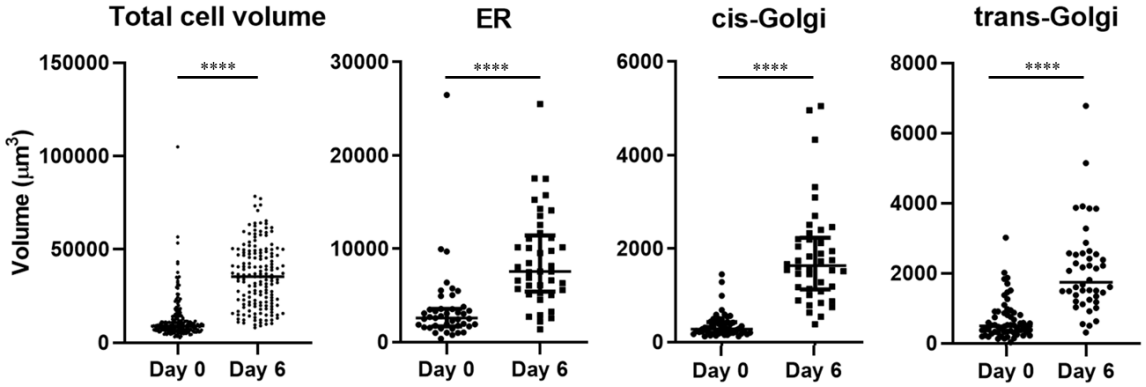


Figure 10. Volume of the secretory pathway organelles increases during decidualization. Immunofluorescence-based morphometric analysis of total cell volume and secretory pathway organelles. Quantification based on plasma membrane (HLA1), ER (calreticulin), *cis*-Golgi (giantin) and *trans*-Golgi (golgin 97) markers, in two independent experiments. The plots show the median ± SEM and the individual values. ****: $p \leq 0.0001$, t-test.

When the organelles were expressed in relation with the total volume of the corresponding cell, clear differences could be observed among the different compartments during decidualization: while the *cis*-Golgi volume increased also in relative terms, the ER volume remained substantially proportional to the total cell volume, possibly with a slight decrease (Figure 11). These results were rather surprising, and quite unexpected: a massive expansion of the endoplasmic reticulum is observed in most secretory cell types, while a significant enlargement of the Golgi complex is observed only in some cases.

No significant difference was observed in the relative volume of the *trans*-Golgi compartment, a surprising observation considering the close proximity and the functional coupling with the *cis* component of the organelle (Figure 11). It is possible to speculate that this observation may indeed have a functional meaning: the *cis* and *medial* components of the organelle, where the glycosylation enzymes are localized, may actually be particularly enlarged, to allow an efficient processing of the cargo proteins; a more limited expansion of the *trans*-Golgi, might instead be sufficient, as increased vesicular transport would be more critical than an enlargement of the compartment.

However, it is not possible to exclude that this result may be due to technical aspects of the analysis: the *trans*-Golgi network displays a variety of morphologies, often including a complex vesicular system. As the microscopy system and the analysis pipeline are not optimized for the detection of very small objects, which may therefore be excluded from the quantification. Significant changes in the expression or distribution of the protein markers could also impact the quantification, modifying the apparent size of the compartments.

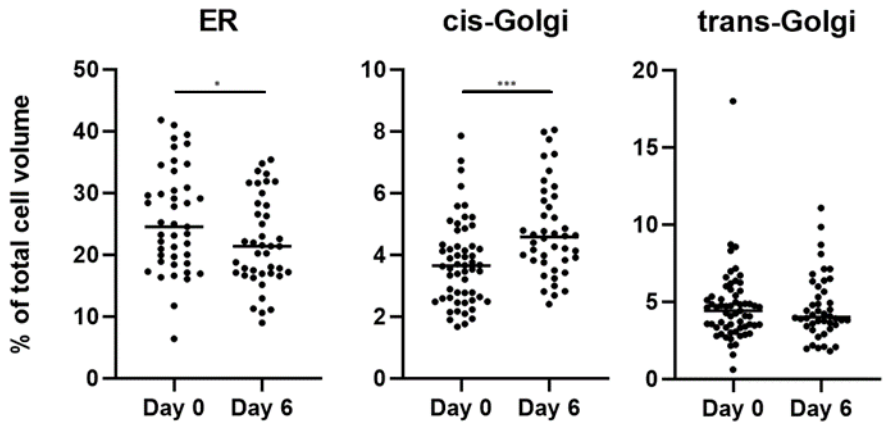


Figure 11. Relative proportions of secretory pathway organelles change in decidualization. Immunofluorescence-based morphometric analysis of secretory pathway organelles. Quantification expressed as relative cell occupancy, based on the calculated volume of each marker and the total volume of the corresponding cell. The plots represent median and individual values. *: $p \leq 0.05$; ***: $p \leq 0.01$

Although a significant expansion of the secretory organelles is observed, this is not as massive as it could have been expected for a secretory differentiation program, especially if relative volumes are considered. This is clearly different from what can be observed for other

secretory cell types, such as plasma cells, in which the ER enlarges dramatically and occupies most of the cell volume (Shaeffer 2004, van Anken 2003).

The peculiarities of the organelle enlargement observed in T-HESC decidualization, with a limited expansion of the ER and a prioritization of the Golgi, likely reflect the specific nature of the protein cargoes and the dynamics of secretion. For complex cargoes such as highly glycosylated ECM proteins, for instance, assembly and glycosylation probably represent the limiting step for the synthesis, thus explaining the expansion of the Golgi.

1.3 Characterization of chaperone and enzyme induction

The expansion of the secretory pathway organelles was further investigated through a detailed analysis of chaperones, enzymes and structural proteins representative of the different functions and compartments.

Transcriptional induction of the genes of interest was measured by qPCR at different days after the exposure to decidualization stimuli. In parallel, the amount of the corresponding proteins was analyzed by western blot at the corresponding time-points.

The results obtained (Figures 11-13) confirmed a general induction of the different components of the secretory pathway, coherently with the increased secretory activity of decidualized cells. In line with the organelle rearrangements observed in microscopy, however, significant differences in the extent of the upregulation were observed among proteins belonging to different compartments of the secretory pathway.

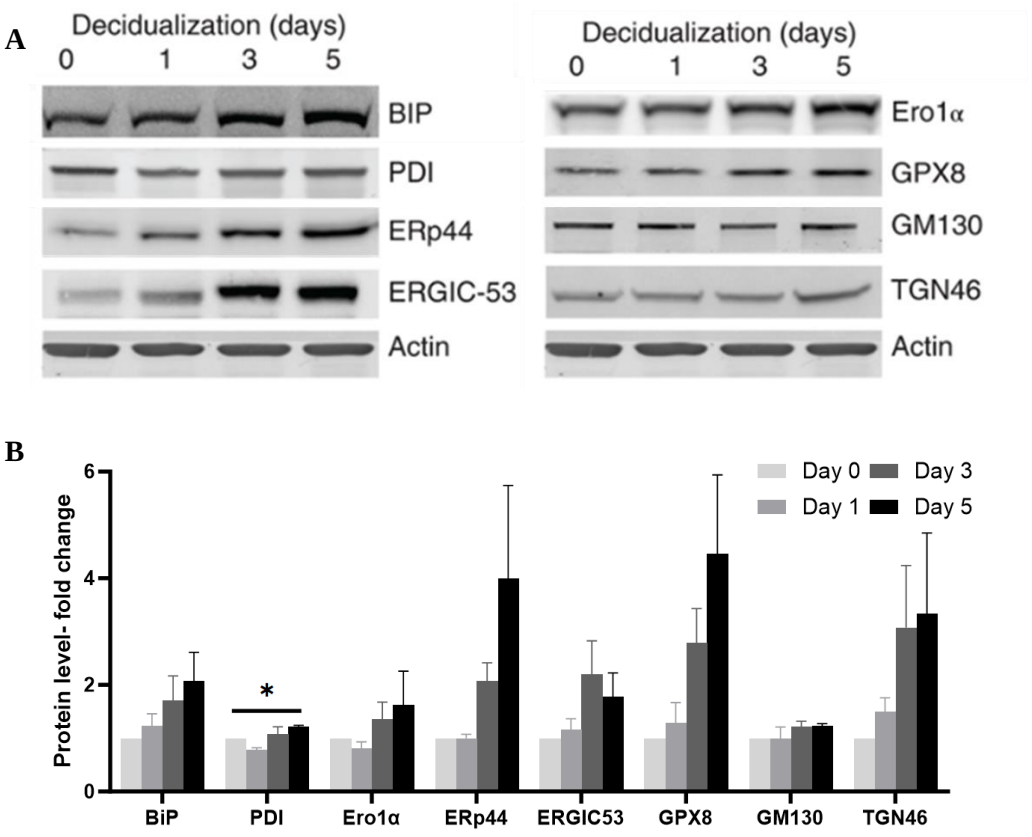


Figure 12. Decidualization induces re-adjustment of the organelle composition.

A. Western Blot assay of chaperones and enzymes of the early secretory pathway during *in vitro* T-HESC decidualization. Image representative of at least three independent experiments. B. Densitometric analysis of the Western Blot shown in A, normalized on the loading control (actin). Data are expressed as fold change of the basal value. The graphs show the mean of a minimum of three independent experiments, ±SEM. *: $p \leq 0.05$, one-way ANOVA of each time-point versus Day 0. The low statistical significance can be attributed to the small sample size and to the high variability observed for Day 3 and Day 5 measurements.

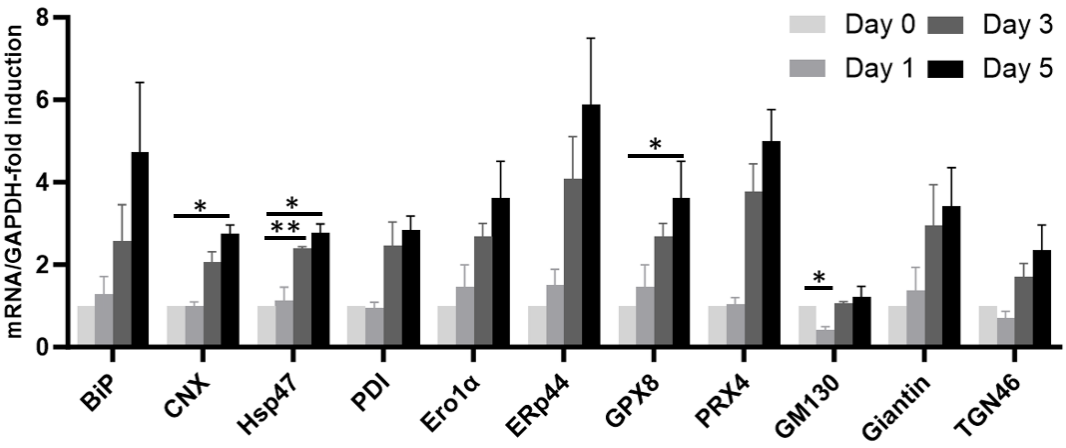


Figure 13. Genes encoding for secretory pathway chaperones and enzymes are induced during decidualization.

Real-time qPCR analysis of early secretory pathway genes during *in vitro* T-HESC decidualization. Results corresponding to three independent experiments, normalized on GAPDH mRNA and represented as mean ± SEM. *: $p \leq 0.05$; ** $p \leq 0.01$, one-way ANOVA of each time-point versus Day 0. The low statistical significance can be attributed to the small sample size and to the high variability observed for Day 3 and Day 5 measurements.

Interestingly, BiP (binding immunoglobulin protein) and PDI, which are known to be strongly upregulated during plasma cell differentiation (van Anken 2003), are only weakly induced; instead, the functional couple ERp44-ERGIC53 (Tempio 2021), as well as most redox enzymes and Golgi proteins, are strongly induced in the decidualization process.

These results, taken together, highlight a general upregulation of the secretory pathway organelles, but also show important differences among their different components. The different behavior observed for the different chaperones likely depends on a different induction pattern, but also on a different expression at basal state. Indeed, as all the observation are relative to cells in control conditions, proteins already highly expressed before decidualization appear as "not induced", regardless their absolute abundance.

The increase observed for ERp44 and ERGIC53, fundamental components of the ERGIC compartment, appears to be particularly interesting from the functional point of view. As shown in Figure 9, this compartment is dramatically expanded in the decidualization process,

with an enlargement of the corresponding immunostaining in the Golgi region, and the appearance of a large number of vesicles. The ERGIC represents a dynamic compartment, acting as an intermediate station between the ER and the Golgi (Appenzeller-Herzog 2006), where cargoes are specifically selected for downstream transport, and incomplete polymeric proteins are instead recognized and retrieved to the ER (Anelli 2008).

Considering the specific functions of the ERGIC, it is possible to speculate that its enlargement, and the upregulation of its components, may actually correspond to specific requirements of decidualized EnSC protein cargoes: for instance, the abundant production of complex, multimeric proteins (such as collagen) may specifically rely on the post-ER quality control, thus requiring an extensive development of this compartment.

The comparison of T-HESC decidualization with the *in vitro* differentiation of primary murine EnSCs revealed strong similarities, but also some interesting differences. Indeed, the comparison by western blot of proliferative and decidualized cells revealed a general enrichment of secretory pathway proteins, thus further confirming the validity of T-HESC as a decidualization model. Differently from what was observed for human cells, however, ER proteins such as BiP, PDI and Ero1α appear to be strongly up-regulated in the differentiation process (Figure 14).

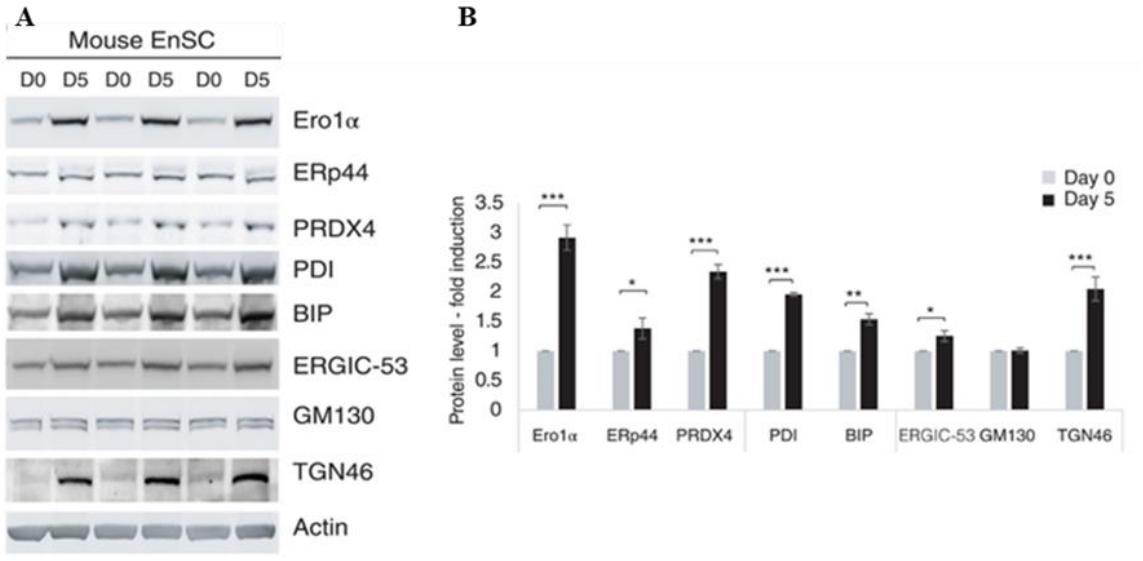


Figure 14. *In vitro* decidualization of primary murine EnSCs validates the secretory pathway reshaping observed in the T-HESC cell line.

A. Western of chaperones and enzymes of the early secretory pathway. Primary endometrial stromal cells derived from the same animal were analyzed in the proliferative state or after *in vitro* decidualization. Representative results based on samples derived from three animals. B. Densitometric analysis of the Western Blot shown in A, normalized on the loading control (actin). Data are expressed as fold change of the basal value. The graphs show the mean of a minimum of three independent experiments, ±SEM. *: $p \leq 0.05$, t-test; **: $p \leq 0.01$; ***: $p \leq 0.001$; t-test of each time-point versus d0.

While the precise biological meaning of the differences observed was not investigated in detail in the present study, it is possible to speculate that they depend on the different physiology of decidualization in the two species. In humans, proliferating EnSCs reconstitute the *stratum functionalis* of the endometrium during each menstrual cycle, a process requiring the secretion of collagen and other extracellular matrix proteins, even if in limited amount compared with the massive matrix deposition of decidualized cells (Carbone 2006, Gellersen 2014). In non-menstruating animals, such as mice, this tissue reconstitution process does not occur, and proliferative EnSCs only have a homeostatic role in the tissue.

These differences in the secretory capacity at the baseline can likely explain why all the components of the secretory pathway appear strongly induced in murine, but not in human EnSCs: the latter, indeed, are probably better prepared for the secretory activity, and this is reflected by more limited changes in the relative quantifications.

1.4 A broader view: time-course transcriptome analysis

The analysis of selected genes and proteins, together with the morphological analysis, suggests an extensive reorganization of the entire secretory pathway. Therefore, to extend the analysis also to other components of the secretory pathway, an unbiased transcriptome analysis of T-HESC decidualization was performed.

The bulk RNAs corresponding to control conditions (0h) and to various time-points after the addition of MPA and cAMP (6h, 18h, 24h, 36h, 48h, 72h and 144h) were analyzed: the intervals were selected to obtain a comprehensive view of both full decidualization and early events of the differentiation program.

As more extensively described in Materials and Methods, genes were considered *differentially expressed* based on changes of their expression compared to the basal conditions (log_2 fold change >0.5), and on the statistical significance of the differences observed (adjusted p-value <0.01).

Differential Expression Analysis (DEA), based on the comparison between each sample and the untreated cells, revealed that the decidualization process entails an extensive reshaping of the cell transcriptome, which begins immediately after the addition of the exposure to the decidualization stimuli (Figure 15). Indeed, almost one thousand genes are already up- or down-regulated at the first time-point (984 genes at 6h), a number that quickly rises to roughly five-thousand as decidualization proceeds (5136 at day 3, 4780 at day 6). The changes observed in the very first hours of the differentiation program, when no change in the cell phenotype has occurred yet, likely represent the primary response to the decidualization stimuli, or to the signaling cascades activated in response to them. The later events, and in particular the transcriptional changes observed between day 3 and day 6, likely correspond to later stages of the differentiation program, including adaptation to the massive production of cargo proteins.

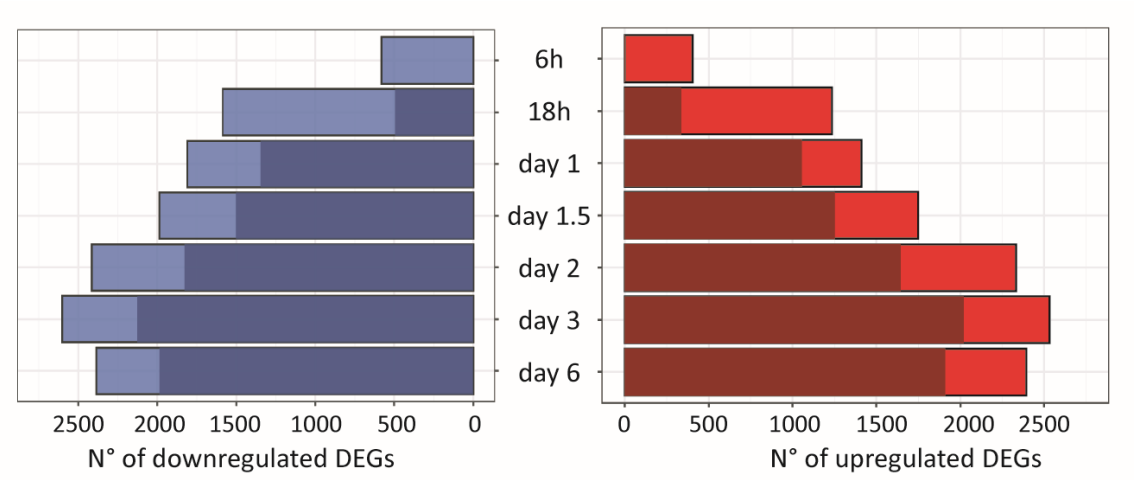


Figure 15. Decidualization entails an extensive transcriptional reshaping.
Graphical representation of differentially expressed genes (DEGs) at different time-points of the decidualization process, based on bulk RNA sequencing. DEGs are divided based on the expression pattern: downregulation (left side, blue) or upregulation (right side, red) genes. For each bar, the darker shade represents genes that were already differentially expressed at the previous time-point.

Differentially expressed genes (DEGs) were analyzed in terms of biological process mediated (BP), or cellular compartment (CC) of the encoded protein, based on over-representation analysis (ORA) of the Gene Ontology (GO) terms. This analysis revealed a strong enrichment, among the up-regulated genes, of all the terms corresponding to the endoplasmic reticulum, the Golgi complex, the vesicular compartment and the extracellular matrix. As expected, this corresponded to secretory pathway-related biological processes, such as glycosylation, vesicular trafficking, Golgi organization and extracellular matrix secretion (Figure 16).

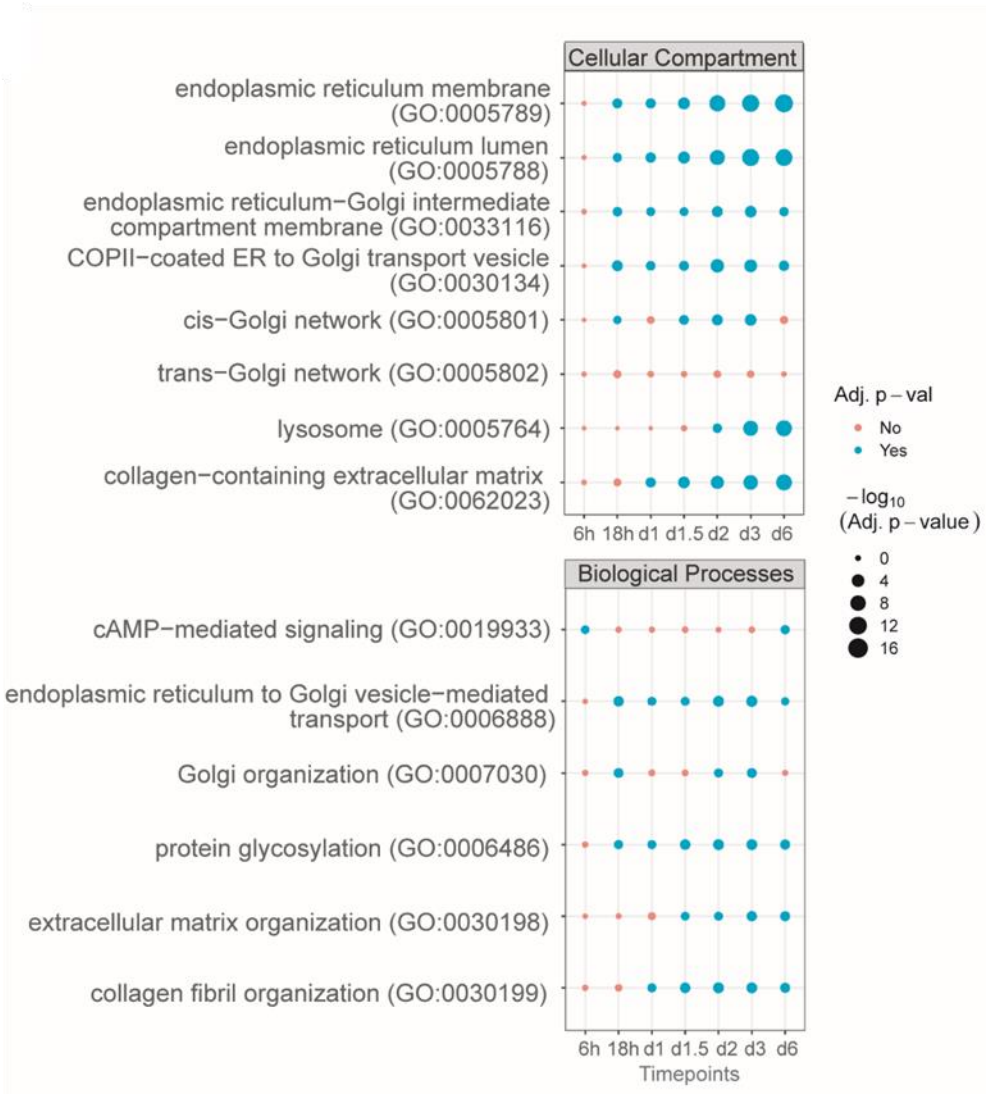


Figure 16. Transcriptional reshaping of the secretory organelles is an early event in decidualization.

Over-Representation Analysis for the genes upregulated at different time points. GO terms associated with secretory pathway organelles (Cellular Compartment) and associated functions (Biological Process) were analyzed in the time-course RNA sequencing. Statistical significance of the over-representation is graphically represented by the different size of the circles.

The analysis of individual genes during the different transcription time-points confirmed and extended the results obtained by qPCR analysis (Figure 17). The upregulation of genes encoding for ER redox enzymes and Golgi structural proteins was observed starting from the first time-points of decidualization. Something similar can be observed for genes involved in vesicle trafficking between the ER and the Golgi, and for lysosomal genes.

This coordinated induction of key components of the secretory pathway organelles, beginning in the very first phases of the decidualization program, can be considered as a *transcriptional preparation* of then secretory organelles, and likely represents an integral part of the decidualization program, and not an adaptation to the secretory activity.

Indeed, a strong induction of the decidualization markers (PRL, IGFBP1 and TF), that also represent secretory cargo proteins, was observed only later in the time-course analysis. As expected for cells undergoing a terminal differentiation program, genes involved in DNA replication and cell cycle progression are instead downregulated.

Interestingly, T-HESC decidualized *in vitro* faithfully reflect the cargo reshuffling observed during *in vivo* decidualization: collagen type VI, produced by proliferating EnSC, is largely replaced by collagen type I, IV and VIII in decidualized cells (Carbone 2006, Shi 2020), as mirrored by the transcriptome analysis. Similar changes are observed also for transcripts encoding for laminins and metalloproteases.

The precise temporal dynamics of expression of secretory pathway genes, the different dynamics of genes involved in different functions, and some regulatory mechanisms will be more extensively discussed in the following paragraphs.

However, the mismatch observed between the upregulation of secretory pathway genes and the expression of the secretory cargoes offers by itself some interesting insights about the decidualization program. As the upregulation of the folding, transport and secretion machineries anticipates the bulk production of cargo proteins, indeed, EnSCs don’t need to

adapt their organelles in response to an accumulation of the cargo, and can increase their secretory activity efficiently and without additional delays.

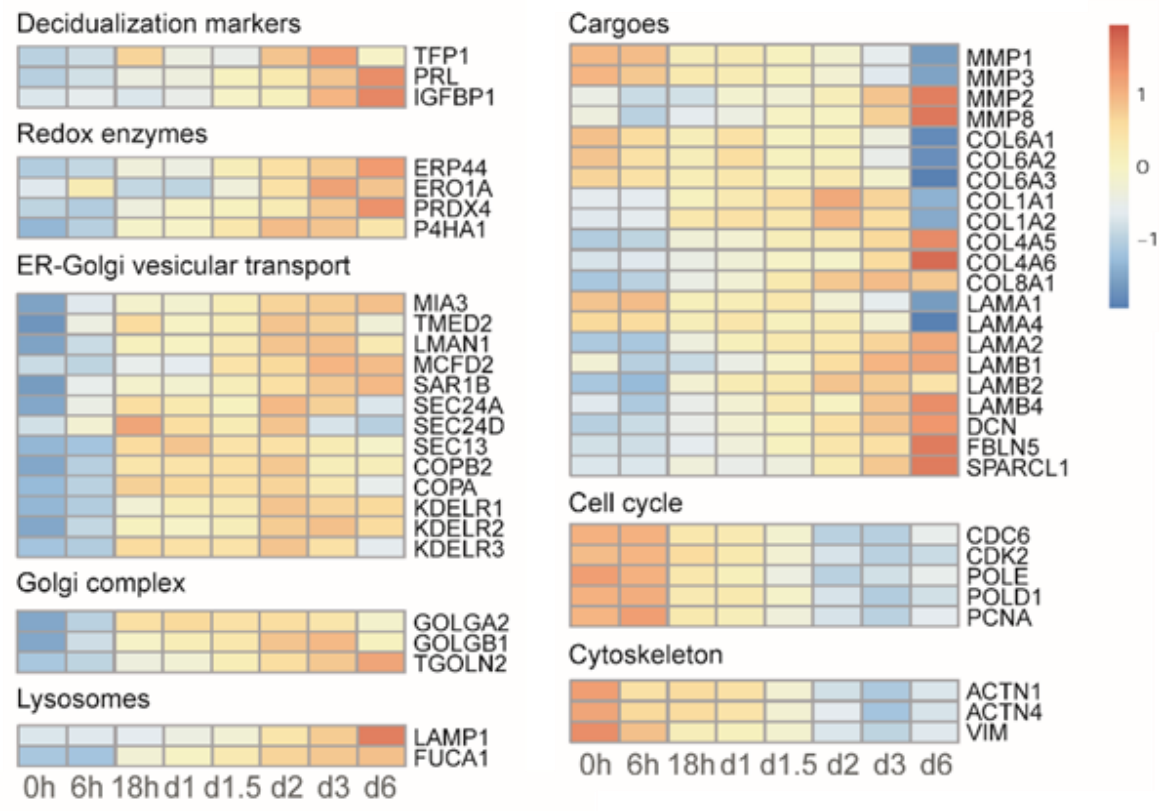


Figure 17. Transcriptional profile of decidualizing T-HESC reflects the physiological differentiation program.

Heatmap of genes differentially expressed during the decidualization program. Expression values were z-normalized and represented as a color scale. The genes were selected as representative for different secretory pathway functions and compartments, or based on their relevance for the decidualization program.

2 Regulation of the secretory organelles: CREB3L1 and CREB3L2

The transcriptome analysis of decidualizing cells revealed contemporary expression of genes encoding for different components of the secretory pathway, belonging to different organelles. As a result of this transcriptional program, secretory organelles significantly increase their size and their capacity, allowing a massive increase in the production and secretion of cargo proteins.

To ensure efficiency of the secretory process, several different functions must be upregulated in a precisely coordinated way, and with the correct timing: the upregulation of the protein folding machinery, for instance, must be coordinated with physical enlargement of the ER, increase in the Golgi processing capacity, improvement of the vesicular transport, and with the expression of the cargo proteins themselves. Defects or delays in the induction of any of those functions would indeed result in critical problems, such as intracellular cargo accumulation, proteotoxicity, or defective glycosylation processing (Aridor 2007, De Matteis 2011).

In the following section, I analyzed the co-regulation of secretory pathway genes during the decidualization process, identified defined clusters of gene expression, and investigated the regulation mechanism of early-induced secretory pathway genes.

2.1 Identification of co-regulated transcriptional clusters of secretory pathway genes

In order to identify pattern of co-expression, and possibly co-regulation, secretory pathway genes identified in the time-course RNA sequencing were further analyzed.

The genes identified as differentially expressed in the first 3 days of decidualization, and annotated for the GO terms corresponding to the secretory pathway organelles were selected, defining a subset of 626 DEGs. In this way, the analysis focused on the early events of decidualization, therefore considering the "proper" transcriptional program and not the adaptation to massive synthesis of cargo proteins. Moreover, given the shorter distance between the time-points considered, the temporal expression analysis was expected to be more reliable in this time-frame.

Partitional clustering divided the secretory pathway genes in five groups, based on their temporal expression pattern. Interestingly, three clusters showed different up-regulation trends, while the other two described down-regulation: this result highlights a transcriptional reshaping, rather than a general induction, of secretory pathway genes (Figure 18A).

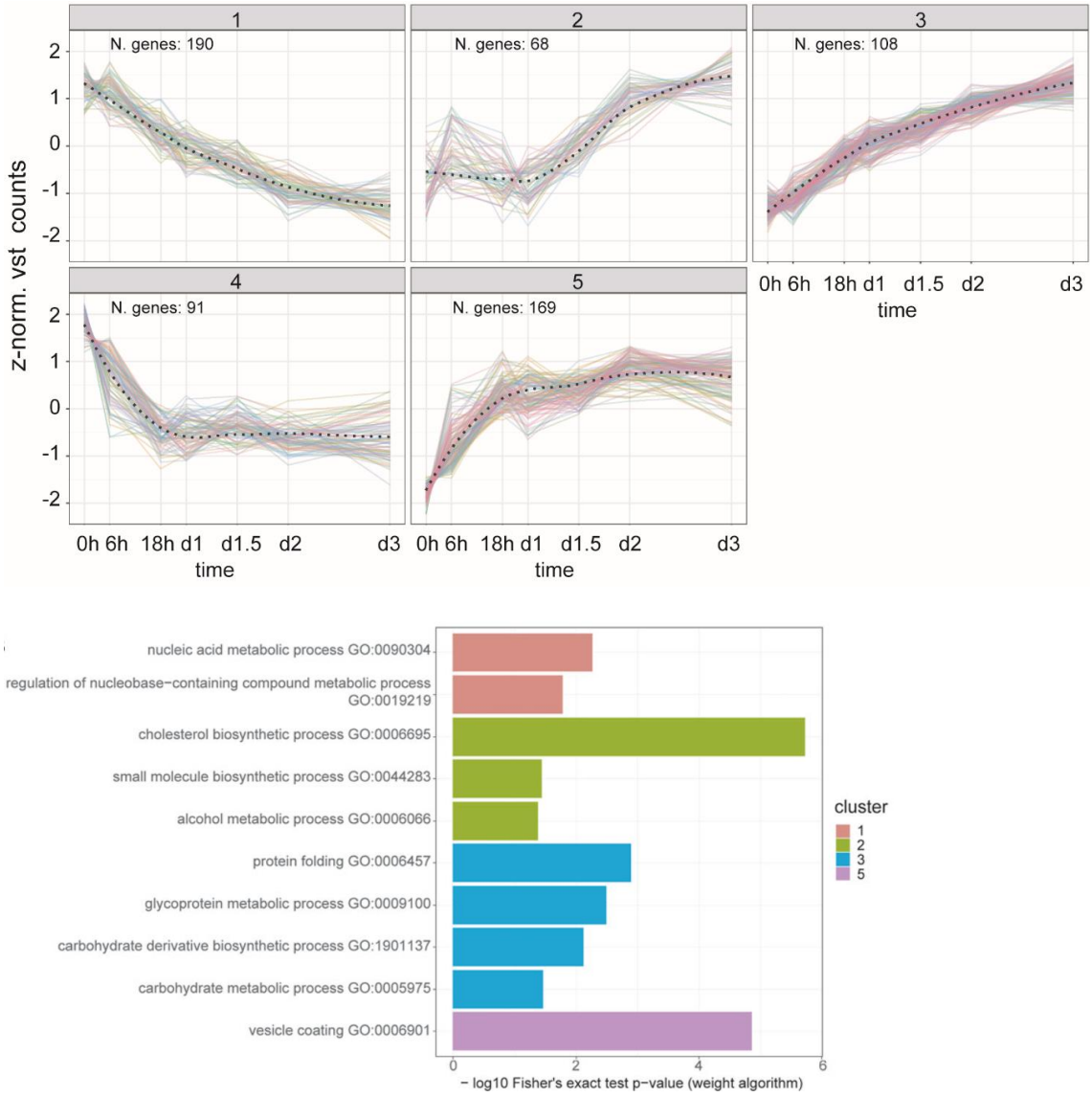


Figure 18. Time-series clustering dissects the transcriptional orchestration of secretory pathway reshaping.

A. Temporal expression trends for DEGs annotated to “Golgi Apparatus” and/or “Endoplasmic Reticulum” GO cellular component terms. Y-axis represents the z-normalized, averaged expression value transformed using DESEQ2 variance stabilized transformation. The overall trends for each cluster (dashed line) were estimated using a LOESS fit. B. Over-representation analysis for biological processes in the different clusters. Fisher’s exact test was carried out using the weight algorithm proposed in Alexa et al., 2006, implemented in TopGO. Cluster 4 did not show terms with a significant enrichment (i.e. p value < 0.05).

An analysis of the genes contained in each cluster, and of their biological functions, provided an interesting picture about the transcriptional dynamics of secretory pathway genes during the decidualization program.

The clusters were generated exclusively by similarities in the expression pattern of the different genes. However, each cluster showed a clear enrichment for genes involved in specific biological processes (Figure 18B), thus indicating that the temporal patterns observed could indeed correspond to the selective induction or repression of different functions during decidualization.

Cluster 1 is steadily repressed during decidualization. The genes contained in this cluster mostly encode for metabolic enzymes, some signaling proteins regulating organelle morphology, coherently with the change in the cellular secretome (thus requiring a new array of processing enzymes), and the extensive morphological reshaping of the secretory organelles. Moreover, this cluster includes several genes involved in DNA replication and repair, or in cell cycle: their products, variably localized in the nucleus, in the cytosol of at the Golgi complex, are probably no longer required upon proliferation arrest.

Cluster 2 mostly contains genes involved in complex metabolic reactions, such as the biosynthesis of cholesterol, but also contains some important redox enzymes of the ER and some lysosomal transport proteins.

Cluster 3, progressively induced during the decidualization process, corresponds to the bulk of the protein folding and processing machinery, including most chaperones and glycosylation enzymes.

Cluster 2 and cluster 3, peaking at the third day of decidualization, likely correspond to the induction of the biosynthetic machinery allowing both the expansion of the endomembrane system, and the massive production, folding and modification of secretory proteins.

No specific enrichment was observed for cluster 4, which genes variously encode for metabolic enzymes, signaling proteins and proteins with unclear function.

Cluster 5 appeared particularly interesting, especially for the analysis of the early events of the decidualization process. The genes belonging to this cluster, indeed, are already

upregulated in the very first phases of decidualization, before a significant expression of protein cargoes: therefore, more than others, they probably represent the transcriptional preparation of the cell for its secretory task.

Cluster 5 includes the genes coding for several key components of the vesicular transport machinery (most of the COP and SEC genes), cargo receptors (LMAN1, MIA3, KDELR3), and proteins that are crucial for Golgi complex structure and organization (GLG, GOLGA2, GOLGA3, GOLGA5). Accordingly, the ORA identified a clear enrichment for GO terms related to vesicle coating and transport.

I decided to focus my attention on the last cluster: indeed, it corresponded to the first secretory pathway genes induced during decidualization, and to functions particularly important for decidualized cells, considering the selective enlargement of the Golgi complex and the high number of transport vesicles observed. Moreover, as this cluster corresponded to genes involved in a limited number of highly connected functions, the identification of a common regulatory mechanism appeared more feasible than for the other groups.

To verify whether the common pattern of expression also corresponds to a co-regulation, the presence of common cis-regulatory elements in the promoters of genes belonging to the same cluster was analyzed with the RcisTarget tool with the help of a collaborating bioinformatician. Interestingly, the highest enrichment values were obtained in cluster 5 for CREB3L1, CREB3L2, CREB3, ATF6 and Xbp1; these factors, among other things, are known to be involved in secretory pathway homeostasis, protein secretion, and differentiation into secretory phenotypes (Iwakoshi 2003, Hetz 2012, Kondo 2012, So 2018).

The same analysis, performed on the other clusters, also identified common transcription factors signatures for large groups of genes. No univocal signature could be identified for the other clusters, even if an interesting enrichment for the binding sites of CREB3L1 and CREB3L2 was detected also in cluster 3.

A detailed analysis of all the different transcription factors identified, and their role in the transcriptional regulation of clusters 1-4 during decidualization, was considered beyond the scope of this project.

2.2 CREB3L1 and CREB3L2: candidates for secretory pathway gene induction

Previous results about a possible involvement of UPR mediators in decidualization had already excluded a major role of ATF6 and of the IRE1-Xbp axis in decidualization, especially in the early phases. Indeed, only minimal activation of the corresponding signal cascades was observed (Anelli 2021), and pharmacological inhibition of the UPR branches didn't have significant effects on decidualization (my Master Thesis results, unpublished). These factors were therefore excluded from further analyses.

CREB3L1 and CREB3L2, instead, were considered promising candidates for the induction of genes belonging to cluster 5.

These transcription factors, characterized by high sequence similarity, and an almost identical DNA binding motif (Sampieri 2019, Yuxiong 2023), belong to the CREB3 transcription factor family (Fox 2010).

As their other homologs (CREB3, CREB3L3, and CREB3L4), CREB3L1 and CREB3L2 have been reported to regulate the secretory capacity in different physiological contexts (Fox 2010). CREB3L1 and CREB3L2, in particular, are required for the differentiation of various secretory cell types (Garcia 2014, Tomoishi 2017), and for the proper development of their secretory capacity (Chen 2014, Tomoishi 2017).

CREB3-like transcription factors ER-localized proteins, formed by a small luminal domain, a single, highly conserved transmembrane passage, and a cytosolic N-terminal domain, representing the "proper" transcription factor (Bailey 2007): upon activation, indeed, these proteins are transported from the ER to the Golgi complex, where they undergo regulated intramembrane proteolysis by S1P and S2P (Brown 2000, Bailey 2007); this releases the cytosolic domain, a bZIP transcription factor, which can translocate in the nucleus, and activate a transcriptional response (Bailey 2007, Kondo 2012). As the others bZIP transcription factors, CREB3-like transcription factors mediate their effect as dimers, with a possible preference for homodimers (Vinson 2006).

If they are not activated, CREB3L1/2 are rapidly ubiquinated by HRD1 (an ER-resident E3 ubiquitin ligase), extracted from the ER membrane, and degraded in the proteasome.

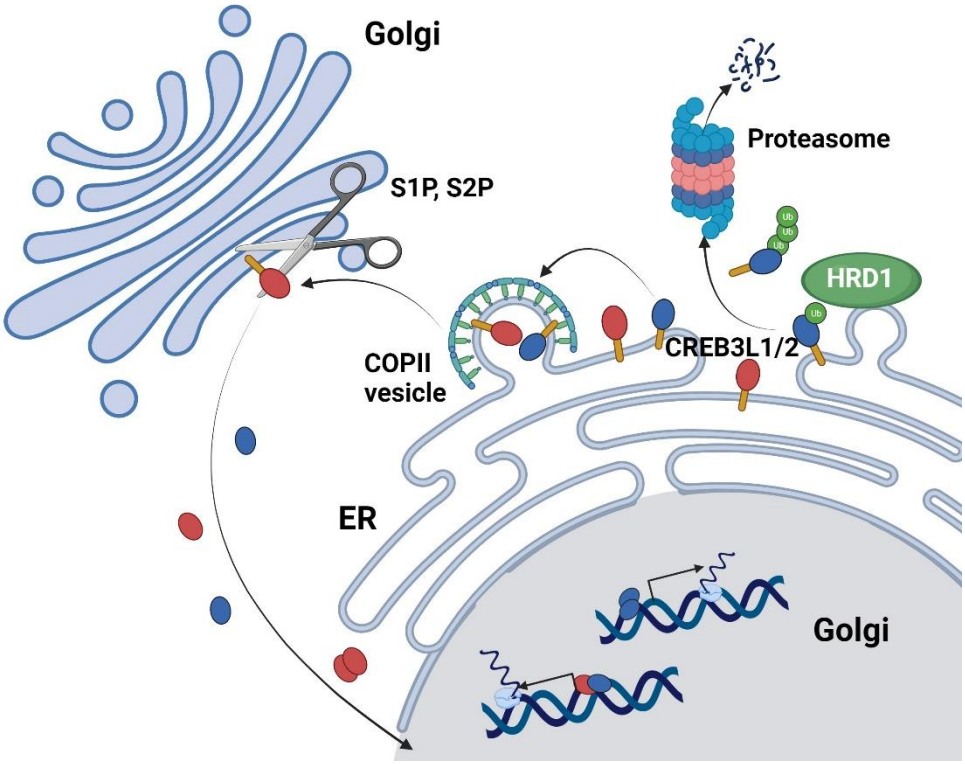


Figure 19. Representation of CREB3L1/2 activation mechanism.
CREB3-like proteins are rapidly ubiquitinated by HRD1, extracted from the ER membrane, and sent to proteasomal degradation. Upon activation, they are inserted into COPII-coated vesicles, transported to the Golgi complex, and cleaved by the Golgi-resident S1P and S2P proteases. In this way, their DNA binding domains can translocate into the nucleus, dimerize, and activate the transcription of their targets. Created in BioRender, publication agreement number VY26A0WYT2.

While the process leading to the release of the bZIP-domain have been well characterized, the activation mechanisms of CREB3L1 and CREB3L2 are not completely understood (Kondo 2012, Yuxiong 2023).

Activation of these transcription factors has been reported in conditions of ER stress (Kondo 2005, Kondo 2012). However, the mechanisms anchoring them in the ER membrane, or eliciting their movement upon activation, are still largely unknown (Kondo 2012).

Moreover, CREB3L1 has also been reported to be activated by extracellular signals, such as TGFβ, in a process required for sustained collagen secretion in osteoblasts (Chen 2014). In this context, the activation of CREB3L1 seems to depend on the downregulation of TM4SF20, which in turn has been proposed to inhibit CREB3L1 proteolysis (Chen 2014).

Segregation in specific ER subdomains, devoid of HRD1, has also been proposed for CREB3L1 activation (Kamikawa 2021); whether this represents a specific case, or a general mechanism of activation, remains to be demonstrated.

2.3 CREB3L1 and CREB3L2 are induced during decidualization

During *in vitro* decidualization of T-HESC, a clear upregulation of CREB3L1 and CREB3L2 mRNA was observed in real-time qPCR, although with a different pattern.

In both cases, a steady transcriptional induction was observed from the beginning of the differentiation program to complete decidualization (Figure 20).

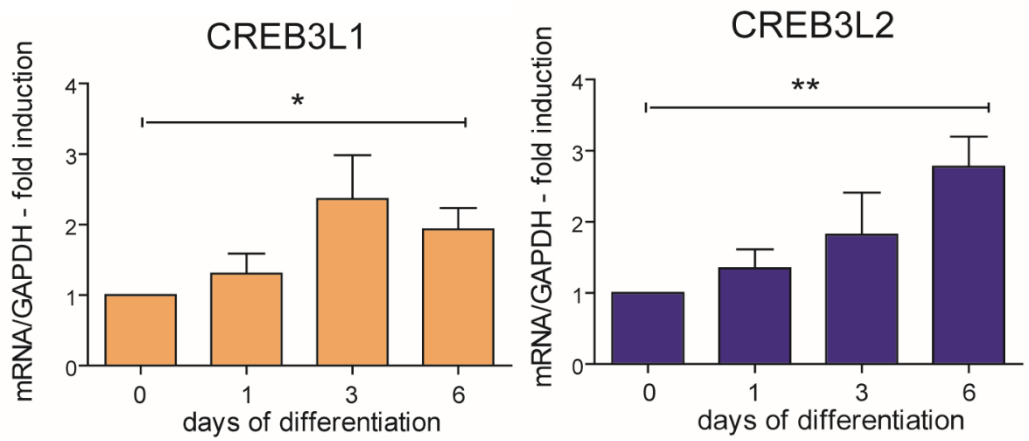


Figure 20. CREB3L1 and CREB3L2 are transcriptionally induced in T-HESC decidualization.

Real-time qPCR analysis of CREB3L1 and CREB3L2. Results corresponding to six independent replicates, normalized on GAPDH mRNA and represented as mean ± SEM. *: $p \leq 0.05$; ** $p \leq 0.01$, t-test of each time-point versus d0.

This result is particularly important as the transcriptional induction of CREB3L1 and CREB3L2 was reported to be sufficient for their activation, possibly due to a larger number of these transcription factors stochastically escaping the degradation pathway (Kondo 2012).

The presence of the two transcription factors at the protein level was also analyzed by western blot assay in lysates collected at different days of decidualization. Silencing of the transcription factor or transient overexpression of its cytoplasmic domain were used as negative and positive controls, respectively (Figure 21).

For both CREB3L1 and CREB3L2, the bands corresponding to the full-length and the cleaved, active form could be identified, both in control conditions and during decidualization. Considering the low stability of these transcription factors, continuously ubiquitinated and degraded, the detection of full-length forms could either indicate a very high expression of CREB3L1/2, or the stabilization of these transcription factors.

The presence of the cleaved form, moreover, indicates that both the transcription factors are activated in the experimental system, both in control conditions and upon decidualization. Therefore, CREB3L1 and CREB3L2 can be expected to play a role in the transcriptional regulation of secretory pathway genes, both in basal conditions and upon decidualization, a process in which most secretory pathway genes are indeed upregulated.

Due to the low signal obtained and the reduced specificity of the antibodies (especially for CREB3L2), no clear conclusion about the abundance of the transcription factors could be obtained with this approach.

An attempt to further investigate the dynamics of synthesis, stabilization, ubiquitination and degradation of CREB3L1 and CREB3L2 was performed, by repeating the experiment upon pharmacological blocking of the proteasome. However, the high background and the presence of several nonspecific bands impaired a precise analysis of the transcription factors, leading to a discontinuation of that experimental approach (not shown).

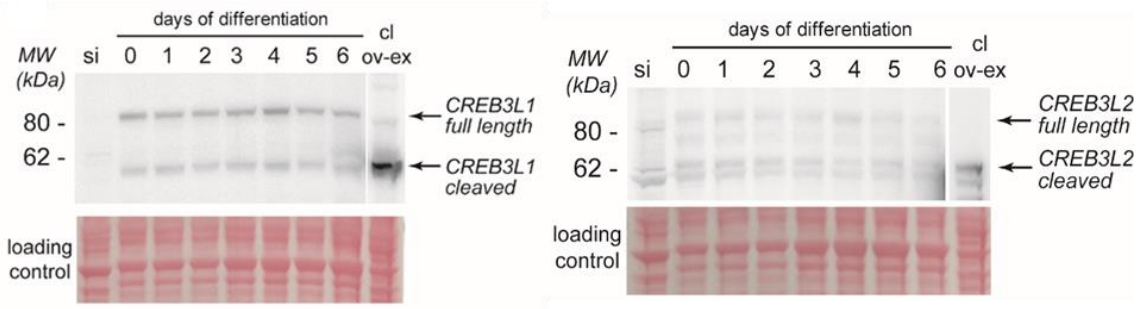


Figure 21. CREB3L1 and CREB3L2 are expressed and activated during decidualization
Western Blot analysis of CREB3L1 (left panel) and CREB3L2 (right panel) at different days of T-HESC *in vitro* decidualization. Arrows indicate the bands corresponding to the two forms of these proteins, observed at the expected molecular weight: the upper band corresponds to the full-length form of the transcription factors, while the lower one to the cytosolic domain, released by proteolytic cleavage. For each blot, a sample in which CREB3L1 or CREB3L2 was silenced was loaded in parallel with the decidualization curve, as a negative control (si). As a positive control, and to better identify the cleaved forms, lysate of HeLa cells overexpressing the cytosolic domain of CREB3L1 or CREB3L2 were also loaded (cl ov-ex). The ponceau staining of the nitrocellulose

membranes is shown to confirm an even loading of the samples. The blots shown are representative of five independent experiments.

2.4 CREB3L1 and CREB3L2 are required for efficient decidualization

The results previously presented suggest that CREB3L1 and CREB3L2 could be involved in the decidualization program, and in particular in the correct induction of genes involved in vesicular transport and Golgi morphogenesis.

To test this hypothesis, CREB3L1 and CREB3L2 were silenced by small interfering RNAs (siRNA), either individually or in combination. The procedure was performed the day before decidualization induction (day -1) and repeated after 3 days (day 2), so that the silencing was maintained for the whole differentiation program.

The effectiveness and the specificity of the silencing procedure were confirmed by qPCR, which also excluded the compensatory induction of one factor upon silencing of the other (Figure 22). Silencing of CREB3L1 and/or CREB3L2 in decidualization didn't show any effect on the induction of decidualization markers, thus excluding a general, nonspecific effect on the decidualization program (Figure 23).

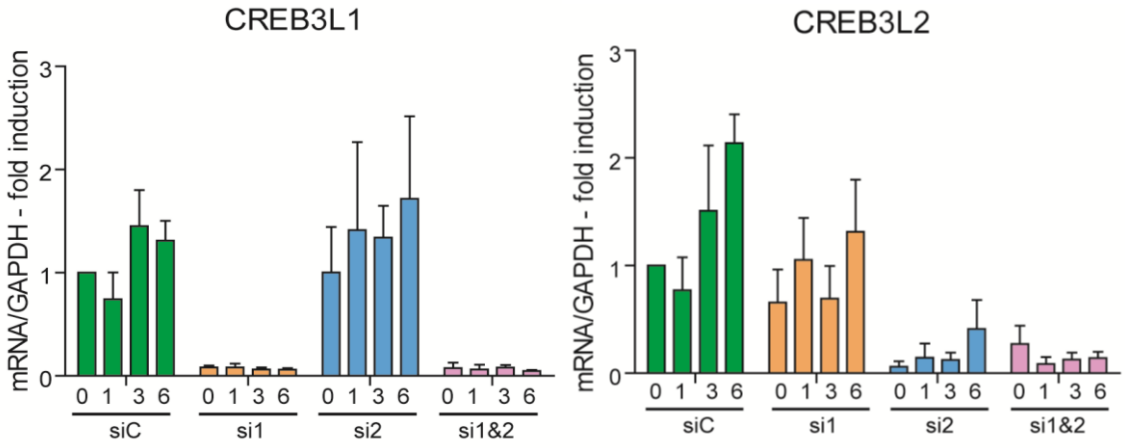


Figure 22. Silencing of CREB3L1 and CREB3L2 is effective and specific.
Real-time qPCR analysis of CREB3L1 and CREB3L2 during T-HESC decidualization upon different RNA silencing conditions. The silencing procedure was performed with silencing oligonucleotides specific for CREB3L1 (si1), CREB3L2 (si2), or a combination of both (si1&2); cells in control conditions (siC) were treated with scrambled oligonucleotides. Results corresponding to three independent replicates, normalized on GAPDH mRNA and represented as mean ± SEM.

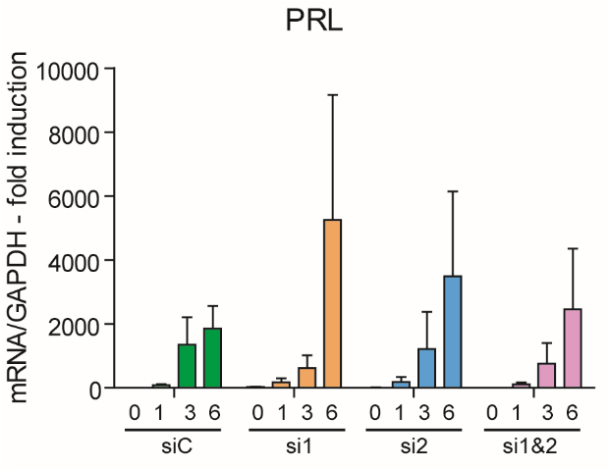


Figure 23. Silencing of CREB3L1 and CREB3L2 does not affect the transcriptional induction of the decidualization marker prolactin.

Real-time qPCR analysis of PRL during decidualization, either in control conditions of upon silencing of CREB3L1, CREB3L2, or combined silencing of both the transcription factors. Results corresponding to three independent replicates, normalized on GAPDH mRNA and represented as mean ± SEM.

Conversely, the silencing of CREB3L1 and CREB3L2 affected dramatically the expression of genes involved in ER-to-Golgi trafficking and in Golgi complex organization, normally upregulated during the decidualization program (Figure 24).

The panel of genes I analyzed included ERp44 and ERGIC53 (LMAN1), key players in distal protein quality control and retrieval of proteins to the ER; KDELR1-3, cargo receptors involved in the retrieval to the ER of KDEL-bearing proteins; genes encoding for structural components of the Golgi complex (GOLGA2, encoding for GM130, and GOLGB1, encoding for giantin); TGN46 (encoded by TGOLN2), regulating vesicular trafficking at the *trans*-Golgi network; SEC24A and D, encoding for components of the COPII vesicle system.

Most of the genes belonged to the cluster 5 (Figure 18A), or have a clear functional association with members of that cluster: KDELR1 and KDELR2 actually belong to cluster 3, but their transcriptional induction is similar to the one observed for KDEL3, and they display an enrichment for CREB3L1/2 binding site in their promoters; ERp44, also part of cluster 3, forms a functional couple with ERGIC53 (Tempio 2021).

Silencing of CREB3L1, CREB3L2, or the combined silencing of both the transcription factors affected the expression of the genes of the panel with a variable extent.

For most of the genes, an effect of the silencing was observed also in basal conditions (day 0), suggesting that CREB3L1 and CREB3L2 are not only involved in decidualization, but also in the homeostasis of secretory pathway organelles in EnSCs.

The most severe effects were observed for SEC24A/D, ERGIC53, KDELR2 and KDELR3. A reduction of expression, although below statistical significance, was observed for Giantin, TGN46 and, in a limited measure, for GM130.

For some genes (e.g. ERGIC53), the basal expression level was strongly reduced, but transcription increased with decidualization; for others, even when the basal effect was limited (e.g. KDELR2), the transcriptional induction was completely abrogated.

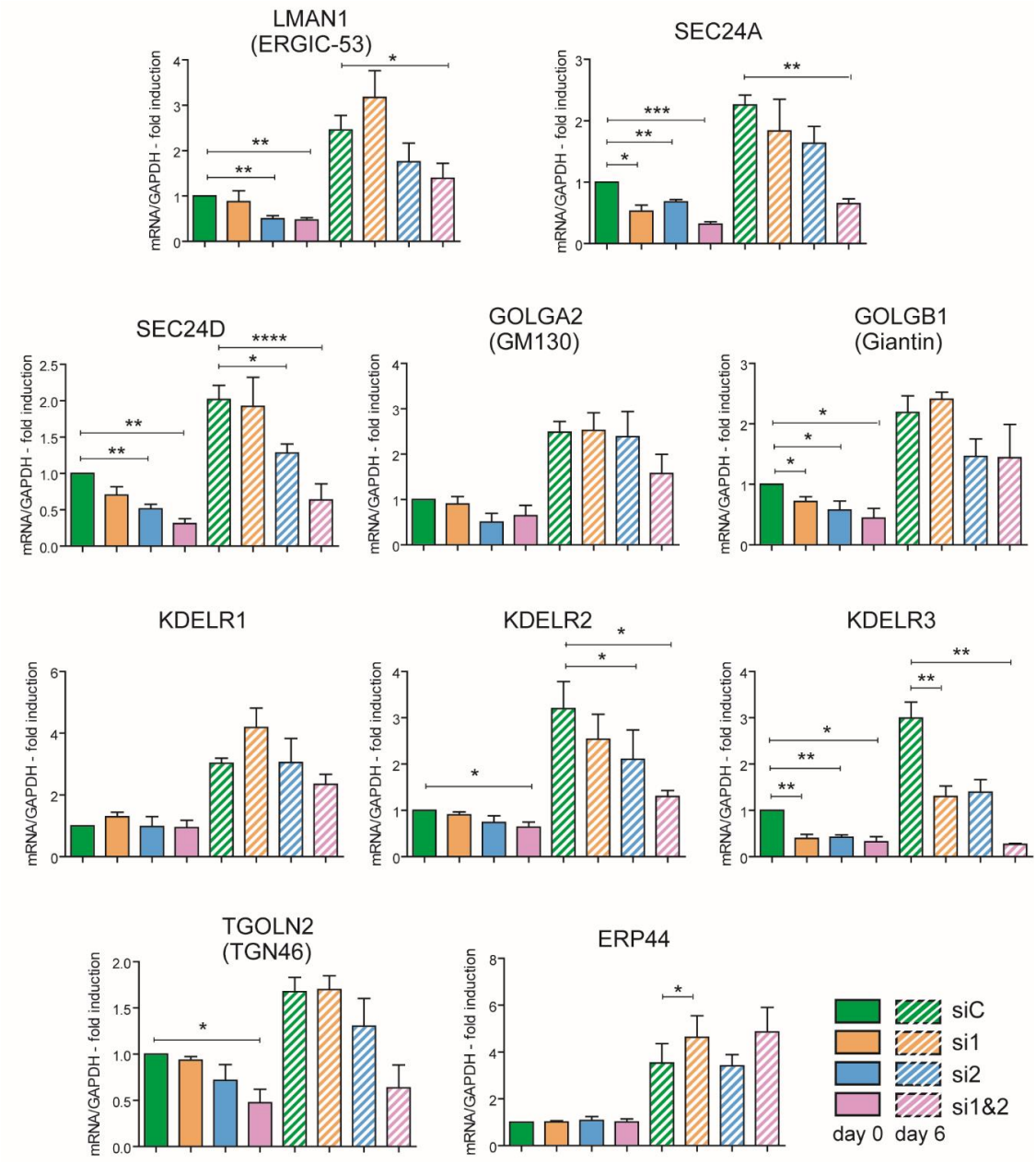


Figure 24. Silencing of CREB3L1 and CREB3L2 impairs expression and induction of secretory pathway genes during decidualization.

Real-time qPCR analysis of secretory pathway genes during *in vitro* T-HESC decidualization, either in control conditions of upon silencing of CREB3L1, CREB3L2, or combined silencing of both the transcription factors. Results corresponding to a minimum of three independent experiments, normalized on GAPDH mRNA and represented as mean ± SEM. *: $p \leq 0.05$; **: $p \leq 0.01$, t-test of each time-point versus siC day 0 or siC day 6, as indicated by bars and asterisks.

The different silencing conditions resulted in similar, but not superimposable effects: most genes displayed a stronger sensitivity for the downregulation of one transcription factor or were only affected by the combined silencing.

This result is particularly interesting, considering the high homology of CREB3L1 and CREB3L2, the similarity of their binding sites, and the possibility for these TFs to heterodimerize: even though CREB3L1 and 2 are similar, and share most of their transcriptional targets, the role of the two transcription factors in decidualization is not identical. Quite unsurprisingly, the combined silencing of CREB3L1 and CREB3L2 invariably resulted in the strongest effects on the affected genes.

Interestingly, some of the analyzed genes were not influenced by CREB3L1/2 silencing, despite their close association with some of the most affected ones.

This was the case of ERp44, colocalized and functionally associated with ERGIC53 (Tempio 2021), but normally expressed and induced even upon combined CREB3L1/2 silencing. Similarly, no effect was observed on KDELR1 expression, differently from the other members of the same family.

Together, these results highlight the important role of CREB3L1 and CREB3L2 in the regulation of secretory pathway gene expression, but also the complexity of the signaling network. In general, most of the secretory pathway genes analyzed relied on CREB3L1 and CREB3L2 for their expression in EnSCs, and their correct induction during decidualization.

However, the role of these transcription factors is not identical, as different effects are observed for the silencing of CREB3L1 and CREB3L2. Moreover, some secretory pathway genes don’t seem to rely on these transcription factors for their expression, thus suggesting the existence of a wide variety of induction and compensatory mechanisms.

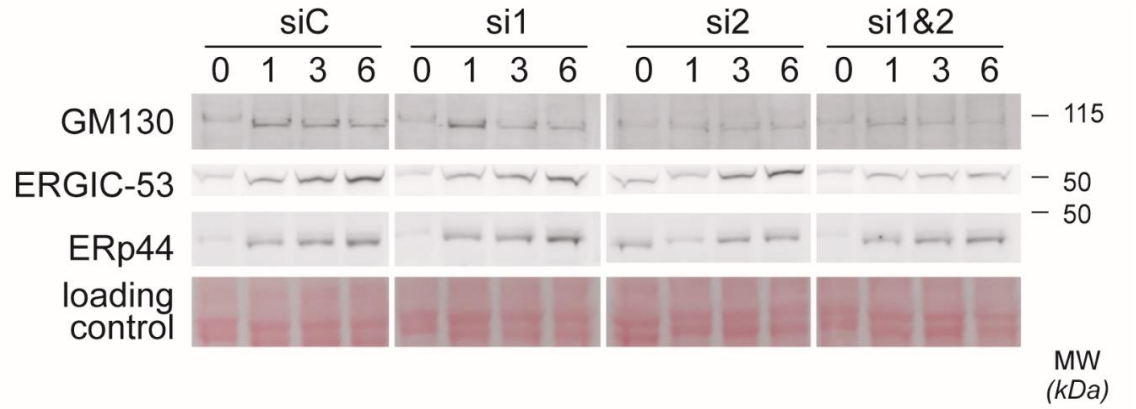


Figure 25. Silencing of CREB3L1 and CREB3L2 impairs the expression of specific secretory pathway proteins.

Western Blot analysis of GM130 (upper panel), ERGIC-53 (middle panel) and ERp44 (lower panel) during T-HESC decidualization, either in control conditions or upon silencing of CREB3L1 and/or CREB3L2. The blots shown are representative of at least three independent experiments.Ponceau staining of the nitrocellulose membranes is shown to confirm an even loading of the samples.

As a further confirmation of the role of CREB3L1 and CREB3L2 in the homeostasis of EnSC secretory pathway during decidualization, the effect of their silencing on the amount of selected proteins was analyzed by western blotting (Figure 25).

As expected from the mRNA analysis, the combined silencing of CREB3L1 and 2 reduced the expression of ERGIC53, and completely abrogated its induction during decidualization; the silencing of CREB3L1 or CREB3L2 alone, instead, only had a limited effect.

Conversely, ERp44 was not affected, and its amount increased in decidualization, regardless CREB3L1/2 silencing.

For GM130, some discrepancies between RNA and protein level were observed: while only combined CREB3L1/2 silencing induced a limited reduction in GM130 mRNA, all the silencing conditions resulted in a dramatic reduction in the protein amount. A possible explanation of this unexpected result may be represented by the concurrent downregulation of the vesicular transport system, possibly interfering with GM130 correct localization and therefore resulting in the degradation of the protein.

2.5 Effect of CREB3L1/2 silencing on secretory organelle volume and morphology

Based on the previous results, CREB3L1 and CREB3L2 appear to be necessary for the correct induction of vesicular transport and Golgi organization genes during the decidualization program.

To verify whether the transcriptional effects of CREB3L1/2 silencing also correspond to structural alterations of the secretory pathway organelles, the morphology of ER and Golgi was analyzed by immunofluorescence.

Consistently with the previous morphometric analysis, calreticulin, giantin and golgin 97 were selected as markers for the ER, the cis-Golgi and the trans-Golgi, respectively. Cells were analyzed in control conditions (day 0) or after complete decidualization (day 6), with or without the silencing of CREB3L1, CREB3L2, or of both the transcription factors. The combined staining with the membrane marker HLAI allowed the comparison between organelle volume and total cell volume, as described in Results, paragraph 1.2.

Silencing of the transcription factors, as expected, didn't result in an overall impairment of the decidualization program, with cells acquiring the predicted epithelioid morphology upon decidualization. Moreover, no significant effect on ER or Golgi volume was observed in basal conditions (not shown).

On the contrary, the enlargement of secretory pathway organelles normally observed in decidualization was partially impaired. The volume of the Golgi complex appeared to be particularly affected by the silencing of CREB3L1, both alone and in combination with CREB3L2. Coherently with what was observed in gene expression analysis, the role of the two transcription factors in Golgi homeostasis appears to be similar, but not identical.

Of note, the expression of giantin was not affected by CREB3L1 silencing (Figure 24), thus excluding that the volume reduction observed may actually be due to a decreased expression of this protein marker.

Both the *cis* and the *trans* components of the organelle were affected in the same way, although only for the *cis*-Golgi the difference among the different conditions was larger, and had a stronger statistical significance. Similarly to what was outlined in the description of

Figure 11, this discrepancy could either have a biological significance, or due to technical aspects of the quantification procedure.

In the first hypothesis, this result would indicate that CREB3L1 role is mostly required for the enlargement of proximal components of the organelle, possibly also due to its role in the regulation of genes involved in ER-to-Golgi transport.

Alternatively, the difference might only due to the higher variability of size and morphology observed for the *trans*-Golgi, determining a higher dispersion of the measurements and thus a reduced statistical significance.

The ER volume, instead, appears to be only minimally affected, even if some morphological anomalies could be noticed. (Figure 26-27)

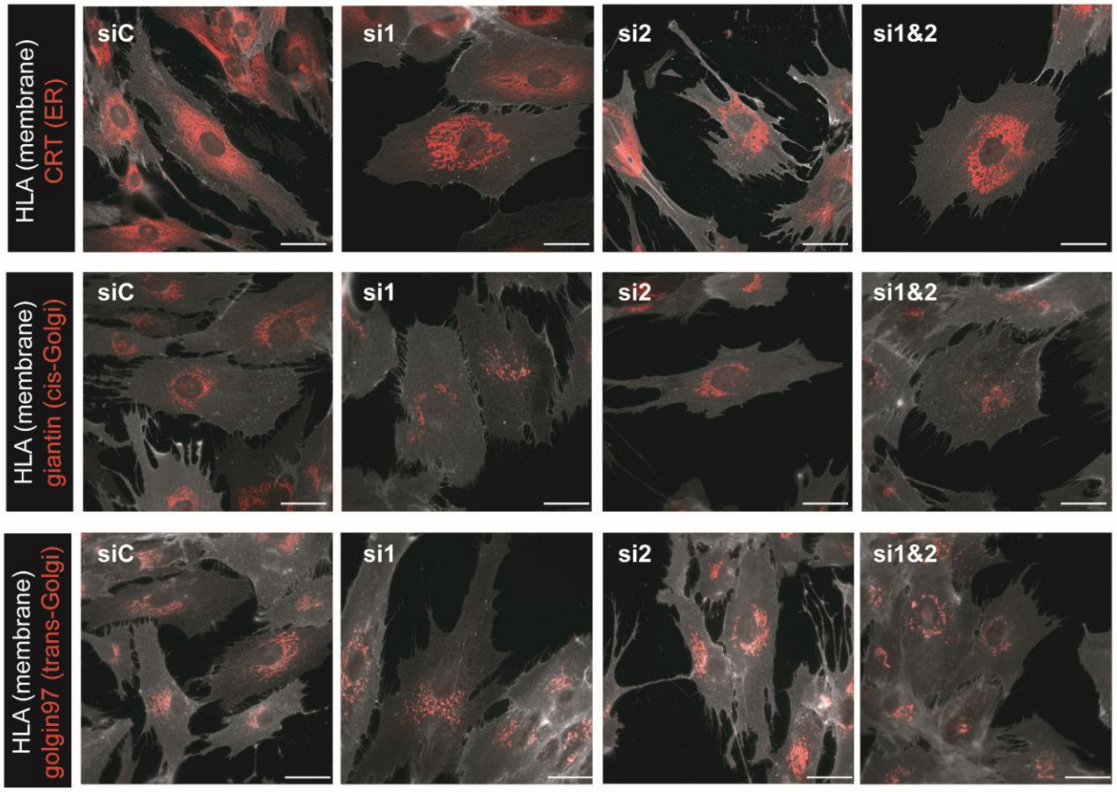


Figure 26. Silencing of CREB3L1/2 in decidualization does not impair the overall morphological reshaping, but affects the morphology of ER and Golgi.
Combined immunofluorescence of secretory pathway organelle and plasma membrane markers on cells decidualized in control conditions (siC), or upon silencing of CREB3L1 and/or CREB3L2. 60x magnification, bar: 15 µm.

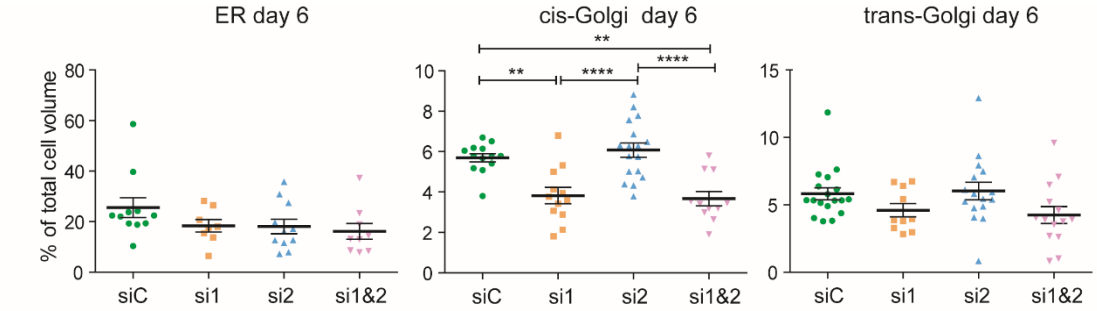


Figure 27. Silencing of CREB3L1/2 in decidualization impairs Golgi complex enlargement. Immunofluorescence-based morphometric analysis of secretory pathway organelles. Cells were decidualized in control conditions (siC), or upon silencing of CREB3L1 and/or CREB3L2. Quantification expressed as relative cell occupancy, based on the calculated volume of each marker and the total volume of the corresponding cell. The plots represent the median ± SEM and individual values of a minimum of two independent experiments. **: $p \leq 0.01$; ***: $p \leq 0.001$; ****: $p \leq 0.0001$; one-way ANOVA with Tukey correction.

Moreover, important morphological alterations could be observed for the Golgi complex upon silencing of the transcription factors. Upon CREB3L1 silencing, the size of the organelle was reduced, coherently with the morphometric analysis; the overall structure, instead, was maintained, even if it appeared to be less complex and intricated than in control conditions. The effect of CREB3L2 silencing, instead, was a complete fragmentation of the Golgi complex, possibly due to insufficient expression of Golgi-organizing proteins: interestingly, the two transcription factors regulate the same group of target genes, but their precise role in the regulation of Golgi homeostasis appears to be different.

The scattering caused by CREB3L2 silencing on the Golgi complex could also partially account for the apparent lack of effect on the organelle volume: as the *cisternae* are scattered on a larger surface, the analysis pipeline could overestimate their apparent size.

As predictable, the combination of CREB3L1 and CREB3L2 silencing produced the most severe morphological defects, with a dramatic decrease of the Golgi volume, disorganization of the overall organelle structure and, in some cells, a general fragmentation and scattering of the Golgi *cisternae* (Figure 28).

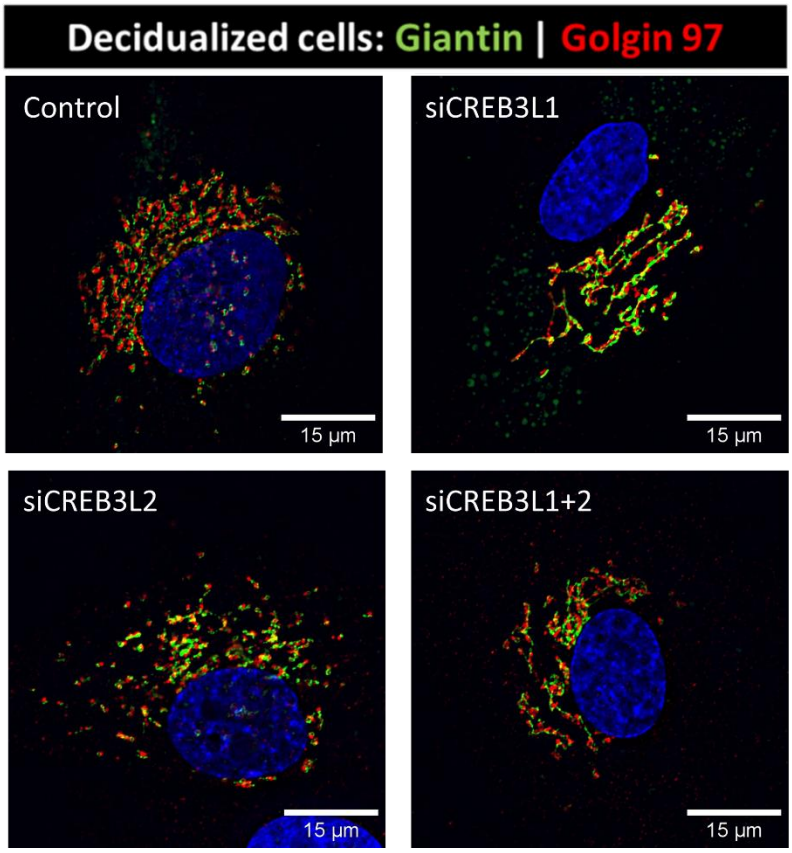


Figure 28. Silencing of CREB3L1/2 disrupts Golgi morphology in decidualized cells. Immunofluorescence of Golgi complex markers in cells decidualized in control conditions, or upon silencing of CREB3L1/2. Giantin and golgin 97 were used as *cis*-Golgi and *trans*-Golgi markers, respectively. Nuclei were counter-stained with DAPI. 100x magnification, bar: 20 µm.

2.6 Silencing of CREB3L1 and CREB3L2 impairs protein trafficking and secretion

In a physiological context, EnSCs mediate their function mostly through their secretory activity. Decidualized cells secrete large amounts of proteins, ranging from small cargoes, such as PRL and cytokines, to ECM proteins and collagen (Dunn 2003, Gellersen 2014). The increased expression of genes coding for protein cargoes, including different collagen types (I, IV and VIII), was indeed observed also in the transcriptome analysis described in Results, paragraph 1.4.

CREB3L1 and CREB3L2 had been previously described as necessary for collagen secretion in osteoblast and chondrocytes (Murakami 2009, Saito 2009, Chen 2014), as well as for the correct differentiation of other secretory cell types (Tomoishi 2017, Khetchoumian

2019). Moreover, a previous paper reported CREB3L1 as one of the genes directly induced during decidualization and demonstrated that the transcription factor is required in decidualization, even if it didn't provide a mechanistic explanation (Ahn 2016).

Therefore, I decided to investigate the role of these transcription factors in the increased secretory capacity of decidualized cells.

Silencing of CREB3L1 and CREB3L2 dramatically impaired the intracellular trafficking of proteins, especially when the combined silencing of both transcription factors was performed. Immunofluorescence for procollagen 1A1 (the precursor of collagen type I) revealed an aberrant intracellular accumulation of this protein, resulting in the formation of enlarged ER *lacunae*, and the appearance of aggregate-like structures (Figure 29).

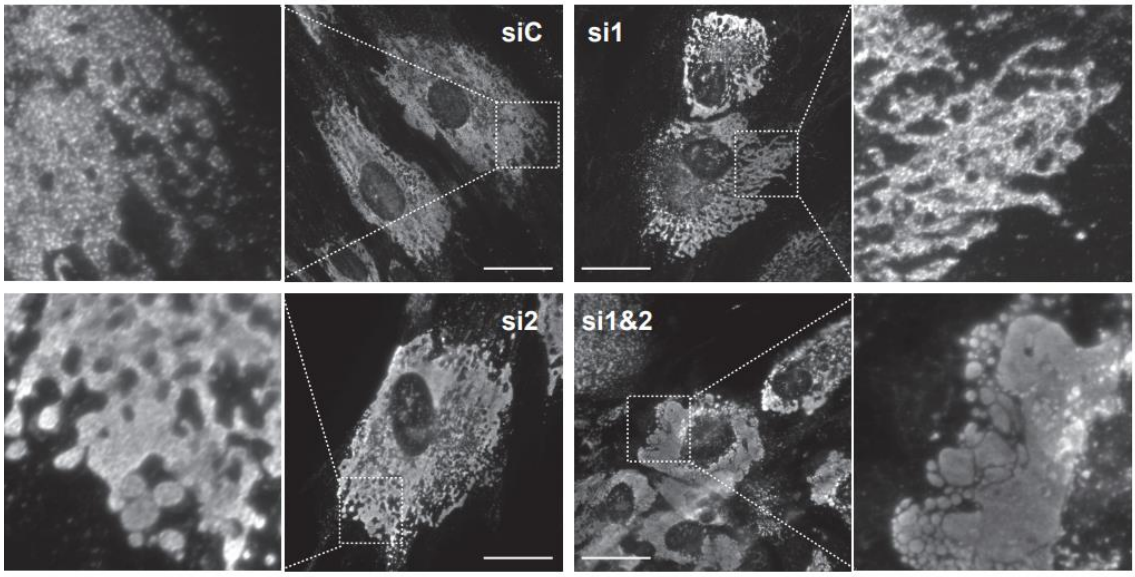


Figure 29. Silencing of CREB3L1/2 induces aberrant ER accumulation of secretory protein cargoes in decidualized EnSCs.
Immunofluorescence of procollagen 1A1 in cells decidualized in control conditions, or upon silencing of CREB3L1/2. For each panel, a representative area is shown with a 4x magnification factor. Acquired with a 60x objective, bar: 20 µm.

This phenotype clearly resembles other example of protein aggregation and impaired secretion, as observed for T-HESC decidualized upon ascorbic acid deprivation (Anelli 2021), or for mutated immunoglobulins leading to Russell Body formation (Valetti 1991).

In accordance with these results, the silencing of CREB3L1/2 caused procollagen 1A1 to significantly accumulate in the intracellular material, as clearly shown by western blot assay (Figure 30A). The experiments was performed in non-reducing conditions, in order to visualize the pro-collagen assembly intermediates (Di Chiara 2018), which indeed appear to be the most accumulated form. A limited amount of monomeric collagen was also detected, with no significant difference between the conditions; the band, with an apparent molecular weight of 170 kDa, likely represents individual procollagen polypeptides, not yet assembled in a triple helix structure.

Conversely, the secretion of mature collagen type I was almost completely abrogated by the combined silencing of CREB3L1 and CREB3L2, further confirming the protein traffic problems experienced by cells decidualized in the absence of these transcription factors (Figure 30B).

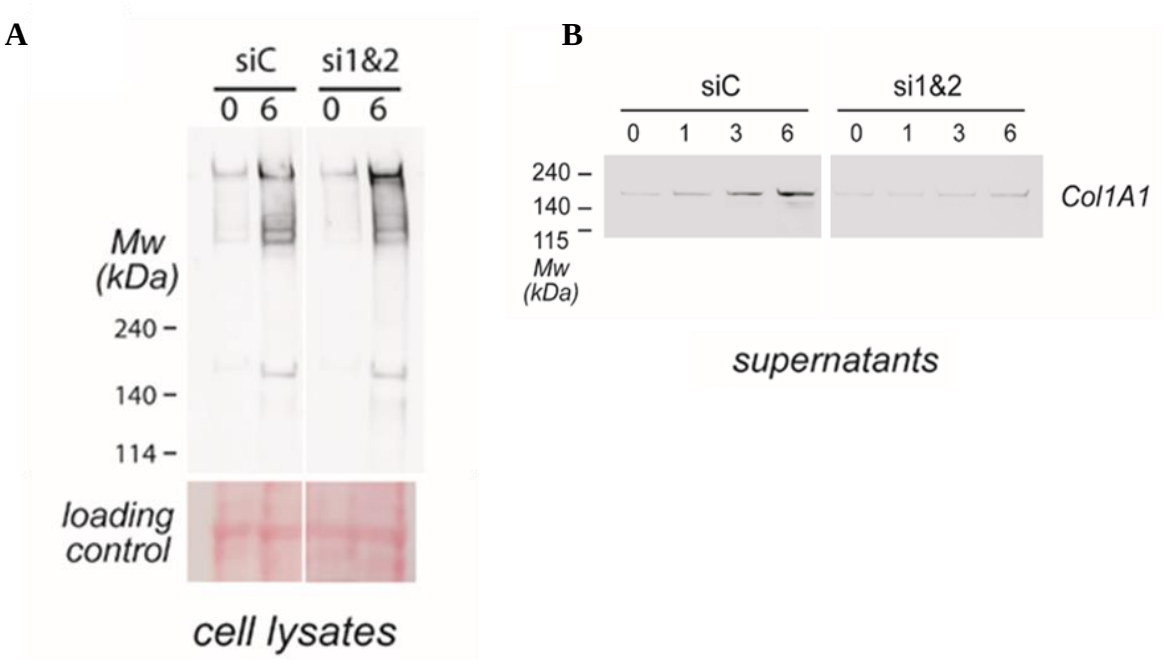


Figure 30. Silencing of CREB3L1 and CREB3L2 causes intracellular accumulation of procollagen and impairs collagen secretion.

A. Non-reducing western blot assay of procollagen 1A1 in T-HESC lysates. The samples correspond to cells kept in proliferative state (0) or decidualized (6), either upon treatment with a scrambled oligonucleotide (siC), or with silencing oligonucleotides specific for CREB3L1 and CREB3L2. Ponceau staining of the membrane is shown as a loading control.

B.Reducing western blot assay of secreted collagen type I. The samples represent the proteins secreted in 6 hours in a reduced-serum medium (Optimem) by 10,000 cells at different days of

decidualization (from 0 to 6). Cells were either decidualized in control conditions (siC) or upon combined silencing of CREB3L1 and CREB3L2.

Silencing of CREB3L1/2 doesn't only impair collagen secretion, but seems instead to interfere with the overall secretory capacity of decidualized cells: SYPRO staining revealed an overall reduction in the protein amount secreted by decidualized cells, with the strongest reduction observed for high-molecular weight proteins (Figure 31A).

Prolactin, a small (23 kDa) and not particularly complex protein, was also affected by the downregulation of these transcription factors: while prolactin expression does not depend on CREB3L1 or CREB3L2 (Figure 23), its secretion was dramatically reduced by the silencing of these transcription factors (Figure 31B).

The protein, clearly detected in the supernatant of cells decidualized in control conditions (Figure 5), was significantly reduced by CREB3L1 silencing, and disappeared almost completely upon the double silencing condition (Figure 31B).

Interestingly, PRL secretion was not affected by CREB3L2 silencing alone, but still the absence of this transcription factor worsened the phenotype in the combined silencing.

This result, combined with previous observations, highlighted some interesting difference between CREB3L1 and CREB3L2. These factors have a similar role in controlling the expression of secretory pathway genes, and both of them are required to increase the secretory capacity of EnSCs during decidualization. However, the interaction between these two factors is complex and, even if they seem to act in combination, their precise role in the regulation of different genes and functions appears to be slightly different (see Figures 24, 27 and 28).

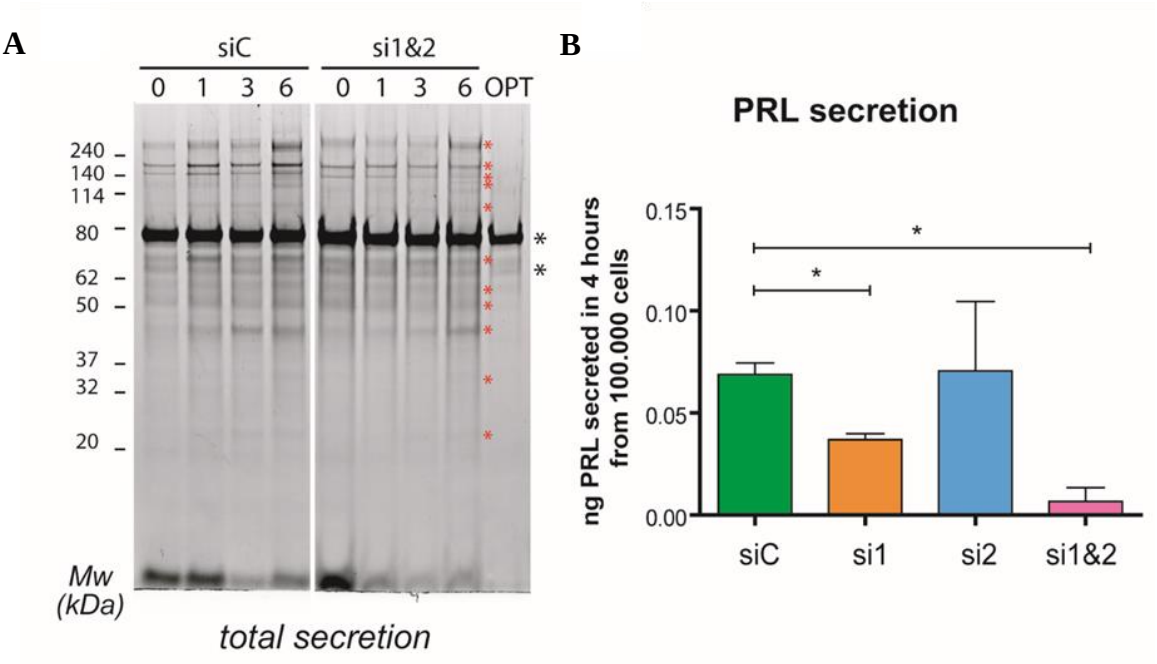


Figure 31. CREB3L1 and CREB3L2 are required for efficient protein secretion in decidualized endometrial stromal cells.

A. SYPRO Ruby Stain for total protein secretion. The supernatant of 10,000 cells was analyzed after 6 hours of secretion in reduced-serum medium. The samples correspond to T-HESCs at different days of *in vitro* decidualization, in control conditions or upon CREB3L1/2 silencing. Red asterisks indicate bands which intensity is reduced by the silencing of the transcription factors. Optimem was used to normalize sample volume and was loaded in the gel (OPT) to identify background bands (indicated by black asterisks).

B. ELISA assay for prolactin secretion. Samples correspond to the amount of proteins secreted in complete medium by 100,000 decidualized cells in 4 hour, with or without CREB3L1/2 silencing. Mean of three independent experiments ± SEM. *: $p \leq 0.05$.

The identification of CREB3L1 and CREB3L2 as critical factors for the correct reorganization of the secretory pathway organelles, and for the acquisition of an increased secretory capacity represents an interesting discovery in the characterization of endometrial stromal cell decidualization, as the molecular bases of the process are, to the state of the art, largely unknown.

Moreover, it is important to remind that decidualized EnSCs mediate almost all their physiological functions through the secretion of protein cargoes, and any alteration of their secretory phenotype may have dramatic consequences for the endometrial microenvironment.

For example, in a physiological context, the effects observed on collagen accumulation and defective secretion (Figures 29-30) would have deleterious effects on the organization of the extracellular matrix.

Similarly, prolactin seems to require CREB3L1 and CREB3L2 for its secretion: as prolactin represents one of the most important protein cargoes of decidualized EnSCs, and is fundamental for their physiological cross-talk with other cell populations of the endometrium, any defect in its secretion would be detrimental for the success of embryo implantation.

3 Not only a matter of secretory organelles: mitochondrial network rewiring

In the previous sections, I characterized the extensive rearrangements of the secretory pathway organelles observed during the decidualization, and identified the transcription factors CREB3L1 and CREB3L2 as key regulators of the process.

However, the morphological and functional reorganization of EnSCs during decidualization is likely not limited to the upregulation of endoplasmic reticulum and Golgi, but instead is expected to involve most of the organelles and most of the cellular functions.

The increase in protein synthesis and secretion, in particular, is an extremely demanding event in terms of energy and biosynthetic intermediates. Indeed, it has been calculated that the formation of a single peptide bond roughly corresponds to the hydrolysis of 5 ATP molecules (Princiotta 2003). Glycosylation also requires high-energy intermediates, in the form of nucleotide-activated monosaccharides (Aebi 2013, Freeze 2022). This corresponds therefore to a minimum of two ATP molecules for each carbohydrate monomer added in post-translational modification (Aebi 2013). Apart from the synthesis and modification of proteins, several other functions upregulated in decidualized cells are known to be energy-demanding, from chaperone-mediated quality control, to vesicle coating, transport and fusion (Alberts, 2015). Decidualization can therefore be expected to entail a significant rewiring of the cell metabolism, to support the secretory phenotype acquired by EnSCs.

In eukaryotic cells, mitochondria represent the main contributors to the energy production, as they mediate the controlled oxidation of high-energy molecules and the production of ATP, the "energy currency" of the cell (Alberts 2015). Moreover, these organelles also mediate other functions that can be crucial for a highly secretory cell type, including ROS scavenging, calcium homeostasis and biosynthesis of membrane lipids (Rowland 2012).

Taking this into consideration, I decided to investigate the dynamics of the mitochondrial network in decidualization, in terms of morphological rearrangements, functional changes, and interactions with the endoplasmic reticulum.

3.1 Mitochondria enlarge in decidualization

To determine if and how EnSC reorganize their mitochondrial network during decidualization, I followed the same experimental strategy I had employed for the analysis of the secretory pathway organelles (Results, paragraph 1.2).

Briefly, I induced *in vitro* differentiation of the model system T-HESC, stained the organelle of interest by immunofluorescence, and performed morphological and morphometric analyses to evaluate the changes.

The combined immunostaining of the mitochondrial protein TOM20 (Translocase of the Outer Membrane 20) and of class I HLA revealed that the mitochondrial nework is indeed rearranged during decidualization (Figure 32-33). Mitochondria expand and reorganize, acquiring a marked radial distribution and reaching the very periphery of the cell. Quantification of the mitochondrial volume confirmed this observation: a clear enlargement of the network can be observed from control conditions to the decidualized state, with a mean increase of 4.5 folds and high statistical significance. This difference is maintained even when the overall changes of cell morphology are considered, and the result is expressed in terms of relative cell occupancy (that is, the ratio between the organelle volume and the total volume of the corresponding cell) (Figure 34).

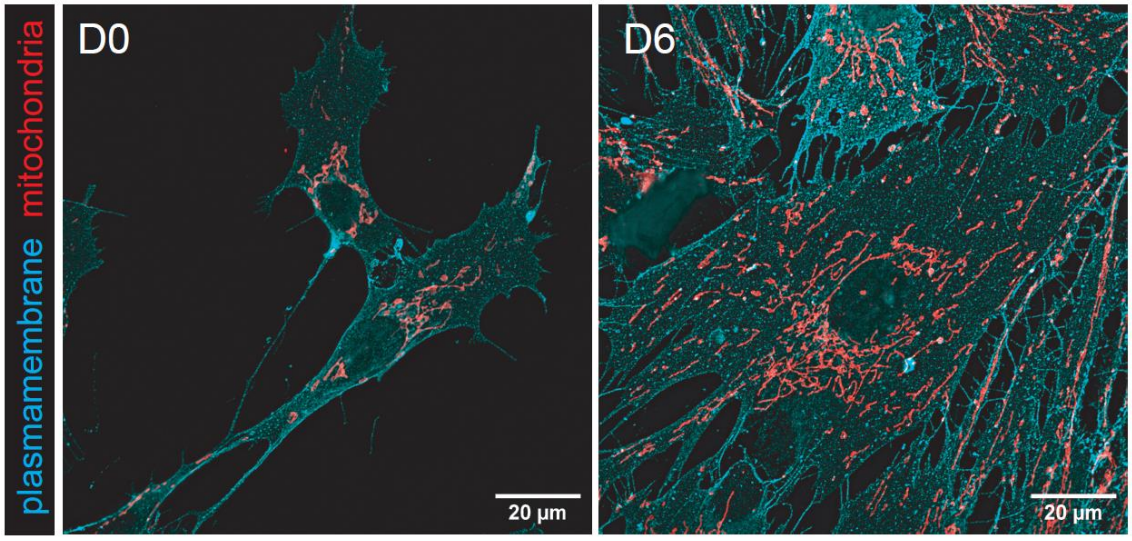


Figure 32. Mitochondria are reorganized and redistributed during decidualization.
Combined immunofluorescence of the mitochondrial marker TOM20 (red) and plasma membrane marker HLA-I (cyan) during in vitro decidualization. 100x magnification, bar: 20 µm.

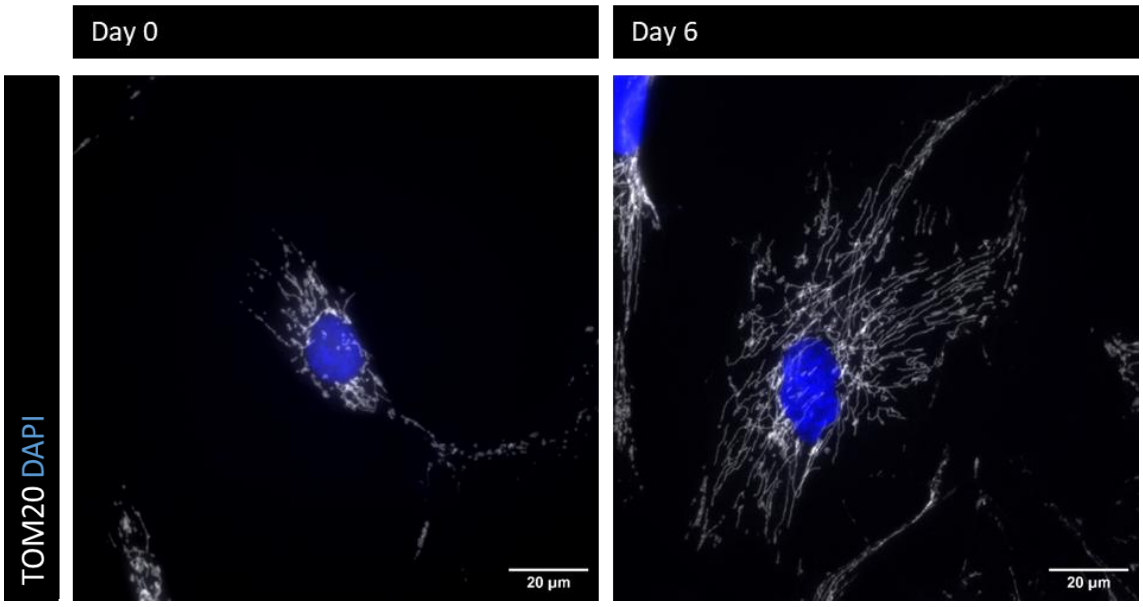


Figure 33. Mitochondrial network enlarges in decidualization.
Alternative visualization of TOM20 immunofluorescence in proliferative and decidualized T-HESC. Nuclei were counter-stained with DAPI. 100x magnification, bar: 20 µm.

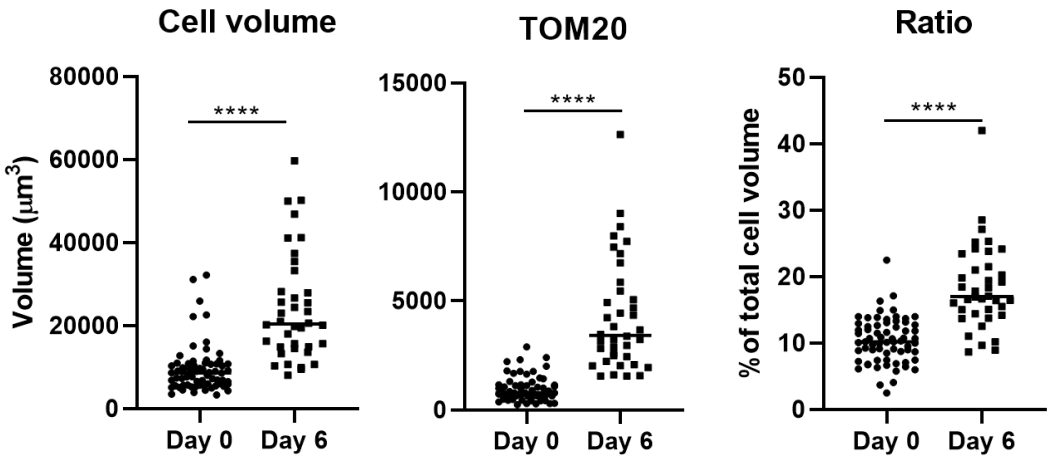


Figure 34. Mitochondrial volume significantly increases upon decidualization.
Immunofluorescence-based morphometric analysis of total cell volume and of the mitochondrial network. Quantification based on plasma membrane (HLA1) and mitochondrial (TOM20) markers, in two independent experiments. Results are expressed as absolute volumes or as percentage of the total volume of the corresponding cell. The plots show median and individual values of each group. ****: $p \leq 0.0001$, t-test.

To evaluate the increase of mitochondrial mass with an independent approach, I analyzed by Western Blot assay TOM20 (the same protein analyzed by immunofluorescence) and VDAC (Voltage Dependent Anion Channel), a well-established mitochondrial marker. As expected, the levels of both proteins steadily increased in decidualization, with differences already visible at 2-3 days post induction. In this way, the morphometric analysis was confirmed, decreasing the impact of possible artefacts in the microscopy-based quantification (Figure 35). These results, combined, suggest a selective enlargement of the mitochondrial compartment, to an extent significantly larger than what was previously observed for the secretory pathway organelles.

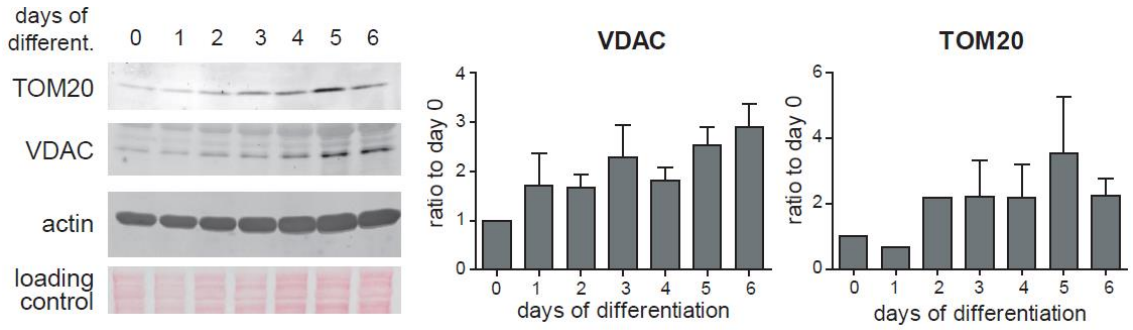


Figure 35. Decidualization increases the expression of mitochondrial proteins.
Western blot assay and densitometric quantification of the mitochondrial proteins TOM20 and VDAC at different time-points of decidualization. Quantifications are normalized on the loading control (actin) and expressed as fold change of the basal value (Day 0). The graphs show the mean of a minimum of three independent experiments, ±SEM.

3.2 Morphological reshaping of the mitochondrial network

It is generally established (Westermann 2010; Skulachev, 2001) that elongated and interconnected mitochondria are more efficient than small fragmented ones in terms of proton potential generation, energy distribution and ROS scavenging, especially in peripheral areas of the cell (Westermann 2010, Napolitano 2021). As a consequence, networks of elongated, highly interconnected mitochondria are often observed in cells with high metabolic activity (Skulachev 2001, Gomes 2011).

To determine whether this also represents an element of the decidualization program, I performed a three-dimensional reconstruction of the immunofluorescence stacks, using the image analysis software Arivis (Figure 36). Afterwards, I measured and compared the morphological parameters of mitochondria in control and decidualized cells: the main axis, in particular, was chosen as the parameter better representing their elongation state.

Comparison of the two conditions clearly showed that decidualized cells contain an increased proportion of tubular, elongated mitochondria, balanced by the decrease of mitochondria belonging to the shortest length classes. To provide an example, mitochondria with the main axis between 5 µm and 10 µm double in proportion during the differentiation process, while longer mitochondria (main axis >10 µm) increase of more than three times (Figure 37).

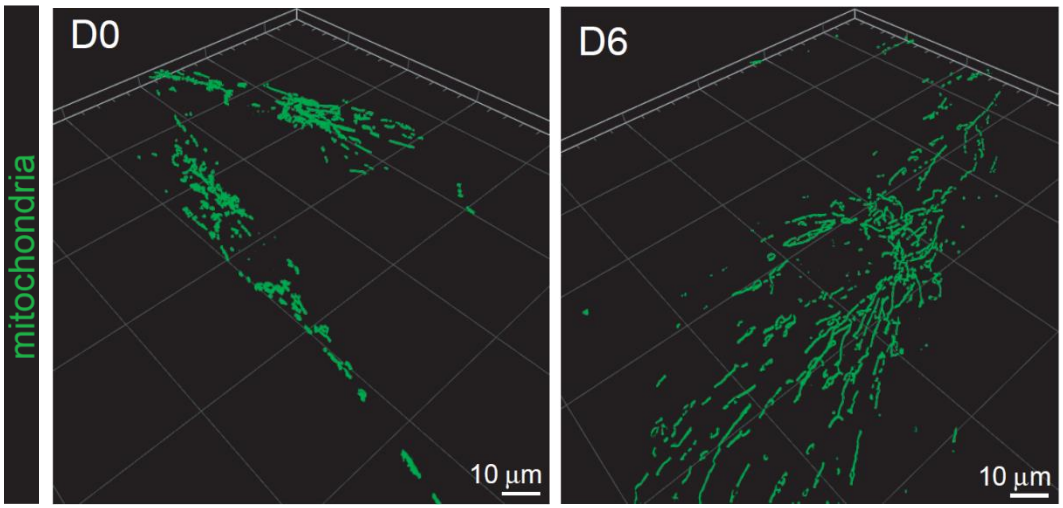


Figure 36. Decidualization reshapes the mitochondrial network morphology.
Three-dimensional representation of the mitochondrial network of proliferative (D0) and decidualized (D6) T-HESCs. The reconstruction was performed with Arivis 4D software based on representative immunofluorescences of TOM20 at 100x magnification (see Figure 28-29). Scale bar: 10 µm

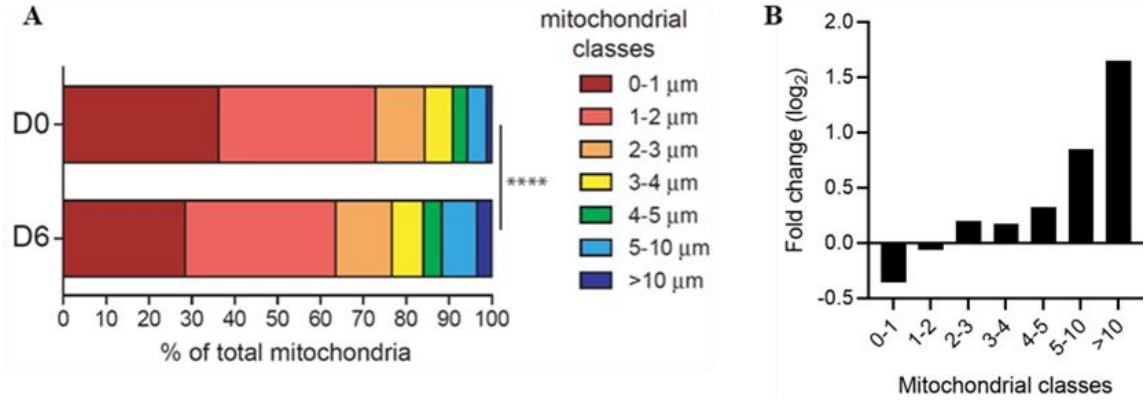


Figure 37. The elongation of mitochondria increases with decidualization.
Morphological analysis of mitochondrial elongation: analysis of the main axis. A. Length distribution analysis. Mitochondria were grouped in arbitrary length classes, based on their main axes. Results were expressed in proportion with the total number of mitochondria analyzed in two independent replicates (≥ 25 cells for both conditions). ****: $p \leq 0.0001$, Kolmogorov-Smirnov test. B. Comparison between the distribution of mitochondria in different length classes. Results expressed as $\log_2$ of the fold change calculated for each length class.

The effectiveness of the approach followed was limited in the perinuclear area of EnSC, as the mitochondria of the perinuclear area form a net-like, highly interconnected network, that cannot be properly segmented and was therefore excluded by the morphological analysis. This was not completely unexpected, as functional networks of fused mitochondria had been

previously described in other cell types (Skulachev 2001, Zamponi 2018). As these structures were mostly observed in decidualized cells, the morphological analysis partially underestimates the shift of mitochondria towards a fused state.

However, it is also important to underline that both proliferative and decidualized cells as required for homeostasis, quality control and organelle transport (Westerman 2010, Zamponi 2018, Li 2022). This confirms that the mitochondrial network remains indeed dynamic, and that the elongation observed in decidualized cells doesn't represent a state of dysfunctional hyperfusion.

This was further confirmed by live imaging, based on the fluorescent probe Mitotracker Red. As expected from the previous immunofluorescences, decidualized cells displayed a core of elongated, static mitochondria, but also several smaller mitochondria, actively transported along the cell, as well as several examples of fusion and fission events (Figure 38).

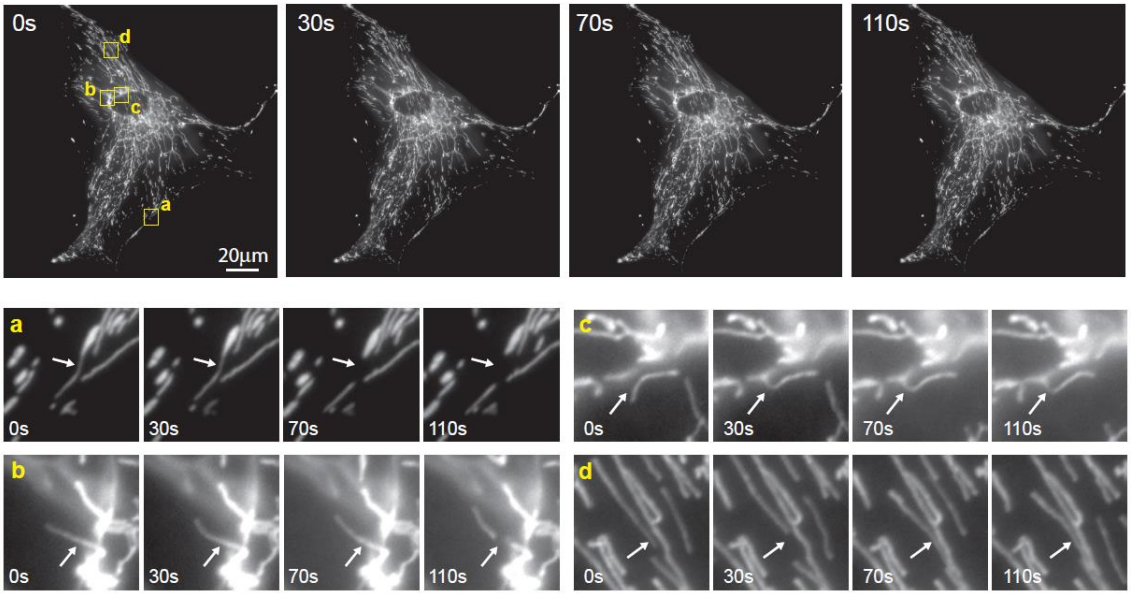


Figure 38. Despite their elongation, mitochondrial of decidualized cells are highly dynamic. Live fluorescence imaging of the mitochondrial network in a decidualized cell (day 6 of decidualization). Representative time-lapse acquisition after Mitotracker Red staining. Details showing event of mitochondrial fission (a-b) and fusion (c-d) events are shown in the lower panels. 60x magnification; bar: 20 µm

3.2 Ultrastructural analysis of mitochondria and ER-mitochondria interactions

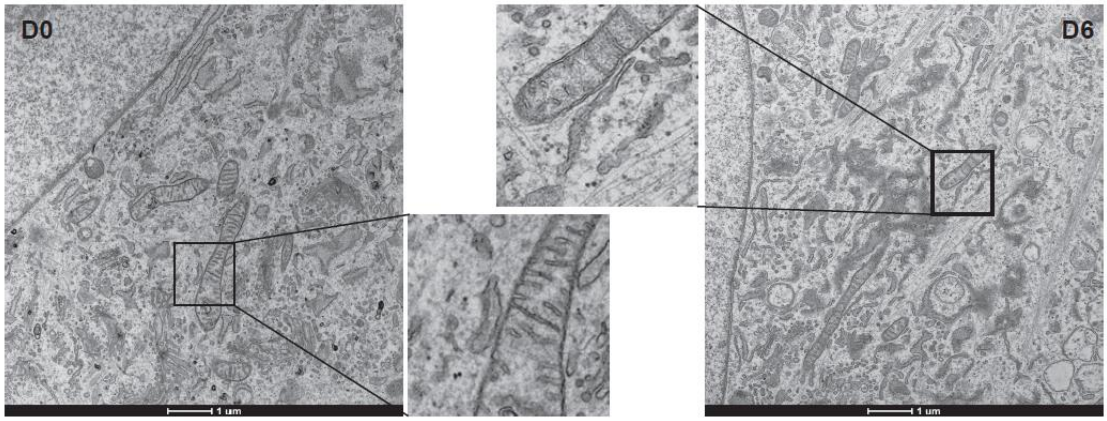


Figure 39. Transmission electron microscopy reveals close interactions between ER and mitochondria.
Transmission electron microscopy of proliferative (left) and decidualized (right) T-HESCs. Details including contacts between ER and mitochondria are shown for both panels with the same magnification factor. Representative images of three independent replicates. Scale bar: 1 µm

To better characterize the morphological changes of the mitochondrial network, I analyzed control and decidualized cells with transmission electron microscopy (TEM), focusing my attention on mitochondria and on their interaction with the ER (Figure 39).

In most of the sections derived from both control and decidualized cells, I could detect a high number of mitochondria. The organelles were identified based on standard morphological parameters, namely the presence of the double membrane and of the *cristae*. In case of dubious identification, the organelle was not included in the analysis (Figure 39-40).

Although the morphology of individual mitochondria varied greatly, the majority of the organelles had normal structure and well-organized *cristae*. When visually inspected, however, mitochondria of decidualized cells displayed a reduced number of morphological alterations compared to the ones of cells in control conditions (80.05% vs 60.84% of completely correct morphology respectively, based on visual evaluation of morphological parameters). This could possibly reflect a more stringent or more efficient quality control of the organelles in decidualized cells (Figure 39).

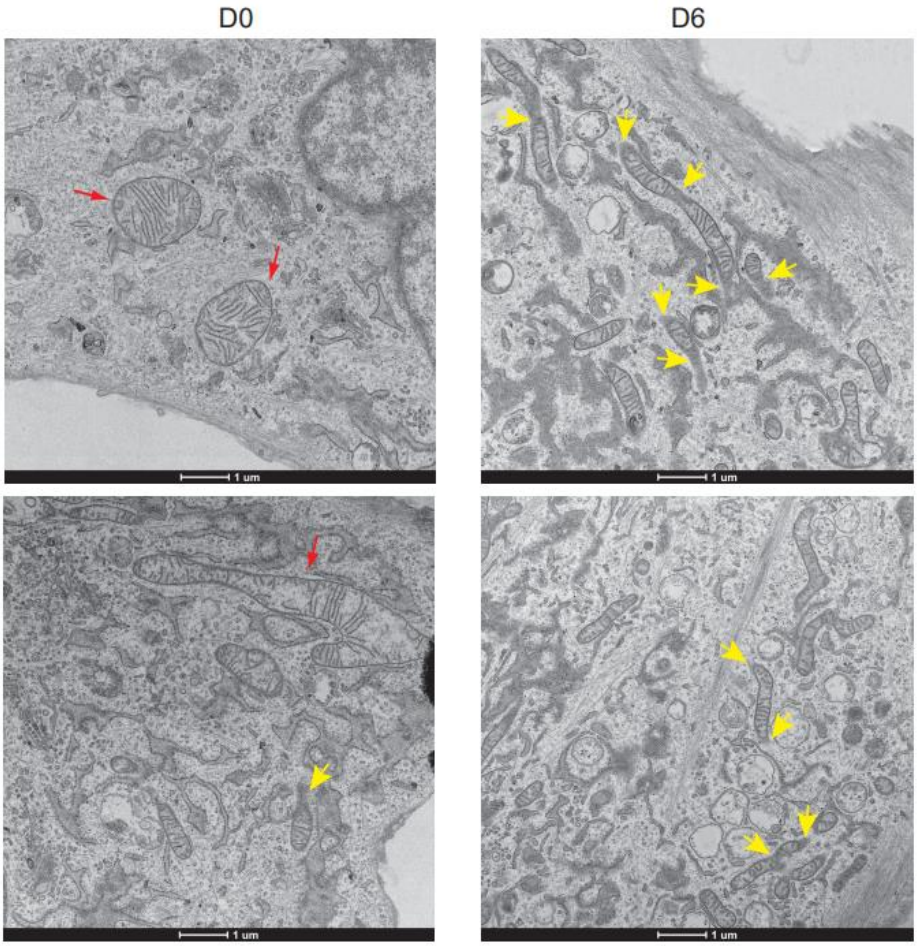


Figure 40. Highly elongated mitochondria are detected by TEM in decidualized T-HESCs
Transmission electron microscopy of proliferative (left) and decidualized (right) T-HESCs. Yellow arrowheads indicate points in which mitochondria would have crossed the sectioning plane. Red arrowheads indicate mitochondria with morphological abnormalities. Scale bar: 1 µm.

Coherently with what observed in immunofluorescence, some extremely elongated mitochondria could be observed, especially in slides derived from decidualized cells (Figure 40). However, it is well established (e.g. Bereiter-Hahn 1990) that mitochondrial morphology in ultrathin TEM sections does not completely recapitulate the physiological situation, as it reduces complex and dynamic three-dimensional objects to two dimensional snapshots.

It was therefore not surprising that most of the mitochondria identified in the EM sections, both in proliferative and decidualized cells, appeared as *bean-like* objects, roughly 1-2 µm long along the main axis.

Prevalence of short, highly fragmented mitochondria has been observed in both physiological and pathological conditions (Galloway 2012), and mitochondrial fission required for the transport and degradation of these organelles, as well as during cell division (Zorov 2019). This organization, however, appears to be in sharp contrast with what was previously observed in both immunofluorescence and live microscopy (Figures 42-43, 36-40). In this experimental setting, indeed, several of the small mitochondria observed in TEM actually correspond to individual, elongated objects, crossing several times the plane of the ultrathin section. This conclusion was supported by the presence of "shades" at one or both the ends of the objects (corresponding to transversal cuts), and the organization of the small mitochondria in clearly recognizable chains (actually corresponding to individual mitochondria), as indicated in Figure 40. Despite this, highly elongated mitochondria could be directly observed, especially in decidualized cells, when their main axis was parallel to the sectioning plane.

The artefactual sectioning of long mitochondria in smaller objects was observed in both conditions, even if it was apparently more frequent in decidualized cells. This was possibly due to the more complex and convoluted organization acquired by mitochondrial network in decidualization (see Figures 32, 33, 36 and 38).

As a result, the average size of individual mitochondrial objects (measured in the TEM images as area and perimeter) is apparently significantly decreased in decidualized cells (data not shown), in spite of other morphological parameters clearly highlighting elongation (decreased roundness and increased *aspect ratio*) (Figure 41).

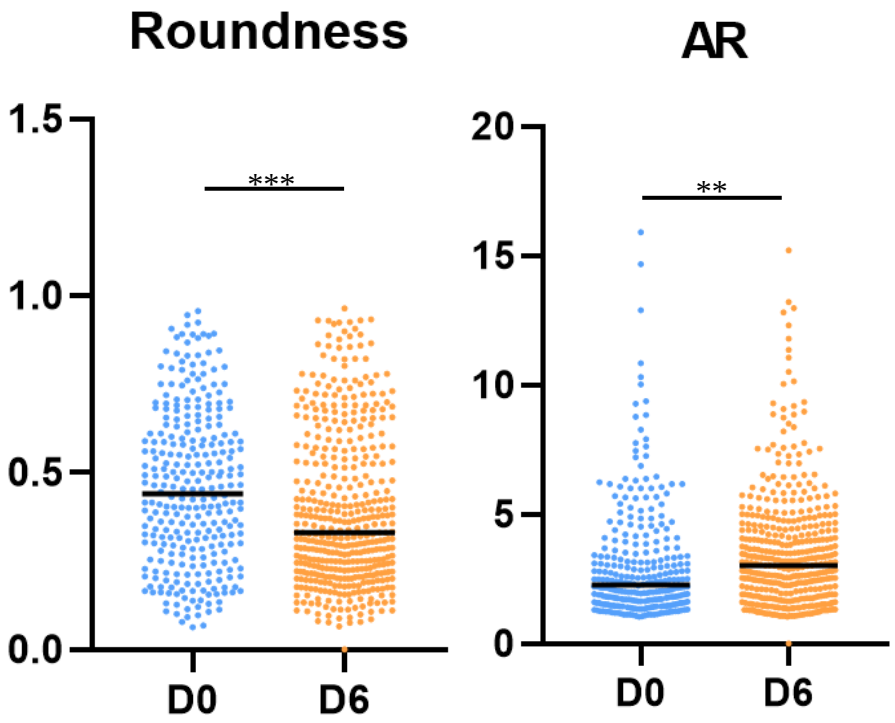


Figure 41. Ultrastructural analysis confirms mitochondrial elongation in decidualized cells. Morphological analysis of mitochondria based on the TEM images acquired in three independent replicates. The elongation of individual objects was expressed as roundness and aspect ratio (that is, the ratio between the major and the minor axes of the ellipse best fitting the object shape). The plots show the median and the individual values D0 = proliferative cells; D6 = decidualized cells. **: $p \leq 0.01$; ***: $p \leq 0.001$; t-test.

In several of the TEM images, a clear association between smooth ER and mitochondria was observed, either as simple proximity or as close, organized contacts, with precise alignment of the organelle membranes (Figure 39).

The precise definition of "contact" between ER and mitochondria has been widely debated in the literature (e.g. Simmen 2018), and an in-depth analysis of these aspects is beyond the scope of the project. Briefly, different types of Mitochondria-ER Contact sites (MERCs) exist in the cell, and one type can dynamically convert into another one based on the metabolic needs of the cell (Sood 2014, Simmen 2018).

Close interactions between the two organelles (10-25 nm, up to 50 nm according to some classifications) represent well-organized structures, stabilized by tethering molecules and enriched in specific transporters and enzymes (Vance 2014): this type of contacts, indeed

mediates the exchange of calcium (Szabadkai 2006), lipid biosynthesis intermediates (Vance 2014), and reactive oxygen species (Debattisti 2017), as well as mitochondrial fusion and fission events (Friedman 2011, Abrisch 2020).

However, sites presenting a larger cleft between the membranes (up to 80-90 nm), not particularly organized in terms of membrane juxtaposition, and even presenting ribosomes on the ER membrane (ribo-MERCs), have been proposed to play a role in the crosstalk between mitochondria and ER, in particular for calcium exchange (Giacomello 2016).

In my analysis, I decided to focus on the canonical Mitochondria-ER contacts, more characterized in terms of function and clearly recognizable based on morphological features.

Based on previous literature (Sorrentino 2022), MERCs were identified based on a distance threshold of 30 nm between aligned membranes, in the absence of other elements clearly interfering with the contact (e.g. ribosomes on the ER membrane, cytoskeleton filaments crossing the putative contact…).

The analysis showed that the number and the length of the contacts established by ER and mitochondria is significantly increased in decidualized cells, especially when normalized on mitochondrial size (Figure 42).

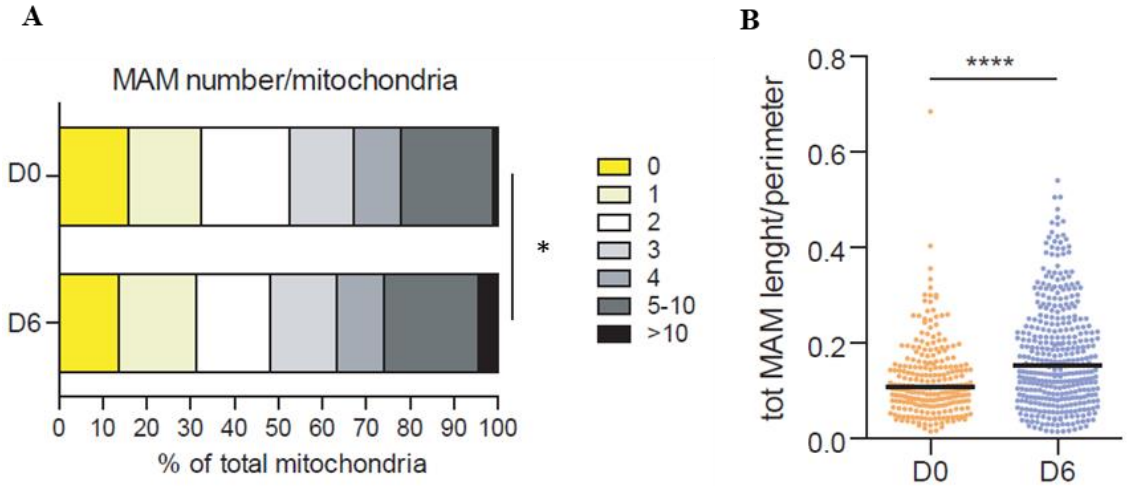


Figure 42. ER and mitochondria increase their association during decidualization.
TEM-based analysis of mitochondria-ER contact sites. A. Classification of mitochondria based on the number of contact sites established with the ER. Results expressed in proportion with the total number of mitochondria analyzed for each condition. *: p≤ 0.05, Mann-Whitney test. B. Analysis

of the total length of the MERCs established by each mitochondrion, normalized over the size of the mitochondrion itself (that is, the perimeter of the object in TEM images). ****: $p \leq 0.0001$, t-test.

This, combined with the other results, suggests that the reorganization of the mitochondrial network observed in decidualization is indeed instrumental to support the functional reshaping of EnSC: a closer association between the organelles, indeed, would provide a more efficient exchange of high-energy molecules, phospholipid intermediates, calcium ions and reactive oxygen species.

It can instead be excluded that the observed increase of the MERCs only depends on confounding factors, such as stochastic proximity of the organelles due to ER expansion: indeed, no dramatic difference in the cellular crowding was observed, and the stringent threshold reduces the possible impact of random juxtaposition of organelles in the quantification of the contacts.

3.3 ER and mitochondria closely associate in endometrial stromal cells

Given the results obtained in the TEM analysis, I verified the association between the mitochondria and different components of the ER on a larger scale, by co-immunofluorescence.

As previously described (Results, section 1.2), the protein markers corresponding to the protein-folding and quality control machinery of the ER, such as PDI (Figure 9 and 43) and CRT (Figure 6 and 43) are largely concentrated in the perinuclear area. The staining for structural components of the organelle, such as reticulon 4 (RTN4), display instead a broader staining, with ER tubules detected also in the very periphery of the cell (Figure 9 and 43).

Mitochondria, stained with the Mitotracker Red dye, appear to co-localize only partially with the markers of the protein-folding compartments. Conversely, they appear to be more closely associated with more general ER markers, corresponding to both the rough and the smooth ER components (Figure 43).

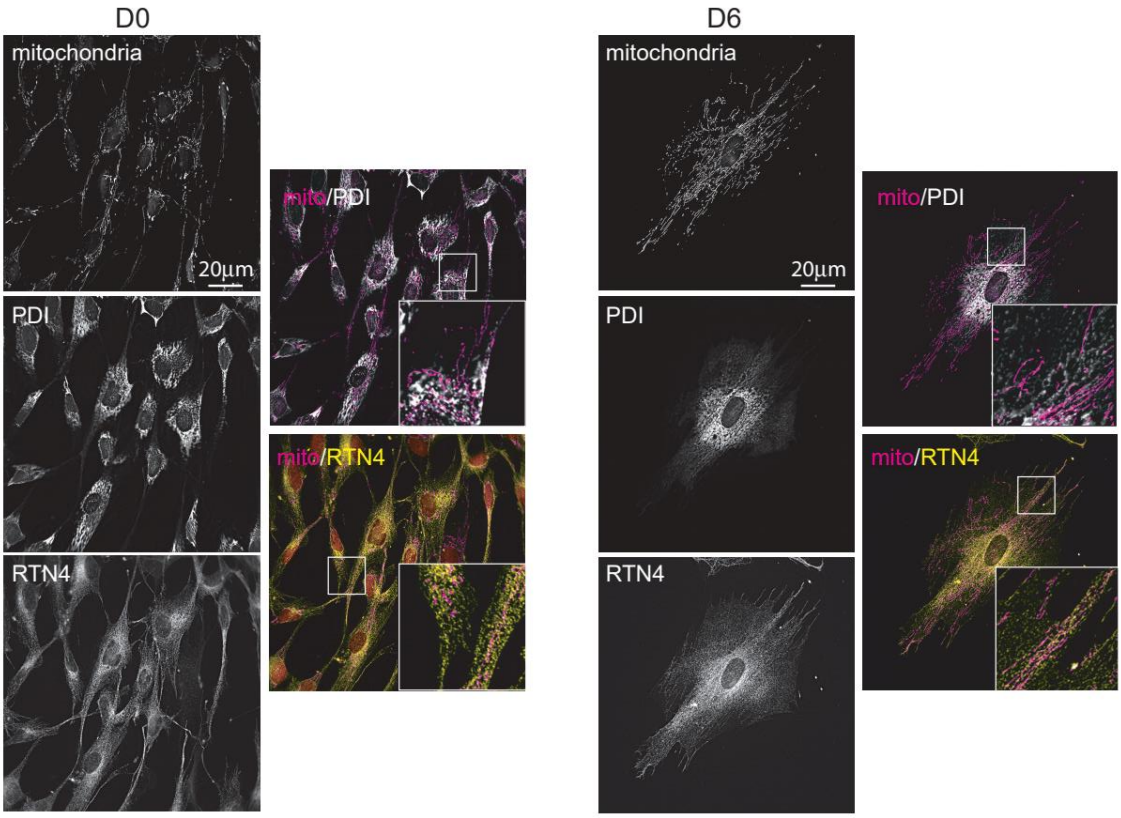


Figure 43. Mitochondria partially colocalize with different ER markers.
Co-immunofluorescence of mitochondria (stained by Mitotracker Red), PDI (rough ER) and RTN4 (smooth and rough ER). Details of the co-localization of ER markers and mitochondria are shown. Scale bar: 20 µm.

The relative distribution of ER and mitochondria, combined with the high number of MERCs observed in TEM, provides interesting insights about the role of mitochondria in EnSCs. Mitochondria are partially associated with the protein-folding compartment of the ER in the perinuclear area, and that part of the mitochondrial network is dramatically expanded in decidualization. This likely corresponds to the most intuitive functions of mitochondria in a secretory cell type, such as providing an adequate energy supply to protein synthesis and folding machineries.

Instead, the peripheral components of the network, substantially extended during decidualization, are likely dedicated to alternative functions, such local production of ATP

for vesicular transport and cytoskeleton dynamics, but also exchange of lipid intermediates and calcium with the smooth ER, and/or ROS scavenging (Skulachev 2001, Rowland 2012).

3.4 A metabolic switch: increase in respiration, decrease in glycolysis

As the results previously presented supported the idea of mitochondrial network enlargement as an intrinsic element of the decidualization process, I decided to evaluate if this also corresponds to a readjustment of the energy metabolism.

To this aim, T-HESC in control condition and in decidualized state were compared in a Seahorse Mito Stress Test for mitochondrial respiration. In this assay, acidification (ECAR) and oxygen consumption (OCR) are quantified by microelectrodes in the volume of medium immediately above the cell layer, as drugs interfering with the mitochondrial function are sequentially added. Briefly, cells were first exposed to oligomycin (a blocker of the ATP synthase), followed by FCCP (an uncoupling agent, allowing free movement of protons across the mitochondrial membrane), and antimycin and rotenone (blocking respectively respiratory complex I and III), as schematized in Figure 44.

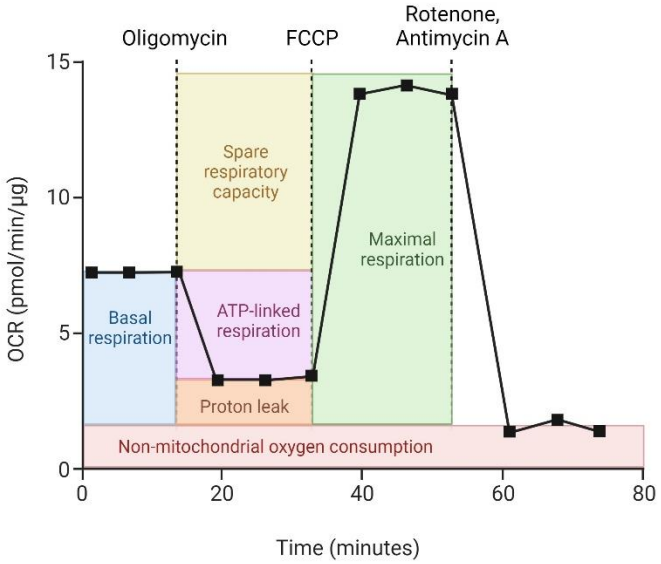


Figure 44. Seahorse mitochondrial stress test.
Schematic representation of the Seahorse metabolic assay for mitochondrial activity, showing in detail the different components of the respiratory profile. Created in BioRender on a template by Daisy Shu, PhD, Harvard Medical School.

In this way, detailed information about mitochondrial respiration and glycolysis in the cells could be precisely dissected (Figure 45-47).

The assay showed that decidualization significantly modifies the respiratory profile of the cells, with a general increase of oxygen consumption, but also an improvement in the efficiency of the process (Figure 45-46).

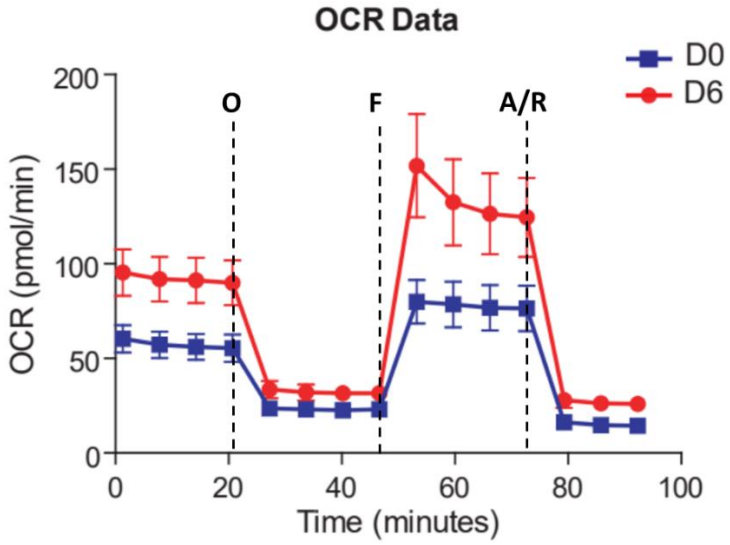


Figure 45. Decidualization increases mitochondrial respiration of T-HESC and modifies their respiratory profile.
Seahorse mito-stress test assay for mitochondrial respiration. Respiratory profile representative of two independent replicates. The addition of drugs is indicated on the graph by the dashed lines. O: oligomycin; F: FCCP; A/R: antimycin and rotenone

Indeed, the basal respiration and the amount of oxygen devoted to ATP production are higher in decidualized than in proliferative cells; the proton leak, a parameter roughly corresponding to incomplete mitochondrial coupling (Jastroch 2010), is instead reduced after the differentiation process (Figure 45-46).

Interestingly, our results also showed a dramatic increase of both the maximal mitochondrial respiration and the spare respiratory capacity (Figure 45-46): this finding indicates that the mitochondria of decidualized cells could produce significantly more energy, to eventually cope with a sudden increase of the metabolic needs of the cell.

Moreover, it further suggests that a significant fraction of mitochondria, in decidualized cells, may be mostly involved in functions independent from energy production, such as calcium buffering, ROS scavenging and lipid biosynthesis.

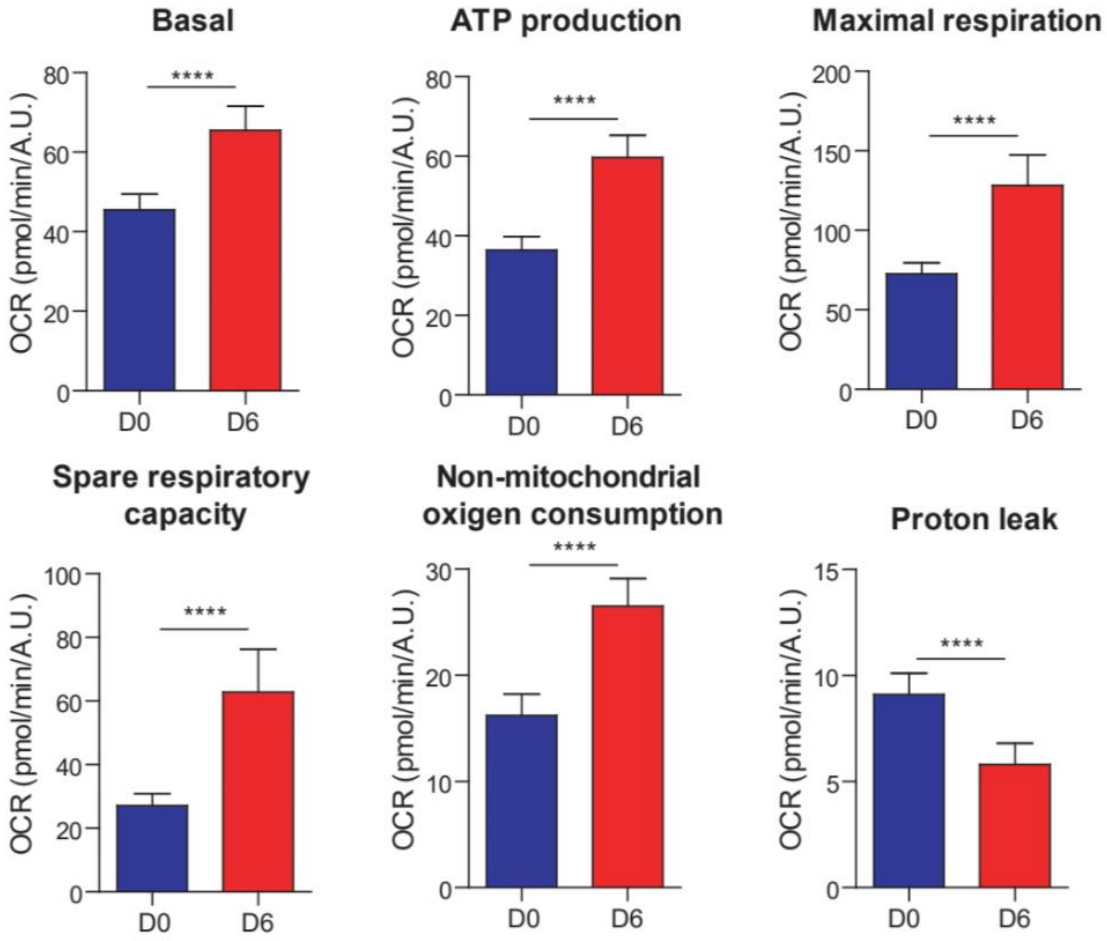


Figure 46. Detailed analysis of mitochondrial respiration rewiring in decidualization.
Comparative representation of the mitochondrial respiration parameters, based on the respiratory curves shown in Figure 45. All the parameters are expressed as oxygen consumption rate normalized over the fluorescence intensity of a DNA-binding dye (roughly corresponding to normalization on cell number). ****: $p \leq 0.0001$, t-test, calculated on the biological replicates analyzed in the experiment.

It is important to highlight that the rewiring of the energy metabolism observed during decidualization seems to be more profound than a simple increase of the mitochondrial

activity: indeed, the increased mitochondrial respiration is paralleled by a contemporary decrease of glycolysis, and thus by a dramatic change in the OCR/ECAR ratio (Figure 47).

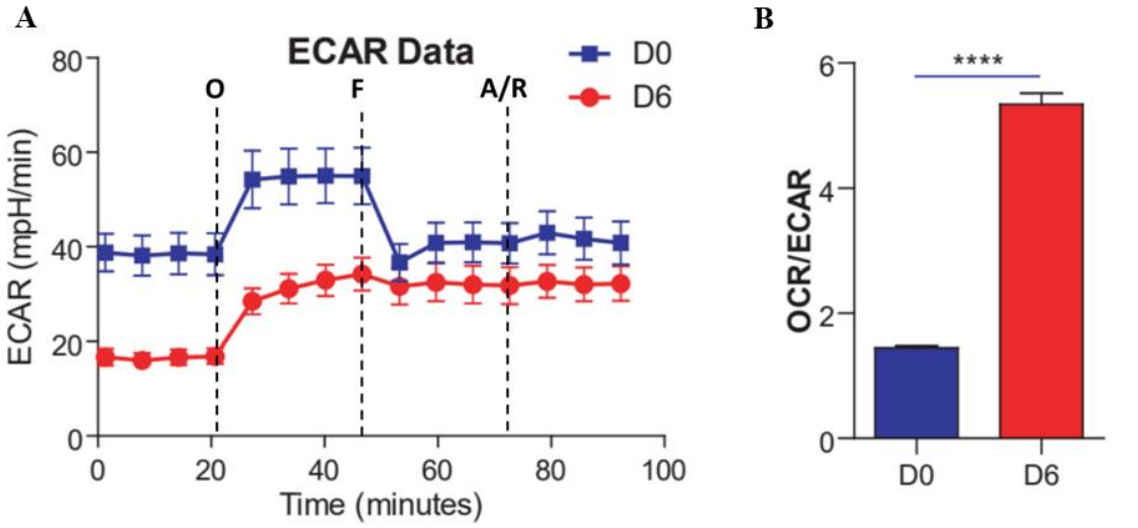


Figure 47. Decidualization reduces glycolysis and induces a switch in the energy metabolism. A. Extracellular acidification profile, measured in parallel with the respiratory profile described in Figure 45-46. B. OCR/ECAR, that is ratio between basal respiration and basal extracellular acidification (which is representative of glycolysis). ****: $p \leq 0.0001$, t-test, calculated on the biological replicates analyzed in the experiment.

Even if a more detailed characterization of the EnSC energy metabolism is beyond the scope of this project, the results obtained provide an interesting insight about the coupling between protein secretion and bioenergetics. Indeed, the results suggest that decidualized EnSC are in general terms more metabolically active than cells in proliferative state, coherently with the increased production of secretory cargoes and the extensive vesicular trafficking. At the same time, cells seem to be more parsimonious in the use of glucose, with a switch from glycolysis to oxidative phosphorylation, and possibly the use of alternative energy sources (as briefly discussed in the following section).

The metabolic rewiring observed in our *in vitro* model of decidualization likely reflects some important aspects of the physiological process. On one side, the extension of the spiral arteries in the endometrial tissue provide the tissue with oxygenated blood, allowing efficient mitochondrial respiration (Pijnenborg 2006). On the other, it seems logical that glucose consumption is reduced, in a context in which epithelial and endometrial stromal cells

accumulate glycogen deposits, required for the successful implantation of the embryo (Gellersen 2014).

3.5 Transcriptional analysis of mitochondrial genes

To better characterize mitochondrial network remodeling, an unbiased transcriptional analysis of the mitochondria-related genes was performed (Figure 48), similarly to what was previously described for secretory pathway genes (Results, paragraph 1.5). To validate the transcriptome analysis, selected genes from the pathways of interest were then individually analyzed by qPCR (Figure 49).

This approach, although lacking the depth of a complete functional analysis, provided a general overview about changes in mitochondrial activities not considered in the previous analyses.

As expected from the previous results, genes involved in the oxidative phosphorylation (OXPHOS) were in general upregulated, with a general induction of both the nuclear and the mitochondrial encoded OXPHOS genes (Figure 48-49). Accordingly, the ORA of the up-regulated genes detected the induction of the terms corresponding to the assembly factors of the respiratory chain (OXPHOS assembly factors), and to the respiratory complexes themselves (OXPHOS subunits), with the former preceding the latter in the induction (Figure 49).

Interestingly, the mitochondrial encoded OXPHOS genes displayed a peculiar expression pattern, different from the one observed for nuclear genes: while at the end of decidualization both the groups are clearly up-regulated, all the mitochondrial genes seem to decrease their expression in the first phase of decidualization, reaching their minimum at 24 hours.

As the products of the two groups of genes must be present with a precise stoichiometry in the respiratory complexes, an imbalance in their expression is unlikely to have a functional meaning. Instead, the pattern observed at the beginning of decidualization could correspond to the superimposition of two opposite events: the replication arrest of EnSCs, corresponding to a block in mitochondrial duplication; and a general enlargement of the mitochondrial network, widely described in this section of the thesis. Apart from these speculations, however, a detailed analysis of mtDNA expression is beyond the scope of this project.

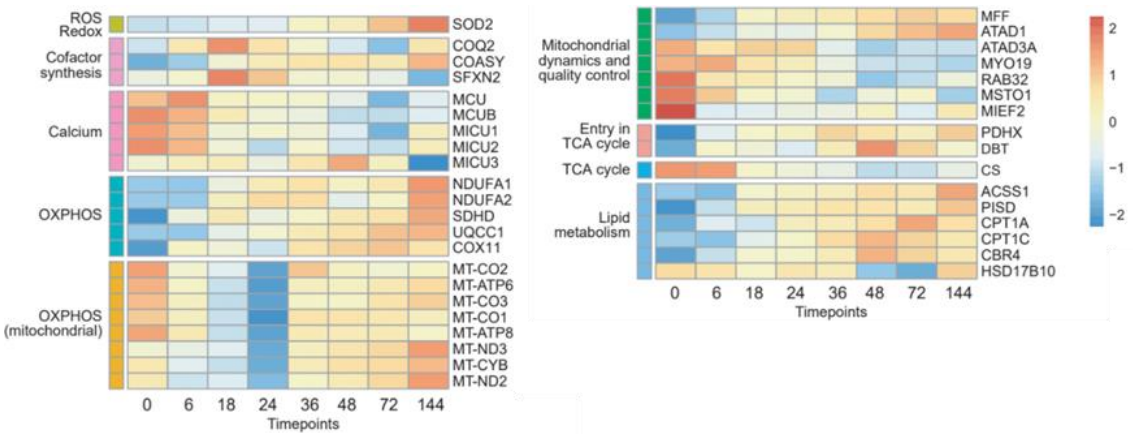


Figure 48. Decidualization reshapes the transcription pattern of mitochondrial genes.

Heat map of genes differentially expressed during the decidualization program. Expression values were z-normalized and represented as a color scale. The genes were selected as grouped based on the biological functions mediated by their products. Mitochondrial encoded OXPHOS genes were considered as a separated group, based on the peculiarity of their expression mechanisms.

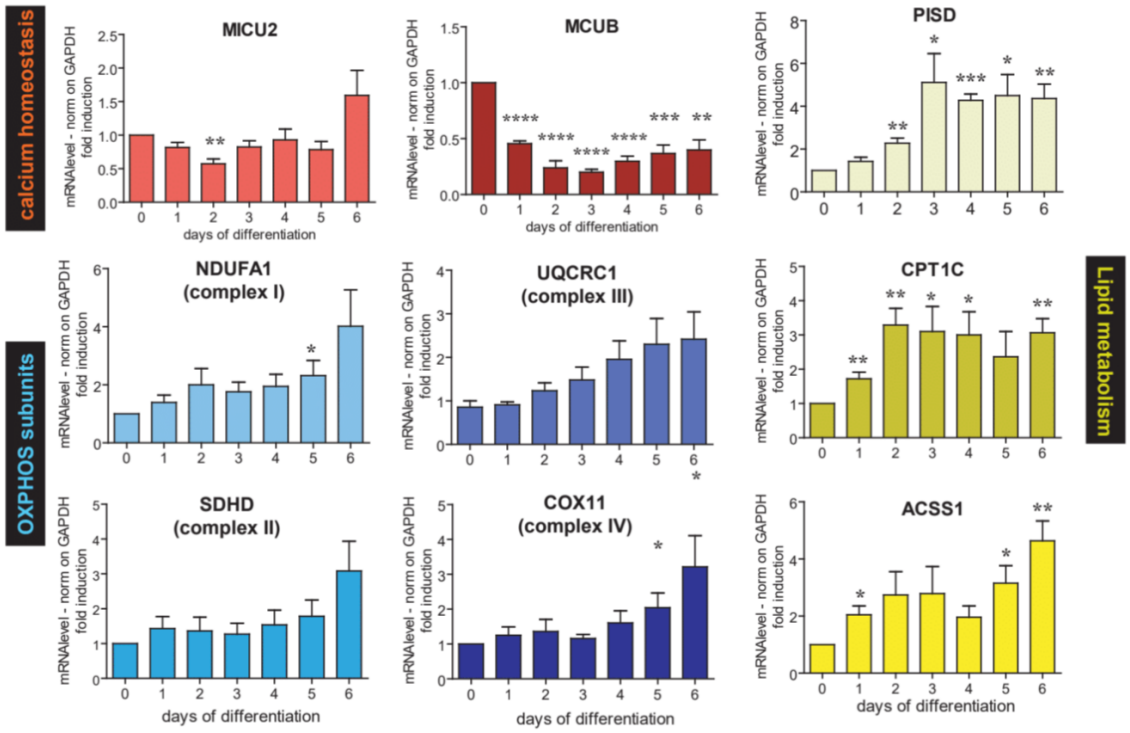


Figure 49. Analysis of individual genes confirms transcriptional induction or repression of key mitochondrial functions.

Real-time qPCR analysis of genes involved in mitochondrial calcium homeostasis, lipid metabolism and oxidative phosphorylation. The samples correspond to RNAs collected at different days of *in vitro* decidualiation of T-HESC, with a minimum of three independent

replicates. Results were normalized on GAPDH mRNA and represented as mean ± SEM. *: $p \leq 0.05$; ** $p \leq 0.01$; ***: $p \leq 0.001$; ****: $p \leq 0.0001$; t-test of each time-point versus d0.

In support of our hypotheses about the importance of ER-mitochondria connection for decidualized cells, the genes related to functions such as ROS detoxification and phospholipids biosynthesis were also induced during the decidualization process. Quite surprisingly, genes involved in mitochondrial calcium import and homeostasis, another function depending on the MERCs (Patergnani 2011), are instead downregulated. This likely underlines slight changes in the nature of the interaction between the organelles (Figure 48-49). Lipid and amino acid metabolism are also among the most up-regulated mitochondrial functions, with a clear transcriptional induction of key enzymes for fatty acid beta-oxidation (ACSS1, CPT1A, CPT1C). Even though a functional validation would be required to draw any definitive conclusion, these results further support the concept of a radical switch in the metabolism of decidualizing cells, possibly including a change in the prevailing energy sources. (Figure 48-50).

Interestingly, genes related to mitochondrial DNA (mtDNA) replication and maintenance, and to translation in the mitochondrial matrix were instead mostly classified as down-regulated. These was reflected by the expression pattern of individual genes (some of which are shown in Figure 48 in the group *Mitochondrial dynamics and quality control*), but even more strikingly by the ORA, in which *mtDNA replication and maintenance* emerged by far as the most down-regulated mitochondrial process along the decidualization program.

This result is probably due to the switch of EnSC a proliferative phenotype (in which the mitochondria are duplicated, with their protein content and genomes, at every cell replication), to the terminal differentiation of decidualized cells (in which mitochondria are enlarged and maintained, but not as actively replicated) (Figure 48-50).

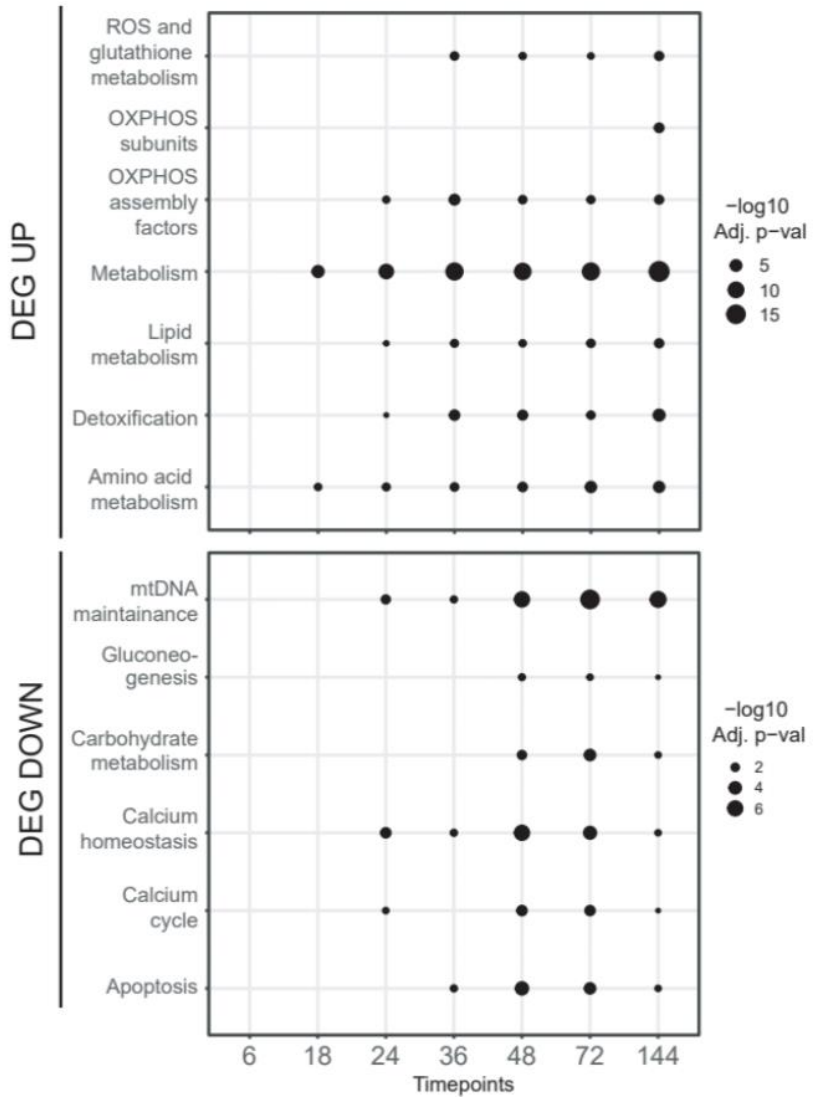


Figure 50. Time-course analysis of mitochondrial gene transcription reveals early and profound functional changes during the decidualization process.
Over-Representation Analysis for the genes upregulated (DEG UP) or downregulated (DEG DOWN) at different time points. GO terms associated with different biological functions of mitochondria were analyzed in the time-course RNA sequencing. Statistical significance of the over-representation is graphically represented by the different size of the circles.

3.6 A glimpse of regulation: the nuclear translocation of PGC-1a

The results previously described show that mitochondria are extensively remodeled during decidualization, and that rewiring of the mitochondrial network and function is likely important for the decidualization process. However, they don't explain whether

mitochondrial reshaping represents a response to the increased metabolic needs of the cell, or are instead an intrinsic element of the differentiation program itself.

The extensive changes observed in the transcriptome analysis as early as 24-48 h after induction, far before any major change in the expression of the cargo (Figure 48-50, support the idea of a transcriptional regulation of mitochondrial genes as an early event of EnSC decidualization.

To validate this hypothesis, I decided to verify whether the transcriptional activation of mitochondrial genes can actually be observed in the very first phases of the decidualization program. The induction of mitochondrial genes is a complex process, controlled by specific transcription factors. As the majority of mitochondrial proteins are nuclear-encoded, their transcription mostly depends on the nuclear translocation of factors such as Nrf1, Nrf2, PPARα, PPARγ and PGC-1α; the last one, in particular, is considered to be the master regulator of mitochondrial biogenesis and factors, due to its capacity to interact with and regulate the activity of the other ones (Abu Shelbayeh 2023).

Therefore, I considered the nuclear translocation of PGC-1α as a readout for a general transcriptional induction of mitochondrial genes.

As hypothesized, the fluorescence signal corresponding to this transcription factor is re-localized from the cytoplasm to the nucleus in the earliest phases of decidualization: the nuclear signal already peaks at 6 hours after decidualization induction and remains high for at least the following 24 hours (Figure 51).

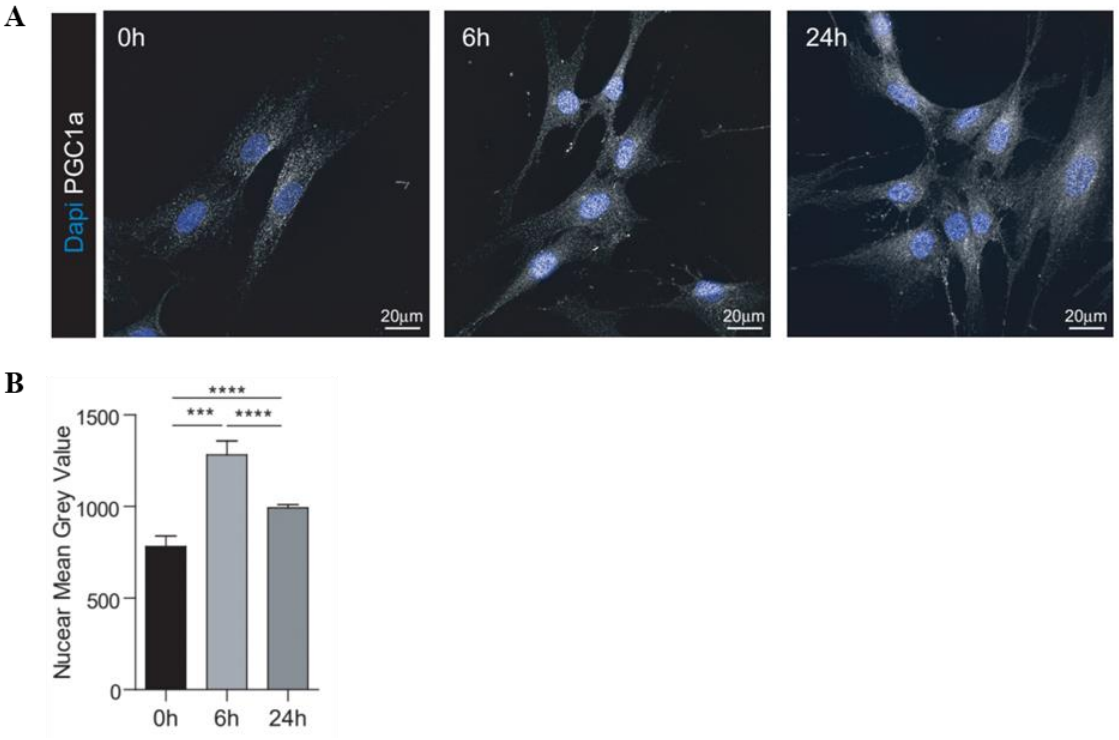


Figure 51. Nuclear translocation of PGC-1α is an early event of T-HESC decidualization.

A. Immunofluorescence of PGC-1α at early time-points of decidualization. Nuclei were counter-stained with DAPI to verify the nuclear translocation of the transcription factor. Images representative of two independent replicates. 60x magnification; scale bar: 20 µm.

B. Quantification of the nuclear translocation of PGC-1α. The graph represents the average intensity of PGC-1α immunostaining in the nucleus, ± SEM. ***: $p \leq 0.001$; ****: $p \leq 0.0001$; one-way ANOVA.

This result further suggests the idea of mitochondrial induction as a part of the decidualization program itself. Similarly to what was observed for the secretory pathway organelle, the mitochondrial network is preventively enlarged and enhanced. This preparation strategy, compared to a strategy based on on-demand responses, ensures that the bioenergetic needs of the cell will be always and completely covered during decidualization, allowing an efficient development of the secretory capacity.

4 A general change in the cellular landscape: preliminary data on zinc quantification in EnSC secretory pathway

As highlighted by the results presented in the previous sections, endometrial stromal cell decidualization entails a complete reshaping of the secretory pathway organelles, but also a general rewiring of the cellular metabolism. Almost all the aspects considered, from cell morphology to the expression of groups of genes, from mitochondrial respiration to vesicular transport are somehow modified, to support the production, transport, and secretion of large amounts of secretory proteins. Inside the secretory organelles, the *toolbox* of chaperones and enzymes is also reorganized, to create the optimal environment for the folding and processing of the new protein cargoes. This, most likely, is not limited to protein expression, but instead involves also inorganic ions and other cofactors.

To further investigate this aspect, rarely considered in the study of cell differentiation programs, I decided to analyze the dynamics of zinc in the secretory pathway organelles of EnSC during decidualization.

Zinc represents a fundamental cofactor for several proteins, ranging from factors to metalloproteases (Maret 2016); the physiological levels of this metal ion are tightly regulated by dedicated transporters and metal-binding proteins (Roohani 2013). In the secretory pathway, the concentration of zinc is significantly higher in the Golgi complex than in the ER (Kowada 2021), by effect of a precise localization of zinc importers and exporters (Amagai 2023).

The loading of a zinc ion in the catalytic site is fundamental for the activity of metalloproteases and other enzymes, a process called *metalation* (Kambe 2017); moreover, zinc concentration seems to play important roles in the homeostasis of the secretory organelles (Amagai 2023), and in the formation of secretory granules of some hormones, including prolactin (Vang 2022).

In the following paragraphs, I described the strategy I followed to determine the zinc concentration in the Golgi complex, and the results obtained by the comparison of control and decidualized cells.

4.1 Generation and validation stable cell lines for subcellular zinc quantification

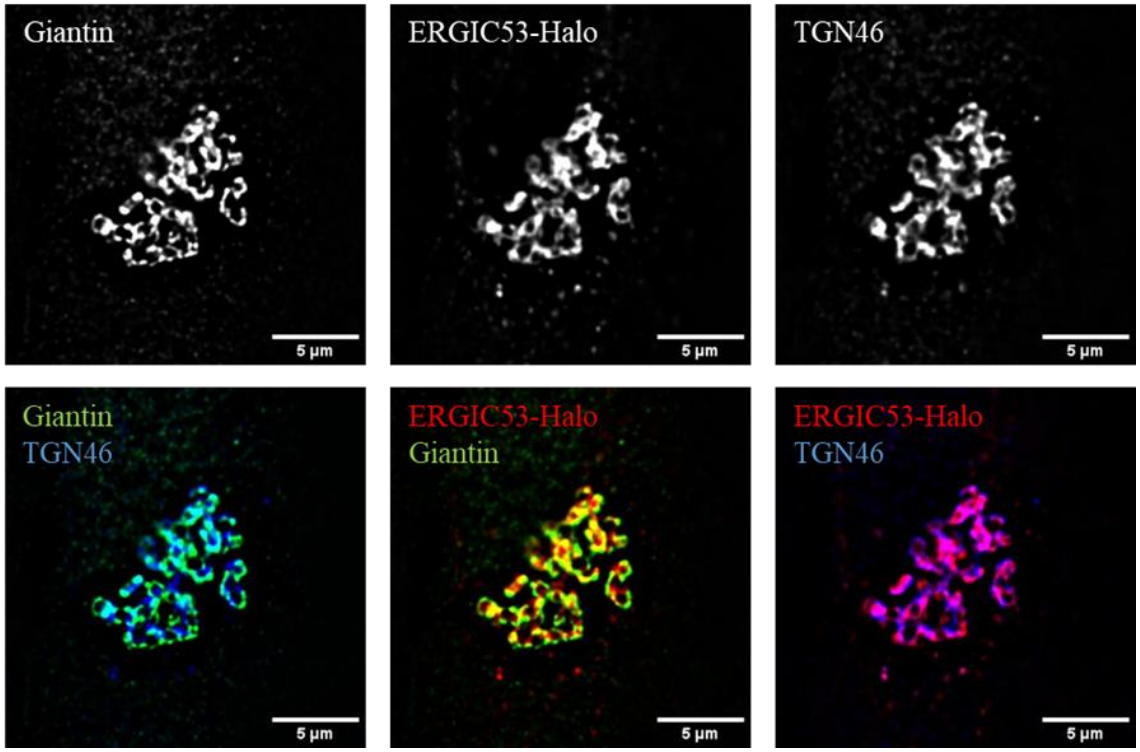
To evaluate the impact of decidualization on the concentration of zinc ions in the secretory pathway organelles, I took advantage of constructs generated by our collaborators from Professor Kenji Inaba's lab, in Tohoku University, Sendai.

These plasmids encode for fusion proteins, containing a Halo-tag and a single transmembrane domain of different Golgi proteins: this allows a precise localization of the probes in different Golgi sub-compartments, from the ERGIC to the *trans*-Golgi.

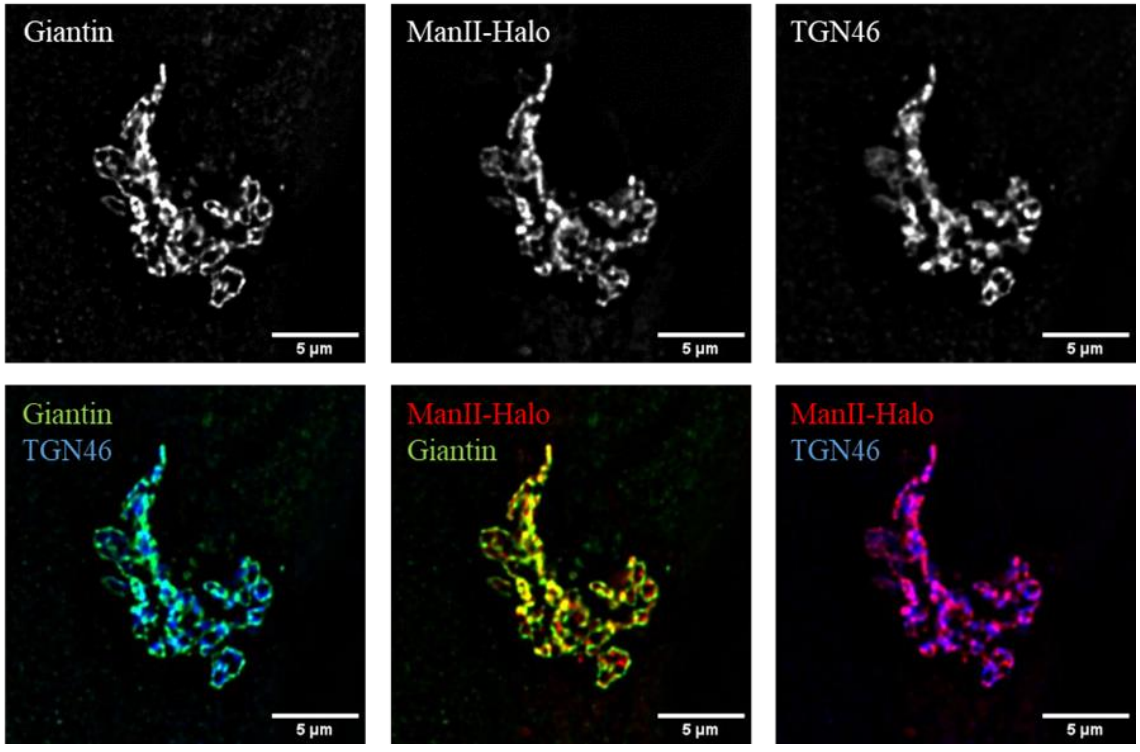
More in detail, the fusion proteins included ERGIC53, the transmembrane portion of ManII (amino acids 1-117), and the transmembrane portion of GalT (amino acids 1-61). The Halo was positioned at the N-terminus in the ERGIC53 fusion protein, and at the C-terminus for the other ones, so that it was localized in the lumen of the organelle.

The probes were transiently expressed in T-HESC cells, and their localization was confirmed by co-immunofluorescence with different Golgi markers. Based on the different degrees of co-localization observed, I confirmed that the different constructs were expressed in the expected compartment. As expected, ERGIC53-Halo and ManII-Halo showed a greater degree of co-localization with cis-Golgi marker giantin, while GalT-Halo was more closely associated with the trans-Golgi marker TGN46 (Figure 52).

A


Giantin
ERGIC53-Halo
TGN46
5 µm
Giantin
TGN46
ERGIC53-Halo
Giantin
ERGIC53-Halo
TGN46

B


Giantin
ManII-Halo
TGN46
5 µm
Giantin
TGN46
ManII-Halo
Giantin
ManII-Halo
TGN46

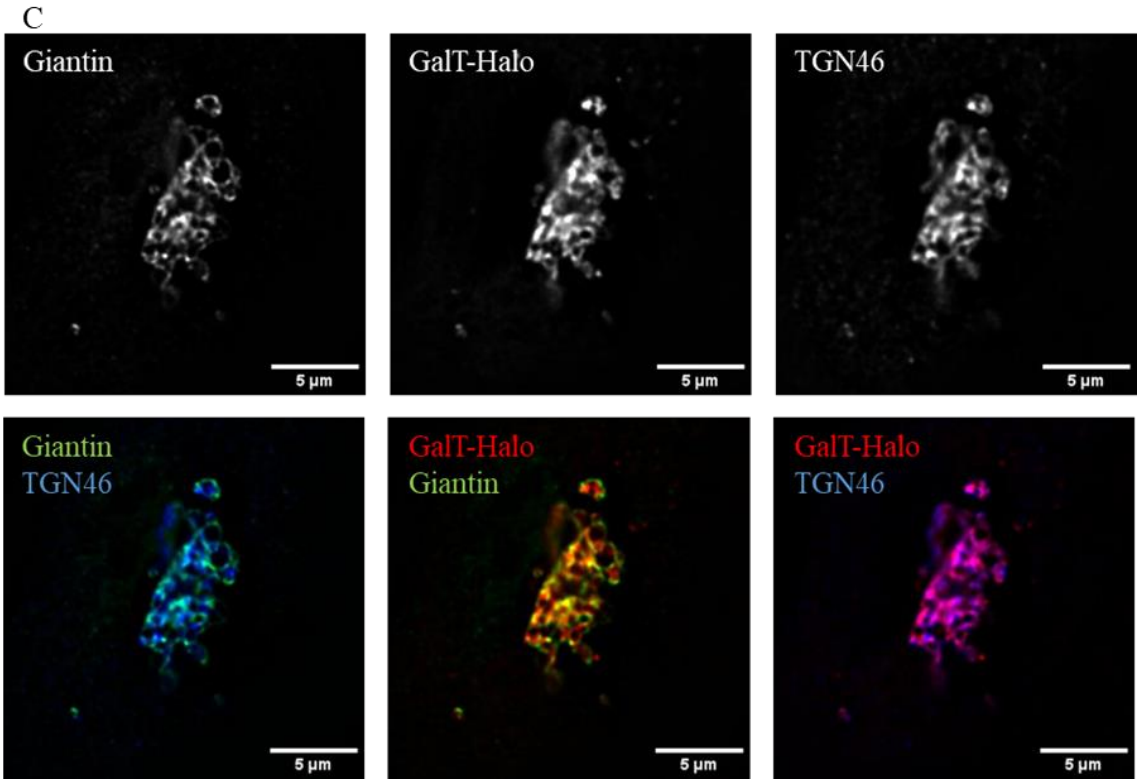


Figure 52. Co-immunofluorescence with Golgi markers confirmed the correct sub-organelle organelle localization of the Halo-tagged probes.

Co-immunofluorescence of the Halo-tagged probes (labeled by TMR Red Halo direct ligand) with the *cis*-Golgi marker giantin and the *trans*-Golgi marker TGN-46. Representative images for each probe are displayed in panels A-C. Single channel images and merges of each couple of channels are shown. 100x magnification, scale bar 5 µm.

Due to the low efficiency of T-HESC transfection, and the technical difficulties of combining the transfection and the decidualization protocols, I decided to generate lines stably expressing the construct of interest.

Although single cell cloning of T-HESC by limiting dilution is technically possible, as demonstrated by proof-of-principle experiments, the growth of isolated T-HESC was extremely slow, and a very low number of colonies could be obtained. Therefore, I decided to proceed with a pool-based approach, based on transfection and selection by acquisition of antibiotic resistance. The protocol resulted in mixed populations, expressing the Halo-tagged constructs at various levels, but with only a minimal fraction of Halo-negative cells.

In the stable cell lines, the localization of the Halo-tagged proteins corresponded to what observed in transient expression, and to the expected localization of the corresponding proteins. Despite the overexpression, no significant accumulation in the ER was observed for any of the probes (Figure 53). Despite the manipulations and the prolonged culture time, all the cell lines maintained the correct morphological features, and responded as expected to the decidualization stimuli: both the transgenic protein and endogenous protein markers revealed a general enlargement of the secretory pathway organelles (Figure 54).

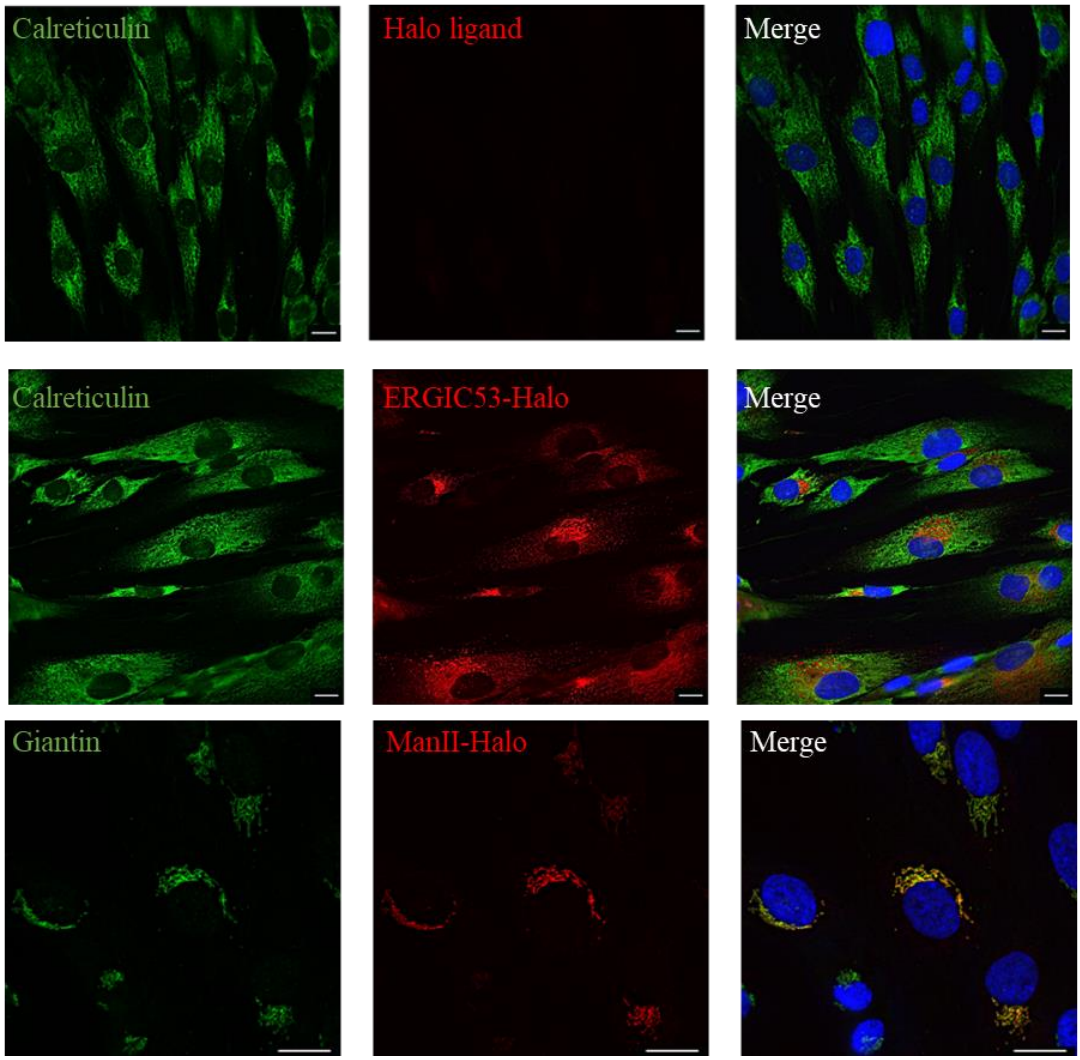


Figure 53. The Halo-tagged probes are expressed and correctly localized in the stable T-HESC cell lines.

Co-immunofluorescence of the Halo-tagged probes (labeled by TMR Red Halo direct ligand) with the ER and *cis*-Golgi markers. Upper panel: Negative control, included to evaluate background or nonspecific signals. Middle panel: Immunofluorescence for calreticulin on cells expressing

ERGIC53-Halo. The distribution of the probe corresponds to the localization of the endogenous proteins, as shown in Figure 9. Lower panel: Immunofluorescence for giantin on cells expressing ManII-Halo; a cell not expressing the probe can be seen in the lower left angle of the image. Upper and middle panels: acquired with a 60x magnification, scale bar 15 µm; lower panel: acquired with a 100x magnification, scale bar 20 µm.

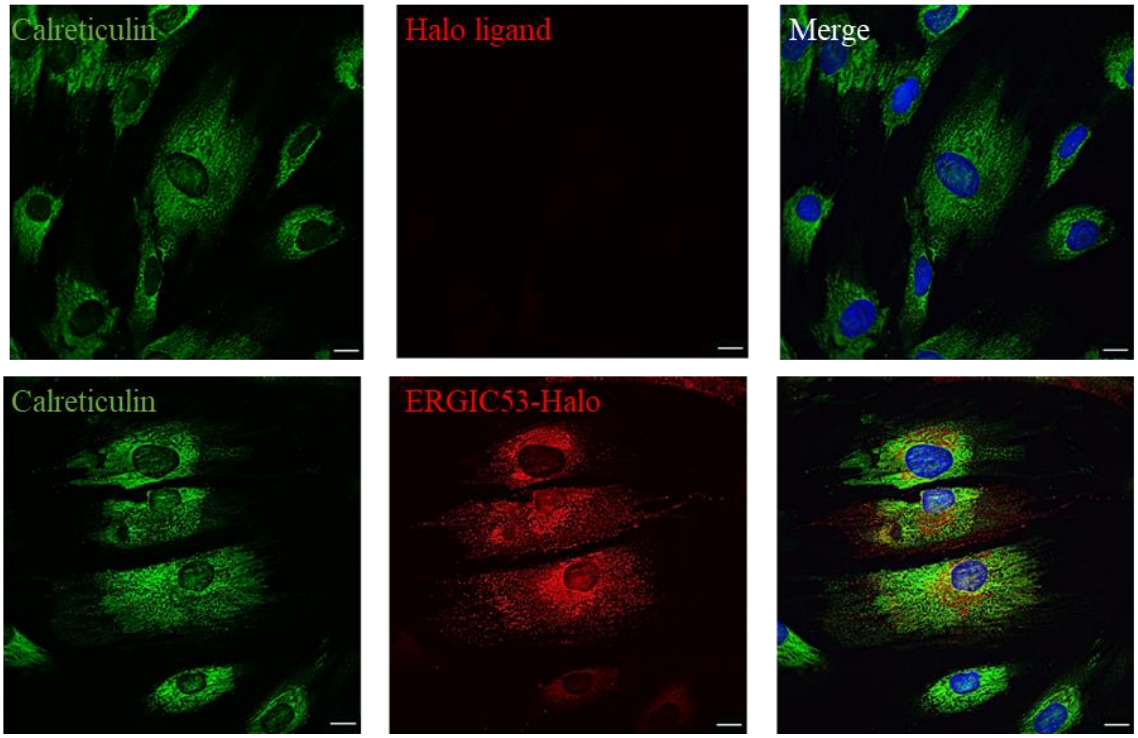


Figure 54. Cell lines expressing the Halo-tagged probes can be correctly decidualized. Co-immunofluorescence of the Halo-tagged ERGIC53 (labeled by TMR Red Halo direct ligand) with the ER marker calreticulin in decidualized T-HESC stable cell lines. Cells display the expected morphological changes, and the localization of the probe corresponds to the distribution observed for endogenous ERGIC-53 in decidualized cells. Cells not expressing the probe were used as a negative control for background or nonspecific signals. Images acquired with a 60x magnification.

4.2 Golgi measurement of pH and zinc at a sub-organelle level

With the cell lines I obtained and validated, I proceeded to the comparative quantification of labile zinc in the secretory pathway of proliferative and decidualized cells.

The strategy I followed was based on what previously described by Kowada et al. (Kowada 2021, Amagai 2023), duly adapted to my experimental system. Briefly, the Halo-expressing cells were incubated with a zinc-sensitive fluorescent Halo ligand (ZnDA-1H),

and with a zinc-insensitive ligand (HaloTMR Direct ligand), used to localize the cells and verify focus stability (Figure 55). The measurement of the basal zinc-depended fluorescence, combined with an appropriate calibration (Figure 56), provided the quantification of the labile zinc pool in the compartment of interest, as more extensively described in Materials and Methods.

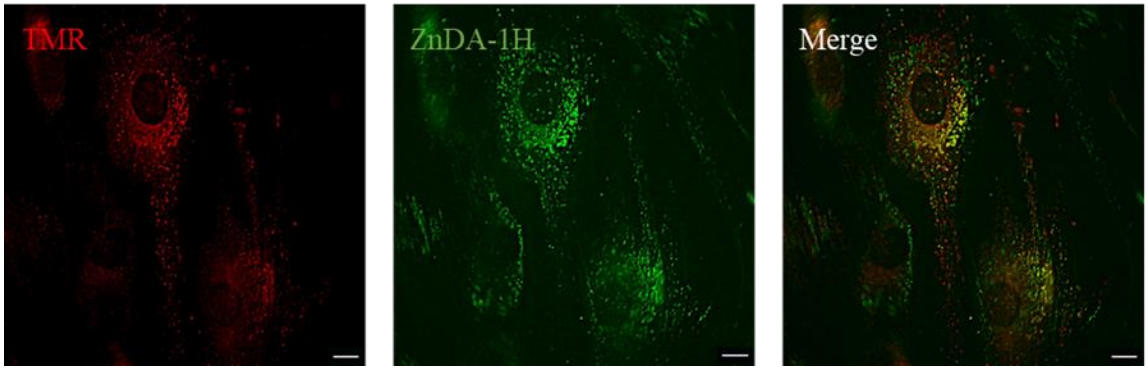


Figure 55. TMR and ZnDA-1H can be correctly detected in the T-HESC lines expressing the Halo-tagged probes, as required for the labile zinc quantification.
Live-imaging microscopy of T-HESC stably expressing Halo-tagged ERGIC53, labeled with a combination of HaloTMR Direct ligand and ZnDA-1H zinc-sensitive fluorescent ligand. Representative images, acquired with a 40x magnification.

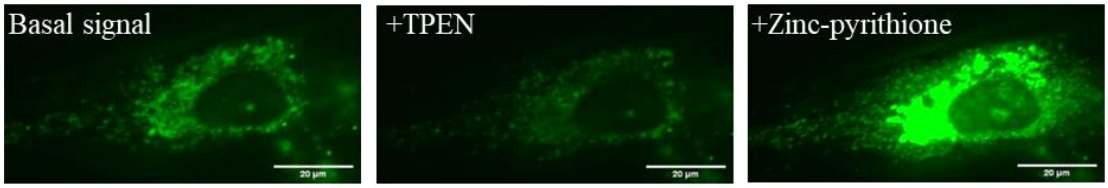


Figure 56. ZnDA-1H fluorescent signal can be modulated, as expected, by zinc chelation and by addition of exogenous zinc.
Representative live imaging of ZnDA-1H signal calibration in T-HESC lines expressing the Halo-tagged protein ERGIC53. The three panels display signal intensity in basal conditions (Ringer buffer containing 2 µM Zn-SO_4), upon addition of the zinc chelator TPEN, and upon addition of the membrane permeant zinc-pyrithione complex, as described in Materials and Methods. Representative images, acquired with a 40x magnification. Scale bar: 20 µm.

In the literature, ZnDA-1H is described as a relatively robust probe, characterized by a high specificity for zinc and a minimal affinity for other biologically relevant metal ions, such as copper or iron (Kowada 2021). However, the apparent affinity of this probe for zinc

can be influenced by pH, even if only wide variations of this parameter (e.g. 1 pH unit) can significantly impact the final results (Kowada 2021, Amagai 2023).

For this reason, in parallel with the labile zinc quantification, I performed a pH measurement based on the fluorescent probe pHluorin2. This small, fluorescent protein changes its excitation spectrum in response to pH, thus allowing a microscopy-based evaluation of this parameter (Mahon 2011).

The same transmembrane domains used for the Halo-tag constructs were used to localize the pHluorin2 in the different compartments of the Golgi complex (Figure 57), thus allowing a direct comparison between the pH and zinc measurement (Kowada 2021).

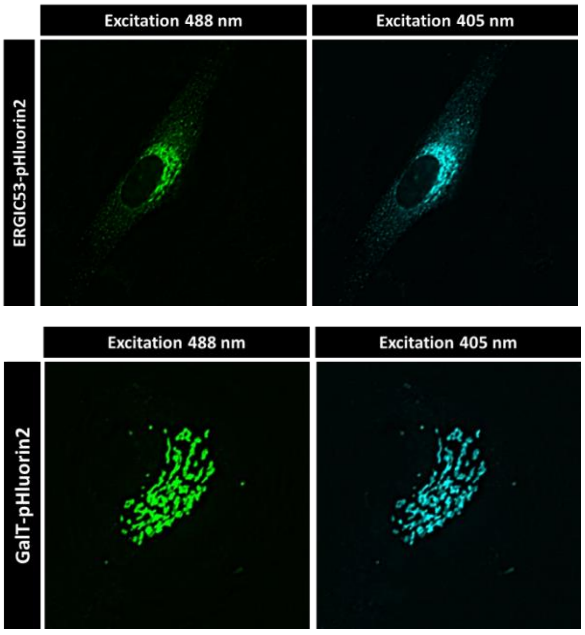


Figure 57. Golgi-localized fluorescent pH probes (pHluorin-2) can be correctly expressed in control and decidualized T-HESC by transient transfection.
Representative fluorescent images of pHluorin-2 probe transfection in T-HESC. Upper panel: ERGIC-localized pHluorin-2 in proliferative cells. Lower panel: *trans*-Golgi localized pHluorin-2 in decidualized cells. The two channels represent emission at 525 nm, after excitation at the indicated wavelengths. Images acquired with a 60x magnification.

At the time of the writing, the results obtained are rather preliminary, but promising. Both the quantifications could be performed successfully, and revealed some interesting differences between cells in proliferative and decidualized cells.

The pH measurement provided results in line with the previous literature, with values between 6.5 and 6.0, and a progressive acidification from the *cis* to the *trans* side of the organelle (Ma L. 2017, Rivinoja 2012). In decidualized cells, interestingly, a strong reduction of the pH was observed in the ERGIC, probably corresponding to a steeper acidification gradient in the early secretory pathway; slightly lower pH values were observed also in the other Golgi sub-compartments (Figure 58).

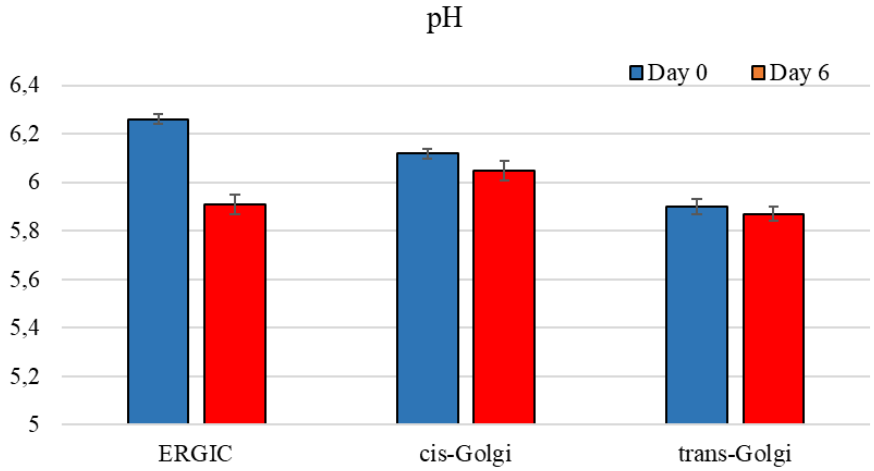


Figure 58. Decidualization induces a slight acidification of different sub-compartments of the Golgi complex.
Fluorescence-based pH quantification in the Golgi, based on the transient expression of Golgi-localized pHluorin-2 probes. Results representative of a minimum of three independent experiments, represented as mean ± SD.

On the base of the pH quantification, the apparent K_d of ZnDA-1H was set to 0.54 µM in the calculations (Kowada 2021). The concentration of labile zinc measured in T-HESC secretory pathway was higher than what observed in other studies (Amagai 2023), but comparable with them. Interestingly, the observed zinc distribution changed with decidualization: in decidualized cells, a higher concentration was observed in the ERGIC, while the opposite was observed in the *cis*-Golgi. The quantification in the *trans*-Golgi

compartment, based on the GalT-Halo probe, were incomplete at the time of the writing, and were not included in this thesis.

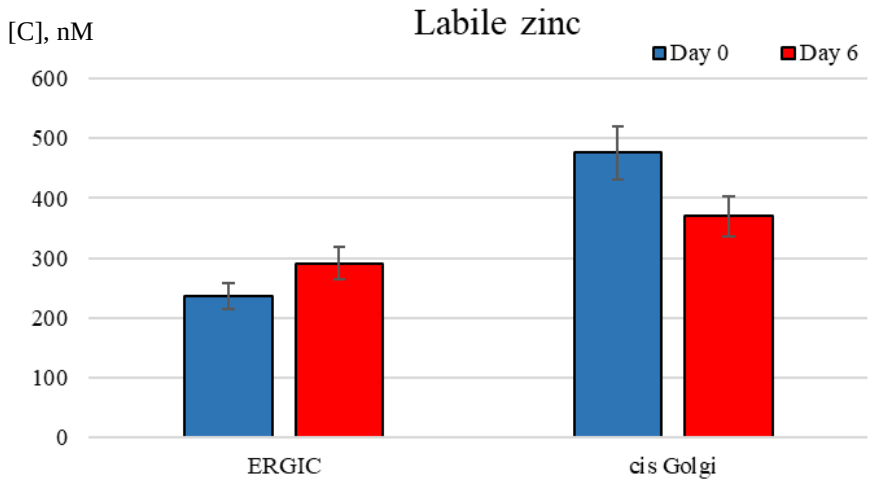


Figure 59. The labile fraction of zinc in different sub-compartments of the Golgi complex is modified by decidualization.
Fluorescence-based quantification of labile zinc fraction, measured by ZnDA-1H in cells stably expressing Golgi-localized Halo-tagged proteins. Results representative of multiple cells in a minimum of three independent experiments, represented as mean ± SD.

The results presented, although very preliminary, highlight some general changes in the intra-organelle *landscape* of the secretory pathway, with differences not only in the content of enzymes, chaperones and protein cargoes, but also in the concentration and distribution of inorganic ions. These differences likely depend on the tightly regulated expression of channels and transporters, of proteins binding and buffering metal ions, and of proteins using them for their biological functions.

In this regard, it is important to underline that the quantification performed can only detect the labile zinc pool (that is, the fraction susceptible to chelation), and provides no details about the fraction strongly associated with proteins.

Even if this part of the project was only explorative, and doesn't lead to definitive conclusions, it is possible to speculate that zinc regulation in the secretory pathway may represent a crucial aspect of decidualization.

Zinc-metalloproteases are some of the most upregulated cargoes in EnSC differentiation program (see Figure 17), and the formation of zinc-prolactin complexes has important roles in the secretion of this hormone (Lorenson 1996, Vang 2022).

In line with the increased production of zinc-requiring proteins, key regulators of Golgi zinc homeostasis appear to be transcriptionally induced in decidualization, according to preliminary results obtained in the lab (data not shown). Real-time qPCR, indeed, showed an interesting up-regulation of zinc importers localized along the Golgi complex (ZnT4, ZnT5, ZnT6 and ZnT7), as well as of metallothioneins (MT1 and MT2), small proteins that bind metal ions in the cytosol and allow their safe transport across the cell by preventing stochastic reactivity.

Similarly, GPHR, the ion transporter responsible for Golgi acidification (Maeda 2008), is also induced in decidualization. This result seems particularly relevant, as the ZnTs are antiporters that counterbalance the import of zinc with an efflux of hydrogen ions (Ishihara 2006). These results were partially confirmed by the transcriptome analysis of decidualization, in which a similar transcriptional induction is observed for the zinc transporters (not shown).

The strong upregulation of ERp44 consistently observed in decidualization may also represent an interesting aspect of zinc homeostasis in EnSC secretory pathway: this protein, involved in disulfide quality control and in the retrieval of ER chaperones, is directly regulated by zinc, which controls its function, its subcellular localization, and its secretion (Tempio 2021, Amagai 2023).

Based on these observations, a detailed investigation of zinc dynamics, zinc transporters and zinc-binding proteins could represent an interesting direction for a more complete understanding of EnSC decidualization physiology.

DISCUSSION

The results obtained during my PhD provide new, interesting insights about the peculiar morphological and functional rewiring program that characterize the decidualization of endometrial stromal cells.

Even though the dynamics of the endometrial tissue have been extensively investigated, indeed, very little focus has been put on the most "basic" aspects of the decidualization, such as the precise morphological changes of EnSCs, or the dynamic rearrangements of their organelles.

At a first sight, these aspects may appear very distant from the clinics, and may only seem important for a descriptive characterization of decidualized cell phenotype. It is important to remember, however, that decidualization is a fundamental secretory differentiation program, and that the physiological functions of EnSCs depend on their capacity to efficiently produce and secrete cargo proteins. Any alteration in the dynamic rearrangements of the organelles, or in the expression of the correct cocktail of chaperones and enzymes, would inevitably affect the secretory capacity of decidualized cells, with severe consequences for health and -especially- fertility.

On the other hand, EnSC decidualization could also represent a powerful system for the study of secretory pathway organelles. Indeed, the decidualization program can be induced in vitro in a simple and reproducible way, by means of well-established differentiation protocols and robust cellular systems. EnSCs can be studied almost in real time during their differentiation program, and both early events and terminal differentiation can be investigated.

Therefore, the analysis of decidualization could also provide new insights about the induction, regulation, and function of the secretory pathway organelles, and of the Golgi complex in particular.

1 Morphological and functional reshaping of the secretory pathway organelles

In my study, I demonstrated how profound is the reshaping of EnSCs, from fibroblast-like cells to protein factories. As parts of a well-oiled machine, all the components of the cell

reorganize to acquire the new morpho-functional phenotype: for sure, becoming a secretory cell doesn't only mean producing and secreting more proteins: it entails a complete commitment of all the organelles and cellular functions.

A general enlargement of the secretory pathway organelles was expected, considering the massive increase of the secretory capacity observed upon decidualization. This was also previously described in another in vitro model of decidualization, but no precise characterization was provided (Kajihara 2014).

The detailed analysis of the organelles, based on immunofluorescence for different organelle markers and on the morphometric analysis, revealed a surprisingly limited expansion of the endoplasmic reticulum, which remained substantially proportional to the total cell volume; this result was rather unexpected for a secretory cell, considering that a massive expansion of the ER is commonly observed in most secretory differentiation programs (Shaeffer 2004, van Anken 2003).

Conversely, a significant enlargement of the Golgi complex was observed, both in absolute terms and compared to the cell size. This aspect had been previously observed in samples derived from the murine endometrium (Bijovsky 1992), but never functionally linked to the secretory activity of EnSCs.

A significant development of the Golgi complex had also been described in some secretory cell types, such as pancreatic beta cells (Noske 2008), and prolactin-secreting cells of the mammary gland (Clermont 1993), but was not particularly significant in others, such as plasma cells (Shaeffer 2004). The size of this organelle in secretory cell types, indeed, seems to depend more on specific features of the cargo produced (for instance, the presence of complex glycan processing), than on the mere amount of the secretory cargoes themselves.

The physical enlargement of the secretory pathway organelles, as predictable, was paralleled by a general increase in the expression of chaperones, redox enzymes and Golgi proteins. While all the components of the protein folding, transport and processing machinery were in general terms upregulated, as expected for cells acquiring a secretory phenotype, EnSC decidualization presented interesting peculiarities.

Coherently with the morphological observations, proteins localized in the ERGIC and Golgi compartments (ERp44, ERGIC53, TGN46, and Giantin) were strongly upregulated during the decidualization program, together with some redox enzymes of the ER (PRDX4, GPX8, Ero1α). Instead, only a limited induction was observed for BiP or PDI, fundamental for the ER protein folding and massively up-regulated during the B-to-plasma cell transition (Shaeffer 2004, van Anken 2003).

Taken together, these results support the idea of secretory differentiation as a precise tailoring of the secretory organelles for the specific protein cargoes produced by the cell, and for the dynamics of secretion required for the cellular functions.

Upon decidualization, endometrial stromal cells secrete a wide array of different cargo proteins, some of which extensively glycosylated; the secretome of EnSCs evolves over time, in a complex interplay between the cells and the extracellular environment.

The type of cargoes and the pattern of secretion, therefore, are completely different, for instance, from the ones of a plasma cell, for which fast response and massive secretion of a single cargo are probably more relevant than long-term efficiency of the secretory organelles.

Interestingly, my results suggest that, in EnSC decidualization, the upregulation of the secretory organelles begins immediately after the exposure to decidualization stimuli, significantly anticipating the massive expression of the secretory cargoes. Possibly for this reason, the production of protein cargoes never exceeds the processing capacity of the cell: previous results demonstrated that –unlike in plasma cells- unfolded protein response is only minimally activated in decidualization (Anelli 2021), and that inhibition of the three UPR branches has no significant effect on the decidualization program (my Master Thesis results, unpublished).

2 Transcriptional regulation of organelle reshaping

The time-course transcriptome analysis of EnSC decidualization further demonstrated how deep and extensive is the reshaping entailed by this differentiation program. With thousands of genes already upregulated or downregulated in less than 24 hours after the

addition of the stimuli, EnSCs don't "simply" increase their secretory capacity, but instead they seem to undergo a functional metamorphosis.

Interestingly, important differences can be observed also among the genes encoding for different components of the secretory pathway organelles, thus suggesting a transcriptional reshaping, rather than a general induction.

A detailed analysis of the secretory pathway genes, indeed, revealed the existence of different clusters, characterized by peculiar patterns of expression, and enriched for genes encoding for specific functions. For two of the clusters, a strong downregulation trend was already observed at the first time-point, corresponding to 6 hours after the addition of the decidualization stimuli.

In the transcriptional regulation of secretory pathway reshaping, timing appears to be a crucial aspect: changes in the expression of some groups of genes (and the induction or inhibition of the corresponding biological functions) represented an immediate event of the decidualization program, while a significant delay was observed for other groups.

These patterns of induction likely correspond to co-regulation mechanisms acting on genes of the same cluster, and have an important functional meaning in the dynamics of secretory pathway organelles. To provide an example, most of the genes involved in ER-to-Golgi transport and in the organization of Golgi cisternae are induced very early in decidualization (cluster 5 of expression, Figure 18A), while the induction of Golgi glycosylation enzymes is delayed (cluster 3, Figure 18A). Thinking in terms of function, these patterns would provide the maximal efficiency to Golgi complex development, preventing upstream accumulation of the glycosylation enzymes.

The identification of CREB3L1 and CREB3L2 as key regulators of vesicular transport and Golgi dynamics provides an interesting insight about the molecular mechanisms regulating the secretory pathway dynamics. These factors, indeed, are induced and activated during the decidualization process, and appear to be fundamental for the correct induction of several secretory pathway genes.

The activation of CREB3L1 and CREB3L2 depends on the balance between their transport to the Golgi complex and their proteasomal degradation (Kondo 2007, Murakami

2009). Thus, these factors could also represent a link between the differentiation program itself and organelle homeostasis and autoregulation, similarly to what observed for UPR in other secretory cell types (Hetz 2012, So 2018, Iwakoshi 2003, Gao 2012)

These transcription factors had been previously described in contexts of secretion and secretory differentiation: indeed CREB3L1 and CREB3L2 are known to regulate collagen secretion (Saito 2009, Chen 2014). Accordingly, both spontaneous mutations in patients and experimental inactivation in animal models cause severe defects in skeletal development (Symoens 2013, Keller 2018, Lindahl 2018, Saito 2009). Moreover, they are fundamental for the correct development of some secretory cell types, such as thyrocytes (Garcia 2017) and hormone-producing cells of the pituitary gland (Khetchoumian 2019), both characterized by a well-developed Golgi complex.

In my experimental system, the correct expression of these transcription factors proved fundamental for the correct enlargement of the Golgi complex, and their inactivation had dramatic consequences on the secretory capacity of decidualized endometrial stromal cells. Upon silencing of CREB3L1 and CREB3L2, indeed, a dramatic ER accumulation of procollagen was observed, and the secretory activity of the cells is almost completely abrogated. In a physiological context, this would correspond to a complete impairment of EnSC functions, which require the efficient and timely secretion of cargo proteins.

To date, no association between CREB3L1/2 and fertility-related phenotypes have been reported in the literature; this is not very surprising, considering the severity of the skeletal phenotypes caused by CREB3L1/2 inactivating mutations, and the extremely low incidence of these pathological conditions (Symoens et al., 2013; Keller et al., 2018; Lindahl et al., 2018). Milder polymorphisms, or defects in CREB3L1/2 induction and activation during the decidualization process, however, could be involved in alterations of EnSC secretome, and therefore have a negative impact of embryo implantation. A detailed investigation of CREB3L1 and CREB3L2 in patients with unexplained infertility or recurrent early-stage pregnancy loss, therefore, could represent a promising direction for future research.

3 Mitochondrial network reshaping and rewiring of the mitochondrial metabolism

As demonstrated by my results, decidualization entails a complete reorganization of the mitochondrial network, and a significant modification of the mitochondrial metabolism. Similar to the rearrangements of the secretory pathway organelles, also the reshaping of the mitochondrial network emerges as an integral part of the decidualization program, regulated by an early induction of mitochondrial genes and by the activation of specific transcription factors.

In my experiments, I observed a dramatic enlargement of the mitochondrial volume, with important changes in the morphology of the network: decidualized cells, indeed, contained more mitochondria, and their morphology appeared to be significantly more elongated.

It is generally established (Skulachev 2001, Westermann 2010) that elongated and interconnected mitochondria are more efficient than small fragmented ones in terms of proton potential generation, energy distribution and ROS scavenging, especially in peripheral areas of the cell (Westermann 2010, Rowland, 2012). Therefore, networks of elongated, highly interconnected mitochondria are often observed in cells with high metabolic activity (Westermann 2010).

In accordance with these observations, functional analyses revealed a strong increase of mitochondrial respiration, highlighted by the increase in oxygen consumption and mitochondrial coupling. At the same time, in our experimental system glycolysis appeared to be significantly reduced. Being based on an *in vitro* model, these results represent only in part the dynamics of cellular metabolism *in vivo*. Indeed, key parameters such as glucose concentration in the medium and oxygen tension are significantly different from the ones experienced by the cells in physiological conditions.

However, the metabolic rewiring observed in my experiments are perfectly coherent with known aspects of endometrial decidualization: the development of spiral arteries provides the tissue with highly oxygenated blood (Pijnenborg 2006), thus allowing EnSC switch to mitochondrial metabolism. At the same time, decidualized EnSCs and cells of the endometrial epithelium accumulate glucose in the form of glycogen granules, required to

support the early stages of embryo development (Gellersen 2014). In this context, mitochondrial respiration probably represents the most efficient solution for the energy requirements of decidualized cells.

Our transcriptome analyses of the mitochondrial genes revealed, as expected from the functional assays, a strong induction of the genes involved in oxidative phosphorylation, with a simultaneous overexpression of both nuclear and mitochondrial encoded genes. However, the induction of other mitochondrial functions was also observed: genes connected for lipid and amino acid metabolism are among the most upregulated, including the ones encoding for key enzyme of lipid β-oxidation (ACSS1, CPT1A, CPT1C).

Even though a functional validation would be required to draw any definitive conclusions, these results further support the concept of a radical switch in the metabolism of decidualizing cells, possibly including a change in the prevailing energy sources. In particular, an increased energy intake provided by fatty acids would allow the cell to channel glucose in metabolic pathways different from energy production, as suggested also by the downregulation of *carbohydrate metabolism* in the Over Representation Analysis of mitochondrial functions. In this way, the glucose up-taken by decidualized cells could be stored in glycogen granules, as previously described (Gellersen 2014), used in amino acid biosynthesis, or funneled in pentose phosphate pathway, fundamental for the synthesis of aromatic amino acids and of the essential cofactor NADPH (Alberts 2015, Alfarouk 2020).

Apart from the changes in energy metabolism, also other functions of the mitochondrial network appear to be significantly modified by decidualization: genes involved in the biosynthesis of phospholipids are upregulated, coherently with the massive increase of the membrane-bound organelles and of the transport vesicles; genes involved in ROS detoxification, such as SOD2, are also strongly induced.

Both these fundamental functions depend on the close interaction between ER and the mitochondrial network (Rowland 2012); accordingly, a significant increase in the length and number of the MERCs was confirmed by the microscopy-based analyses.

Although a further characterization of the ER-mitochondria interactions in decidualization was beyond the scope of my project, it could be interesting to better investigate the

interactions between these organelles. MERCs, indeed, have been implicated in various fundamental mechanisms, ranging from the dynamics of mitochondrial fusion and fission (Rowland 2012), to the exchange of hydrogen peroxide, during the oxidative folding of proteins in the ER (Sorrentino 2022), with the assembly of specialized protein complexes on both the ER and the mitochondrial membranes (Gilady 2010, Rowland 2012). Considering the marked spatial regionalization of both the ER and mitochondria in EnSCs, it would be interesting to investigate whether also the contacts between the two organelles present may mediate specialized functions in different areas of the cell.

As previously observed also for the secretory pathway genes, the transcriptional reshaping of mitochondria begins immediately after the exposure of the cells to the decidualization stimuli, far before any change in the cellular phenotype. This was also confirmed by the early nuclear translocation of PGC-1α, transcription factor described as master regulator of mitochondrial biogenesis (Abu Shelbayeh 2023). PGC-1α activation has been described as a crucial mechanism for the up-regulation of important mitochondrial functions, such as oxidative phosphorylation, lipid metabolism, and detoxification of reactive oxygen radicals (Mastropasqua 2018), which seem to be fundamental elements in the decidualization program. Moreover, previous studies reported that PGC-1α is highly expressed in decidualized cells (Bombail 2008), and that this transcription factor is directly involved in the transcriptional induction of PRL and IGFBP-1 (Takagi 2022).

Therefore, even though the precise mechanism inducing nuclear translocation of PGC-1α at the beginning of decidualization was not characterized, it can be speculated that this represents a fundamental step in the process, directly linking the transcriptional induction of important cargoes, with the increase in the mitochondrial capacity.

As previously described for the secretory pathway compartment, it is important to highlight that the architectural and functional reorganization of the mitochondrial network precedes the production of cargo proteins. Preparing well in advance, indeed, appears to be a crucial aspect of secretory differentiation programs, as observed also for other cell types (e.g. plasma cells, in van Anken 2003). The details and the implications of these aspects will be discussed further below, in the concluding remarks.

4 The dynamics of zinc in EnSC secretory pathway

The analysis of biophysical parameters of the secretory pathway organelles could provide a new perspective about the dynamic modifications of the secretory pathway organelles.

The results presented in this thesis are preliminary, and far from providing a complete overview about the precise rearrangements of the secretory pathway "landscape". Clear differences were observed between the organelles of proliferative and decidualized cells; however, additional analyses are required to decipher the functional meaning of these changes.

Even if it still at a rather embryonic level, the analysis of zinc in the secretory compartments of EnSCs appears to be particularly promising.

In the secretory pathway organelles, the concentration of this metal ion is regulated by the precise localization of zinc exporters and importers (Roohani 2013, Kowada 2021): based on the distribution of the different transporters, precise zinc concentrations are established and maintained in the different compartments, at both an organelle and sub-organelle levels (Kowada 2021, Amagai 2023).

To the state of the art, however, the mechanisms regulating and maintaining the different distribution of the transporters are poorly characterized; moreover, almost nothing is known about how zinc concentration is modified during secretory differentiation programs.

To complete decidualization, EnSCs must precisely regulate zinc concentration at a sub-organelle level. Fundamental secretory cargoes of these cells require zinc for their activity, as several matrix metalloproteases (Kambe 2017) or for their correct assembly into secretory granules, as described for prolactin (Vang 2022).

In this connection, the induction of ERp44 during decidualization could be linked to zinc.

ERp44 has fundamental roles in distal quality control and in the retrieval of chaperones and enzymes from downstream secretory organelles (Anelli 2002, Anelli 2003, Tempio 2021). To mediate its function, ERp44 continuously cycles between the ERGIC-Golgi, where it binds its client proteins, and the ER, where the clients are released (Anelli 2003).

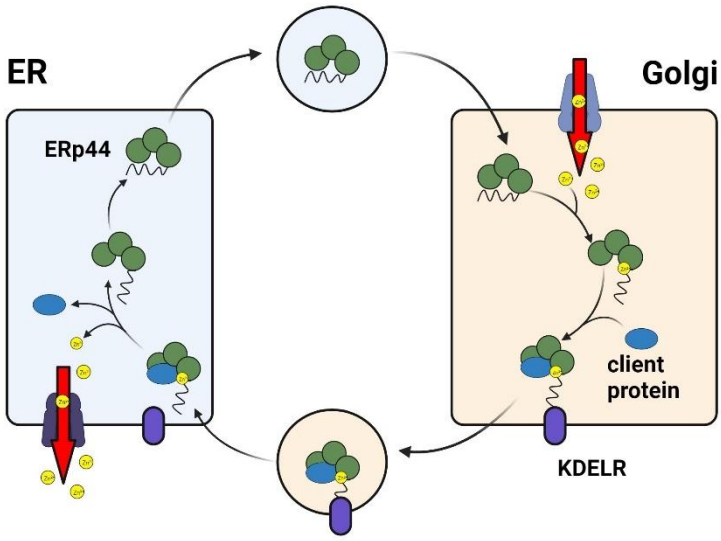


Figure 60. Zinc concentration controls localization and function of ERp44.
Graphical representation of ERp44 movements between the ER and the Golgi complex. ERp44 is transported from the ER to the Golgi in a closed conformation. In the Golgi, the high zinc concentration induces the opening of the tail, allowing the binding of client proteins and the retrieval by the KDELR system. Back in the ER, the decreased zinc concentration induces the release of ERp44 client proteins and the closure of its tail. Based on Anelli 2003. Created in BioRender, publication agreement number HO26A11KRC.

In decidualized EnSCs, for unknown reasons, a small fraction of ERp44 is O-glycosylated and partly secreted in the medium, as consistently observed in my experiments and previously described by other members of the group (Sannino 2014).

As to the function of secreted ERp44, we know only that is does not serve obvious pro-inflammatory functions (unpublished results, Master Thesis project on Anna Maria Naso in Protein Transport and Secretion Unit, UniSR).

Since the interactions of ERp44 with both its clients and the retrieval system (the KDELRs) are controlled by zinc and pH (Watanabe 2019, Tempio 2021), the experimental modulation of these parameters can modify the localization of this protein and cause its glycosylation and secretion (Watanabe 2019, Tempio 2021, Amagai 2023).

Thus, zinc fluxes in the secretory pathway of decidualizing EnSC may similarly influence the localization of ERp44 and/or its secretion.

From the preliminary quantification of zinc and pH in decidualization, both these parameters appear to be particularly affected in the ERGIC compartment. This could have a profound impact on ERp44 dynamics: zinc and acidification both contribute to the opening of ERp44 tail (Watanabe 2019), allowing the binding of ERp44 to its clients and thus their retrieval. Therefore, it can be speculated that the parameters measured in decidualized cells could allow an earlier activation of this mechanism, possibly to counterbalance an increased transport of ER proteins in the compartment.

Moreover, it would be interesting to understand if the secretion of this protein only represents a "leakage" with no functional meaning, or if it could instead mediate functions in the extracellular environment, such as signaling or extracellular zinc buffering. The functional connections between decidualization, zinc concentration and ERp44, to the state of the art based only on preliminary results and speculations, will probably be investigated in a future development of the project.

5 Closing remarks

During my project, I investigated the dynamics of endometrial stromal cell decidualization, with a particular focus on the morphological and functional changes of the organelles.

The explosive success of science in the last half millennium is largely based on reductionism. Even if my experiments were performed on cellular models, a clear reduction of the system complexity, they allowed me to dissect key aspects of decidualization with unprecedented details and with a complete control over the experimental conditions. Moreover, most if not all the results are compatible with the known features of the *in vivo* processes of decidualization, and are consistent with what observed in physiological contexts, whenever a comparison was possible.

As expected, decidualization entails an increase in the secretory capacity, but is not limited to that: all the components of the cell appear to reorganize in coordination, to support the novel secretory task and ensure the maximum efficiency to the process. The secretory organelles themselves are finely reshaped, in order to provide the optimal conditions for the

processing of the secretory cargo proteins. All these processes appear to be integrated and coordinated, with the activation of the differentiation program interacting with a complex network of feedback signals, organelle autoregulation mechanisms, and stress responses. Possibly, the cargo itself also influences this process. Indeed, a comparison between decidualization and other secretory differentiation programs revealed some similarities, but also some important differences: while some aspects are always required to build a secretory cell, others determine the peculiarities of each cell type, in a precise tailoring of the phenotype. Moreover, the presence of secretory proteins itself can affect cell homeostasis in general, by delivering tonic signals through cargo and vesicle movements along the secretory pathway.

In conclusion, the results of my PhD project provide a new insight about the decidualization program of EnSCs, which represents both a fundamental process for human health and fertility, and a powerful model to investigate coordinated organelle remodeling.

The latter aspect, indeed, represents a relatively unexplored frontier of Cell Biology, as the physiological signaling mechanisms controlling homeostasis and autoregulation of the cellular organelles are still largely unknown.

MATERIALS AND METHODS

Reagents

Unless otherwise specified, all the chemicals and reagents were purchased from Sigma-Aldrich (Saint-Louis, MO). Synthetic oligonucleotides, listed in Table 1, were purchased from Metabion (Planegg, Germany). A detailed list of the antibodies used for immunofluorescence and/or biochemical assays is reported in Table 2.

Cell lines and culture conditions

Experiments were performed on the human immortalized EnSC cell line T-HESC, obtained from ATCC (ATCC CRL-4003). Cells were cultured, according to manufacturer's instructions, in a 1:1 mixture of Dulbecco's modified Eagle's medium and Ham's F-12 medium without Phenol Red, containing 3.1 g/L glucose and 1 mM sodium pyruvate, and supplemented with 1.5 g/L sodium bicarbonate, 1% ITS + Premix (Corning), 500 ng/ml puromycin, and 10% charcoal/dextran treated fetal bovine serum. Medium was supplemented every 3–4 days with 50 µg/ml ascorbic acid, unless otherwise specified.

A few test and validation were performed in HeLa cells, maintained in High Glucose DMEM supplemented with 10% fetal bovine serum and with penicillin/streptomycin (100 U/ml and 100 µg/ml respectively).

In vitro decidualization protocol

Decidualization was induced by direct addition into the medium of 0.5 mM cAMP (8-bromoadenosine 3′, 5′ cyclic monophosphate) and 1µM MPA (medroxyprogesterone acetate) as previously described (Brosens 1999, Gellersen 2014, Anelli 2021). After 3 days, the medium and the decidualization stimuli were replaced.

Isolation, culture and *in vitro* decidualization of murine EnSC

Experiments involving animals were conducted in accordance with the National Institute of Health standards for the use and care of animals. The protocol was approved by the Animal Care and Use Committee of the San Raffaele Hospital. Female mice (C57BI/6, 10 weeks old) were sacrificed after a 48 h exposure to male urine via soiled bedding to standardize the estrous cycle. Uterine tissue of 5 mice was collected, washed with Hank's balanced salt solution (HBSS), and placed into HBSS containing 0.5 g/L of type IA collagenase. After incubation for 45 minutes at 37°C, the tubes were vortexed for roughly 10 seconds to isolate cells from the digested tissue; cell dispersion was then passed through a 70 µm-gauze filter (Millipore), to remove tissue fragments and large cell aggregates.

Cells were resuspended in the same DMEM-F12 medium used for T-HESC (prepared without puromycin but supplemented with 100U/L penicillin, 0.1 g/L streptomycin), and seeded in 35 mm Petri dishes. After a few days in culture, EnSCs expanded, while all the other cell populations isolated from the tissue were lost.

To analyze decidualization, EnSCs were detached with trypsin/EDTA (Gibco) split and reseeded: one dish was induced with cAMP and MPA, while the other was kept in proliferative state as a matched control.

Immunofluorescence

T-HESC were plated on glass slides (0.13-0.16 mm thickness) and maintained for the time indicated, with or without decidualization induction. Cells were fixed in formalin solution (neutral buffered, 10%) for 10 minutes (min) at room temperature (RT) and then washed with PBS.

Cells were permeabilized with 0.1% Triton X100 in PBS, incubated with blocking solution (PBS-5% FCS) for 30 min at RT. They were then incubated with primary and secondary antibodies and/or with Phalloidin-FITC, 30 min each, diluted in blocking solution as indicated in Table 1. Nuclei were counter-stained with DAPI, 1:5000 in PBS, for 5 min at RT.

For double staining with anti-HLA antibody and other primary antibodies produced in mouse, a different protocol was used to avoid cross-reactivity. Briefly, cells were reversibly permeabilized with 0.1% saponin, and the primary and secondary staining were performed with 0.1% saponin in the antibody diluting solution. Afterwards, cells were incubated in PBS for 5 min and in PBS 5% FCS for 30 min, to allow membrane pore closure, and then incubated with anti-HLA W6/32 antibody and the corresponding secondary antibody, without re-permeabilization steps.

Images were acquired with DeltavisionUltra microscope (GE Healthcare) with oil immersion objective at 60x (Olympus 60X/1.42, 1-U2B933) or 100x (Olympus 100X/1.45, 1-UXB240) magnification, and deconvolved with the instrument software.

Haematoxylin/Eosin staining

Microscope slides for haematoxylin/eosin staining was performed as described in immunofluorescence section: slides were directly transferred in PFA 4%, incubated for 10 minutes at room temperature, and then washed twice with PBS. After that, they were stored at 4°C until processing could be performed.

Staining with haematoxylin and eosin was performed with a standard staining protocol. Images were acquired with bright field Axio Imager Microscope (Zeiss AxioImager M2m with AxioCam MRc5 and Nuance FX Multispectral Tissue Imaging System).

Morphometric and morphological analysis

Image stacks for the morphometric analysis were deconvolved with Huygens software (CMLE algorithm, SNR:10, 40 iterations).

Volume quantification was performed with Huygens Object Analyzer plugin, with a threshold of 10%, a seed value of 4% and a garbage value of 1 used to identify the mitochondria objects inside the cells. The results were expressed in voxels, and converted in μm^3 based on the metadata of the IF images. Relative cell occupancy was then calculated dividing the volume calculated for the organelles by the total volume of the corresponding cell.

Morphological analysis was performed with the Arivis 4D software (version 3.6.2), using a custom analysis pipeline. For each object, the dimensions along the three axes and the sphericity parameters were measured. The objects visually inspected, and the ones corresponding to an incorrect segmentation (visually recognized as not separated, or with a calculated main axis longer than 25 µm) were excluded from the analysis. Three-dimensional reconstruction of the mitochondrial network was performed on representative cells using the 3D visualization tool of Arivis, using the "*glass"* texture tool to improve volumetric rendering.

Secretome collection

To analyze the secreted proteins, the cultured cells were washed three times with DPBS (Euroclone), and incubated for 4 or 6 hours in the protein-low OptiMEM medium (Gibco), supplemented with 50 µg/mL Ascorbic Acid. The supernatants were collected and centrifuged at 3500 rpm with a tabletop centrifuge (~1200 g), to precipitate detached cells and large debris; then, they were added with 10 mM N-ethylmaleimide (NEM) and cOmplete EDTA-free protease inhibitor cocktail (Roche).

In parallel, cells were detached with Trypsin/0.1% EDTA (Gibco), counted with Neubauer chamber, and lysed as described below. In this way, normalization by cell number and comparison between intra- and extracellular material were performed.

ELISA

PRL and IL-6 levels in T-HESC culture media were determined using two step-sandwich ELISA assays (R&D Systems), according to the manufacturer's protocols. Briefly, plates were coated overnight at RT with the capture antibody. Then, the calibration standards and the samples were added in the wells, and incubated for 2 h at RT. After washing, the detection antibody was added, and plates were incubated again for 2 h at RT. Lastly, the plates were washed again, and streptavidin-HRP was added, followed by chromogenic substrate and stop solution. The optical density was determined at 450 nm, and the concentrations were determined based on the standard sample curves and the blank wells.

Western Blot

Western Blot assay was performed as previously described (Anelli et al., 2021). Briefly, cells were detached with Trypsin/0.5% EDTA (ThermoFisher), counted with Neubauer chamber, and washed with ice-cold DPBS containing 10 mM N-ethylmaleimide (NEM) to block disulfide bond rearrangements; lysis was performed in 150 mM NaCl, 1% NP-40, 2% SDS, 50 mM Tris HCl pH 7.4 containing 10 mM NEM and cOmplete EDTA-free protease inhibitor cocktail (Roche) and phosphatase inhibitors. 10uL of lysis buffer for 100.000 cells. Samples were then processed with Benzonase nuclease according to manufacturer's instructions, to remove nucleic acids. Lysate volumes corresponding to 50.000 cells were loaded under reducing conditions (50 mM DTT) on SDS-PAGE (3-8%, 4-12% or 4-20% gradient gel, Invitrogen). After transfer on nitrocellulose (0.2 µm, Ahmersham), membranes were incubated in blocking solution (5% w/v nonfat dry milk in PBS, 0.1% Tween 20) and incubated with primary and secondary antibodies prepared in PBS-Tween, 3% milk.

Signals were detected by fluorescence, with FujiFilm FLA 9000 (FujiFilm Life Science, Tokyo, Japan), or by chemoluminescence, with Uvitec Alliance Mini HD9 (Cambridge, United Kingdom). Densitometric analysis of the images was performed with ImageJ, based on the Mean Grey Value of the bands of interest.

SYPRO Ruby protein staining

For total protein staining, samples were collected and prepared as for Western Blot assay and run in a 4-12% gradient precast polyacrylamide gel (Invitrogen), which was stained with SYPRO Ruby Protein Gel Stain (Sigma-Merck) as from manufacturer's instructions. Briefly, the gel was fixed in 50% methanol, 7% acetic acid (two incubations, 30 min each, RT), incubated with the staining reagent, and then washed in 10% methanol, 7% acetic acid (30 min at RT).

Fluorescent signal was acquired with FujiFilm FLA 9000 (FujiFilm Life Science, Tokyo, Japan).

Real time qPCR

Total RNA was extracted from T-HESC at different decidualization days by Trizol RNA lysis reagent (Invitrogen), and immediately stored at -80°C. When all the samples of the series were collected, they were retrotranscribed with MV reverse transcriptase (Promega) and random primers (Promega), according to manufacturer's instructions.

Semi-quantitative real time PCR (qPCR) was performed with the SYBR Green PCR Master Mix (Applied Biosystems) and the Rotor Gene Q (Qiagen), or with the iTAQ Universal SYBR Green Supermix (BioRad) and the CFX96 Real Time System (BioRad).

Briefly, 1 μL of primer couples (25 μM each, to a final concentration of 2.5 μM, for the RotorGene; 5 μM each, to a final concetration 0.5 μM, for the CFX96), 5 μL of SYBR mix and 4 μL of cDNA and nuclease-free water (corresponding to 8 ng of template DNA) were added to each reaction well, in a total volume of 10 μL. All the samples were loaded in triplicate.

The amplification was performed with a denaturation step of 10 min at 95°C, followed by 40 cycles of PCR amplification (15 sec at 95°C, 1 min at 60°C), and by a step-by-step temperature increase from 60°C to 95°C, to calculate the melting curve.

For each sample, the C_t (cycle number at which the fluorescence signal crosses the threshold) was measured, and the value of the replicates was averaged. To compare different conditions, the C_t of the reference gene GAPDH (which expression is constant along the decidualization process) was subtracted from the C_t of the gene of interest in the same condition (ΔC_t); then, each ΔC_t was expressed in relation with the corresponding value in the control condition (by subtraction, giving the $\Delta\Delta C_t$), and expressed as fold change of gene expression ($2^{-\Delta\Delta Ct}$).

Most primer sequences were chosen based on previous literature or on UCSC qPCR primer database (Zeisel 2013), as detailed in Table 2; primers for the KDELRs, instead, were purchased from Qiagen (Hilden, Germany). Primers with an optimal amplification temperature of 60°C were chosen.

Silencing of gene expression

Silencing of gene expression was performed with Lipofectamine RNAiMax reagent (ThermoFisher), according to manufacturer's instructions. Briefly, 3 µL the oligonucleotide (at 20 µM concentration) and 4 µL RNAiMax were prepared separately in 250 µL of OptiMEM (Gibco) for each 35 mm dish, incubated for 5 min at RT, mixed, and further incubated for 15 min at RT. The reagent was then added to the dish, containing 1 mL of fresh medium; medium was replaced approximately 24 hours after the procedure. A double volume of each reagent was used for 60 mm dishes, accounting for the larger number of cells.

When coupled with decidualization, the silencing procedure was performed the day before the addition of the stimuli (Day -1), and repeated after three days (Day 2), to minimize the number of medium changes.

SiRNA oligos against CREB3L2 were previously described by Tomoishi et al. (Tomoishi, 2017), while oligos against CREB3L1 were custom designed, and their effectiveness was validated by qPCR. Non-targeting duplexes used as control (SiC) were purchased from Darmachon (Lafayette, Colorado, United States; catalog number D-001810–01).

Transmission electron microscopy

Cells were fixed with 2.5% glutaraldehyde in 100 mM sodium-cacodylate buffer pH 7.4 for 1h at RT, washed three times with cacodylate buffer, and incubated with 1% osmium tetroxide and 1.5% potassium ferrocyanide in 100 mM cacodylate for 1h on ice. After repeated washes with distilled water, en bloc staining was performed overnight at 4°C with 0.5% uranyl acetate (in water).

Then, the samples were dehydrated in a graded ethanol series (30%, 50%,70%, 80%,90%,96%, 5 min each; absolute ethanol, three washes, 10 min each), infiltrated in 1:1 ethanol/Epon 812 solution for 2 h, in 100% Epon twice for 1 h, and finally covered with a layer of Epon and polymerized in an oven at 60°C for 48 h.

A part of the sample was glued on an Epon block, and sectioned with a Leica Ultracut UCT ultramicrotome. Ultrathin (70-90 nm) sections were collected on copper grids, stained

with uranyl acetate and lead citrate, and finally examined with a transmission electron microscope (TALOS L120C ThermoScientific) at 120 kV.

Mitochondria were identified based on standard morphological parameters, that is the presence of a double membrane and the identification of the *cristae.* In case of dubious identification, the objects were not included in the following analyses.

The objects identified as mitochondria were visually inspected, in order to evaluate possible morphological alterations, either with a biological meaning or due to fixation artefacts. Mitochondria with 1) clear disruption of the outer membrane and/or of the cristae, or 2) swollen appearance, with rounded shape, disruption of the cristae organization, and unusually large distance between the different membrane layers, were classified as "abnormal" in terms of morphology. No distinction was made in the classification was made between clear artefacts (e.g. damages due to the sectioning) or alterations with a biological meaning; the former were present only in a very limited number, and appeared evenly distributed between the two conditions. Unless the alterations impaired the evaluation of ER-mitochondria contacts (e.g. significant loss of continuity of the mitochondrial membrane), the "abnormal" mitochondria were included in the subsequent analyses.

Morphometric analysis was performed as previously described (Sorrentino 2022). A minimum of 50 images were acquired for each condition, and all the mitochondria present in them were analyzed. Area and perimeter of the mitochondria were defined as regions of interest (ROIs) using the freehand selection tool of ImageJ. Then, each ROI was extended by 30 nm with the enlarge function, and all the ER structures present were scored as MAMs, and the length of the contact was measured. Regions of close proximity between ER and mitochondria, but in which other elements excluded the presence of a functional MERC (e.g. clear presence of ribosomes on the ER membrane, or of other structures between the organelles in the putative contact region) were excluded from the analysis.

All the parameters acquired were analyzed and represented in GraphPad Prism, release 8.2.

Mitotracker staining

Mitochondrial staining was performed with MitoTracker™ Red CMXRos (ThermoFisher, M7512), as from manufacturer's instructions. Briefly, mitotracker was diluted in medium to a final concentration of 20 nM; cells were incubated with the dye for 30 min at 37°C, 5% CO_2, washed twice with PBS, and kept in complete medium until further processing.

Then, slides were either fixed and prepared for immunofluorescence, or transferred in a ring support for live imaging, covered with 500 µl Ringer buffer (140 mM NaCl, 2 mM CaCl2, 1 mM MgSO4, 1.5 mM K2HPO4, 10 mM glucose, 10 mM Hepes, buffered to pH 7.4) and imaged with DeltaVision Ultra microscope, 60x magnification, in a 37°C, 5% CO2 chamber and with automatic focus stabilization (UltimateFocus).

To prevent mitochondrial fragmentation in response to thermal shock, all the buffers and mediums were pre-warmed to 37°C before use.

Seahorse assay for mitochondrial activity

Mito Stress Test was performed with Seahorse XF96, Agilent. Control and decidualized cells were plated in the 96-well plate 24 hours before the experiment. Cell number was previously determined by pilot experiments: 10,000 and 20,000 cells for each condition were plated, with 15 replicated wells per experiment; 20,000 cells, corresponding to a confluence of 90%, were chosen as optimal. As from manufacturer's protocol, cells were sequentially treated with 1µM oligomycin, 1.5µM FCCP, 0.5µM (each) antimycin and rotenone. Oxygen Consumption Rate (OCR) and Extra-Cellular Acidification Rate (ECAR) were measured for each well at the indicated timepoints. At the end of the experiment, cell nuclei were stained with CyQuant (Invitrogen, C7026) and the fluorescence signal was used for normalization. Two independent experimental replicates were performed.

Molecular biology: plasmid generation

Cytosolic domains of CREB3L1 and CREB3L2 were cloned from RNA of T-HESC cell line, retrotranscribed with MV reverse transcriptase (Promega) and oligo-dT primers (Promega) according to manufacturer's instructions. To ensure high expression of the

transcripts and avoid cross-contamination, RNAs at day 3 of decidualization with silencing of CREB3L2 and CREB3L1 (confirmed by RealTime quantitative PCR) were used to amplify CREB3L1 and CREB3L2 respectively. PCR was performed with Pfu DNA Polymerase (Promega), with the following conditions: 95°C 2 min; 95°C 30 s, 52°C (CREB3L1)/56°C (CREB3L2) 30 s, 72°C 3 min × 35 cycles; 72°C, 5 min (CREB3L1 fw: CTAGCTAGCTAGGGCTGCGATGGACGCCGTC; rev: CCGGATATCTTATTATGG TCCCAGTCTGGGTG; CREB3L2 fw: CTAGCTAGCTAGGGCCCGCACCGCCATG; rev: CCGGATATCTTATTAGCAGGTGCCAGTCTGCGTG). Vector pcDNA3.1 (+) and PCR products were digested with NheI-HF and EcoRV (New England Biolabs), run in 1% agarose gel and purified (ZymoClean Gel DNA Recovery Kit, Zymo Research). Ligation was performed with T4 DNA ligase (Promega), with a 3:1 insert/plasmid ratio. Plasmid identity was then confirmed by site-specific enzymatic digestion with NotI (New England Biolabs) and BstxI (Promega) and by sequencing (Eurofins Genomics, Ebersberg, Germany).

The construct used for microscopy-based measurements of zinc and pH were kindly provided us by Professor Kenji Inaba's Group (Amagai 2023). The plasmids were developed by Dr. Yuta Amagai (ManII-Halo, hTPST2-Halo, GalT-Halo, pH2-ERGIC53, ManII-pH2, hTPST2-pH2, GalT-pH2), and by Dr. Momo Yamada (Halo-ERGIC53).

For the generation of stable cell lines, ManII-Halo, hTPST2-Halo and GalT-Halo were extracted from the original pEF4/myc-HisB backbone by BamHI-HF and XbaI-HF (New England Biolabs), and transferred into a pcDNA3.1(+) backbone.

The identity of all the constructs (original and modified) was verified by enzymatic restriction and sequencing, as described above.

T-HESC transfection

As a result of pilot experiments, Lipofectamine 3000 (Thermo Fisher) was chosen as optimal reagent for T-HESC transfection. After titration experiments with plasmids routinely used in the lab (Halo-tagged ERp44, described e.g. in Tempio et al., 2021), a ratio of 2.5 µL of lipofectamine and 2 µL of p3000 reagent for 1 µg of plasmid DNA was used.

As from manufacturer's instructions, DNA and p3000 reagent were mixed in OptiMEM (Gibco), while lipofectamine was prepared separately in the same medium. After 5 min of incubation at room temperature, the reagents were mixed, further incubated for 20 min at RT, and added to the cell culture dishes. For 35 mm cell culture dishes, cells were transfected with 1 µg of DNA (with the transfection reagents prepared in 125 µL OptiMEM each, and the dish containing 1 mL of fresh medium); as for the silencing procedure, all the volumes were doubled for the 60 mm dishes.

For transfection of decidualized cells, the procedure was performed at the third day of the differentiation protocol, concomitantly with the medium change and the re-addition of the decidualization stimuli.

Transcriptome analysis

Cell samples were collected in duplicate before the stimulus (0 h), and at different time-points after decidualization induction (6h, 18h, 24h, 36h, 48h, 72h, 144h), using TRIzol (Invitrogen) according to the manufacturer's instructions.

The library was created starting from 500 ng of total RNA per sample, and processed using the TruSeq Stranded mRNA kit (Illumina); sequencing was then performed of an Illumina HiSeq 3000 platform (Illumina).

Raw sequencing data were analyzed using *snakePipes* with standard parameters (Bhardwaj 2019), a pipeline that employs *STAR aligner* to map the reads on the human reference genome (*genome build hg38*). *FeatureCounts* was utilized to count the number of reads per annotated gene using *gencode gtf file* (release 27).

All the raw sequencing data are available on the Gene Expression Omnibus Repository with the accession number GSE200200.

Differential expression analysis (DEA), over-representation analysis (ORA), time series clustering and data visualization were performed using the R programming language (v. 4.1.0).

Before DEA, the matrix was prefiltered, removing all the genes with a total number of counts (across all the samples) lower than 30. The analysis is based on the pairwise

comparison of each timepoint versus the control condition (0h), using the DESEQ2 package (v. 1.32.0) (Love 2014). Genes were called differentially expressed (DEGs) based on absolute expression change (log_2 fold change >0.5) and statistical significance (adjusted p-value <0.01).

ORA was then performed with the enrichR package (v. 3.0), using Gene Ontology (GO) terms based on the 2021 release. For mitochondria-related genes, ORA for MitoCarta terms (version 3.0) was performed via classical Fisher's exact test based on upregulated and downregulated terms, respectively. Multiple testing correction was performed using the Benjamini–Hochberg method.

Gene clustering was performed on DEGs identified between 6h and 72h, and annotated for either the GO cell compartment ER (GO:0005783) or Golgi apparatus (GO:0005794); annotations were downloaded from AmiGO2, considering "*Homo sapiens*" and "*experimental evidence*" as "*organism*" and "*evidence*" respectively. The input matrix for clustering was then retrieved by subsetting the time-course expression of the genes of interest, transformed using DESeq2 variance stabilizing transformation. Then, the replicates were averaged, and z-normalization was performed to optimize the subsequent analysis.

Time-series clustering was performed with the dtwclust package (v. 5.5.10) (Sardà-Espinosa 2019), using shape-based distance (SBD) as distance metric (Paparrizos and Gravano, 2015) and partition around medioids (PAM) as clustering algorithm.

SBD consists of a normalized version of the cross-correlation measure, which recognizes the shape similarity of time signals, even if they are not properly aligned.

As PAM requires to set the number of clusters (k) *a priori*, the optimal number was determined by a heuristic approach, based on the maximization of the average Silhouette Index. Optimal clustering was obtained with k=5 and the *seed* set to 23. Genes showing a dramatic out-of-phase temporal expression (more than two standard deviation difference from the mean z-score of the time-point considered) were filtered out in a final cluster polishing step.

Enrichment for BP GO terms for each cluster was carried out on topGO package (v.2.44.0) (Alexa and Rahnenfuhrer, 2023). ORA was performed by adjusting the gene Universe to the

genes contained in the polished version of the clustering output. The weighted algorithm proposed in Alexa et al., 2006 was used to reduce the impact of local dependencies in the GO graph.

Enrichment for shared transcription factor binding motif (TFBM) for the genes in each cluster was performed using RcisTarget (v. 1.12.1) (Aibar 2017). The analysis was performed by evaluating the shared motifs found at ± 10 kb from the transcription start site of the genes in the input list. Data visualization was performed using the packages ggplot2 (v. 3.3.6) (Wickham 2016) and pheatmap (v. 1.0.12) (Kolde 2019).

HeLa cell transfection

HeLa cells were transfected with JetPEI transfection reagent (Polyplus), as from manufacturer's instructions. For a 35 mm cell culture dish, 2 µg of the plasmid of interest and 4 µL of the transfection reagent were prepared in 42 µL of 150 mM NaCl, mixed, incubated for 20 min at RT, and added to the cells, covered by 1 mL of fresh medium. After 24 hours, cell culture medium was replaced.

Generation of stable T-HESC cell lines

An approach based on transfection followed by antibiotic selection was used to generate T-HESC lines stably expressing the construct of interest. Cells were seeded in 60 mm dishes, transfected as previously described and, 48 hours after the procedure, incubated with 400 µg/mL of Geneticin/G418 (Gibco). After 48-72 hours, medium and antibiotic were replaced. After the first week of selection, when most of the cells were killed by the treatment, the antibiotic concentration was progressively lowered to 100 µg/mL, to allow a better recovery of the selected cells. The clones identified in each plate were pooled and expanded, and the effective expression of the construct of interest was subsequently confirmed by microscopy.

The efficiency of the procedure was slightly improved by the addition of 1:3 spent medium from untransfected cells, but the procedure was discontinued due to the increased risk of bacterial contamination.

A similar selection procedure was attempted for different plasmids with zeocin as selection antibiotic (Invitrogen), but the selection velocity and effectiveness was not sufficient for the experimental purposes.

Microscopy-based in vivo measurement of pH and zinc

Measurment of zinc and pH in the secretory pathway of T-HESC were performed with a modified version of the protocol developed by Professor Kenji Inaba's group (Kowada 2021). For zinc quantification, T-HESC lines stably expressing Golgi-localized Halo probes were used. For pH measurement, transient expression of pHluorin-2 in control or decidualized cells was preferred.

As described for mitotracker live imaging, slides were transferred in a ring support for live imaging, covered with 500 µL Ringer buffer, and imaged with DeltaVision Ultra microscope, 40x magnification, in a 37°C, 5% CO2 chamber and with automatic focus stabilization (UltimateFocus).

For pH measurement, calibration of the fluorescence signal was performed with a series of calibration solutions, as from Ma et al., 2017: 125 mM KCl, 25 mM NaCl, 10 µM Monensin, 25 mM MES (for buffers ar pH 5.5, 6.0 and 6.5) or HEPES (for buffers at pH 7.0 and 7.5), and NaOH for final pH adjustment. Both for the calibration step and for the signal measurement, the probe was alternatively excited with 390 nm and 475 nm wavelength light, and the ratio between the two emission signals (both at 525 nm) was calculated in Fiji software in the corresponding ROIs (Figure 62).

For zinc measurement, cells were pre-incubated with the zinc-sensitive fluorescent ligand ZnDA-1H, 250 nM, and HaloTMR Direct Ligand (Promega), 5 nM, in complete medium for 30 min, 37°C, 5% CO_2. Then, the slides were washed with pre-warmed Ringer buffer, and imaged in Ringer buffer containing 2 µM $ZnSO_4$. The red channel (excitation 575 nm, emission 625nm) was used for focusing and organelle localization, both in visualization and in the quantification steps. The green channel (excitation 475 nm, emission 525 nm), corresponding to the zinc-dependent signal, was acquired at 30 second intervals, first in basal conditions, and then after the sequential addition of the zinc-chelator TPEN 10 µM (3 min

after the beginning of the acquisition) and of 400 µM $ZnSO_4$ and 20 µM pyrithione (5 min after TPEN addition). The optimal concentration of the different reagents and the acquisition parameters were first validated on HeLa cells transiently expressing Golgi-localized Halo probes, and then applied to the T-HESC lines stably expressing them.

Signal was then calculated in Fiji software in the ROI of interest in the time-lapse images. Labile zinc concentration was then calculated as previously proposed (Kowada 2021, Amagai 2023), based on the signal calibration and the pH-corrected dissociation coefficient (K_d) of ZnDA-1H, with the following equation:

$[Zn^{2+}] = Kd \times (Rss - Rmin)/(Rmax - Rss)$

Where $[Zn^{2+}]$ is the zinc concentration, R_{ss} the basal signal at the steady state, R_{min} the signal upon zinc chelation, R_{max} the signal upon zinc addition.

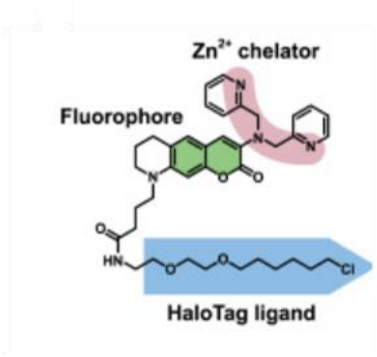


Figure 61. Structure of the ZnDA-1H fluorescent probe.
Structure of ZnDA-1H fluorescent probe. The zinc-binding group, the fluorescent region and the Halo-binding tail of the molecule are highlighted in the structure (Kowada 2021).

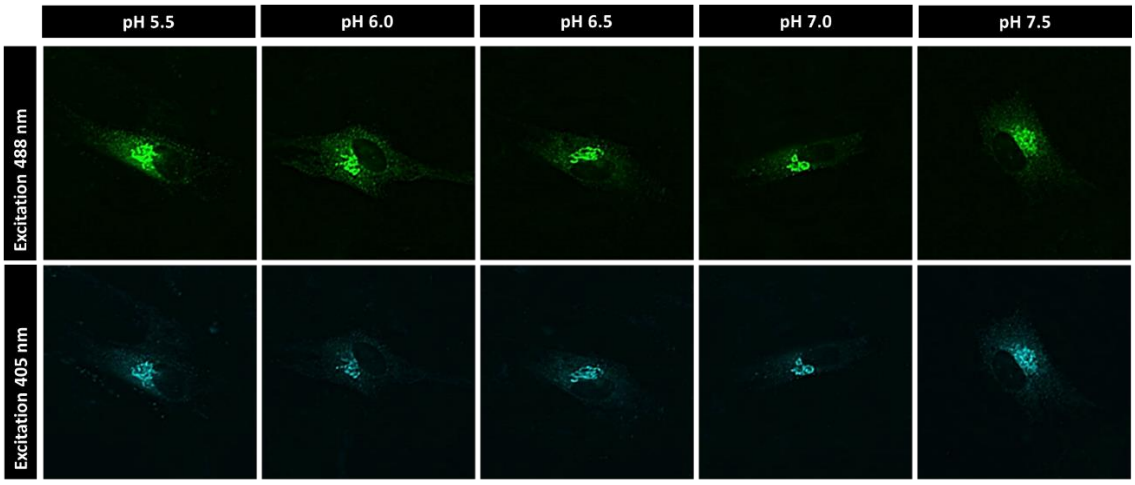


Figure 62. Graphical representation of pHluorin-2 signal calibration.
Representative images of ERGIC-localized pHluorin-2 probe at different pH values. The two channels represent emission at 525 nm, after excitation at the indicated wavelengths. Images acquired with a 40x magnification.

Graphical representations and statistical analysis

Graphical representation and statistical analysis of the results were performed with GraphPad Prism 8.2. Based on the type of dataset, t-test, one-way ANOVA, Mann-Whitney test or Kolmogorov-Smirnov non-parametric test were performed, as indicated in the text or the figure legends. Statistically significance was set at p-value <0.05, unless otherwise specified.

When elaboration of the raw data was required before analysis (e.g. ratio between two values), calculations were performed in Microsoft Office Excel.

Table 1: Antibodies

Antibody -immunoblotting	***Species***	***Dilution***
BiP (sc-1015, Santa Cruz Biotechnology)	*Goat*	*1:500 in 3% milk*
Collagen type I	*Rabbit*	*1:1500 in 3% milk*
CREB3L1 (EMD, clone 10H1, MABE1151)	*Mouse*	*1:500 in 2% milk*
CREB3L2 (EMD, clone 28G9, MABE1018)	*Mouse*	*1:500 in 2% milk*

ERGIC-53 (E1031, Sigma-Aldrich)	*Rabbit*	*1:500 in 1% BSA; blocking in 1% BSA*
Ero1α (3264P, Cell Signaling)	*Mouse*	*1:500 in 3% milk*
ERp44 (3C9, in house)	*Mouse*	*1:1000 in 3% milk*
GAPDH (6C5, Santa Cruz Biotechnology)	*Mouse*	*1:500 in 3% milk*
GM130 (710823, BD Biosciences)	*Mouse*	*1:500 in 3% milk*
GPX8 (AG-25B-0028-C100)	*Rabbit*	*1:500 in 3% milk*
PDI (C81H6, Cell Signaling)	*Rabbit*	*1:2000 in 3% milk*
PRDX4 (LF-PA009, TermoFisher)	*Rabbit*	*1:500 in 3% milk*
Procollagen type I (SP1.D8, DSHB)	*Mouse*	*1:1000 in 3% milk*
TGN46 (ABT95, Merck)	*Rabbit*	*1:500 in 3% milk*
TOM-20 (BD 612278)	*Mouse*	*1:500 in 3% milk*
VDAC (Biovision 3594-100)	*Rabbit*	*1:500 in 3% milk*
β-actin (A5441, Sigma-Aldrich)	*Mouse*	*1:2000 or 1:5000 in 3% milk*
Alexa secondary antibodies 488, 546 or 647	*Goat, Chicken*	*1:1000 in 3% milk*
Antibody-immunofluorescence		
Calreticulin (C4606, Sigma)	*Rabbit*	*1:500 in 5% FCS*
ERGIC-53 (clone G1/93)	*Mouse*	*1:100 in 5% FCS*
ERp44 (3C9, in house)	*Mouse*	*1:500 in 5% FCS*
Giantin (Biolegend)	*Rabbit*	*1:2000 in 5% FCS*
GM130 (BD Biosciences)	*Mouse*	*1:500 in 5% FCS*
Golgin-97 (CDF4, Invitrogen)	*Mouse*	*1:500 in 5% FCS, 0.1% saponin*
HLA (W6-32), hybridoma supernatant	*Mouse*	*No dilution*
PDI (Invitrogen, MA3-019)	*Mouse*	*1:250 in 5% FCS*

PGC-1α (Invitrogen, PA5-72948)	*Rabbit*	*1:500 in 5% FCS*
Procollagen type I (SP1.D8, DSHB)	*Mouse*	*1:100 in 5% FCS or 1:500 in 10% FCS*
Reticulon 4 (Invitrogen, PA1-412209)	*Rabbit*	*1:250 in 5% FCS*
TGN46 (Biorad, AHP500)	*Sheep*	*1:500 in 5% FCS*
TGN46 ABT95 (Merck-Millipore)	*Rabbit*	*1:500 in 10% FCS*
TOM-20 (BD 612278)	*Mouse*	*1:100 in 5% FCS, 0.1% saponin*
Vimentin (Sigma-Aldrich, V4-630)	*Goat*	*1:500 in 5% FCS*
Alexa secondary antibodies 488, 546 and 647	*Goat, Donkey, Rabbit*	*1:500 in 5% or 10% FCS*

Table 2: Synthetic oligonucleotides

Oligonucleotide	**Sequence**
CREB3L1 siRNA	CCACCAAGUACCUGAGUGA (dT)(dT)
CREB3L2 siRNA	GAGUCUUGUUCAACUGAGA (dT)(dT)
GAPDH fw	TGAAGGTCGGAGTCAACGGATTT
GAPDH rev	CATGTAAACCATGTAGTTGAGGT
CREB3L1 fw	ACAATGCGCACTTTCCTGAG
CREB3L1 rev	GAGGGCTCTTCTCATCCAGC
CREB3L2 fw	AGAATACATGGACAGCCTGGAG
CREB3L2 rev	TCTAGAACCTCTACCTTCTTCCGA
ERp44 fw	CAGCACTCTGACATAGCCCA
ERp44 rev	CTGATCGCTGACCCCTGTAT
LMAN1 fw	TCAGGAGGAATTTGAGCACTTT
LMAN1 rev	GCTCTCGATCTCCTACACTCTCA
GOLGA2 fw	CAGCCGCCTGCAGTATTC
GOLGA2 rev	TGAGGGCGTCTCTCTCTTTG

GOLGB1 fw	AGCATCTCAGACTTCTTTCCCA
GOLGB1 rev	GAGCAAGGCTCCCTTTTCAT
TGOLN2 fw	GAGCAGCCACTTCTTTGCAT
TGOLN2 rev	TTCCTTCCAGGACAAAAGCA
SEC24A fw	ACACTGGAGGCTGAGGTGG
SEC24A rev	ACACTGGAGGCTGAGGTGG
SEC4D fw	ACCCCATCAGTTTGGTCAGA
SEC24D rev	CCACATTGTTGACAGGTGGA
PRL fw	AGCCAGGTTCATCCTGAAA
PRL rev	AGCAGAAAGGCGAGACTCTT
TF fw	CCAAACCCGTCAATCAAGTC
TF rev	GTCGGTGAGGTCACACTCTGT
CNX fw	GTAGCCCTTCCTGTGTTCCT
CNX rev	TGACAGTGCCACCATCTTCT
PDI fw	TCACATCCTGCTGTTCTTGC
PDI rev	GTCGCTGTCGATGAAGATGA
BIP fw	TAGCGTATGGTGCTGCTGTC
BIP rev	TGACACCTCCCACAGTTTCA
PRDX4 fw	AACAGCTGTGATCGATGGAG
PRDX4 rev	TCAAGTCTGTCGCCAAAAGC
ERO1α fw	GTGTGGCTGCTCAGCTCG
ERO1α rev	TCAATGGTTTCAACATCACAGG
GPX8 fw	CTACGGAGTAACTTTCCCCATCTTCCACAAG
GPX8 rev	CTGCTATGTCAGGCCTGATGACTTCAATGG
IGFBP1 fw	TTACCTGCCAAACTGCAACA
IGFBP1 rev	CATTCCAAGGGTAGACGCAC
HSP47 fw	ATGCAGAAGAAGGCTGTTGC
HSP47 rev	GGCCTTGTTCTTGTCAATGG

REFERENCES

Abrisch, R. G., Gumbin, S. C., Wisniewski, B. T., Lackner, L. L., & Voeltz, G. K. (2020). Fission and fusion machineries converge at ER contact sites to regulate mitochondrial morphology. Journal of Cell Biology, 219(4). https://doi.org/10.1083/jcb.201911122

Abu Shelbayeh, O., Arroum, T., Morris, S., & Busch, K. B. (2023). PGC-1α Is a Master Regulator of Mitochondrial Lifecycle and ROS Stress Response. *Antioxidants*, *12*(5), 1075. https://doi.org/10.3390/antiox12051075

Adams, B. M., Canniff, N. P., Guay, K. P., & Hebert, D. N. (2021). The Role of Endoplasmic Reticulum Chaperones in Protein Folding and Quality Control (pp. 27–50). https://doi.org/10.1007/978-3-030-67696-4_3

Aebi, M. (2013). N-linked protein glycosylation in the ER. *Biochimica et Biophysica Acta (BBA) - Molecular Cell Research*, *1833*(11), 2430–2437. https://doi.org/10.1016/j.bbamcr.2013.04.001

Ahn, J. I., Yoo, J.-Y., Kim, T. H., Kim, Y. I., Ferguson, S. D., Fazleabas, A. T., Young, S. L., Lessey, B. A., Ahn, J. Y., Lim, J. M., & Jeong, J.-W. (2016). cAMP-Response Element-Binding 3-Like Protein 1 (CREB3L1) is Required for Decidualization and its Expression is Decreased in Women with Endometriosis. Current Molecular Medicine, 16(3), 276–287. https://doi.org/10.2174/1566524016666160225153659

Aibar, S., González-Blas, C. B., Moerman, T., Huynh-Thu, V. A., Imrichova, H., Hulselmans, G., Rambow, F., Marine, J.-C., Geurts, P., Aerts, J., van den Oord, J., Atak, Z. K., Wouters, J., & Aerts, S. (2017). SCENIC: single-cell regulatory network inference and clustering. Nature Methods, 14(11), 1083–1086. https://doi.org/10.1038/nmeth.4463

Alberts, B., A. J. J. L. D. M. M. R. K. R. P. W. S. B. (2015). *Molecular Biology of the Cell, Sixth Edition; ISBN: 9780815344643; and Molecular Biology of the Cell, Sixth Edition, The Problems Book; ISBN 9780815344537* (Vol. 16). https://doi.org/10.3390/ijms161226074

Albrecht, E. D., & Pepe, G. J. (2010). Estrogen regulation of placental angiogenesis and fetal ovarian development during primate pregnancy. *The International Journal of Developmental Biology*, *54*(2–3), 397–408. https://doi.org/10.1387/ijdb.082758ea

Alexa, A., Rahnenfuhrer, J. (2023). topGO: Enrichment Analysis for Gene Ontology. doi:10.18129/B9.

Alexa, A., Rahnenführer, J., & Lengauer, T. (2006). Improved scoring of functional groups from gene expression data by decorrelating GO graph structure. Bioinformatics, 22(13), 1600–1607. https://doi.org/10.1093/bioinformatics/btl140

Alfarouk, K. O., Ahmed, S. B. M., Elliott, R. L., Benoit, A., Alqahtani, S. S., Ibrahim, M. E., Bashir, A. H. H., Alhoufie, S. T. S., Elhassan, G. O., Wales, C. C., Schwartz, L. H., Ali, H. S., Ahmed, A., Forde, P. F., Devesa, J., Cardone, R. A., Fais, S., Harguindey, S., & Reshkin, S. J. (2020). The Pentose Phosphate Pathway Dynamics in Cancer and Its Dependency on Intracellular pH. Metabolites, 10(7), 285. https://doi.org/10.3390/metabo10070285

Amagai, Y., Yamada, M., Kowada, T., Watanabe, T., Du, Y., Liu, R., Naramoto, S., Watanabe, S., Kyozuka, J., Anelli, T., Tempio, T., Sitia, R., Mizukami, S., & Inaba, K. (2023). Zinc homeostasis governed by Golgi-resident ZnT family members regulates ERp44-mediated proteostasis at the ER-Golgi interface. *Nature Communications*, *14*(1), 2683. https://doi.org/10.1038/s41467-023-38397-6

Anelli, T. (2002). ERp44, a novel endoplasmic reticulum folding assistant of the thioredoxin family. *The EMBO Journal*, *21*(4), 835–844. https://doi.org/10.1093/emboj/21.4.835

Anelli, T. (2003). Thiol-mediated protein retention in the endoplasmic reticulum: the role of ERp44. *The EMBO Journal*, *22*(19), 5015–5022. https://doi.org/10.1093/emboj/cdg491

Anelli, T., & Sitia, R. (2008). Protein quality control in the early secretory pathway. The EMBO Journal, 27(2), 315–327. https://doi.org/10.1038/sj.emboj.7601974

Anelli, T., Dalla Torre, M., Borini, E., Mangini, E., Ulisse, A., Semino, C., Sitia, R., & Panina-Bordignon, P. (2022). Profound architectural and functional readjustments of the secretory pathway in decidualization of endometrial stromal cells. *Traffic*, *23*(1). https://doi.org/10.1111/tra.12822

Anelli, T., & Sitia, R. (2018). *CHAPTER 3.4. Mechanisms of Oxidative Protein Folding and Thiol-dependent Quality Control: Tales of Cysteines and Cystines* (pp. 249–266). https://doi.org/10.1039/9781788013253-00249

Anfinsen, C. B. (1973). Principles that Govern the Folding of Protein Chains. Science, 181(4096), 223–230. https://doi.org/10.1126/science.181.4096.223

Appenzeller-Herzog, C., & Hauri, H.-P. (2006). The ER-Golgi intermediate compartment (ERGIC): in search of its identity and function. *Journal of Cell Science*, *119*(11), 2173–2183. https://doi.org/10.1242/jcs.03019

Araki, K., Iemura, S., Kamiya, Y., Ron, D., Kato, K., Natsume, T., & Nagata, K. (2013). Ero1-α and PDIs constitute a hierarchical electron transfer network of endoplasmic reticulum oxidoreductases. Journal of Cell Biology, 202(6), 861–874. https://doi.org/10.1083/jcb.201303027

Aridor, M. (2007). Visiting the ER: The endoplasmic reticulum as a target for therapeutics in traffic related diseases. Advanced Drug Delivery Reviews, 59(8), 759–781. https://doi.org/10.1016/j.addr.2007.06.002

Bailey, D., & O'Hare, P. (2007). Transmembrane bZIP Transcription Factors in ER Stress Signaling and the Unfolded Protein Response. Antioxidants & Redox Signaling, 9(12), 2305–2322. https://doi.org/10.1089/ars.2007.1796

Bar-Lavan, Y., Shemesh, N., & Ben-Zvi, A. (2016). Chaperone families and interactions in metazoa. Essays in Biochemistry, 60(2), 237–253. https://doi.org/10.1042/EBC20160004

Barr, F. A., Preisinger, C., Kopajtich, R., & Körner, R. (2001). Golgi matrix proteins interact with p24 cargo receptors and aid their efficient retention in the Golgi apparatus. *The Journal of Cell Biology*, *155*(6), 885–892. https://doi.org/10.1083/jcb.200108102

Baumann, O., & Walz, B. (2001). Endoplasmic reticulum of animal cells and its organization into structural and functional domains (pp. 149–214). https://doi.org/10.1016/S0074-7696(01)05004-5

Ben-Jonathan, N., Mershon, J. L., Allen, D. L., & Steinmetz, R. W. (1996). Extrapituitary Prolactin: Distribution, Regulation, Functions, and Clinical Aspects*. *Endocrine Reviews*, *17*(6), 639–669. https://doi.org/10.1210/edrv-17-6-639

Bereiter-Hahn, J. (1990). *Behavior of Mitochondria in the Living Cell* (pp. 1–63). https://doi.org/10.1016/S0074-7696(08)61205-X

Betz, S. F. (1993). Disulfide bonds and the stability of globular proteins. *Protein Science*, *2*(10), 1551–1558. https://doi.org/10.1002/pro.5560021002

Bhardwaj V., Heyne S., Sikora K., Rabbani L., Rauer M., Kilpert F., et al. (2019). snakePipes: facilitating flexible, scalable and integrative epigenomic analysis. Bioinformatics 35, 4757–4759. 10.1093/bioinformatics/btz436

Bijovsky, A. T., Zorn, T. M. T., & Abrahamsohn, P. A. (1992). Remodeling of the Mouse Endometrial Stroma during the Preimplantation Period. Cells Tissues Organs, 144(3), 231–234. https://doi.org/10.1159/000147311

Bischof, P. (2001). Endocrine, paracrine and autocrine regulation of trophoblastic metalloproteinases. Early Pregnancy, 5(1), 30–31.

Blond-Elguindi, S. (1993). Affinity panning of a library of peptides displayed on bacteriophages reveals the binding specificity of BiP. Cell, 75(4), 717–728. https://doi.org/10.1016/0092-8674(93)90492-9

Bombail, V., MacPherson, S., Critchley, H. O. D., & Saunders, P. T. K. (2008). Estrogen receptor related beta is expressed in human endometrium throughout the normal menstrual cycle. Human Reproduction, 23(12), 2782–2790. https://doi.org/10.1093/humrep/den298

Braakman, I., & Bulleid, N. J. (2011). Protein Folding and Modification in the Mammalian Endoplasmic Reticulum. *Annual Review of Biochemistry*, *80*(1), 71–99. https://doi.org/10.1146/annurev-biochem-062209-093836

Brar, A. K., Frank, G. R., Kessler, C. A., Cedars, M. I., & Handwerger, S. (1997). Progesterone-dependent decidualization of the human endometrium is mediated by cAMP. *Endocrine*, *6*(3), 301–307. https://doi.org/10.1007/BF02820507

Brosens, I., Puttemans, P., & Benagiano, G. (2019). Placental bed research: I. The placental bed: from spiral arteries remodeling to the great obstetrical syndromes. *American Journal of Obstetrics and Gynecology*, *221*(5), 437–456. https://doi.org/10.1016/j.ajog.2019.05.044

Brosens, J. J., Hayashi, N., & White, J. O. (1999). Progesterone Receptor Regulates Decidual Prolactin Expression in Differentiating Human Endometrial Stromal Cells1. *Endocrinology*, *140*(10), 4809–4820. https://doi.org/10.1210/endo.140.10.7070

Brown, M. S., Ye, J., Rawson, R. B., & Goldstein, J. L. (2000). Regulated Intramembrane Proteolysis. Cell, 100(4), 391–398. https://doi.org/10.1016/S0092-8674(00)80675-3

Cancino, J., Capalbo, A., Di Campli, A., Giannotta, M., Rizzo, R., Jung, J. E., Di Martino, R., Persico, M., Heinklein, P., Sallese, M., & Luini, A. (2014). Control Systems of Membrane Transport at the Interface between the Endoplasmic Reticulum and the Golgi. *Developmental Cell*, *30*(3), 280–294. https://doi.org/10.1016/j.devcel.2014.06.018

Capitani, M., & Sallese, M. (2009). The KDEL receptor: New functions for an old protein. *FEBS Letters*, *583*(23), 3863–3871. https://doi.org/10.1016/j.febslet.2009.10.053

Carbone, K., Pinto, N. M. P., Abrahamsohn, P. A., & Zorn, T. M. T. (2006). Arrangement and fine structure of collagen fibrils in the decidualized mouse endometrium. Microscopy Research and Technique, 69(1), 36–45. https://doi.org/10.1002/jemt.20265

Carter, A. M., Hills, F., O'Gorman, D. B., Roberts, C. T., Sooranna, S. R., Watson, C. S., & Westwood, M. (2004). The Insulin-like Growth Factor System in Mammalian Pregnancy—A Workshop Report. *Placenta*, *25*, S53–S56. https://doi.org/10.1016/j.placenta.2004.01.019

Centonze, F. G., Reiterer, V., Nalbach, K., Saito, K., Pawlowski, K., Behrends, C., & Farhan, H. (2019). LTK is an ER-resident receptor tyrosine kinase that regulates secretion. *Journal of Cell Biology*, *218*(8), 2470–2480. https://doi.org/10.1083/jcb.201903068

Chaiworapongsa, T., Chaemsaithong, P., Yeo, L., & Romero, R. (2014). Pre-eclampsia part 1: current understanding of its pathophysiology. *Nature Reviews Nephrology*, *10*(8), 466–480. https://doi.org/10.1038/nrneph.2014.102

Chen, Q., Lee, C.-E., Denard, B., & Ye, J. (2014). Sustained Induction of Collagen Synthesis by TGF-β Requires Regulated Intramembrane Proteolysis of CREB3L1. PLoS ONE, 9(10), e108528. https://doi.org/10.1371/journal.pone.0108528

Choi, H., Liao, Y.-C., Yoon, Y. J., Grimm, J., Lavis, L. D., Singer, R. H., & Lippincott-Schwartz, J. (2023). Lysosomal release of amino acids at ER three-way junctions regulates transmembrane and secretory protein mRNA translation. BioRxiv : The Preprint Server for Biology. https://doi.org/10.1101/2023.08.01.551382

Christian, M., Marangos, P., Mak, I., McVey, J., Barker, F., White, J., & Brosens, J. J. (2001). Interferon-γ Modulates Prolactin and Tissue Factor Expression in Differentiating Human Endometrial Stromal Cells 1. Endocrinology, 142(7), 3142–3151. https://doi.org/10.1210/endo.142.7.8231

Christis C, Fullaondo A, Schildknegt D, Mkrtchian S, Heck AJR, Braakman I. Regulated increase in folding capacity prevents unfolded protein stress in the ER. J Cell Sci. 2010;123(5):787-794. doi:10.1242/jcs.041111

Clermont, Y., Xia, L., Rambourg, A., Turner, J. D., & Hermo, L. (1993). Structure of the Golgi apparatus in stimulated and nonstimulated acinar cells of mammary glands of the rat. The Anatomical Record, 237(3), 308–317. https://doi.org/10.1002/ar.1092370303

Conneely, O. (2000). Progesterone receptors in reproduction: functional impact of the A and B isoforms. *Steroids*, *65*(10–11), 571–577. https://doi.org/10.1016/S0039-128X(00)00115-X

Conway, C. D., Howe, K. M., Nettleton, N. K., Price, D. J., Mason, J. O., & Pratt, T. (2011). Heparan Sulfate Sugar Modifications Mediate the Functions of *Slits* and Other Factors Needed for Mouse Forebrain Commissure Development. *The Journal of Neuroscience*, *31*(6), 1955–1970. https://doi.org/10.1523/JNEUROSCI.2579-10.2011

Cooper, G. M. (2000). *The Cell: A Molecular Approach* (2nd ed.). Sinauer Associates 2000.

Coppock, H. A., White, A., Aplin, J. D., & Westwood, M. (2004). Matrix Metalloprotease-3 and -9 Proteolyze Insulin-Like Growth Factor-Binding Protein-11. *Biology of Reproduction*, *71*(2), 438–443. https://doi.org/10.1095/biolreprod.103.023101

Corbacho, A., Martinez De La Escalera, G., & Clapp, C. (2002). Roles of prolactin and related members of the prolactin/growth hormone/placental lactogen family in angiogenesis. *Journal of Endocrinology*, *173*(2), 219–238. https://doi.org/10.1677/joe.0.1730219

Cornillie, F. J., Lauweryns, J. M., & Brosens, I. A. (1985). Normal Human Endometrium. An ultrastructural survey. *Gynecologic and Obstetric Investigation*, *20*(3), 113–129. https://doi.org/10.1159/000298983

Cousins, F. L., Pandoy, R., Jin, S., & Gargett, C. E. (2021). The Elusive Endometrial Epithelial Stem/Progenitor Cells. *Frontiers in Cell and Developmental Biology*, *9*. https://doi.org/10.3389/fcell.2021.640319

Coutinho, M. F., Prata, M. J., & Alves, S. (2012). Mannose-6-phosphate pathway: A review on its role in lysosomal function and dysfunction. *Molecular Genetics and Metabolism*, *105*(4), 542–550. https://doi.org/10.1016/j.ymgme.2011.12.012

Cox, J. S., & Walter, P. (1996). A Novel Mechanism for Regulating Activity of a Transcription Factor That Controls the Unfolded Protein Response. Cell, 87(3), 391–404. https://doi.org/10.1016/S0092-8674(00)81360-4

Danilczyk, U. G., Cohen-Doyle, M. F., & Williams, D. B. (2000). Functional Relationship between Calreticulin, Calnexin, and the Endoplasmic Reticulum Luminal Domain of Calnexin. *Journal of Biological Chemistry*, *275*(17), 13089–13097. https://doi.org/10.1074/jbc.275.17.13089

De Matteis, M. A., & Luini, A. (2011). Mendelian Disorders of Membrane Trafficking. New England Journal of Medicine, 365(10), 927–938. https://doi.org/10.1056/NEJMra0910494

Deb, S., Tessier, C., Prigent-Tessier, A., Barkai, U., Ferguson-Gottschall, S., Srivastava, R. K., Faliszek, J., & Gibori, G. (1999). The Expression of Interleukin-6 (IL-6), IL-6 Receptor, and gp130-Kilodalton Glycoprotein in the Rat Decidua and a Decidual Cell Line: Regulation by 17β-Estradiol and Prolactin1. Endocrinology, 140(10), 4442–4450. https://doi.org/10.1210/endo.140.10.7063

Debattisti, V., Gerencser, A. A., Saotome, M., Das, S., & Hajnóczky, G. (2017). ROS Control Mitochondrial Motility through p38 and the Motor Adaptor Miro/Trak. Cell Reports, 21(6), 1667–1680. https://doi.org/10.1016/j.celrep.2017.10.060

Deshaies, R. J., Sanders, S. L., Feldheim, D. A., & Schekman, R. (1991). Assembly of yeast Sec proteins involved in translocation into the endoplasmic reticulum into a membrane-bound multisubunit complex. Nature, 349(6312), 806–808. https://doi.org/10.1038/349806a0

Di Chiara, A. S., Li, R. C., Suen, P. H., Hosseini, A. S., Taylor, R. J., Weickhardt, A. F., Malhotra, D., McCaslin, D. R., & Shoulders, M. D. (2018). A cysteine-based molecular code informs collagen C-propeptide assembly. Nature Communications, 9(1), 4206. https://doi.org/10.1038/s41467-018-06185-2

Di Martino, R., Sticco, L., & Luini, A. (2019). Regulation of cargo export and sorting at the trans-Golgi network. *FEBS Letters*, *593*(17), 2306–2318. https://doi.org/10.1002/1873-3468.13572

Dimitriadis, E. (2002). Interleukin 11 advances progesterone-induced decidualization of human endometrial stromal cells. *Molecular Human Reproduction*, *8*(7), 636–643. https://doi.org/10.1093/molehr/8.7.636

Dudley, D. J., Trautman, M. S., Araneo, B. A., Edwin, S. S., & Mitchell, M. D. (1992). Decidual cell biosynthesis of interleukin-6: regulation by inflammatory cytokines. The Journal of Clinical Endocrinology & Metabolism. https://doi.org/10.1210/jcem.74.4.1548355

Dunn, C. L., Kelly, R. W., & Critchley, H. O. D. (2003). Decidualization of the human endometrial stromal cell: an enigmatic transformation. *Reproductive Biomedicine Online*, *7*(2), 151–161. https://doi.org/10.1016/s1472-6483(10)61745-2

DuRose, J. B., Tam, A. B., & Niwa, M. (2006). Intrinsic Capacities of Molecular Sensors of the Unfolded Protein Response to Sense Alternate Forms of Endoplasmic Reticulum Stress. *Molecular Biology of the Cell*, *17*(7), 3095–3107. https://doi.org/10.1091/mbc.e06-01-0055

Ellgaard, L., McCaul, N., Chatsisvili, A., & Braakman, I. (2016). Co- and Post-Translational Protein Folding in the ER. Traffic, 17(6), 615–638. https://doi.org/10.1111/tra.12392

Ellgaard, L., & Ruddock, L. W. (2005). The human protein disulphide isomerase family: substrate interactions and functional properties. EMBO Reports, 6(1), 28–32. https://doi.org/10.1038/sj.embor.7400311

Farhan, H., & Rabouille, C. (2011). Signalling to and from the secretory pathway. *Journal of Cell Science*, *124*(2), 171–180. https://doi.org/10.1242/jcs.076455

Farquhar, M. G. (1985). Progress in Unraveling Pathways of Golgi Traffic. Annual Review of Cell Biology, 1(1), 447–488. https://doi.org/10.1146/annurev.cb.01.110185.002311

Finka, A., & Goloubinoff, P. (2013). Proteomic data from human cell cultures refine mechanisms of chaperone-mediated protein homeostasis. Cell Stress and Chaperones, 18(5), 591–605. https://doi.org/10.1007/s12192-013-0413-3

Fischer, A. H., Jacobson, K. A., Rose, J., & Zeller, R. (2008). Hematoxylin and Eosin Staining of Tissue and Cell Sections. Cold Spring Harbor Protocols, 2008(5), pdb.prot4986. https://doi.org/10.1101/pdb.prot4986

Ford, C., Parchure, A., von Blume, J., & Burd, C. G. (2021). Cargo sorting at the trans-Golgi network at a glance. Journal of Cell Science, 134(23). https://doi.org/10.1242/jcs.259110

Fox, R. M., Hanlon, C. D., & Andrew, D. J. (2010). The CrebA/Creb3-like transcription factors are major and direct regulators of secretory capacity. Journal of Cell Biology, 191(3), 479–492. https://doi.org/10.1083/jcb.201004062

Freeze HH, Boyce M, Zachara NE, et al. Glycosylation Precursors. In: Varki A, Cummings RD, Esko JD, et al., editors. Essentials of Glycobiology [Internet]. 4th edition. Cold Spring Harbor (NY): Cold Spring Harbor Laboratory Press; 2022. Chapter 5. doi:10.1101/glycobiology.4e.5

Friedman, J. R., Lackner, L. L., West, M., DiBenedetto, J. R., Nunnari, J., & Voeltz, G. K. (2011). ER Tubules Mark Sites of Mitochondrial Division. Science, 334(6054), 358–362. https://doi.org/10.1126/science.1207385

Galloway, C. A., Lee, H., & Yoon, Y. (2012). Mitochondrial morphology—emerging role in bioenergetics. Free Radical Biology and Medicine, 53(12), 2218–2228. https://doi.org/10.1016/j.freeradbiomed.2012.09.035

Gao, C., Cai, Y., Wang, Y., Kang, B.-H., Aniento, F., Robinson, D. G., & Jiang, L. (2014). Retention mechanisms for ER and Golgi membrane proteins. *Trends in Plant Science*, *19*(8), 508–515. https://doi.org/10.1016/j.tplants.2014.04.004

Gao, Y., Sartori, D. J., Li, C., Yu, Q.-C., Kushner, J. A., Simon, M. C., & Diehl, J. A. (2012). PERK Is Required in the Adult Pancreas and Is Essential for Maintenance of Glucose Homeostasis. *Molecular and Cellular Biology*, *32*(24), 5129–5139. https://doi.org/10.1128/MCB.01009-12

Garrido-Gomez, T., Quiñonero, A., Dominguez, F., Rubert, L., Perales, A., Hajjar, K. A., & Simon, C. (2020). Preeclampsia: a defect in decidualization is associated with deficiency of Annexin A2. *American Journal of Obstetrics and Gynecology*, *222*(4), 376.e1-376.e17. https://doi.org/10.1016/j.ajog.2019.11.1250

Gary-Bobo, M., Nirde, P., Jeanjean, A., Morere, A., & Garcia, M. (2007). Mannose 6-Phosphate Receptor Targeting and its Applications in Human Diseases. *Current Medicinal Chemistry*, *14*(28), 2945–2953. https://doi.org/10.2174/092986707782794005

Gaynor, L. M., & Colucci, F. (2017). Uterine Natural Killer Cells: Functional Distinctions and Influence on Pregnancy in Humans and Mice. *Frontiers in Immunology*, *8*. https://doi.org/10.3389/fimmu.2017.00467

Gellersen, B., & Brosens, J. (2003). Cyclic AMP and progesterone receptor cross-talk in human endometrium: a decidualizing affair. *Journal of Endocrinology*, *178*(3), 357–372. https://doi.org/10.1677/joe.0.1780357

Gellersen, B., & Brosens, J. J. (2014). Cyclic Decidualization of the Human Endometrium in Reproductive Health and Failure. *Endocrine Reviews*, *35*(6), 851–905. https://doi.org/10.1210/er.2014-1045

Giacomello, M., & Pellegrini, L. (2016). The coming of age of the mitochondria–ER contact: a matter of thickness. Cell Death & Differentiation, 23(9), 1417–1427. https://doi.org/10.1038/cdd.2016.52

Gidalevitz, T., Stevens, F., & Argon, Y. (2013). Orchestration of secretory protein folding by ER chaperones. *Biochimica et Biophysica Acta (BBA) - Molecular Cell Research*, *1833*(11), 2410–2424. https://doi.org/10.1016/j.bbamcr.2013.03.007

Gilady, S. Y., Bui, M., Lynes, E. M., Benson, M. D., Watts, R., Vance, J. E., & Simmen, T. (2010). Ero1α requires oxidizing and normoxic conditions to localize to the mitochondria-associated membrane (MAM). Cell Stress and Chaperones, 15(5), 619–629. https://doi.org/10.1007/s12192-010-0174-1

Girling, J. E., & Rogers, P. A. W. (2009). Regulation of endometrial vascular remodelling: role of the vascular endothelial growth factor family and the angiopoietin–TIE signalling system. *REPRODUCTION*, *138*(6), 883–893. https://doi.org/10.1530/REP-09-0147

Gleeson, L. M., Chakraborty, C., McKinnon, T., & Lala, P. K. (2001). Insulin-Like Growth Factor-Binding Protein 1 Stimulates Human Trophoblast Migration by Signaling through α5β1 Integrin via Mitogen-Activated Protein Kinase Pathway [1]. *The Journal of Clinical Endocrinology & Metabolism*, *86*(6), 2484–2493. https://doi.org/10.1210/jcem.86.6.7532

Glick, B. S., & Luini, A. (2011). Models for Golgi Traffic: A Critical Assessment. *Cold Spring Harbor Perspectives in Biology*, *3*(11), a005215–a005215. https://doi.org/10.1101/cshperspect.a005215

Gosavi, P., & Gleeson, P. A. (2017). The Function of the Golgi Ribbon Structure – An Enduring Mystery Unfolds! *BioEssays*, *39*(11). https://doi.org/10.1002/bies.201700063

Graner, M. W., Lillehei, K. O., & Katsanis, E. (2015). Endoplasmic Reticulum Chaperones and Their Roles in the Immunogenicity of Cancer Vaccines. Frontiers in Oncology, 4. https://doi.org/10.3389/fonc.2014.00379

Gu, F., Crump, C. M., & Thomas, G. (2001). Trans-Golgi network sorting. *Cellular and Molecular Life Sciences*, *58*(8), 1067–1084. https://doi.org/10.1007/PL00000922

Hanna, J., Goldman-Wohl, D., Hamani, Y., Avraham, I., Greenfield, C., Natanson-Yaron, S., Prus, D., Cohen-Daniel, L., Arnon, T. I., Manaster, I., Gazit, R., Yutkin, V., Benharroch, D., Porgador, A., Keshet, E., Yagel, S., & Mandelboim, O. (2006). Decidual NK cells regulate key developmental processes at the human fetal-maternal interface. *Nature Medicine*, *12*(9), 1065–1074. https://doi.org/10.1038/nm1452

Hansson, S. R., Bottalico, B., Noskova, V., & Casslen, B. (2008). Monoamine transporters in human endometrium and decidua. *Human Reproduction Update*, *15*(2), 249–260. https://doi.org/10.1093/humupd/dmn048

Haze, K., Yoshida, H., Yanagi, H., Yura, T., & Mori, K. (1999). Mammalian Transcription Factor ATF6 Is Synthesized as a Transmembrane Protein and Activated by Proteolysis in Response to Endoplasmic Reticulum Stress. Molecular Biology of the Cell, 10(11), 3787–3799. https://doi.org/10.1091/mbc.10.11.3787

Henderson, T. A., Saunders, P. T. K., Moffett-King, A., Groome, N. P., & Critchley, H. O. D. (2003). Steroid Receptor Expression in Uterine Natural Killer Cells. *The Journal of Clinical Endocrinology & Metabolism*, *88*(1), 440–449. https://doi.org/10.1210/jc.2002-021174

Hetz, C. (2012). The unfolded protein response: controlling cell fate decisions under ER stress and beyond. *Nature Reviews Molecular Cell Biology*, *13*(2), 89–102. https://doi.org/10.1038/nrm3270

Hetz, C., & Papa, F. R. (2018). The Unfolded Protein Response and Cell Fate Control. Molecular Cell, 69(2), 169–181. https://doi.org/10.1016/j.molcel.2017.06.017

Houserman, V. L., Todd, H., & Hertelendy, F. (1989). Progesterone treatment in vitro enhances prostaglandin E and forskolin-promoted cyclic AMP production in human endometrial stromal cells. Reproduction, 85(1), 195–202. https://doi.org/10.1530/jrf.0.0850195

Ishihara, K., Yamazaki, T., Ishida, Y., Suzuki, T., Oda, K., Nagao, M., Yamaguchi-Iwai, Y., & Kambe, T. (2006). Zinc Transport Complexes Contribute to the Homeostatic Maintenance of Secretory Pathway Function in Vertebrate Cells. Journal of Biological Chemistry, 281(26), 17743–17750. https://doi.org/10.1074/jbc.M602470200

Iwakoshi, N. N., Lee, A.-H., Vallabhajosyula, P., Otipoby, K. L., Rajewsky, K., & Glimcher, L. H. (2003). Plasma cell differentiation and the unfolded protein response intersect at the transcription factor XBP-1. *Nature Immunology*, *4*(4), 321–329. https://doi.org/10.1038/ni907

Jabbour, H., & Critchley, H. (2001). Potential roles of decidual prolactin in early pregnancy. *Reproduction*, 197–205. https://doi.org/10.1530/rep.0.1210197

Jastroch, M., Divakaruni, A. S., Mookerjee, S., Treberg, J. R., & Brand, M. D. (2010). Mitochondrial proton and electron leaks. *Essays in Biochemistry*, *47*, 53–67. https://doi.org/10.1042/bse0470053

Jessop, C. E., Watkins, R. H., Simmons, J. J., Tasab, M., & Bulleid, N. J. (2009). Protein disulphide isomerase family members show distinct substrate specificity: P5 is targeted to BiP client proteins. Journal of Cell Science, 122(23), 4287–4295. https://doi.org/10.1242/jcs.059154

Johnson, A. E., & van Waes, M. A. (1999). The Translocon: A Dynamic Gateway at the ER Membrane. Annual Review of Cell and Developmental Biology, 15(1), 799–842. https://doi.org/10.1146/annurev.cellbio.15.1.799

Jones, M. C., Fusi, L., Higham, J. H., Abdel-Hafiz, H., Horwitz, K. B., Lam, E. W.-F., & Brosens, J. J. (2006). Regulation of the SUMO pathway sensitizes differentiating human endometrial stromal cells to progesterone. Proceedings of the National Academy of Sciences, 103(44), 16272–16277. https://doi.org/10.1073/pnas.0603002103

Jones, R. L., Stoikos, C., Findlay, J. K., & Salamonsen, L. A. (2006). TGF-β superfamily expression and actions in the endometrium and placenta. Reproduction, 132(2), 217–232. https://doi.org/10.1530/rep.1.01076

Kajihara, T., Tanaka, K., Oguro, T., Tochigi, H., Prechapanich, J., Uchino, S., Itakura, A., Šućurović, S., Murakami, K., Brosens, J. J., & Ishihara, O. (2014). Androgens Modulate the Morphological Characteristics of Human Endometrial Stromal Cells Decidualized In Vitro. *Reproductive Sciences*, *21*(3), 372–380. https://doi.org/10.1177/1933719113497280

Kambe, T., Matsunaga, M., & Takeda, T. (2017). Understanding the Contribution of Zinc Transporters in the Function of the Early Secretory Pathway. *International Journal of Molecular Sciences*, *18*(10), 2179. https://doi.org/10.3390/ijms18102179

Kamikawa, Y., Saito, A., Matsuhisa, K., Kaneko, M., Asada, R., Horikoshi, Y., Tashiro, S., & Imaizumi, K. (2021). OASIS/CREB3L1 is a factor that responds to nuclear envelope stress. Cell Death Discovery, 7(1), 152. https://doi.org/10.1038/s41420-021-00540-x

Keller, R. B., Tran, T. T., Pyott, S. M., Pepin, M. G., Savarirayan, R., McGillivray, G., Nickerson, D. A., Bamshad, M. J., & Byers, P. H. (2018). Monoallelic and biallelic CREB3L1 variant causes mild and severe osteogenesis imperfecta, respectively. Genetics in Medicine, 20(4), 411–419. https://doi.org/10.1038/gim.2017.115

Khetchoumian, K., Balsalobre, A., Mayran, A., Christian, H., Chénard, V., St-Pierre, J., & Drouin, J. (2019). Pituitary cell translation and secretory capacities are enhanced cell autonomously by the transcription factor Creb3l2. Nature Communications, 10(1), 3960. https://doi.org/10.1038/s41467-019-11894-3

Kim, M. R., Park, D. W., Lee, J. H., Choi, D. S., Hwang, K. J., Ryu, H. S., & Min, C. K. (2005). Progesterone-dependent release of transforming growth factor-beta1 from epithelial cells enhances the endometrial decidualization by turning on the Smad signalling in stromal cells. MHR: Basic Science of Reproductive Medicine, 11(11), 801–808. https://doi.org/10.1093/molehr/gah240

Kim, S.-M., & Kim, J.-S. (2017). A Review of Mechanisms of Implantation. *Development & Reproduction*, *21*(4), 351–359. https://doi.org/10.12717/DR.2017.21.4.351

Klemmt, P. A. B., Carver, J. G., Kennedy, S. H., Koninckx, P. R., & Mardon, H. J. (2006). Stromal cells from endometriotic lesions and endometrium from women with endometriosis have reduced decidualization capacity. *Fertility and Sterility*, *85*(3), 564–572. https://doi.org/10.1016/j.fertnstert.2005.08.046

Kolde, R. (2019) "pheatmap: Pretty Heatmaps. R package version 1.0. 12".

Kondo, S., Hino, S.-I., Saito, A., Kanemoto, S., Kawasaki, N., Asada, R., Izumi, S., Iwamoto, H., Oki, M., Miyagi, H., Kaneko, M., Nomura, Y., Urano, F., & Imaizumi, K. (2012).

Activation of OASIS family, ER stress transducers, is dependent on its stabilization. Cell Death & Differentiation, 19(12), 1939–1949. https://doi.org/10.1038/cdd.2012.77

Kondo, S., Murakami, T., Tatsumi, K., Ogata, M., Kanemoto, S., Otori, K., Iseki, K., Wanaka, A., & Imaizumi, K. (2005). OASIS, a CREB/ATF-family member, modulates UPR signalling in astrocytes. Nature Cell Biology, 7(2), 186–194. https://doi.org/10.1038/ncb1213

Kondo, S., Saito, A., Asada, R., Kanemoto, S., & Imaizumi, K. (2011). Physiological unfolded protein response regulated by OASIS family members, transmembrane bZIP transcription factors. IUBMB Life, 63(4), 233–239. https://doi.org/10.1002/iub.433

Kowada, T., Watanabe, T., Liu, R., & Mizukami, S. (2021). Protocol for synthesis and use of a turn-on fluorescent probe for quantifying labile Zn2+ in the Golgi apparatus in live cells. *STAR Protocols*, *2*(2), 100395. https://doi.org/10.1016/j.xpro.2021.100395

Krikun, G., Mor, G., Alvero, A., Guller, S., Schatz, F., Sapi, E., Rahman, M., Caze, R., Qumsiyeh, M., & Lockwood, C. J. (2004). A Novel Immortalized Human Endometrial Stromal Cell Line with Normal Progestational Response. *Endocrinology*, *145*(5), 2291–2296. https://doi.org/10.1210/en.2003-1606

Kusama, K., Yoshie, M., Tamura, K., Kodaka, Y., Hirata, A., Sakurai, T., Bai, H., Imakawa, K., Nishi, H., Isaka, K., Nagai, T., Nagao, T., & Tachikawa, E. (2013). Regulation of decidualization in human endometrial stromal cells through exchange protein directly activated by cyclic AMP (Epac). Placenta, 34(3), 212–221. https://doi.org/10.1016/j.placenta.2012.12.017

Lee, P. D. K., Conover, C. A., & Powell, D. R. (1993). Regulation and Function of Insulin-Like Growth Factor-Binding Protein-1. Experimental Biology and Medicine, 204(1), 4–29. https://doi.org/10.3181/00379727-204-43630

Li, A., Gao, M., Liu, B., Qin, Y., chen, L., Liu, H., Wu, H., & Gong, G. (2022). Mitochondrial autophagy: molecular mechanisms and implications for cardiovascular disease. Cell Death & Disease, 13(5), 444. https://doi.org/10.1038/s41419-022-04906-6

Li, J., Ahat, E., & Wang, Y. (2019). *Golgi Structure and Function in Health, Stress, and Diseases* (pp. 441–485). https://doi.org/10.1007/978-3-030-23173-6_19

Li, Q., Kannan, A., Wang, W., DeMayo, F. J., Taylor, R. N., Bagchi, M. K., & Bagchi, I. C. (2007). Bone Morphogenetic Protein 2 Functions via a Conserved Signaling Pathway Involving Wnt4 to Regulate Uterine Decidualization in the Mouse and the Human. Journal of Biological Chemistry, 282(43), 31725–31732. https://doi.org/10.1074/jbc.M704723200

Lindahl, K., Åström, E., Dragomir, A., Symoens, S., Coucke, P., Larsson, S., Paschalis, E., Roschger, P., Gamsjaeger, S., Klaushofer, K., Fratzl-Zelman, N., & Kindmark, A. (2018). Homozygosity for CREB3L1 premature stop codon in first case of recessive osteogenesis imperfecta associated with OASIS-deficiency to survive infancy. Bone, 114, 268–277. https://doi.org/10.1016/j.bone.2018.06.019

Lorenson, M. Y. (1996). Prolactin (PRL) is a zinc-binding protein. I. Zinc interactions with monomeric PRL and divalent cation protection of intragranular PRL cysteine thiols. *Endocrinology*, *137*(3), 809–816. https://doi.org/10.1210/en.137.3.809

Love M. I., Huber W., Anders S. (2014). Moderated estimation of fold change and dispersion for RNA-seq data with DESeq2. Genome Biol. 15, 550. 10.1186/s13059-014-0550-8

Lucas, E. S., Vrljicak, P., Muter, J., Diniz-da-Costa, M. M., Brighton, P. J., Kong, C.-S., Lipecki, J., Fishwick, K. J., Odendaal, J., Ewington, L. J., Quenby, S., Ott, S., & Brosens, J. J. (2020). Recurrent pregnancy loss is associated with a pro-senescent decidual response during the peri-implantation window. *Communications Biology*, *3*(1), 37. https://doi.org/10.1038/s42003-020-0763-1

Lynes, E. M., & Simmen, T. (2011). Urban planning of the endoplasmic reticulum (ER): How diverse mechanisms segregate the many functions of the ER. Biochimica et Biophysica Acta (BBA) - Molecular Cell Research, 1813(10), 1893–1905. https://doi.org/10.1016/j.bbamcr.2011.06.011

Ma, L., Ouyang, Q., Werthmann, G. C., Thompson, H. M., & Morrow, E. M. (2017). Live-cell Microscopy and Fluorescence-based Measurement of Luminal pH in Intracellular Organelles. *Frontiers in Cell and Developmental Biology*, *5*. https://doi.org/10.3389/fcell.2017.00071

Ma, W., Goldberg, E., & Goldberg, J. (2017). ER retention is imposed by COPII protein sorting and attenuated by 4-phenylbutyrate. *ELife*, *6*. https://doi.org/10.7554/eLife.26624

Mader, S. L., Libal, N. L., Pritchett-Corning, K., Yang, R., & Murphy, S. J. (2009). Refining timed pregnancies in two strains of genetically engineered mice. *Lab Animal*, *38*(9), 305–310. https://doi.org/10.1038/laban0909-305

Maeda, Y., Ide, T., Koike, M., Uchiyama, Y., & Kinoshita, T. (2008). GPHR is a novel anion channel critical for acidification and functions of the Golgi apparatus. Nature Cell Biology, 10(10), 1135–1145. https://doi.org/10.1038/ncb1773

Mahon, M. J. (2011). pHluorin2: an enhanced, ratiometric, pH-sensitive green florescent protein. *Advances in Bioscience and Biotechnology*, *02*(03), 132–137. https://doi.org/10.4236/abb.2011.23021

Maret, W. (2016). The Metals in the Biological Periodic System of the Elements: Concepts and Conjectures. *International Journal of Molecular Sciences*, *17*(1), 66. https://doi.org/10.3390/ijms17010066

Maruyama, T., & Yoshimura, Y. (2008). Molecular and cellular mechanisms for differentiation and regeneration of the uterine endometrium. *Endocrine Journal*, *55*(5), 795–810. https://doi.org/10.1507/endocrj.k08e-067

Mastropasqua, F., Girolimetti, G., & Shoshan, M. (2018). PGC1α: Friend or Foe in Cancer? Genes, 9(1), 48. https://doi.org/10.3390/genes9010048

Matsuoka, A., Kizuka, F., Lee, L., Tamura, I., Taniguchi, K., Asada, H., Taketani, T., Tamura, H., & Sugino, N. (2010). Progesterone Increases Manganese Superoxide Dismutase Expression via a cAMP-Dependent Signaling Mediated by Noncanonical Wnt5a Pathway in Human Endometrial Stromal Cells. The Journal of Clinical Endocrinology & Metabolism, 95(11), E291–E299. https://doi.org/10.1210/jc.2010-0619

Modest, A. M., Wise, L. A., Fox, M. P., Weuve, J., Penzias, A. S., & Hacker, M. R. (2018). IVF success corrected for drop-out: use of inverse probability weighting. *Human Reproduction*. https://doi.org/10.1093/humrep/dey309

Mori, K., Ma, W., Gething, M.-J., & Sambrook, J. (1993). A transmembrane protein with a cdc2+CDC28-related kinase activity is required for signaling from the ER to the nucleus. Cell, 74(4), 743–756. https://doi.org/10.1016/0092-8674(93)90521-Q

Munro, S. (2011). The Golgin Coiled-Coil Proteins of the Golgi Apparatus. Cold Spring Harbor Perspectives in Biology, 3(6), a005256–a005256. https://doi.org/10.1101/cshperspect.a005256

Murakami, T., Saito, A., Hino, S., Kondo, S., Kanemoto, S., Chihara, K., Sekiya, H., Tsumagari, K., Ochiai, K., Yoshinaga, K., Saitoh, M., Nishimura, R., Yoneda, T., Kou, I., Furuichi, T., Ikegawa, S., Ikawa, M., Okabe, M., Wanaka, A., & Imaizumi, K. (2009). Signalling mediated by the endoplasmic reticulum stress transducer OASIS is involved in bone formation. Nature Cell Biology, 11(10), 1205–1211. https://doi.org/10.1038/ncb1963

Nagata, K. (2003). HSP47 as a collagen-specific molecular chaperone: function and expression in normal mouse development. Seminars in Cell & Developmental Biology, 14(5), 275–282. https://doi.org/10.1016/j.semcdb.2003.09.020

Napolitano, G., Fasciolo, G., & Venditti, P. (2021). Mitochondrial Management of Reactive Oxygen Species. Antioxidants, 10(11), 1824. https://doi.org/10.3390/antiox10111824

Nelson, D. L., & Michael M. Cox. (2017). *Lehninger Principles of Biochemistry.* (W.H. Freeman, Ed.; 7th ed.).

Ng, S.-W., Norwitz, G. A., Pavlicev, M., Tilburgs, T., Simón, C., & Norwitz, E. R. (2020). Endometrial Decidualization: The Primary Driver of Pregnancy Health. *International Journal of Molecular Sciences*, *21*(11), 4092. https://doi.org/10.3390/ijms21114092

Norwitz, E. R., Schust, D. J., & Fisher, S. J. (2001). Implantation and the Survival of Early Pregnancy. *New England Journal of Medicine*, *345*(19), 1400–1408. https://doi.org/10.1056/NEJMra000763

Noske, A. B., Costin, A. J., Morgan, G. P., & Marsh, B. J. (2008). Expedited approaches to whole cell electron tomography and organelle mark-up in situ in high-pressure frozen pancreatic islets. *Journal of Structural Biology*, *161*(3), 298–313. https://doi.org/10.1016/j.jsb.2007.09.015

Okada, H., Nakajima, T., Yasuda, K., & Kanzaki, H. (2004). Interleukin-1 inhibits interleukin-15 production by progesterone during in vitro decidualization in human. *Journal of Reproductive Immunology*, *61*(1), 3–12. https://doi.org/10.1016/j.jri.2003.10.002

Okada, H., Tsuzuki, T., & Murata, H. (2018). Decidualization of the human endometrium. *Reproductive Medicine and Biology*, *17*(3), 220–227. https://doi.org/10.1002/rmb2.12088

Okada, H., Tsuzuki, T., Shindoh, H., Nishigaki, A., Yasuda, K., & Kanzaki, H. (2014). Regulation of decidualization and angiogenesis in the human endometrium: Mini review. *Journal of Obstetrics and Gynaecology Research*, *40*(5), 1180–1187. https://doi.org/10.1111/jog.12392

Okada, S. (2000). Expression of interleukin-15 in human endometrium and decidua. *Molecular Human Reproduction*, *6*(1), 75–80. https://doi.org/10.1093/molehr/6.1.75

Palejwala, S., Tseng, L., Wojtczuk, A., Weiss, G., & Goldsmith, L. T. (2002). Relaxin Gene and Protein Expression and Its Regulation of Procollagenase and Vascular Endothelial Growth Factor in Human Endometrial Cells1. Biology of Reproduction, 66(6), 1743–1748. https://doi.org/10.1095/biolreprod66.6.1743

Paparrizos J., Gravano L. (2015). “k-Shape: Efficient and accurate clustering of time series,” in SIGMOD '15: Proceedings of the 2015 ACM SIGMOD International Conference on Management of Data, Melbourne Victoria Australia, 31 May 2015- 4 June 2015, 1855–1870.

Paroutis, P., Touret, N., & Grinstein, S. (2004). The pH of the Secretory Pathway: Measurement, Determinants, and Regulation. Physiology, 19(4), 207–215. https://doi.org/10.1152/physiol.00005.2004

Patergnani, S., Suski, J. M., Agnoletto, C., Bononi, A., Bonora, M., de Marchi, E., Giorgi, C., Marchi, S., Missiroli, S., Poletti, F., Rimessi, A., Duszynski, J., Wieckowski, M. R., & Pinton, P. (2011). Calcium signaling around Mitochondria Associated Membranes (MAMs). Cell Communication and Signaling : CCS, 9, 19. https://doi.org/10.1186/1478-811X-9-19

Pelham, H. R. B., & Rothman, J. E. (2000). The Debate about Transport in the Golgi—Two Sides of the Same Coin? Cell, 102(6), 713–719. https://doi.org/10.1016/S0092-8674(00)00060-X

Petracco, R. G., Kong, A., Grechukhina, O., Krikun, G., & Taylor, H. S. (2012). Global Gene Expression Profiling of Proliferative Phase Endometrium Reveals Distinct Functional Subdivisions. *Reproductive Sciences*, *19*(10), 1138–1145. https://doi.org/10.1177/1933719112443877

Phillips, M. J., & Voeltz, G. K. (2016). Structure and function of ER membrane contact sites with other organelles. Nature Reviews Molecular Cell Biology, 17(2), 69–82. https://doi.org/10.1038/nrm.2015.8

Pietro, L., Bottcher-Luiz, F., Velloso, L. A., Morari, J., Nomura, M., & Lucci De Angelo Andrade, L. A. (2020). Expression of interleukin-6 (IL-6), signal transducer and activator of transcription-3 (STAT-3) and telomerase in choriocarcinomas. Surgical and Experimental Pathology, 3(1), 28. https://doi.org/10.1186/s42047-020-00080-1

Pijnenborg, R., Vercruysse, L., & Hanssens, M. (2006). The Uterine Spiral Arteries In Human Pregnancy: Facts and Controversies. *Placenta*, *27*(9–10), 939–958. https://doi.org/10.1016/j.placenta.2005.12.006

Pincus, D., Chevalier, M. W., Aragón, T., van Anken, E., Vidal, S. E., El-Samad, H., & Walter, P. (2010). BiP Binding to the ER-Stress Sensor Ire1 Tunes the Homeostatic Behavior of the Unfolded Protein Response. PLoS Biology, 8(7), e1000415. https://doi.org/10.1371/journal.pbio.1000415

Pittari, D., Dalla Torre, M., Borini, E., Hummel, B., Sawarkar, R., Semino, C., van Anken, E., Panina-Bordignon, P., Sitia, R., & Anelli, T. (2022). CREB3L1 and CREB3L2 control Golgi remodelling during decidualization of endometrial stromal cells. *Frontiers in Cell and Developmental Biology*, *10*. https://doi.org/10.3389/fcell.2022.986997

Pobre, K. F. R., Poet, G. J., & Hendershot, L. M. (2019). The endoplasmic reticulum (ER) chaperone BiP is a master regulator of ER functions: Getting by with a little help from ERdj friends. Journal of Biological Chemistry, 294(6), 2098–2108. https://doi.org/10.1074/jbc.REV118.002804

Princiotta, M. F., Finzi, D., Qian, S.-B., Gibbs, J., Schuchmann, S., Buttgereit, F., Bennink, J. R., & Yewdell, J. W. (2003). Quantitating protein synthesis, degradation, and endogenous antigen processing. *Immunity*, *18*(3), 343–354. https://doi.org/10.1016/s1074-7613(03)00051-7

Pulvirenti, T., Giannotta, M., Capestrano, M., Capitani, M., Pisanu, A., Polishchuk, R. S., Pietro, E. S., Beznoussenko, G. V., Mironov, A. A., Turacchio, G., Hsu, V. W., Sallese, M., & Luini, A. (2008). A traffic-activated Golgi-based signalling circuit coordinates the secretory pathway. *Nature Cell Biology*, *10*(8), 912–922. https://doi.org/10.1038/ncb1751

Queckbörner, S., Syk Lundberg, E., Gemzell-Danielsson, K., & Davies, L. C. (2020). Endometrial stromal cells exhibit a distinct phenotypic and immunomodulatory profile. *Stem Cell Research & Therapy*, *11*(1), 15. https://doi.org/10.1186/s13287-019-1496-2

Rämö, O., Kumar, D., Gucciardo, E., Joensuu, M., Saarekas, M., Vihinen, H., Belevich, I., Smolander, O.-P., Qian, K., Auvinen, P., & Jokitalo, E. (2016). NOGO-A/RTN4A and NOGO-B/RTN4B are simultaneously expressed in epithelial, fibroblast and neuronal cells and maintain ER morphology. Scientific Reports, 6(1), 35969. https://doi.org/10.1038/srep35969

Rivinoja, A., Pujol, F. M., Hassinen, A., & Kellokumpu, S. (2012). Golgi pH, its regulation and roles in human disease. *Annals of Medicine*, *44*(6), 542–554. https://doi.org/10.3109/07853890.2011.579150

Roohani, N., Hurrell, R., Kelishadi, R., & Schulin, R. (2013). Zinc and its importance for human health: An integrative review. *Journal of Research in Medical Sciences : The Official Journal of Isfahan University of Medical Sciences*, *18*(2), 144–157.

Rothman, J. E., & Wieland, F. T. (1996). Protein Sorting by Transport Vesicles. Science, 272(5259), 227–234. https://doi.org/10.1126/science.272.5259.227

Rowland, A. A., & Voeltz, G. K. (2012). Endoplasmic reticulum–mitochondria contacts: function of the junction. *Nature Reviews Molecular Cell Biology*, *13*(10), 607–615. https://doi.org/10.1038/nrm3440

Rutanen, E.-M., Koistinen, R., Wahlstrom, T., Bohn, H., Ranta, T., & Seppala, M. (1985). Synthesis of Placental Protein 12 by Human Decidua. *Endocrinology*, *116*(4), 1304–1309. https://doi.org/10.1210/endo-116-4-1304

Saibil, H. (2013). Chaperone machines for protein folding, unfolding and disaggregation. *Nature Reviews Molecular Cell Biology*, *14*(10), 630–642. https://doi.org/10.1038/nrm3658

Saito, A., Hino, S., Murakami, T., Kanemoto, S., Kondo, S., Saitoh, M., Nishimura, R., Yoneda, T., Furuichi, T., Ikegawa, S., Ikawa, M., Okabe, M., & Imaizumi, K. (2009). Regulation of endoplasmic reticulum stress response by a BBF2H7-mediated Sec23a pathway is essential for chondrogenesis. Nature Cell Biology, 11(10), 1197–1204. https://doi.org/10.1038/ncb1962

Saleh, L., Otti, G. R., Fiala, C., Pollheimer, J., & Knöfler, M. (2011). Evaluation of human first trimester decidual and telomerase-transformed endometrial stromal cells as model systems of in vitro decidualization. *Reproductive Biology and Endocrinology*, *9*(1), 155. https://doi.org/10.1186/1477-7827-9-155

Salker, M., Teklenburg, G., Molokhia, M., Lavery, S., Trew, G., Aojanepong, T., Mardon, H. J., Lokugamage, A. U., Rai, R., Landles, C., Roelen, B. A. J., Quenby, S., Kuijk, E. W., Kavelaars, A., Heijnen, C. J., Regan, L., Macklon, N. S., & Brosens, J. J. (2010). Natural Selection of Human Embryos: Impaired Decidualization of Endometrium Disables Embryo-Maternal Interactions and Causes Recurrent Pregnancy Loss. *PLoS ONE*, *5*(4), e10287. https://doi.org/10.1371/journal.pone.0010287

Sampieri, L., di Giusto, P., & Alvarez, C. (2019). CREB3 Transcription Factors: ER-Golgi Stress Transducers as Hubs for Cellular Homeostasis. Frontiers in Cell and Developmental Biology, 7. https://doi.org/10.3389/fcell.2019.00123

Sannino, S., Anelli, T., Cortini, M., Masui, S., Degano, M., Fagioli, C., Inaba, K., & Sitia, R. (2014). Progressive quality control of secretory proteins in the early secretory compartment by ERp44. *Journal of Cell Science*. https://doi.org/10.1242/jcs.153239

Santoni, A., Carlino, C., & Gismondi, A. (2008). Uterine NK cell development, migration and function. *Reproductive BioMedicine Online*, *16*(2), 202–210. https://doi.org/10.1016/S1472-6483(10)60575-5

Sardà-Espinosa A. (2019). Time-series clustering in R using the dtwclust package. R J. 11, 22–43. 10.32614/RJ-2019-023

Sasaki, K., & Yoshida, H. (2019). Golgi stress response and organelle zones. *FEBS Letters*, *593*(17), 2330–2340. https://doi.org/10.1002/1873-3468.13554

Sathe, A., & Gerriets, V. (2023). *Medroxyprogesterone*.

Schatz, F., Guzeloglu-Kayisli, O., Arlier, S., Kayisli, U. A., & Lockwood, C. J. (2016). The role of decidual cells in uterine hemostasis, menstruation, inflammation, adverse pregnancy outcomes and abnormal uterine bleeding. *Human Reproduction Update*, *22*(4), 497–515. https://doi.org/10.1093/humupd/dmw004

Segerer, S. E., Rieger, L., Kapp, M., Dombrowski, Y., Müller, N., Dietl, J., & Kämmerer, U. (2012). MIC-1 (a multifunctional modulator of dendritic cell phenotype and function) is produced by decidual stromal cells and trophoblasts. *Human Reproduction*, *27*(1), 200–209. https://doi.org/10.1093/humrep/der358

Shaffer, A. L., Shapiro-Shelef, M., Iwakoshi, N. N., Lee, A.-H., Qian, S.-B., Zhao, H., Yu, X., Yang, L., Tan, B. K., Rosenwald, A., Hurt, E. M., Petroulakis, E., Sonenberg, N., Yewdell, J. W., Calame, K., Glimcher, L. H., & Staudt, L. M. (2004). XBP1, Downstream of Blimp-1, Expands the Secretory Apparatus and Other Organelles, and Increases Protein Synthesis in Plasma Cell Differentiation. *Immunity*, *21*(1), 81–93. https://doi.org/10.1016/j.immuni.2004.06.010

Sharma, S., Godbole, G., & Modi, D. (2016). Decidual Control of Trophoblast Invasion. *American Journal of Reproductive Immunology*, *75*(3), 341–350. https://doi.org/10.1111/aji.12466

Shi, J.-W., Lai, Z.-Z., Yang, H.-L., Yang, S.-L., Wang, C.-J., Ao, D., Ruan, L.-Y., Shen, H.-H., Zhou, W.-J., Mei, J., Fu, Q., & Li, M.-Q. (2020). Collagen at the maternal-fetal interface in human pregnancy. International Journal of Biological Sciences, 16(12), 2220–2234. https://doi.org/10.7150/ijbs.45586

Shibata, Y., Voeltz, G. K., & Rapoport, T. A. (2006). Rough Sheets and Smooth Tubules. Cell, 126(3), 435–439. https://doi.org/10.1016/j.cell.2006.07.019

Shifren, J. L., Tseng, J. F., Zaloudek, C. J., Ryan, I. P., Meng, Y. G., Ferrara, N., Jaffe, R. B., & Taylor, R. N. (1996). Ovarian steroid regulation of vascular endothelial growth factor in the human endometrium: implications for angiogenesis during the menstrual cycle and in the pathogenesis of endometriosis. *The Journal of Clinical Endocrinology & Metabolism*, *81*(8), 3112–3118. https://doi.org/10.1210/jcem.81.8.8768883

Simmen, T., & Herrera-Cruz, M. S. (2018). Plastic mitochondria-endoplasmic reticulum (ER) contacts use chaperones and tethers to mould their structure and signaling. Current Opinion in Cell Biology, 53, 61–69. https://doi.org/10.1016/j.ceb.2018.04.014

Simón, C., Frances, A., Piquette, G. N., el Danasouri, I., Zurawski, G., Dang, W., & Polan, M. L. (1994). Embryonic implantation in mice is blocked by interleukin-1 receptor antagonist. *Endocrinology*, *134*(2), 521–528. https://doi.org/10.1210/endo.134.2.8299552

Simon, C., Pellicer, A., & Polan, M. L. (1995). Interleukin-1 system crosstalk between embryo and endometrium in implantation. *Human Reproduction*, *10*(suppl 2), 43–54. https://doi.org/10.1093/humrep/10.suppl_2.43

Skulachev, V. P. (2001). Mitochondrial filaments and clusters as intracellular power-transmitting cables. *Trends in Biochemical Sciences*, *26*(1), 23–29. https://doi.org/10.1016/S0968-0004(00)01735-7

Smith, A. D. A. C., Tilling, K., Nelson, S. M., & Lawlor, D. A. (2015). Live-Birth Rate Associated With Repeat In Vitro Fertilization Treatment Cycles. *JAMA*, *314*(24), 2654. https://doi.org/10.1001/jama.2015.17296

So, J.-S. (2018). Roles of Endoplasmic Reticulum Stress in Immune Responses. *Molecules and Cells*, *41*(8), 705–716. https://doi.org/10.14348/molcells.2018.0241

Soares Moretti, A. I., & Martins Laurindo, F. R. (2017). Protein disulfide isomerases: Redox connections in and out of the endoplasmic reticulum. Archives of Biochemistry and Biophysics, 617, 106–119. https://doi.org/10.1016/j.abb.2016.11.007

Sood, A., Jeyaraju, D. V., Prudent, J., Caron, A., Lemieux, P., McBride, H. M., Laplante, M., Tóth, K., & Pellegrini, L. (2014). A Mitofusin-2–dependent inactivating cleavage of Opa1 links changes in mitochondria cristae and ER contacts in the postprandial liver. Proceedings of the National Academy of Sciences, 111(45), 16017–16022. https://doi.org/10.1073/pnas.1408061111

Sorrentino, I., Galli, M., Medraño-Fernandez, I., & Sitia, R. (2022). Transfer of H2O2 from Mitochondria to the endoplasmic reticulum via Aquaporin-11. *Redox Biology*, *55*, 102410. https://doi.org/10.1016/j.redox.2022.102410

Stanley, P. (2011). Golgi Glycosylation. *Cold Spring Harbor Perspectives in Biology*, *3*(4), a005199–a005199. https://doi.org/10.1101/cshperspect.a005199

Stefanoska, I., Jovanović Krivokuća, M., Vasilijić, S., Ćujić, D., & Vićovac, L. (2013). Prolactin stimulates cell migration and invasion by human trophoblast in vitro. *Placenta*, *34*(9), 775–783. https://doi.org/10.1016/j.placenta.2013.06.305

Symoens, S., Malfait, F., D'hondt, S., Callewaert, B., Dheedene, A., Steyaert, W., Bächinger, H. P., de Paepe, A., Kayserili, H., & Coucke, P. J. (2013). Deficiency for the ER-stress transducer OASIS causes severe recessive osteogenesis imperfecta in humans. Orphanet Journal of Rare Diseases, 8(1), 154. https://doi.org/10.1186/1750-1172-8-154

Szabadkai, G., Bianchi, K., Várnai, P., de Stefani, D., Wieckowski, M. R., Cavagna, D., Nagy, A. I., Balla, T., & Rizzuto, R. (2006). Chaperone-mediated coupling of endoplasmic reticulum and mitochondrial Ca2+ channels. The Journal of Cell Biology, 175(6), 901–911. https://doi.org/10.1083/jcb.200608073

Takagi, H., Tamura, I., Fujimura, T., Doi-Tanaka, Y., Shirafuta, Y., Mihara, Y., Maekawa, R., Taketani, T., Sato, S., Tamura, H., & Sugino, N. (2022). Transcriptional coactivator PGC-1α contributes to decidualization by forming a histone-modifying complex with C/EBPβ and p300. Journal of Biological Chemistry, 298(5), 101874. https://doi.org/10.1016/j.jbc.2022.101874

Tamura, M., Sebastian, S., Yang, S., Gurates, B., Fang, Z., & Bulun, S. E. (2002). Interleukin-1β Elevates Cyclooxygenase-2 Protein Level and Enzyme Activity via Increasing Its mRNA Stability in Human Endometrial Stromal Cells: An Effect

Mediated by Extracellularly Regulated Kinases 1 and 2. The Journal of Clinical Endocrinology & Metabolism, 87(7), 3263–3273. https://doi.org/10.1210/jcem.87.7.8594

Telgmann, R. (1998). Marker genes of decidualization: activation of the decidual prolactin gene. Human Reproduction Update, 4(5), 472–479. https://doi.org/10.1093/humupd/4.5.472

Tempio, T., Orsi, A., Sicari, D., Valetti, C., Yoboue, E. D., Anelli, T., & Sitia, R. (2021). A virtuous cycle operated by ERp44 and ERGIC-53 guarantees proteostasis in the early secretory compartment. *IScience*, *24*(3), 102244. https://doi.org/10.1016/j.isci.2021.102244

Thiyagarajan, D. K., Basit, H., & Jeanmonod, R. (2023). *Physiology, Menstrual Cycle*.

Tomoishi, S., Fukushima, S., Shinohara, K., Katada, T., & Saito, K. (2017). CREB3L2-mediated expression of Sec23A/Sec24D is involved in hepatic stellate cell activation through ER-Golgi transport. *Scientific Reports*, *7*(1), 7992. https://doi.org/10.1038/s41598-017-08703-6

Tu, B. P., & Weissman, J. S. (2004). Oxidative protein folding in eukaryotes. The Journal of Cell Biology, 164(3), 341–346. https://doi.org/10.1083/jcb.200311055

Valetti, C., Grossi, C. E., Milstein, C., & Sitia, R. (1991). Russell bodies: a general response of secretory cells to synthesis of a mutant immunoglobulin which can neither exit from, nor be degraded in, the endoplasmic reticulum. The Journal of Cell Biology, 115(4), 983–994. https://doi.org/10.1083/jcb.115.4.983

Valm, A. M., Cohen, S., Legant, W. R., Melunis, J., Hershberg, U., Wait, E., Cohen, A. R., Davidson, M. W., Betzig, E., & Lippincott-Schwartz, J. (2017). Applying systems-level spectral imaging and analysis to reveal the organelle interactome. Nature, 546(7656), 162–167. https://doi.org/10.1038/nature22369

van Anken, E., Romijn, E. P., Maggioni, C., Mezghrani, A., Sitia, R., Braakman, I., & Heck, A. J. R. (2003). Sequential Waves of Functionally Related Proteins Are Expressed When B Cells Prepare for Antibody Secretion. *Immunity*, *18*(2), 243–253. https://doi.org/10.1016/S1074-7613(03)00024-4

van Baelen, K., Dode, L., Vanoevelen, J., Callewaert, G., de Smedt, H., Missiaen, L., Parys, J. B., Raeymaekers, L., & Wuytack, F. (2004). The Ca2+/Mn2+ pumps in the Golgi apparatus. Biochimica et Biophysica Acta (BBA) - Molecular Cell Research, 1742(1–3), 103–112. https://doi.org/10.1016/j.bbamcr.2004.08.018

Vance, J. E. (2014). MAM (mitochondria-associated membranes) in mammalian cells: Lipids and beyond. Biochimica et Biophysica Acta (BBA) - Molecular and Cell Biology of Lipids, 1841(4), 595–609. https://doi.org/10.1016/j.bbalip.2013.11.014

Vang, J., Pustovalova, Y., Korzhnev, D. M., Gorbatyuk, O., Keeler, C., Hodsdon, M. E., & Hoch, J. C. (2022). Architecture of the two metal-binding sites in prolactin. *Biophysical Journal*, *121*(7), 1312–1321. https://doi.org/10.1016/j.bpj.2022.02.024

Vasudevan, K., Raber, J., & Sztein, J. (2010). Fertility comparison between wild type and transgenic mice by in vitro fertilization. *Transgenic Research*, *19*(4), 587–594. https://doi.org/10.1007/s11248-009-9336-2

Vinketova, K., Mourdjeva, M., & Oreshkova, T. (2016). Human Decidual Stromal Cells as a Component of the Implantation Niche and a Modulator of Maternal Immunity. *Journal of Pregnancy*, *2016*, 1–17. https://doi.org/10.1155/2016/8689436

Vinson, C., Acharya, A., & Taparowsky, E. J. (2006). Deciphering B-ZIP transcription factor interactions in vitro and in vivo. Biochimica et Biophysica Acta (BBA) - Gene Structure and Expression, 1759(1–2), 4–12. https://doi.org/10.1016/j.bbaexp.2005.12.005

Voeltz, G. K., Prinz, W. A., Shibata, Y., Rist, J. M., & Rapoport, T. A. (2006). A Class of Membrane Proteins Shaping the Tubular Endoplasmic Reticulum. Cell, 124(3), 573–586. https://doi.org/10.1016/j.cell.2005.11.047

Walter, P., & Ron, D. (2011). The Unfolded Protein Response: From Stress Pathway to Homeostatic Regulation. Science, 334(6059), 1081–1086. https://doi.org/10.1126/science.1209038

Wagner, B. L., Norris, J. D., Knotts, T. A., Weigel, N. L., & McDonnell, D. P. (1998). The Nuclear Corepressors NCoR and SMRT Are Key Regulators of Both Ligand- and 8-Bromo-Cyclic AMP-Dependent Transcriptional Activity of the Human Progesterone

Receptor. Molecular and Cellular Biology, 18(3), 1369–1378. https://doi.org/10.1128/MCB.18.3.1369

Wang, S., Tukachinsky, H., Romano, F. B., & Rapoport, T. A. (2016). Cooperation of the ER-shaping proteins atlastin, lunapark, and reticulons to generate a tubular membrane network. ELife, 5. https://doi.org/10.7554/eLife.18605

Watanabe, S., Amagai, Y., Sannino, S., Tempio, T., Anelli, T., Harayama, M., Masui, S., Sorrentino, I., Yamada, M., Sitia, R., & Inaba, K. (2019). Zinc regulates ERp44-dependent protein quality control in the early secretory pathway. Nature Communications, 10(1), 603. https://doi.org/10.1038/s41467-019-08429-1

Westermann, B. (2010). Mitochondrial fusion and fission in cell life and death. *Nature Reviews Molecular Cell Biology*, *11*(12), 872–884. https://doi.org/10.1038/nrm3013

Westrate, L. M., Lee, J. E., Prinz, W. A., & Voeltz, G. K. (2015). Form Follows Function: The Importance of Endoplasmic Reticulum Shape. Annual Review of Biochemistry, 84(1), 791–811. https://doi.org/10.1146/annurev-biochem-072711-163501

Wickham H (2016). ggplot2: Elegant Graphics for Data Analysis. Springer-Verlag New York. ISBN 978-3-319-24277-4, https://ggplot2.tidyverse.org.

Wilcox, A. J., Baird, D. D., & Weinberg, C. R. (1999). Time of Implantation of the Conceptus and Loss of Pregnancy. *New England Journal of Medicine*, *340*(23), 1796–1799. https://doi.org/10.1056/NEJM199906103402304

Wilcox, A. J., Weinberg, C. R., O'Connor, J. F., Baird, D. D., Schlatterer, J. P., Canfield, R. E., Armstrong, E. G., & Nisula, B. C. (1988). Incidence of Early Loss of Pregnancy. *New England Journal of Medicine*, *319*(4), 189–194. https://doi.org/10.1056/NEJM198807283190401

Yamaguchi, M., Yoshihara, K., Suda, K., Nakaoka, H., Yachida, N., Ueda, H., Sugino, K., Mori, Y., Yamawaki, K., Tamura, R., Ishiguro, T., Motoyama, T., Watanabe, Y., Okuda, S., Tainaka, K., & Enomoto, T. (2021). Three-dimensional understanding of the morphological complexity of the human uterine endometrium. *IScience*, *24*(4), 102258. https://doi.org/10.1016/j.isci.2021.102258

Yoshie, M., Kusama, K., & Tamura, K. (2015). Molecular Mechanisms of Human Endometrial Decidualization Activated by Cyclic Adenosine Monophosphate Signaling Pathways. Journal of Mammalian Ova Research, 32(3), 95–102. https://doi.org/10.1274/jmor.32.95

Yuxiong, W., Faping, L., Bin, L., Yanghe, Z., Yao, L., Yunkuo, L., Yishu, W., & Honglan, Z. (2023). Regulatory mechanisms of the cAMP-responsive element binding protein 3 (CREB3) family in cancers. *Biomedicine & Pharmacotherapy*, *166*, 115335. https://doi.org/10.1016/j.biopha.2023.115335

Zamponi, N., Zamponi, E., Cannas, S. A., Billoni, O. v., Helguera, P. R., & Chialvo, D. R. (2018). Mitochondrial network complexity emerges from fission/fusion dynamics. Scientific Reports, 8(1), 363. https://doi.org/10.1038/s41598-017-18351-5

Zeisel, A., Yitzhaky, A., Bossel Ben-Moshe, N., & Domany, E. (2013). An accessible database for mouse and human whole transcriptome qPCR primers. *Bioinformatics (Oxford, England)*, *29*(10), 1355–1356. https://doi.org/10.1093/bioinformatics/btt145

Zorov, D., Vorobjev, I., Popkov, V., Babenko, V., Zorova, L., Pevzner, I., Silachev, D., Zorov, S., Andrianova, N., & Plotnikov, E. (2019). Lessons from the Discovery of Mitochondrial Fragmentation (Fission): A Review and Update. Cells, 8(2), 175. https://doi.org/10.3390/cells8020175

